

MODELING HOST-MICROBIOTA INTERACTIONS IN DISEASE USING ORGANOID CO-CULTURES

Cayetano Pleguezuelos Manzano

**MODELING HOST-MICROBIOTA INTERACTIONS IN
DISEASE USING ORGANOID CO-CULTURES**

**MODELLEREN VAN GASTHEER-MICROBIOTA-INTERACTIES
BIJ ZIEKTEN MET BEHULP VAN ORGANOÏDE CO-CULTUREN
(met een samenvatting in het Nederlands)**

Proefschrift

ter verkrijging van de graad van doctor aan de
Universiteit Utrecht
op gezag van de
rector magnificus, prof.dr. H.R.B.M. Kummeling,
ingevolge het besluit van het college voor promoties
in het openbaar te verdedigen op

dinsdag 4 juli 2023 des ochtends te 10.15 uur

door

ISBN: 978-94-93278-51-6

Author: Cayetano Pleguezuelos Manzano

Cover: Adriana Martinez-Silgado, Cayetano Pleguezuelos Manzano

Layout: Off Page, Amsterdam

Research in this thesis was performed at the Hubrecht Institute, Utrecht, the Netherlands, in the lab
of Prof. Dr. Hans Clevers.

© All rights reserved. No part of this thesis may be reproduced, stored, or transmitted in any form
by any means without prior permission of the author. The copyright of the published manuscripts
remains with the publishers.

Cayetano Pleguezuelos Manzano

geboren op 25 juni 1992

te Córdoba, Spanje

PROMOTOR

Prof. dr. J.C. Clevers

BEOORDELINGSCOMMISSIE

Prof. dr. M.J.M. Bonten (voorzitter)

Prof. dr. M.M. Maurice

Prof. dr. L. Meyaard

Prof. dr. E.E.S. Nieuwenhuis

Prof. dr. J.P.J. Peters

TABLE OF CONTENTS

Scope of the thesis	7
Chapter 1 Gut microbiota in colorectal cancer: associations, mechanisms and clinical approaches	11
Chapter 2 Organoids and organs-on-chip: insights into human gut-microbe interactions	37
Chapter 3 Establishment and culture of human intestinal organoids derived from adult stem cells	65
Chapter 4 Intestinal organoid co-cultures with microbes	99
Chapter 5 Mutational signature in colorectal cancer caused by <i>pks⁺ E. coli</i>	129
Chapter 6 An analytical framework to detect colibactin-induced mutations in colorectal cancer and <i>E. coli</i> Nissle-exposed organoids	159
Chapter 7.1 The human respiratory tract, cystic fibrosis, and the role of <i>Pseudomonas aeruginosa</i> in the progression of the disease	183
Chapter 7.2 Establishment and characterization of a new <i>Pseudomonas aeruginosa</i> infection model using 2D airway organoids and dual RNA sequencing	189
Chapter 8 Summarizing discussion	219
Appendix Nederlandse samenvatting	231
Resumen en español	235
Curriculum vitae	238
List of Publications	239
Acknowledgments	242

SCOPE OF THE THESIS

Adult stem cell (ASC)-derived organoids are miniature replicas of human organs grown in a dish. They rely on the intrinsic ability of epithelial stem cells to proliferate and/or differentiate upon specific molecular cues. By mimicking these cues *in vitro*, ASC organoids can be grown from healthy tissue and expanded indefinitely, while giving rise to the differentiated cells characteristic of their organ of origin. Today, ASC organoids are used to study diverse biological aspects of human epithelial biology.

The focus of this thesis is to understand mechanisms by which bacteria cause disease. Several bacterial species, *pks*⁺ *E. coli* among them, have been recurrently associated with the development of colorectal cancer (CRC). However, whether their enrichment is causative, or a consequence of the disease remains unclear. Additionally, the increasing rate of antimicrobial resistant (AMR) bacteria is becoming a major problem worldwide. Particularly, AMR strains of *P. aeruginosa* cause chronic infections in individuals with cystic fibrosis, representing a main contributor to its high mortality rate.

In this thesis, we develop organoid-bacteria co-culture models to investigate the direct mechanisms by which these (*pks*⁺ *E. coli* and *P. aeruginosa*) bacteria cause disease. Due to their reductionist nature (being purely epithelial), ASC organoids allow isolation and *in vitro* reconstruction of the interactions occurring between the epithelium and bacteria during infection.

Chapter 1 aims to define the bacteria species commonly associated with CRC. It continues focusing on the current mechanistic knowledge by which the microbiota may cause CRC. Additionally, it discusses current approaches to use or target the gut microbiota in cancer treatment.

Chapter 2 reviews recent developments of bacteria co-cultures with intestinal organoids and organ-on-a-chip models. Additionally, this chapter highlights the biological processes that are better recapitulated by each model. Furthermore, it discusses the current trends and future directions of the use of organoid-bacteria co-cultures to study host-microbiota interactions.

Chapter 3 describes the standard method used to establish and culture ASC-derived human small intestinal and colon 3D organoids, both from healthy and tumor tissue. It includes techniques for cryopreservation, immunofluorescence staining and differentiation of organoids towards specific cell lineages.

Chapter 4 describes the methodology that we have developed to perform co-cultures, with a focus on 3D intestinal organoids and gut bacteria. Furthermore, it covers the most common techniques used in downstream analyses, from the chemical labeling of bacteria to its combination with organoid immunolabeling and imaging, evaluation of bacteria and organoid viability, and the generation of single cell clones from organoids for assessment of bacterial mutagenesis on the epithelium.

Chapter 5 identifies mutational signatures induced by *pks*⁺ *E. coli* in CRC. By establishing long-term co-cultures of intestinal organoids with *pks*⁺ *E. coli*, we identify two

mutational signatures induced by the *pks* product, colibactin. These signatures, termed SBS88 and ID18, can be understood as specific footprints left in the genome by colibactin. Thus, this allows us to identify the mutagenic effect of *pks*⁺ bacteria enriched in a subset of CRC patients. Additionally, our results suggest that colibactin-induced mutations might specifically affect APC, the main driver of CRC tumorigenesis.

Chapter 6 is a follow up study where we evaluate the mutagenic ability of a *pks*⁺ strain of *E. coli* used as a common probiotic. Thus, this strain shows reduced, but detectable mutagenic properties when co-cultured with organoids. As part of this analysis, we develop an analytical approach exploiting the characteristic adenine enrichment of colibactin-induced mutations. This method refines their detection in whole genome sequencing datasets. Additionally, it enables efficient detection of colibactin mutations in samples from whole exome sequencing cohorts.

Chapter 7.1 gives an overview of the human respiratory tract and the current ASC organoid models derived from the airway. Additionally, it describes the cause and consequences of cystic fibrosis (CF), a monogenic disease severely affecting the airways. Often, CF is accompanied by chronic infections of the Gram-negative *P. aeruginosa*, causing severe complications for the patients.

Chapter 7.2 models airway infections with *P. aeruginosa* using a 2D organoid culture system. After establishing the co-culture conditions, we simultaneously characterize the transcriptional response from the epithelium and the bacteria, with a focus on quorum sensing regulation. Using dual RNA sequencing, we show that the epithelium induces bacterial changes in the bacteria that are related to metabolism, expression of virulence factors and antibiotic resistance genes. Importantly, several of these processes are recapitulated in *in vivo* infected samples.

Chapter 8 discusses the implications of the results described in the previous chapters, and the role that organoid-bacteria co-cultures may play in the future developments of the host-microbiota field.



GUT MICROBIOTA IN COLORECTAL CANCER: ASSOCIATIONS, MECHANISMS AND CLINICAL APPROACHES

Cayetano Pleguezuelos-Manzano^{1,2,*}, Jens Puschhof^{1,2,*}, Hans Clevers^{1,2,3}

¹Hubrecht Institute, Royal Netherlands Academy of Arts and Sciences (KNAW) and UMC Utrecht, Utrecht, The Netherlands. ²Oncode Institute, Utrecht, The Netherlands. ³The Princess Máxima Center for Pediatric Oncology, Utrecht, The Netherlands. * Equal contribution

ABSTRACT

Colorectal cancer (CRC) is associated with the presence of particular gut microbes, as observed in many metagenomic studies to date. However, in most cases, it remains difficult to disentangle their active contribution to CRC from just a bystander role. This review focuses on the mechanisms described to date by which the CRC-associated microbiota could contribute to CRC. Bacteria like *pks*⁺ *Escherichia coli*, *Fusobacterium nucleatum*, or enterotoxigenic *Bacteroides fragilis* have been shown to induce mutagenesis, alter host epithelial signaling pathways or reshape the tumor immune landscape in a number of experimental systems. The mechanistic roles of other bacteria, as well as newly identified fungi and viruses which are enriched in CRC, is only starting to be elucidated. Additionally, novel systems like organoids and organs-on-chips are emerging as powerful tools to study the direct effect of gut microbiota on healthy or tumor intestinal epithelium. Thus, the expanding knowledge on tumor-microbiota interactions holds promise for improved diagnosis and treatment of CRC.

KEYWORDS

Colorectal cancer; gut microbiota; organoids; organs-on-chips; clinical translation

GUT MICROBIOTA AND CRC

Colorectal cancer (CRC) is one of the most prevalent cancer types worldwide, with almost 2 million cases and 1 million deaths per year (Sung et al., 2021). The gut mucosa presents the highest concentration of commensal microorganisms in the human body, which intimately affect its homeostatic maintenance and is long hypothesized to be a cause of CRC. Indeed, it is estimated that 2.2 million cases of cancer are attributable to biological infectious agents, accounting for 13% of total cases (Martel et al., 2020). However, despite all the advances in the field, no member of the gut microbiota has been officially recognized as carcinogenic by the WHO to date (Martel et al., 2020).

The advent of next-generation sequencing (NGS)-based metagenomic studies revolutionized our understanding of the human gut microbiota and its relation with CRC. 16S amplicon sequencing studies allow detailed characterization of the gut microbiota species in an unbiased way. Furthermore, shotgun metagenomics enable the study of functional processes encoded in the microbiome of CRC patients (Thomas et al., 2019; Wirbel et al., 2019; Yachida et al., 2019). This has led to the identification of a set of microbes recurrently enriched in fecal and tumor samples (Table 1). Bacteria like genotoxic *pks*⁺ *E. coli*, *Fusobacterium nucleatum* or enterotoxigenic *Bacteroides fragilis* (ETBF) are consistently associated with CRC. Additionally, genera like *Parvimonas*, *Porphyromonas*, *Peptostreptococcus*, *Gemella*, *Streptococcus*, *Prevotella* or the *Clostridiales* order are also recurrently enriched in the disease (Table 1), although how they could contribute to CRC is less studied. While most of the studies to date have focused on bacteria, the microbiota additionally consists of fungi and viruses. Indeed, opportunistic fungal pathogens such as *Malassezia* sp. (Coker et al., 2019) or eukaryotic viruses like *Papillomaviridae* or *Polyomaviridae* (Chen et al., 2015; Turkington et al., 2021) and bacteriophages such as *Caudovirales* (Hannigan et al., 2018; Nakatsu et al., 2018) are starting to arise as potential players in CRC development (Table 1).

Identifying associations of the gut microbiota with CRC and testing their ability to predict the presence of the disease (Thomas et al., 2019; Wirbel et al., 2019; Yachida et al., 2019) has already shown clinical potential as a diagnostic tool (Young et al., 2021a) that is valid for diverse geographical populations (Young et al., 2021b). However, while these associations have proven useful in diagnostics, they do not imply their active role in CRC development. Thus, it is important that studies using a range of biological systems, from human cell lines to mouse models and organoids, help dissecting which microbes contribute causally to CRC, and which are mere bystanders of carcinogenesis. This will contribute to developing strategies to combat relevant CRC processes mediated by microbes (Sepich-Poore et al., 2021).

This review focuses on the current knowledge about how CRC-associated bacteria could contribute to the development of the disease, including the role of gut fungi and viruses. Additionally, we review the advances in the fields of *in vitro* organoid and organs-on-chips to study gut-microbiota interactions in the context of CRC. Finally, we

Table 1. Microbes commonly associated with CRC.

CRC-enriched bacteria	Metagenomic studies describing microbial enrichment in CRC
<i>Fusobacterium nucleatum</i>	Castellarin et al., 2012; Kostic et al., 2012 and 2013; Nakatsu et al., 2015; Baxter et al., 2016; Flemer et al., 2017; Yu et al., 2017; Thomas et al., 2019; Wirbel et al., 2019; Yachida et al., 2019; Young et al., 2021a
<i>Parvimonas</i>	Nakatsu et al., 2015; Baxter et al., 2016; Flemer et al., 2017; Yu et al., 2017; Thomas et al., 2019; Wirbel et al., 2019; Yachida et al., 2019; Young et al., 2021a
<i>Peptostreptococcus</i>	Kostic et al., 2012; Baxter et al., 2016; Flemer et al., 2017; Yu et al., 2017; Thomas et al., 2019; Wirbel et al., 2019; Yachida et al., 2019; Young et al., 2021a
<i>Gemella</i>	Nakatsu et al., 2015; Baxter et al., 2016; Thomas et al., 2021; Wirbel et al., 2019; Yachida et al., 2019; Young et al., 2021a
(<i>pks</i> ⁺) <i>Escherichia coli</i>	Arthur et al., 2012; Wu et al., 2013; Nakatsu et al., 2015; Wirbel et al., 2019; Young et al., 2021a
<i>Porphyromonas</i>	Baxter et al., 2016; Thomas et al., 2019; Wirbel et al., 2019; Yachida et al., 2019; Young et al., 2021a
<i>Solobacterium</i>	Yu et al., 2017; Thomas et al., 2019; Wirbel et al., 2019; Yachida et al., 2019; Young et al., 2021a
<i>Clostridium</i>	Flemer et al., 2019; Thomas et al., 2019; Wirbel et al., 2019; Yachida et al., 2019
<i>Bilophila</i>	Yachida et al., 2019; Nguyen et al., 2020; Young et al., 2021a
<i>Atopobium</i>	Yachida et al., 2019; Young et al., 2021a
<i>Dorea</i>	Yachida et al., 2019; Young et al., 2021a
<i>Streptococcus</i>	Thomas et al., 2019; Yachida et al., 2019
<i>Prevotella</i>	Baxter et al., 2016; Wirbel et al., 2019
Enterotoxigenic <i>Bacteroides fragilis</i>	Nakatsu et al., 2015
CRC-enriched fungi	
Basidiomycota	Gao et al., 2017; Richard et al., 2018; Coker et al., 2019
<i>Malassezia</i>	Gao et al., 2017; Richard et al., 2018; Coker et al., 2019
CRC-enriched viruses	
<i>Papillomaviridae</i>	Chen et al., 2015; Turkington et al., 2021
<i>Polyomaviridae</i>	Chen et al., 2015; Turkington et al., 2021
<i>Caudovirales</i>	(Hannigan et al., 2018; Nakatsu et al., 2018)

discuss how this mechanistic knowledge is already shaping the clinical approach to CRC diagnostics, prognostics and treatment.

MECHANISTIC INSIGHT ON GUT BACTERIA DRIVING CRC TUMORIGENESIS

Genotoxic *pks*⁺ *Escherichia coli*

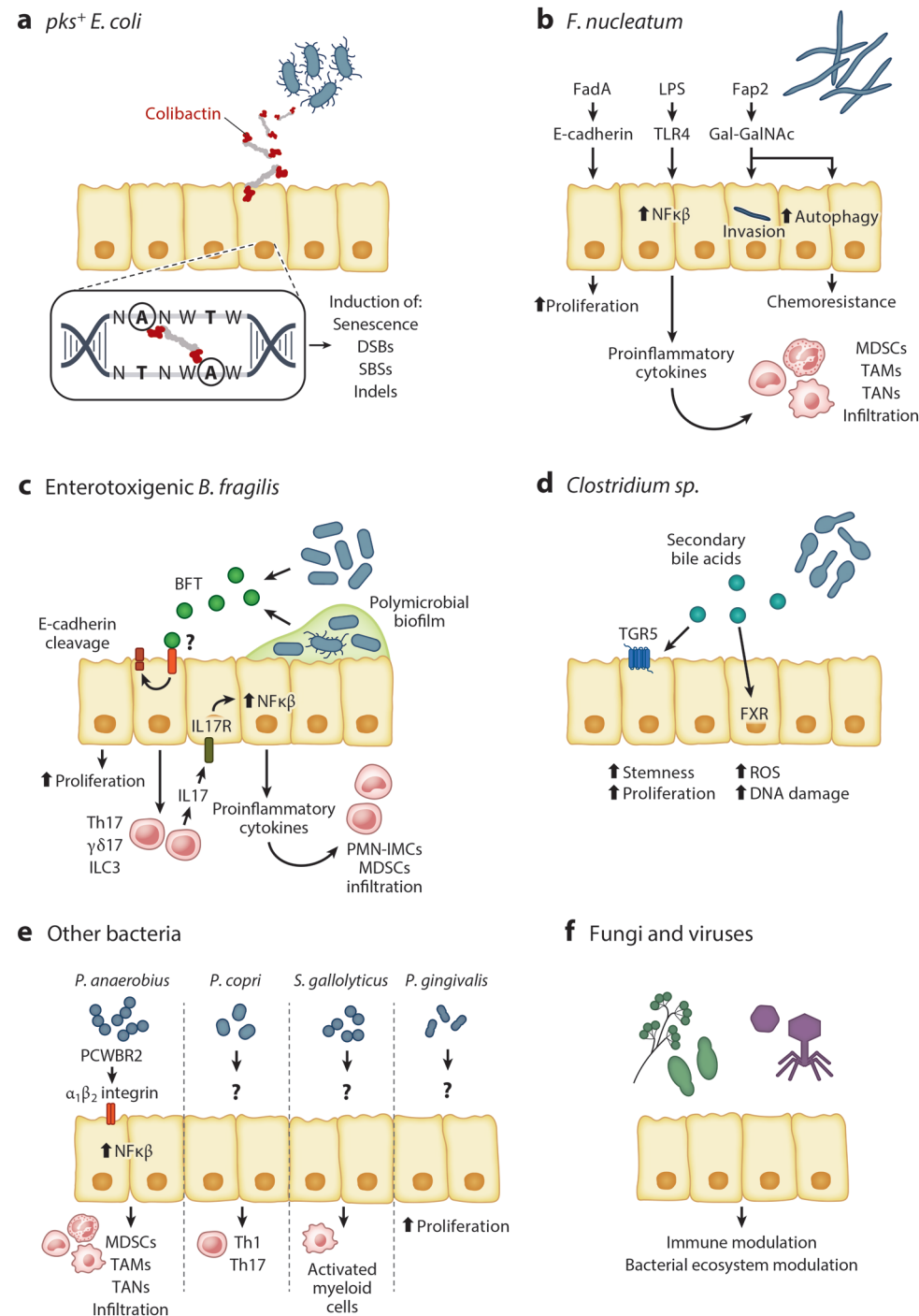
In 2006, a landmark study identified intestinal strains of genotoxic *E. coli* harboring the *pks* operon, putting them on the map of CRC (Nougayrède et al., 2006). Since then,

several investigations have shown the enrichment of genotoxic *pks*⁺ *E. coli* in CRC samples (Arthur et al., 2012; Buc et al., 2013; Wirbel et al., 2019). Indeed, *pks*⁺ strains of *E. coli* are present in approximately 60% of CRC samples compared to only 20% of healthy donors (Arthur et al., 2012; Buc et al., 2013). Additionally, *pks*⁺ *E. coli* has been found enriched in precancerous conditions like inflammatory bowel disease (IBD) and familial adenomatous polyposis (FAP) (Arthur et al., 2012; Dejea et al., 2018).

The *pks* operon encodes a hybrid non-ribosomal peptide synthetase-polyketide synthase assembly line which enables production of the genotoxin colibactin (Faïss et al., 2018). The effects of this -highly labile- molecule on epithelial cells have been studied intensively since its discovery. They range from the induction of DNA interstrand crosslinks (Bossuet-Greif et al., 2018) to cell senescence (Cougoux et al., 2014). Additionally, *pks*⁺ *E. coli* colonization increases DNA damage and tumor burden in mouse models of CRC (Cuevas-Ramos et al., 2010; Arthur et al., 2012; Dejea et al., 2018).

A series of publications in 2019 resolved the long-elusive structure of colibactin and enabled unprecedented insight into its DNA damaging capabilities (Li et al., 2019; Wilson et al., 2019; Xue et al., 2019). Key insights comprise the ability of colibactin to alkylate adenosines (Wilson et al., 2019) and to form interstrand crosslinks through two cyclopropane warheads (Xue et al., 2019). This causes DNA double strand breaks (DSBs) by a copper-mediated mechanism (Li et al., 2019). In turn, this suggests a potential mechanism whereby colibactin induces crosslinking of adenines on opposing DNA strands, leading to DSB induction and/or mutagenesis through improper resolution of these adducts.

More recently, we described the ability of *pks*⁺ *E. coli* to induce a genome-wide mutational signature in CRC (Pleguezuelos-Manzano et al., 2020). Mutational signatures are marks left in the genome through the effect of specific mutagens, and they can be used to explore the past exposure of tumors to these mutagens (Alexandrov et al., 2013, 2020). Thus, healthy human gut organoids, chronically exposed to the bacteria, were used to establish that -beyond DSB induction described previously- *pks*⁺ *E. coli* induces mutations in adenine-rich regions of the DNA, giving rise to readily recognizable SBS-88 and ID-18 mutational signatures. Then, this was used to identify the contribution of *pks*⁺ *E. coli* to the mutational burden of CRC in patients and its potential to mutate CRC-relevant genes like *APC* (Pleguezuelos-Manzano et al., 2020). Furthermore, the genome-wide profile of DSB induced by the bacteria also showed an adenine enrichment in the damaged DNA sequence (Dziubańska-Kusibab et al., 2020). Both observations are in line with the ability of colibactin to crosslink adenines deduced in the previous structural studies (Li et al., 2019; Wilson et al., 2019; Xue et al., 2019). Another study reported Wnt-independent growth of murine intestinal organoids after a 3-hour exposure to genotoxic *E. coli*, associated with wide-ranging genomic effects (Iftekhar et al., 2021) (Figure 1a).



Fusobacterium nucleatum

The presence of *Fusobacterium nucleatum* in CRC tumor samples was first described in two seminal studies (Castellarin et al., 2012; Kostic et al., 2012). Subsequently, metagenomic analyses from fecal (Thomas et al., 2019; Wirbel et al., 2019; Yachida et al., 2019) and tumor (Nakatsu et al., 2015) samples confirmed the association between *F. nucleatum* and CRC. Clinically, the presence of *F. nucleatum* correlates with left-sided, microsatellite instability (MSI) positive CRC tumors (Hamada et al., 2018; Mima et al., 2016). Interestingly, *F. nucleatum* has been found associated from early to late stages of CRC (Hong et al., 2019; Yachida et al., 2019) as well as being detected in CRC-derived liver metastases (Kostic et al., 2012; Bullman et al., 2017). Furthermore, *F. nucleatum* shows no association with Lynch syndrome patients, a familial version of hypermutated CRC (Yan et al., 2020), highlighting the bacterial link with sporadic CRC.

F. nucleatum is a common member of the oral microbiota. Currently, it is thought that its translocation to colonic tumors occurs via the bloodstream (Abed et al., 2016), through the transient elevation of bacterial counts in the bloodstream after toothbrushing. Tail vein injection of *F. nucleatum* led to the specific localization of the bacteria to orthotopic colonic tumors. This tropism was mediated by the bacterial adhesin Fap2 which binds Gal-GalNAc, a sugar moiety specifically overexpressed in CRC cells (Abed et al., 2016). Other possibilities, like tumor translocation via the gastrointestinal tract, remain to be tested.

◀ **Figure 1. Different mechanisms by which CRC-associated bacteria have been proposed to drive CRC carcinogenesis.** **a**, The production of colibactin by *pks*⁺ *Escherichia coli* induces DNA damage (DSBs), senescence, SBSs, and short insertions/deletion mutations (indels) in CRC. **b**, *Fusobacterium nucleatum* enhances proliferation via FadA binding to epithelial E-cadherin and the production of proinflammatory cytokines and the infiltration of MDSCs, TAMs, and TANs via LPS activation of TLR4-NF-κβ. The engagement of Fap2 to epithelial Gal-GalNAc mediates bacterial invasion and increased autophagy-mediated chemoresistance. **c**, By producing BFT, enterotoxigenic *Bacteroides fragilis* induces recruitment of Th17, γδ17, and ILC3 lymphocytes and a proinflammatory environment through the IL-17/NF-κβ axis, resulting in the infiltration of proinflammatory MDSCs and PMN-IMCs. **d**, Secondary bile acids produced by *Clostridium* spp. are proposed to induce stemness and proliferation via TGR5 and FXR activation, increased levels of ROS, and DNA damage. **e**, Proposed mechanisms by which other bacteria could contribute to CRC: *Peptostreptococcus anaerobius* protein PCWBR2 binding to epithelial integrin induces infiltration of MDSCs, TAMs and TANs via NF-κβ activation; *Prevotella copri* induces recruitment of Th1 and Th17 lymphocytes and *Streptococcus gallolyticus* recruits activated myeloid cells, although the mechanisms remain unknown; and *Porphyromonas gingivalis* increases proliferation by unknown mechanisms. **f**, Fungi and viruses from the gut microbiota are supposed to modulate the immune and bacterial compartment. There is no conclusive evidence about whether they could directly induce CRC by their effect on epithelial cells. Abbreviations: BFT, *B. fragilis* toxin; δγ17, IL-17-producing δγ T cells; DSB, double-strand break; ILC3, type 3 innate lymphoid cells; MDSCs, myeloid-derived suppressor cell; PMN-IMC, polymorphonuclear immature myeloid cell; ROS, reactive oxygen species; SBS, single-base substitution; TAM, tumor-associated macrophage; TAN, tumor-associated neutrophil; Th1, T helper type 1 cell; Th17, T helper type 17 cell.

Growing evidence suggests that *F. nucleatum* can induce colon tumorigenesis. *Fusobacterium* was shown to increase proliferation in colorectal cancer cell lines (Rubinstein et al., 2013; Yang et al., 2017), colonic tumor formation in CRC mouse models (Kostic et al., 2013; Yang et al., 2017) and xenograft establishment rate (Bullman et al., 2017). It was suggested using CRC cell lines that *Fusobacterium* surface protein FadA binds to epithelial cell-to-cell adhesion protein E-cadherin, which normally is a binding partner of the Wnt pathway protein β -catenin. As a result, this was suggested to have an impact on Wnt signaling activation levels (Rubinstein et al., 2013). Additionally, *Fusobacterium* could contribute to CRC by altering tumor sensitivity to anti-cancer drugs. Through a TLR4/MYD88 miRNA-mediated mechanism leading to increased autophagy, *F. nucleatum* was shown to induce resistance to chemotherapeutics like oxaliplatin or 5-FU in cancer cell lines and CRC cell line mouse xenografts (Yu et al., 2017).

Besides, *F. nucleatum* has been proposed to induce CRC tumor inflammation. The presence of *F. nucleatum* in CRC patient samples correlated with pro-inflammatory gene profiles (Kostic et al., 2013). This was confirmed later in several CRC mouse models where *Fusobacterium* induced the expression of proinflammatory cytokines and NF κ B pathway activation (Kostic et al., 2013; Yang et al., 2017). In turn, this profile led to the accumulation of tumor-associated macrophages (TAMs), dendritic cells and myeloid-derived suppressor cells (MDSCs) (Kostic et al., 2013), which have been shown to promote tumor development and enhanced immune escape (Veglia et al., 2018). In patients, the presence of *F. nucleatum* was also inversely associated with the presence of CD3⁺, CD3⁺/CD4⁺/CD45RO⁺ and CD8⁺ T cells (Mima et al., 2015; Serna et al., 2020; Borowsky et al., 2021). Furthermore, *Fusobacterium* has been shown to directly inhibit NK cell cytotoxicity by FadA-mediated binding to TIGIT receptor (Gur et al., 2015).

F. nucleatum shows an invasive phenotype in CRC cell lines *in vitro* (Castellarin et al., 2012) and in CRC tumors (Bullman et al., 2017; Serna et al., 2020). However, until recently, the consequences of this invasion remained unexplored. Casasanta and colleagues showed that bacterial invasion into CRC cancer cell lines is dependent on Fap2 expression (Casasanta et al., 2020). Invasion was accompanied by induction of epithelial CXCL1 and IL8 cytokine production, which in turn led to increased tumor cell migration *in vitro*. This, together with the presence of the bacteria in CRC liver metastases (Bullman et al., 2017; Kostic et al., 2012), suggests that by invading epithelial cells *F. nucleatum* could mediate the metastatic process. Although this hypothesis sounds appealing, experimental evidence is not available yet (Figure 1b).

Enterotoxigenic *Bacteroides fragilis*

Bacteroides fragilis is a common human gut commensal, where it contributes to a healthy intestinal tract. However, particular strains termed enterotoxigenic *B. fragilis* (ETBF) were identified in the 90's for their ability to induce diarrhea, inflammation and being associated with IBD (Sack et al., 1994; Prindiville et al., 2000; Basset et al., 2004; Sears et al., 2008, 2014) and later with FAP and CRC patients (Dejea et al., 2014; Boleij et al., 2015; Nakatsu

et al., 2015; Dejea et al., 2018). The toxigenicity of ETBF resides in the production of a matrix metalloproteinase toxin termed *B. fragilis* toxin (BFT), encoded in the genomic *bft* locus (Sears et al., 2014). Despite its association, shotgun metagenomic analysis of BFT presence in fecal samples did not identify an association between the toxin and CRC (Wirbel et al., 2019). This observation could be confounded by differences previously observed between the detection of mucosal and fecal microbes, which was shown to particularly affect *Bacteroides* in mice (Vaga et al., 2020).

The action of ETBF through BFT has been implicated in a number of CRC-inducing mechanisms. Initially, the BFT toxin was shown to induce E-cadherin cleavage and altered Wnt pathway levels, leading to increased proliferation rates in cancer cell lines (Wu et al., 2003, 2007), similar to what has been observed in the case *F. nucleatum* (Rubinstein et al., 2013). Despite these observations, the specific binding partner of BFT on the epithelial cell surface has not been identified yet. Elucidating this interaction could help the development of specific inhibitors to be used as clinical drugs against ETBF and BFT.

The use of several CRC mouse models has uncovered the ability of ETBF to induce distal colon tumorigenesis, via a multi-step pro-inflammatory immune response. In *Apc^{min/+}* and AOM mouse models, ETBF was shown to induce distal tumorigenesis 1 week after gut colonization (Wu et al., 2009; Dejea et al., 2018; Chung et al., 2018). Particularly, ETBF, through the action of BFT, can induce recruitment of Th17, γ δ T17 and ILC3 to the colonic tumors, leading to increased IL17 levels activating the NF- κ B/STAT3 pathway in the epithelium (Wu et al., 2009; Dejea et al., 2018; Chung et al., 2018). In turn, this activates the production of proinflammatory cytokines like CXCL1, CXCL2 or CXCL5 that further recruit CXCR2⁺ polymorphonuclear immature myeloid cells (PMN-IMCs) (Thiele Orberg et al., 2017) and promote their differentiation towards tumor-promoting MDSCs immune cells (Chung et al., 2018).

Furthermore, ETBF is able to grow in polymicrobial bacterial biofilms, enriched in right-side CRC (Dejea et al., 2014, 2018). The significance of bacterial biofilms in colorectal cancer is not yet fully understood, but the presence of these biofilms correlates with higher levels of IL6, pSTAT3 and proliferative cells, even in regions of normal mucosa that are in close proximity to bacterial aggregates (Dejea et al., 2014). Interestingly, Dejea and colleagues (Dejea et al., 2018) showed that ETBF can co-localize with *pks⁺ E. coli* in polymicrobial biofilms on FAP patient polyps. The combined presence of ETBF and *pks⁺ E. coli* increased their tumorigenicity in two mouse models of CRC. Interestingly, ETBF-induced IL17-mediated inflammation and mucosal barrier disruption appear to facilitate the mutagenic effect of *pks⁺ E. coli*. These observations suggest a cooperative contribution to CRC tumorigenesis through these combined effects (Figure 1c).

Other bacteria associated with CRC development

As the number of metagenomic studies increases, so does the evidence that there are other bacteria associated with CRC, i.e., genera like *Parvimonas*, *Peptostreptococcus*, *Gemella*, *Porphyromonas*, *Solobacterium*, *Clostridium*, *Bilophila*, *Atopobium*, *Dorea*,

Streptococcus or *Prevotella* (Table 1). However, proof for their active contribution to the disease is limited or absent in most cases.

A number of these bacteria have been suggested to induce inflammation of the gut. *Peptostreptococcus anaerobius* was shown to bind $\alpha 1/\beta 2$ integrin of CRC cell lines, via its surface protein PCWBR2 (Long et al., 2019), inducing proinflammatory cytokine production and MDSCs, TAMs and tumor-associated neutrophils (TANs) infiltration in *Apc^{min/+}* mouse models. *Prevotella copri* has been shown to induce Th1 and Th17 infiltration (Yu et al., 2019). *Streptococcus gallolyticus* preferentially locates in polyps bearing mutations in APC (Aymeric et al., 2018) and induces pro-inflammatory cytokine secretion and infiltration of CD11b⁺/TLR4⁺ activated myeloid cells (Deng et al., 2020). In other AOM-cancer mouse models, the presence of *S. gallolyticus* increased tumor burden and resulted in higher dysplasia grade (Kumar et al., 2017). Finally, *Porphyromonas gingivalis* can induce proliferation in CRC cell lines, where it displays an epithelial invasive phenotype (Mu et al., 2020). Furthermore, specific proteobacteria including strains of *E. coli*, can produce cytolethal distending toxin (CDT), a molecule that has been shown to induce DSBs and tumorigenesis in mice (He et al., 2019).

The order Clostridiales, and particularly the ability of some species to produce secondary bile acids, is strikingly associated with CRC development (Wirbel et al., 2019; Yachida et al., 2019). Members of this order are able to metabolize bile acids from the human host, producing secondary bile acids, mainly deoxycholic and lithocholic acid (DCA and LCA). These are highly hydrophobic molecules that strongly activate nuclear receptors and TGR5 signaling (Jia et al., 2018). Mechanistically, secondary bile acids were shown to induce colonic stemness and tumorigenesis through their effect on the FXR nuclear receptor in the context of high fat diet in *Apc^{min/+}* CRC mouse model (Fu et al., 2019). Additionally, secondary bile acids could induce chromosomal instability, potentially through increasing reactive oxygen species (ROS) levels (Fu et al., 2019). Furthermore, secondary bile acids have been implicated in liver tumorigenesis. In a key study, Yoshimoto and colleagues demonstrated that high fat diet induced an enrichment of *Clostridium* in the gut microbiota and a stark increase of DCA levels. In turn, DCA promoted a senescence-associated secretory phenotype in liver stellate cells and their proinflammatory state, leading to the development of hepatocellular carcinoma (Yoshimoto et al., 2013) (Figure 1d, e).

FUNGI AND CRC DEVELOPMENT

Past metagenomic studies have focused mostly on the bacterial contribution to CRC. However, the gut fungal microbiota, or mycobiota, is also emerging as a potential player in colon tumorigenesis. In the healthy gut, there are 2 dominating phyla: Ascomycota (70%) and Basidiomycota (30%), with Zygomycetes being detected more rarely (Hallen-Adams and Suhr, 2017; Richard and Sokol, 2019). To date, only few metagenomics studies have attempted to characterize CRC fungal dysbiosis and generally the small sample size makes it difficult to draw definitive conclusions.

CRC is characterized by an increased Basidiomycota:Ascomycota ratio, with an enrichment of *Malassezia* spp. (Gao et al., 2017; Richard et al., 2018; Coker et al., 2019) (Table 1). Interestingly, *Malassezia* has been demonstrated to promote pancreatic ductal adenocarcinoma after migrating from the gut lumen to the pancreas (Aykut et al., 2019), although its role in CRC needs investigation. To date, the most extensive fungi metagenomics study (Coker et al., 2019) identified a set of 14 fungal species, with potential use as CRC biomarkers, allowing to distinguish between healthy and early-stage CRC samples, as done for bacteria. The active role of fungi in CRC development remains largely unknown. Some studies have suggested that the opportunistic pathogen *Candida albicans* can alter immune cell metabolism leading to increased inflammation and tumorigenesis (Zhu et al., 2021). Others have focused on the role of *Debaryomyces hansenii* in Crohn's disease, a subtype of IBD. *D. hansenii* is enriched in inflamed gut regions of patients, and induces a type-I IFN-CCL5 response that impairs wound healing in a DSS-induced colitis mouse model (Jain et al., 2021). Despite these studies, further studies are required, both to validate the associations observed to date as well as to possibly identify new enriched fungi as the sample size and statistical power of the studies increases. This will certainly be accompanied by mechanistic studies that will deepen our understanding of the mycobiota contribution to CRC disease (Figure 1f).

VIRUSES AND CRC DEVELOPMENT

While viruses have been at the forefront of infectious agents causing cancer (White et al., 2014), their role in CRC development has been harder to disentangle. While it remains challenging to separate viral from contaminant sequencing data, as well as to faithfully annotate viral genomes, advances in viral like particle (VLP) purification prior to sequencing and in analytical frameworks have enabled much progress on establishing the baseline human virome (Angly et al., 2005; Virgin et al., 2009; Reyes et al., 2010, 2010; Virgin, 2014; Shkoporov et al., 2019).

Recent studies have reported changes in the human gut virome in CRC (Hannigan et al., 2018; Nakatsu et al., 2018; Emler et al., 2020) and in potential precursor conditions such as IBD (Norman et al., 2015) (Table 1). Of note, most disease associations reported to date stem from the more abundant bacteriophages as opposed to eukaryotic viruses infecting gut epithelium. An increase in overall diversity of bacteriophages (Nakatsu et al., 2018) and *Caudovirales* (Norman et al., 2015) was reported for CRC and IBD cases, respectively, but no changed diversity was observed in a further study of CRC (Hannigan et al., 2018). Identification of CRC-associated individual phage species proves more difficult and noted a smaller effect size compared to bacteria in these early studies. Nevertheless, *Inovirus*, *Tunalikevirus* (Nakatsu et al., 2018) as well as several other phages of the *Caudovirales*, *Siphoviridae* and *Myoviridae* families (Hannigan et al., 2018) have been identified as most strongly associated with CRC cases.

The functional consequences of changed bacteriophage abundances on CRC are only beginning to be unraveled. The impact on bacterial communities is one of the most

plausible, yet indirect, ways by which bacteriophages may impact CRC (Dahlman et al., 2021) (Massimino et al., 2021). Indeed, inhibition of either pro- and anti-tumorigenic bacterial species are mechanisms by which bacteriophages have been shown to modulate CRC risk (Gogokhia et al., 2019; Emlet et al., 2020). A landmark study highlights that - in addition to the direct predation of specific bacterial species - a direct induction of a host immune response is a mechanism by which phages are prone to shape the CRC microbiota (Gogokhia et al., 2019). Further studies will be necessary to elucidate the functional roles of the CRC virome. The emerging insights into the roles of bacteriophages in CRC will not only reveal their contribution to cancer development but could also pave the way to bacteriophage therapies targeted at bacterial species in CRC (Turkington et al., 2021). Beyond these phage-centric studies, eukaryotic viruses such as human papillomaviruses and *Polyomaviridae* (Chen et al., 2015; Turkington et al., 2021) and less characterized infections agents (Hausen, 2012; Bund et al., 2021) have been implicated in CRC development. Detection in large scale sequencing efforts and mechanistic studies may substantiate their role in CRC development and provide new targets for CRC prevention (Figure 1f).

ORGANOID-BASED APPROACHES AS NEW SYSTEMS TO STUDY HEALTHY COLON- AND CRC-MICROBIOTA INTERACTIONS

Developed during the past decade, adult stem cell-based organoid technology (Sato et al., 2009, 2011; Clevers, 2016) has emerged as a novel model to study CRC host-microbiota interactions (Figure 2). Adult stem cell-derived organoids are miniature versions of epithelial organs that can directly be established from human tissue samples. They normally grow embedded in an extracellular matrix as self-organizing 3D structures that recapitulate the cellular and molecular characteristics of the tissue they are derived from. Since they can be derived from healthy or tumor tissue, organoids offer a great opportunity to experimentally study microbe contribution to CRC initiation and development in a human-specific setting. Additionally, intestinal organoids can be generated from induced pluripotent stem cell (iPSC) intestinal organoids (Spence et al., 2011; Múnera et al., 2017; McCauley and Wells, 2017). Despite their advantages, intestinal organoids lack the presence of immune cells, which are important to shape the gut mucosa-microbe relationships, present in more holistic approaches like mouse models.

Several approaches have been already used to study the interactions between the gut and commensal microbiota using organoids co-cultures, from organoid luminal microinjection and inoculation of fragmented organoids, to the generation of polarized 2D organoid cultures that allow for easy apical exposure in hemi-anaerobic systems (Kim et al., 2019; Sasaki et al., 2020). More recently, organoid co-cultures have been applied to CRC-associated bacteria. Mutational signatures were first linked to the genotoxic effect of bacteria, particularly of *pks⁺ E. coli*, through long-term co-culture with healthy

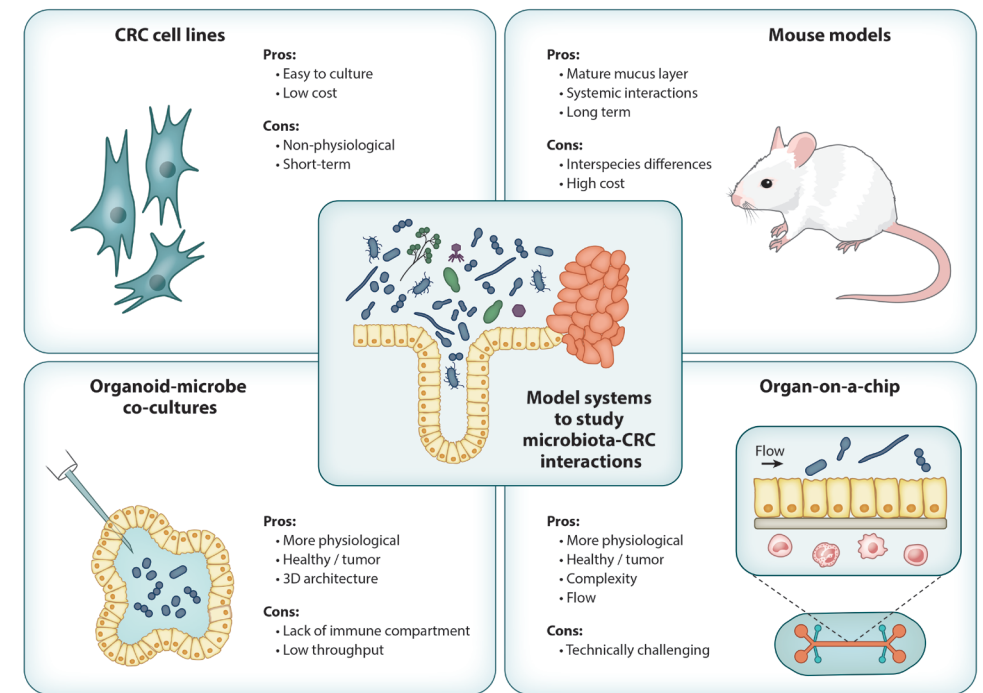


Figure 2. Different models for studying host-microbiota interactions in CRC development. CRC cell lines, mouse models, organoid-microbe cocultures, and organs-on-a-chip.

intestinal organoids (Pleguezuelos-Manzano et al., 2020). Other studies used mouse-derived intestinal organoids to further investigate the mutagenic effect of *pks⁺ E. coli* (Iftexhar et al., 2021), by exposing organoid fragments in suspension to the bacteria for 3h. Furthermore, a recent study explored the effect of an *F. nucleatum*-derived molecule cocktail on healthy colonic organoids grown as 2D monolayers (Engevik et al., 2021). This induces NF- κ B activation, in line with what has been observed before in other CRC models. This suggests that if present in the colon before the onset of CRC, *F. nucleatum* could still induce inflammation and perhaps early steps of CRC tumorigenesis. Finally, murine intestinal organoids have also been used to study the effect of ETBF and BFT on healthy and tumor-derived colon organoids (Liu et al., 2020; Patterson et al., 2020).

Beside organoids, organ-on-a-chip technology holds great promise to model more complex interactions between colorectal cancer and the gut microbiota (Steinway et al., 2020) (Figure 2). The experimental control provided by connection of microfluidic channels and the ability to readily install gradients of growth factors and oxygen make organs-on-chips ideally suited to incorporate colorectal cancer cells, cancer-associated microbial communities and further microenvironmental interaction partners such as vasculature and members of the immune compartment. The past years have seen rapid progress in all of these areas (Bein et al., 2018). While intestine-on-a-chip platforms traditionally rely

on the CRC cell line Caco2, new generations of chips incorporate additional cancer cell lines (Kim et al., 2012; Beurivage et al., 2019; Carvalho et al., 2019), intestinal organoids derived from pluripotent (Workman et al., 2017; Naumovska et al., 2020) or adult stem cells (Nikolaev et al., 2020) and even primary human biopsies (Hinman et al., 2019; Jalili-Firoozinezhad et al., 2019). Microbial communities can be cultured and repeatedly harvested from the lumen over weeks (Jalili-Firoozinezhad et al., 2019, Kim et al., 2016) and assessed for their impact on epithelial barrier integrity, induction of cytokine release and several other features. While the modelling of host-microbe interactions in CRC on organ-on-a-chip platforms is in its infancy, these recent advances set the stage for the rapid expansion of this field.

GUT MICROBIOTA IN CRC FROM A CLINICAL PERSPECTIVE

The intestinal microbiota has been historically regarded as agents that could potentially cause or prevent CRC. Yet, it is becoming clear that the central role of microbiota in CRC has profound implications in many clinical aspects of CRC, from prevention and early diagnosis to treatment. The next section focuses on how the gut microbiota is starting to affect clinical aspects of CRC. The gut microbiota is relevant to many other cancer types or non-cancer diseases which have been reviewed previously (Sepich-Poore et al., 2021).

Intestinal microbiota as a CRC diagnostic tool

Besides the identification of microbial associations with CRC, metagenomic studies have been shown to retrospectively predict the disease status of patients based on fecal microbial markers (Thomas et al., 2019; Wirbel et al., 2019; Yachida et al., 2019). Not only can they discriminate between healthy and CRC, but also between early stages of the disease (Thomas et al., 2019; Yachida et al., 2019). This offers potential to develop non-invasive, clinical diagnostic tests for patient stratification. Recently, the combination of bacterial markers with other parameters like hemoglobin presence in feces was shown to improve the predictive power of such approaches (Young et al., 2021a), which are valid across different geographical and socio-economic populations (Young et al., 2021b). Additionally, recent studies suggest the potential to detect cancer onset based on microbial DNA in blood samples (Poore et al., 2020).

However, all these approaches are based on microbial data collected during or after the onset of the disease. It will be of high interest to elucidate which bacteria are enriched prior to CRC onset. For this, large prospective cohorts can be envisioned, with longitudinal (decades) collection of samples from healthy individuals. During the study, some will be developing the disease, which may identify microbial species that were enriched before the onset of CRC. This will allow implementation of stricter preventive measures and monitoring of individuals at high risk. While these kinds of cohorts already exist, they focus on healthy ageing (Lifelines Cohort: <https://www.lifelines.nl/>) and not particularly on CRC.

Of note, the mutagenic effect of *pks*⁺ *E. coli* has been observed in colonic crypts from healthy individuals (Lee-Six et al., 2019; Pleguezuelos-Manzano et al., 2020), indicating that these bacteria may act before the onset of the disease, most likely very early in life. This example shows that pathogenic effect of the microbiota could occur many years, even decades, before the onset of the disease, increasing the opportunity window to intensify prevention measures for the individuals at risk. Interestingly, the same mutational patterns have been observed in head and neck and uroepithelial tumors (Boot et al., 2020; Pleguezuelos-Manzano et al., 2020), implying that the nocive effect of *pks*⁺ bacteria might expand beyond the gut. Thus, in the case of *pks*⁺ *E. coli*, approaches against the mutagenic effect of colibactin are starting to be envisaged in the lab (Volpe et al., 2019), although their translation to the clinic remains a future goal. This exemplifies how our understanding of bacterially driven CRC mechanisms can promote the development of novel targeted therapies against their pathogenic action.

The gut microbiota in CRC treatment

The gut microbiota can influence the outcome of cancer treatment both in positive and negative directions. During the last decade, it has become evident that immune checkpoint inhibitor treatment response (either positive or negative) is associated with particular microbial communities (Gopalakrishnan et al., 2018; Iida et al., 2013; Routy et al., 2018; Vétizou et al., 2015; Zitvogel et al., 2018). Chemotherapy (Geller et al., 2017; T. Yu et al., 2017) is similarly influenced by the microbiota. *Akkermansia muciniphila* and specific members of *Bacteroidales* can promote a positive response to immune checkpoint inhibitor treatments (Vétizou et al., 2015; Routy et al., 2018). Additionally, a recent study highlights the bacterial metabolite inosine as a key mediator enhancing immune checkpoint inhibitor responsiveness in melanoma (Mager et al., 2020). On the other hand, alterations of the microbiota have also been shown to have negative effects on treatment outcome in diverse cancers (Gopalakrishnan et al., 2018; Routy et al., 2018). Furthermore, a recent study showed that the persistence of *F. nucleatum* in rectal tumors after post-neoadjuvant chemoradiotherapy is strikingly linked to an increased risk of relapse. *F. nucleatum* presence inversely correlated with CD8⁺ infiltration, suggesting the role of the bacteria dampening anti-tumor immune responses allowing tumor relapse (Serna et al., 2020).

There is a long-standing quest to use the gut microbiota to enhance the response to cancer treatment and to modulate its derived side effects, either by using defined probiotics, prebiotics and postbiotics or fecal microbial transplant (FMT) (Helmink et al., 2019; McQuade et al., 2019) (Table 2). However, to date most of these trials aim to reduce the inflammation levels in CRC patients rather than to directly affect the treatment. Preclinical studies in mice have shown the potential of using defined bacterial communities as probiotics to boost CD8⁺ antitumor immune response (Tanoue et al., 2019). Furthermore, bacterial outer membrane vesicles (OMVs) have also been

Table 2. CRC clinical trials using probiotics or fecal microbiota transplantations.

NCT number ^a	Reference	n	Intervention	Outcome	Location	Status
NCT00936572	Gianotti et al., 2010	35	Probiotics: La1, BB536	Bacteria colonization and mucosal inflammation	Italy	Completed
NCT01609660	Consoli et al., 2016	33	Probiotics: <i>Saccharomyces boulardii</i>	Colonic mucosal cytokine gene expression and SCFA levels	Brazil	Completed
NCT03072641	Hibberd et al., 2017	20	Probiotics: ProBion Clinica	Changes in microbiota composition and epigenetics	Sweden	Completed
NCT03782428	Zaharuddin et al., 2019	52	Probiotics: HEXBIO	Post-operative inflammation of CRC patients	Malaysia	Completed
NCT03531606	Park et al., 2020	68	Probiotics: Mechnicov	Markers related to Inflammation, SCFA, Zonulin, other cytokines	South Korea	Completed
NCT04131803		140 ^b	Probiotics: Bifico	Tumor size on patients receiving chemo- and targeted therapy	China	Recruiting
NCT04021589		50 ^b	Probiotics: Weileshu	Progression free survival	China	Recruiting
NCT04729322		15 ^b	Non-autologous FMT	Effect of FMT from anti-PD-1 responders dMMR CRC patients to anti-PD-1 non-responders dMMR CRC	United States	Not yet recruiting

^a<https://clinicaltrials.gov/>.

^bEstimated.

Abbreviations: dMMR, mismatch repair-deficient; FMT, fecal microbiota transfer; NA, not any; SCFA, short-chain fatty acids.

suggested as a potential strategy to induce anti-tumor immunity in CRC mouse models (Kim et al., 2017).

To date, FMT is not used as a common CRC treatment. However, an early phase 1 clinical trial is scheduled to assess the treatment of mismatch repair deficient (dMMR) CRC patients not responding to anti-PD1 treatment with FMT from anti-PD1 responders (NCT04729322; Table 2). If positive, the results will probably serve as a first step to the design of larger and more informative trials. Preclinical studies have shown that anti-PD1 treatment responsiveness can be transferred via FMT from humans to mice (Routy et al., 2018). Beyond CRC, FMT has been recently employed in two trials of melanoma response to anti-PD-1 treatment (Baruch et al., 2021; Davar et al., 2021). Intriguingly, the microbial transfer from long-term immunotherapy responders induced clinical responses in 3/10 and 6/15 patients with anti-PD-1 refractory metastatic melanoma, respectively. The insights derived from these studies, comprising increased CD68⁺ cell infiltration in the gut lamina propria (Baruch et al., 2021) and relationships between species abundance and cytokine profiles (Davar et al., 2021), add substantial insights into the effects of FMT on immunotherapy response in cancer and are set to inspire future approaches in diverse cancer types.

CONCLUSIONS AND FUTURE DIRECTIONS

The development of NGS metagenomics during the last decade is initiating a revolution in our understanding of the microbiota and its association with CRC. Despite these advances, closing the gap between association and causation remains a challenging task in most cases. For some of the bacteria, particularly genotoxic *pkcs*⁺ *Escherichia coli*, *Fusobacterium nucleatum*, and enterotoxigenic *Bacteroides fragilis* there is increasing evidence of the mechanisms by which they elicit CRC tumorigenesis. These range from inducing mutations, reshaping the immune landscape towards pro-inflammatory pro-tumor state to dysregulating key epithelial signaling pathways. However, the active role of most of the CRC-associated bacteria remains elusive. Similarly, some fungi and virus taxa have been associated with CRC, but little is known about their active contribution. Current and future research in the organoid and organ-on-a-chip fields will generate increasingly sophisticated microbial co-cultures models. These will hopefully contribute towards distinguishing microbial species and communities which actively contribute to CRC development from those which play a mere bystander role and bacteria having mixed profiles with regard to the enrichment in and contribution to CRC. Importantly, organoids allow to investigate these questions in healthy tissue and across the different stages of CRC development. Accompanying these efforts by clinical studies on large patient cohorts will be necessary to attribute relevance to these improved mechanistic insights. These should include 1) prospective studies, as mentioned above, that will help disentangling the CRC-associated microbes that are present from pre-cancerous stages onwards and likely play a role in tumor initiation, and 2) cohorts designed based on

new insights obtained from mechanistic *in vitro* and *in vivo* experiments. These could include performing WGS or RNA sequencing on tumor biopsies together with microbial characterization of the samples either by metagenomics or more targeted microbe-specific approaches to link transcriptomic and genomic changes to bacterial effects in patients. Thus, these efforts will lead to a better understanding of the microbial contribution to CRC development and behavior, and will hopefully result in refined approaches that improve CRC prevention as well as the diagnosis, stratification and treatment of CRC patients.

DISCLOSURE STATEMENT

H.C.'s full disclosure is given at <https://www.uu.nl/staff/JCClevers/>.

ACKNOWLEDGEMENTS

This review was supported by CRUK grant OPTIMISTIC (C10674/A27140) (C.P.-M., J.P.), the Gravitation projects CancerGenomiCs.nl, and the Netherlands Organ-on-Chip Initiative (024.003.001) from the Netherlands Organisation for Scientific Research (NWO) funded by the Ministry of Education, Culture and Science of the government of the Netherlands (C.P.-M., J.P.), the OncoCode Institute (partly financed by the Dutch Cancer Society), the European Research Council under ERC Advanced Grant Agreement no. 67013 (J.P., H.C.).

REFERENCES

1. Abed J, Emgård JEM, Zamir G, Faroja M, Almogy G, et al. 2016. Fap2 Mediates *Fusobacterium nucleatum* Colorectal Adenocarcinoma Enrichment by Binding to Tumor-Expressed Gal-GalNAc. *Cell Host & Microbe*. 20(2):215–25
2. Alexandrov LB, Kim J, Haradhvala NJ, Huang MN, Tian Ng AW, et al. 2020. The repertoire of mutational signatures in human cancer. *Nature*. 578(7793):94–101
3. Alexandrov LB, Nik-Zainal S, Wedge DC, Aparicio SAJR, Behjati S, et al. 2013. Signatures of mutational processes in human cancer. *Nature*. 500(7463):415–21
4. Angly F, Rodriguez-Brito B, Bangor D, McNairnie P, Breitbart M, et al. 2005. PHACCS, an online tool for estimating the structure and diversity of uncultured viral communities using metagenomic information. *BMC Bioinformatics*. 6:41
5. Arthur JC, Perez-Chanona E, Mühlbauer M, Tomkovich S, Uronis JM, et al. 2012. Intestinal Inflammation Targets Cancer-Inducing Activity of the Microbiota. *Science*. 338(6103):120–23
6. Aykut B, Pushalkar S, Chen R, Li Q, Abengozar R, et al. 2019. The fungal mycobiome promotes pancreatic oncogenesis via activation of MBL. *Nature*. 574(7777):264–67
7. Aymeric L, Donnadieu F, Mulet C, du Merle L, Nigro G, et al. 2018. Colorectal cancer specific conditions promote *Streptococcus gallolyticus* gut colonization. *Proc Natl Acad Sci U S A*. 115(2):E283–91
8. Basset C, Holton J, Bazeos A, Vaira D, Bloom S. 2004. Are *Helicobacter* Species and Enterotoxigenic *Bacteroides fragilis* Involved in Inflammatory Bowel Disease? *Dig Dis Sci*. 49(9):1425–32
9. Baxter NT, Ruffin MT, Rogers MAM, Schloss PD. 2016. Microbiota-based model improves the sensitivity of fecal immunochemical test for detecting colonic lesions. *Genome Medicine*. 8(1):37
10. Beurivage C, Naumovska E, Chang YX, Elstak ED, Nicolas A, et al. 2019. Development of a Gut-on-a-Chip Model for High Throughput Disease Modeling and Drug Discovery. *Int J Mol Sci*. 20(22):
11. Bein A, Shin W, Jalili-Firoozinezhad S, Park MH, Sontheimer-Phelps A, et al. 2018. Microfluidic Organ-on-a-Chip Models of Human Intestine. *Cell Mol Gastroenterol Hepatol*. 5(4):659–68
12. Boleij A, Hechenbleikner EM, Goodwin AC, Badani R, Stein EM, et al. 2015. The *Bacteroides fragilis* Toxin Gene Is Prevalent in the Colon Mucosa of Colorectal Cancer Patients. *Clinical Infectious Diseases*. 60(2):208–15
13. Borowsky J, Haruki K, Lau MC, Dias Costa A, Väyrynen JP, et al. 2021. Association of *Fusobacterium nucleatum* with Specific T-cell Subsets in the Colorectal Carcinoma Microenvironment. *Clin Cancer Res*. 1078-0432.CCR-20-4009
14. Bossuet-Greif N, Vignard J, Taieb F, Mirey G, Dubois D, et al. 2018. The Colibactin Genotoxin Generates DNA Interstrand Cross-Links in Infected Cells. *MBio*. 9(2):
15. Buc E, Dubois D, Sauvanet P, Raisch J, Delmas J, et al. 2013. High Prevalence of Mucosa-Associated *E. coli* Producing Cyclomodulin and Genotoxin in Colon Cancer. *PLOS ONE*. 8(2):e56964
16. Bullman S, Peadarallu CS, Sicinska E, Clancy TE, Zhang X, et al. 2017. Analysis of *Fusobacterium* persistence and antibiotic response in colorectal cancer. *Science*. 358(6369):1443–48
17. Casasanta MA, Yoo CC, Udayasuryan B, Sanders BE, Umaña A, et al. 2020. *Fusobacterium nucleatum* host-cell binding and invasion induces IL-8 and CXCL1 secretion that drives colorectal cancer cell migration. *Sci. Signal*. 13(641):
18. Castellarin M, Warren RL, Freeman JD, Dreolini L, Krzywinski M, et al. 2012. *Fusobacterium nucleatum* infection is prevalent in human colorectal carcinoma. *Genome Res*. 22(2):299–306
19. Chen H, Chen X-Z, Waterboer T, Castro FA, Brenner H. 2015. Viral infections and colorectal cancer: A systematic review of epidemiological studies. *International Journal of Cancer*. 137(1):12–24
20. Chung L, Orberg ET, Geis AL, Chan JL, Fu K, et al. 2018. *Bacteroides fragilis* Toxin Coordinates a Pro-carcinogenic

- Inflammatory Cascade via Targeting of Colonic Epithelial Cells. *Cell Host & Microbe*. 23(2):203-214.e5
21. Clevers H. 2016. Modeling Development and Disease with Organoids. *Cell*. 165(7):1586-97
 22. Coker OO, Nakatsu G, Dai RZ, Wu WKK, Wong SH, et al. 2019. Enteric fungal microbiota dysbiosis and ecological alterations in colorectal cancer. *Gut*. 68(4):654-62
 23. Consoli MLD, Silva RS da, Nicoli JR, Bruña-Romero O, Silva RG da, et al. 2016. Randomized Clinical Trial. *Journal of Parenteral and Enteral Nutrition*. 40(8):1114-21
 24. Dahlman S, Avellaneda-Franco L, Barr JJ. 2021. Phages to shape the gut microbiota? *Current Opinion in Biotechnology*. 68:89-95
 25. Davar D, Dzutsev AK, McCulloch JA, Rodrigues RR, Chauvin J-M, et al. 2021. Fecal microbiota transplant overcomes resistance to anti-PD-1 therapy in melanoma patients. *Science*. 371(6529):595-602
 26. Dejea CM, Fathi P, Craig JM, Boleij A, Taddese R, et al. 2018. Patients with familial adenomatous polyposis harbor colonic biofilms containing tumorigenic bacteria. *Science*. 359(6375):592-97
 27. Dejea CM, Wick EC, Hechenbleikner EM, White JR, Welch JLM, et al. 2014. Microbiota organization is a distinct feature of proximal colorectal cancers. *PNAS*. 111(51):18321-26
 28. Deng Q, Wang C, Yu K, Wang Y, Yang Q, et al. 2020. *Streptococcus bovis* Contributes to the Development of Colorectal Cancer via Recruiting CD11b+TLR-4+ Cells. *Med Sci Monit*. 26:e921886-1-e921886-9
 29. Dziubańska-Kusibab PJ, Berger H, Battistini F, Bouwman BAM, Iftekhar A, et al. 2020. Colibactin DNA-damage signature indicates mutational impact in colorectal cancer. *Nature Medicine*. 26(7):1063-69
 30. Emler C, Ruffin M, Lamendella R. 2020. Enteric Virome and Carcinogenesis in the Gut. *Dig Dis Sci*. 65(3):852-64
 31. Engevik MA, Danhof HA, Ruan W, Engevik AC, Chang-Graham AL, et al. 2021. *Fusobacterium nucleatum* Secretes Outer Membrane Vesicles and Promotes Intestinal Inflammation. *mBio*. 12(2):
 32. Fu T, Coulter S, Yoshihara E, Oh TG, Fang S, et al. 2019. FXR Regulates Intestinal Cancer Stem Cell Proliferation. *Cell*. 176(5):1098-1112.e18
 33. Gao R, Kong C, Li H, Huang L, Qu X, et al. 2017. Dysbiosis signature of microbiota in colon polyp and colorectal cancer. *Eur J Clin Microbiol Infect Dis*. 36(12):2457-68
 34. Geller LT, Barzily-Rokni M, Danino T, Jonas OH, Shental N, et al. 2017. Potential role of intratumor bacteria in mediating tumor resistance to the chemotherapeutic drug gemcitabine. *Science*. 357(6356):1156-60
 35. Gianotti L, Morelli L, Galbiati F, Rocchetti S, Coppola S, et al. 2010. A randomized double-blind trial on perioperative administration of probiotics in colorectal cancer patients. *World J Gastroenterol*. 16(2):167-75
 36. Gogokhia L, Buhrke K, Bell R, Hoffman B, Brown DG, et al. 2019. Expansion of Bacteriophages Is Linked to Aggravated Intestinal Inflammation and Colitis. *Cell Host & Microbe*. 25(2):285-299.e8
 37. Gopalakrishnan V, Spencer CN, Nezi L, Reuben A, Andrews MC, et al. 2018. Gut microbiome modulates response to anti-PD-1 immunotherapy in melanoma patients. *Science*. 359(6371):97-103
 38. Gur C, Ibrahim Y, Isaacson B, Yamin R, Abed J, et al. 2015. Binding of the Fap2 Protein of *Fusobacterium nucleatum* to Human Inhibitory Receptor TIGIT Protects Tumors from Immune Cell Attack. *Immunity*. 42(2):344-55
 39. Hallen-Adams HE, Suhr MJ. 2017. Fungi in the healthy human gastrointestinal tract. *Virulence*. 8(3):352-58
 40. Hamada T, Zhang X, Mima K, Bullman S, Sukawa Y, et al. 2018. *Fusobacterium nucleatum* in Colorectal Cancer Relates to Immune Response Differentially by Tumor Microsatellite Instability Status. *Cancer Immunol Res*. 6(11):1327-36
 41. Hannigan GD, Duhaime MB, Ruffin MT, Koumpouras CC, Schloss PD. 2018. Diagnostic Potential and Interactive Dynamics of the Colorectal Cancer Virome. *mBio*. 9(6):
 42. Hausen H zur. 2012. Red meat consumption and cancer: Reasons to suspect involvement of bovine infectious factors in colorectal cancer. *International Journal of Cancer*. 130(11):2475-83
 43. Helmkink BA, Khan MAW, Hermann A, Gopalakrishnan V, Wargo JA. 2019. The microbiome, cancer, and cancer therapy. *Nature Medicine*. 25(3):377-88
 44. Hibberd AA, Lyra A, Ouwehand AC, Rolny P, Lindgren H, et al. 2017. Intestinal microbiota is altered in patients with colon cancer and modified by probiotic intervention. *BMJ Open Gastroenterology*. 4(1):e000145
 45. Hinman SS, Wang Y, Allbritton NL. 2019. Photopatterned Membranes and Chemical Gradients Enable Scalable Phenotypic Organization of Primary Human Colon Epithelial Models. *Anal Chem*. 91(23):15240-47
 46. Hong B, Ideta T, Lemos BS, Igarashi Y, Tan Y, et al. 2019. Characterization of Mucosal Dysbiosis of Early Colonic Neoplasia. *npj Precision Oncology*. 3(1):1-10
 47. Iftekhar A, Berger H, Bouznad N, Heuberger J, Boccellato F, et al. 2021. Genomic aberrations after short-term exposure to colibactin-producing *E. coli* transform primary colon epithelial cells. *Nature Communications*. 12(1):1003
 48. Iida N, Dzutsev A, Stewart CA, Smith L, Bouladoux N, et al. 2013. Commensal Bacteria Control Cancer Response to Therapy by Modulating the Tumor Microenvironment. *Science*. 342(6161):967-70
 49. Jain U, Heul AMV, Xiong S, Gregory MH, Demers EG, et al. 2021. *Debaryomyces* is enriched in Crohn's disease intestinal tissue and impairs healing in mice. *Science*. 371(6534):1154-59
 50. Jalili-Firoozinezhad S, Gazzaniga FS, Calamari EL, Camacho DM, Fadel CW, et al. 2019. A complex human gut microbiome cultured in an anaerobic intestine-on-a-chip. *Nat Biomed Eng*. 3(7):520-31
 51. Kim HJ, Li H, Collins JJ, Ingber DE. 2016. Contributions of microbiome and mechanical deformation to intestinal bacterial overgrowth and inflammation in a human gut-on-a-chip. *Proc Natl Acad Sci U S A*. 113(1):E7-15
 52. Kim OY, Park HT, Dinh NTH, Choi SJ, Lee J, et al. 2017. Bacterial outer membrane vesicles suppress tumor by interferon- γ -mediated antitumor response. *Nature Communications*. 8(1):626
 53. Kim R, Attayek PJ, Wang Y, Furtado KL, Tamayo R, et al. 2019. An in vitro intestinal platform with a self-sustaining oxygen gradient to study the human gut/microbiome interface. *Biofabrication*. 12(1):015006
 54. Kostic AD, Chun E, Robertson L, Glickman JN, Gallini CA, et al. 2013. *Fusobacterium nucleatum* Potentiates Intestinal Tumorigenesis and Modulates the Tumor-Immune Microenvironment. *Cell Host & Microbe*. 14(2):207-15
 55. Kostic AD, Gevers D, Pedamallu CS, Michaud M, Duke F, et al. 2012. Genomic analysis identifies association of *Fusobacterium* with colorectal carcinoma. *Genome Res*. 22(2):292-98
 56. Kumar R, Herold JL, Schady D, Davis J, Kopetz S, et al. 2017. *Streptococcus gallolyticus* subsp. *gallolyticus* promotes colorectal tumor development. *PLOS Pathogens*. 13(7):e1006440
 57. Lee-Six H, Olafsson S, Ellis P, Osborne RJ, Sanders MA, et al. 2019. The landscape of somatic mutation in normal colorectal epithelial cells. *Nature*. 574(7779):532-37
 58. Li Z-R, Li J, Cai W, Lai JYH, McKinnie SMK, et al. 2019. Macrocyclic colibactin induces DNA double-strand breaks via copper-mediated oxidative cleavage. *Nat Chem*. 11(10):880-89
 59. Mager LF, Burkhard R, Pett N, Cooke NCA, Brown K, et al. 2020. Microbiome-derived inosine modulates response to checkpoint inhibitor immunotherapy. *Science*. 369(6510):1481-89
 60. Martel C de, Georges D, Bray F, Ferlay J, Clifford GM. 2020. Global burden of cancer attributable to infections in 2018: a worldwide incidence analysis. *The Lancet Global Health*. 8(2):e180-90
 61. Massimino L, Lovisa S, Antonio Lamparelli L, Danese S, Ungaro F. 2021. Gut eukaryotic virome in colorectal carcinogenesis: Is that a trigger? *Computational and Structural Biotechnology Journal*. 19:16-28
 62. McCauley HA, Wells JM. 2017. Pluripotent stem cell-derived organoids: using principles of developmental biology to grow human tissues in a dish. *Development*. 144(6):958-62
 63. McQuade JL, Daniel CR, Helmkink BA, Wargo JA. 2019. Modulating

- the microbiome to improve therapeutic response in cancer. *The Lancet Oncology*. 20(2):e77–91
64. Mima K, Nishihara R, Qian ZR, Cao Y, Sukawa Y, et al. 2016. *Fusobacterium nucleatum* in colorectal carcinoma tissue and patient prognosis. *Gut*. 65(12):1973–80
 65. Mima K, Sukawa Y, Nishihara R, Qian ZR, Yamauchi M, et al. 2015. *Fusobacterium nucleatum* and T Cells in Colorectal Carcinoma. *JAMA Oncol*. 1(5):653
 66. Mu W, Jia Y, Chen X, Li H, Wang Z, Cheng B. 2020. Intracellular *Porphyromonas gingivalis* Promotes the Proliferation of Colorectal Cancer Cells via the MAPK/ERK Signaling Pathway. *Front. Cell. Infect. Microbiol*. 10:
 67. Múnera JO, Sundaram N, Rankin SA, Hill D, Watson C, et al. 2017. Differentiation of Human Pluripotent Stem Cells into Colonic Organoids via Transient Activation of BMP Signaling. *Cell Stem Cell*. 21(1):51–64.e6
 68. Nakatsu G, Li X, Zhou H, Sheng J, Wong SH, et al. 2015. Gut mucosal microbiome across stages of colorectal carcinogenesis. *Nature Communications*. 6(1):8727
 69. Nakatsu G, Zhou H, Wu WKK, Wong SH, Coker OO, et al. 2018. Alterations in Enteric Virome Are Associated With Colorectal Cancer and Survival Outcomes. *Gastroenterology*. 155(2):529–541.e5
 70. Naumovska E, Aalderink G, Wong Valencia C, Kosim K, Nicolas A, et al. 2020. Direct On-Chip Differentiation of Intestinal Tubules from Induced Pluripotent Stem Cells. *Int J Mol Sci*. 21(14):
 71. Nikolaev M, Mitrofanova O, Broguiere N, Geraldo S, Dutta D, et al. 2020. Homeostatic mini-intestines through scaffold-guided organoid morphogenesis. *Nature*. 585(7826):574–78
 72. Norman JM, Handley SA, Baldrige MT, Droit L, Liu CY, et al. 2015. Disease-Specific Alterations in the Enteric Virome in Inflammatory Bowel Disease. *Cell*. 160(3):447–60
 73. Nougayrède J-P, Homburg S, Taieb F, Boury M, Brzuszkiewicz E, et al. 2006. *Escherichia coli* induces DNA double-strand breaks in eukaryotic cells. *Science*. 313(5788):848–51
 74. Park IJ, Lee J-H, Kye B-H, Oh H-K, Cho YB, et al. 2020. Effects of Probiotics on the Symptoms and Surgical Outcomes after Anterior Resection of Colon Cancer (POSTCARE): A Randomized, Double-Blind, Placebo-Controlled Trial. *Journal of Clinical Medicine*. 9(7):2181
 75. Patterson L, Allen J, Posey I, Shaw JJP, Costa-Pinheiro P, et al. 2020. Glucosylceramide production maintains colon integrity in response to *Bacteroides fragilis* toxin-induced colon epithelial cell signaling. *The FASEB Journal*. 34(12):15922–45
 76. Pleguezuelos-Manzano C, Puschhof J, Rosendahl Huber A, van Hoeck A, Wood HM, et al. 2020. Mutational signature in colorectal cancer caused by genotoxic pks + *E. coli*. *Nature*. 580(7802):269–73
 77. Poore GD, Kopylova E, Zhu Q, Carpenter C, Fraccacio S, et al. 2020. Microbiome analyses of blood and tissues suggest cancer diagnostic approach. *Nature*. 579(7800):567–74
 78. Prindiville TP, Sheikh RA, Cohen SH, Tang YJ, Cantrell MC, Silva J. 2000. *Bacteroides fragilis* enterotoxin gene sequences in patients with inflammatory bowel disease. *Emerg Infect Dis*. 6(2):171–74
 79. Reyes A, Haynes M, Hanson N, Angly FE, Heath AC, et al. 2010. Viruses in the faecal microbiota of monozygotic twins and their mothers. *Nature*. 466(7304):334–38
 80. Richard ML, Liguori G, Lamas B, Brandi G, Costa G da, et al. 2018. Mucosa-associated microbiota dysbiosis in colitis associated cancer. *Gut Microbes*. 9(2):131–42
 81. Richard ML, Sokol H. 2019. The gut mycobiota: insights into analysis, environmental interactions and role in gastrointestinal diseases. *Nature Reviews Gastroenterology & Hepatology*. 16(6):331–45
 82. Routy B, Chatelier EL, Derosa L, Duong CPM, Alou MT, et al. 2018. Gut microbiome influences efficacy of PD-1-based immunotherapy against epithelial tumors. *Science*. 359(6371):91–97
 83. Rubinstein MR, Wang X, Liu W, Hao Y, Cai G, Han YW. 2013. *Fusobacterium nucleatum* Promotes Colorectal Carcinogenesis by Modulating E-Cadherin/ β -Catenin Signaling via its FadA Adhesin. *Cell Host & Microbe*. 14(2):195–206
 84. Sack RB, Albert MJ, Alam K, Neogi PK, Akbar MS. 1994. Isolation of enterotoxigenic *Bacteroides fragilis* from Bangladeshi children with diarrhea: a controlled study. *Journal of Clinical Microbiology*. 32(4):960–63
 85. Sasaki N, Miyamoto K, Maslowski KM, Ohno H, Kanai T, Sato T. 2020. Development of a Scalable Coculture System for Gut Anaerobes and Human Colon Epithelium. *Gastroenterology*. 159(1):388–390.e5
 86. Sato T, Stange DE, Ferrante M, Vries RGJ, Es JH van, et al. 2011. Long-term Expansion of Epithelial Organoids From Human Colon, Adenoma, Adenocarcinoma, and Barrett's Epithelium. *Gastroenterology*. 141(5):1762–72
 87. Sato T, Vries RG, Snippert HJ, van de Wetering M, Barker N, et al. 2009. Single Lgr5 stem cells build crypt-villus structures in vitro without a mesenchymal niche. *Nature*. 459(7244):262–65
 88. Sears CL, Geis AL, Housseau F. 2014. *Bacteroides fragilis* subverts mucosal biology: from symbiont to colon carcinogenesis. *J Clin Invest*. 124(10):4166–72
 89. Sears CL, Islam S, Saha A, Arjumand M, Alam NH, et al. 2008. Association of Enterotoxigenic *Bacteroides fragilis* Infection with Inflammatory Diarrhea. *Clinical Infectious Diseases*. 47(6):797–803
 90. Sepich-Poore GD, Zitvogel L, Straussman R, Hasty J, Wargo JA, Knight R. 2021. The microbiome and human cancer. *Science*. 371(6536):eabc4552
 91. Serna G, Ruiz-Pace F, Hernando J, Alonso L, Fasani R, et al. 2020. *Fusobacterium nucleatum* persistence and risk of recurrence after preoperative treatment in locally advanced rectal cancer. *Annals of Oncology*. 31(10):1366–75
 92. Shkoporov AN, Clooney AG, Sutton TDS, Ryan FJ, Daly KM, et al. 2019. The Human Gut Virome Is Highly Diverse, Stable, and Individual Specific. *Cell Host & Microbe*. 26(4):527–541.e5
 93. Spence JR, Mayhew CN, Rankin SA, Kuhar MF, Vallance JE, et al. 2011. Directed differentiation of human pluripotent stem cells into intestinal tissue in vitro. *Nature*. 470(7332):105–9
 94. Steinway SN, Saleh J, Koo B-K, Delacour D, Kim D-H. 2020. Human Microphysiological Models of Intestinal Tissue and Gut Microbiome. *Front. Bioeng. Biotechnol*. 8:
 95. Sung H, Ferlay J, Siegel RL, Laversanne M, Soerjomataram I, et al. 2021. Global Cancer Statistics 2020: GLOBOCAN Estimates of Incidence and Mortality Worldwide for 36 Cancers in 185 Countries. *CA Cancer J Clin*. 71(3):209–49
 96. Tanoue T, Morita S, Plichta DR, Skelly AN, Suda W, et al. 2019. A defined commensal consortium elicits CD8 T cells and anti-cancer immunity. *Nature*. 565(7741):600–605
 97. Thiele Orberg E, Fan H, Tam AJ, Dejea CM, Destefano Shields CE, et al. 2017. The myeloid immune signature of enterotoxigenic *Bacteroides fragilis*-induced murine colon tumorigenesis. *Mucosal Immunology*. 10(2):421–33
 98. Thomas AM, Manghi P, Asnicar F, Pasolli E, Armanini F, et al. 2019. Metagenomic analysis of colorectal cancer datasets identifies cross-cohort microbial diagnostic signatures and a link with choline degradation. *Nature Medicine*. 25(4):667–78
 99. Turkington CJR, Varadan AC, Grenier SF, Grasis JA. 2021. The Viral Janus: Viruses as Aetiological Agents and Treatment Options in Colorectal Cancer. *Frontiers in Cellular and Infection Microbiology*. 10:
 100. Vaga S, Lee S, Ji B, Andreasson A, Talley NJ, et al. 2020. Compositional and functional differences of the mucosal microbiota along the intestine of healthy individuals. *Scientific Reports*. 10(1):14977
 101. Veglia F, Perego M, Gabrilovich D. 2018. Myeloid-derived suppressor cells coming of age. *Nature Immunology*. 19(2):108–19
 102. Vétizou M, Pitt JM, Daillère R, Lepage P, Waldschmitt N, et al. 2015. Anticancer immunotherapy by CTLA-4 blockade relies on the gut microbiota. *Science*. 350(6264):1079–84
 103. Virgin HW. 2014. The Virome in Mammalian Physiology and Disease. *Cell*. 157(1):142–50
 104. Virgin HW, Wherry EJ, Ahmed R. 2009. Redefining Chronic Viral Infection. *Cell*. 138(1):30–50
 105. Volpe MR, Wilson MR, Brotherton CA, Winter ES, Johnson SE, Balskus EP. 2019. In Vitro Characterization of the Colibactin-Activating Peptidase ClbP Enables Design

- of a Fluorogenic Activity Probe. *ACS Chem Biol.* 14(9):2095
106. White MK, Pagano JS, Khalili K. 2014. Viruses and Human Cancers: a Long Road of Discovery of Molecular Paradigms. *Clinical Microbiology Reviews.* 27(3):463–81
 107. Wilson MR, Jiang Y, Villalta PW, Stornetta A, Boudreau PD, et al. 2019. The human gut bacterial genotoxin colibactin alkylates DNA. *Science.* 363(6428):eaar7785
 108. Wirbel J, Pyl PT, Kartal E, Zych K, Kashani A, et al. 2019. Meta-analysis of fecal metagenomes reveals global microbial signatures that are specific for colorectal cancer. *Nature Medicine.* 25(4):679
 109. Workman MJ, Gleeson JP, Troisi EJ, Estrada HQ, Kerns SJ, et al. 2017. Enhanced Utilization of Induced Pluripotent Stem Cell-Derived Human Intestinal Organoids Using Microengineered Chips. *Cell Mol Gastroenterol Hepatol.* 5(4):669-677.e2
 110. Wu S, Rhee K-J, Albesiano E, Rabizadeh S, Wu X, et al. 2009. A human colonic commensal promotes colon tumorigenesis via activation of T helper type 17 T cell responses. *Nature Medicine.* 15(9):1016–22
 111. Wu S, Rhee K-J, Zhang M, Franco A, Sears CL. 2007. *Bacteroides fragilis* toxin stimulates intestinal epithelial cell shedding and γ -secretase-dependent E-cadherin cleavage. *Journal of Cell Science.* 120(11):1944–52
 112. Xue M, Kim CS, Healy AR, Wernke KM, Wang Z, et al. 2019. Structure elucidation of colibactin and its DNA cross-links. *Science.* 365(6457):eaax2685
 113. Yachida S, Mizutani S, Shiroma H, Shiba S, Nakajima T, et al. 2019. Metagenomic and metabolomic analyses reveal distinct stage-specific phenotypes of the gut microbiota in colorectal cancer. *Nature Medicine.* 25(6):968–76
 114. Yan Y, Drew DA, Markowitz A, Lloyd-Price J, Abu-Ali G, et al. 2020. Structure of the Mucosal and Stool Microbiome in Lynch Syndrome. *Cell Host & Microbe.* 27(4):585-600.e4
 115. Yang Y, Weng W, Peng J, Hong L, Yang L, et al. 2017. *Fusobacterium nucleatum* Increases Proliferation of Colorectal Cancer Cells and Tumor Development in Mice by Activating Toll-Like Receptor 4 Signaling to Nuclear Factor- κ B, and Up-regulating Expression of MicroRNA-21. *Gastroenterology.* 152(4):851-866.e24
 116. Yoshimoto S, Loo TM, Atarashi K, Kanda H, Sato S, et al. 2013. Obesity-induced gut microbial metabolite promotes liver cancer through senescence secretome. *Nature.* 499(7456):97–101
 117. Young C, Wood HM, Fuentes Balaguer A, Bottomley D, Gallop N, et al. 2021a. Microbiome Analysis of More Than 2,000 NHS Bowel Cancer Screening Programme Samples Shows the Potential to Improve Screening Accuracy. *Clin Cancer Res.* 1078-0432.CCR-20–3807
 118. Young C, Wood HM, Seshadri RA, Van Nang P, Vaccaro C, et al. 2021b. The colorectal cancer-associated faecal microbiome of developing countries resembles that of developed countries. *Genome Med.* 13:
 119. Yu C, Zhou B, Xia X, Chen S, Deng Y, et al. 2019. *Prevotella copri* is associated with carboplatin-induced gut toxicity. *Cell Death Dis.* 10(10):
 120. Yu J, Feng Q, Wong SH, Zhang D, Liang Q yi, et al. 2017. Metagenomic analysis of faecal microbiome as a tool towards targeted non-invasive biomarkers for colorectal cancer. *Gut.* 66(1):70–78
 121. Zhu Y, Shi T, Lu X, Xu Z, Qu J, et al. 2021. Fungal-induced glycolysis in macrophages promotes colon cancer by enhancing innate lymphoid cell secretion of IL-22. *The EMBO Journal.* n/a(n/a):e105320
 122. Zitvogel L, Ma Y, Raoult D, Kroemer G, Gajewski TF. 2018. The microbiome in cancer immunotherapy: Diagnostic tools and therapeutic strategies. *Science.* 359(6382):1366–70

2

ORGANOIDS AND ORGANS-ON-CHIP: INSIGHTS INTO HUMAN GUT-MICROBE INTERACTIONS

Jens Puschhof^{1,2,*}, Cayetano Pleguezuelos-Manzano^{1,2,*}, Hans Clevers^{1,2}

¹Hubrecht Institute, Royal Netherlands Academy of Arts and Sciences (KNAW) and UMC Utrecht, 3584 CT Utrecht, the Netherlands. ²Oncode Institute, Hubrecht Institute, 3584 CT Utrecht, the Netherlands

* equal contribution

ABSTRACT

The important and diverse roles of the gut microbiota in human health and disease are increasingly recognized. The difficulty of inferring causation from metagenomic microbiome sequencing studies and from mouse-human interspecies differences have prompted the development of sophisticated *in vitro* models of human gut-microbe interactions. Here we review recent advances in the co-culture of microbes with intestinal and colonic epithelium, comparing the rapidly developing fields of organoids and organs-on-a-chip with other standard models. We describe how specific individual processes by which microbes and epithelia interact can be recapitulated *in vitro*. Using examples of bacterial, viral and parasitic infections, we highlight the advantages of each culture model and discuss current trends and future possibilities to build more complex co-cultures.

INTRODUCTION

The human intestinal tract is inhabited by a multitude of microorganisms, collectively referred to as the gut microbiota. This diverse community of bacteria, fungi, protozoans, viruses and bacteriophages is essential to maintaining healthy gut physiology. Infection with pathogenic species like *Clostridium difficile* or norovirus, as well as gut microbiota imbalances have been linked to a variety of disease conditions, ranging from infectious diseases to complex chronic diseases like inflammatory bowel disease, metabolic syndrome and colorectal cancer.

The advent of sophisticated sequencing technologies has enabled detailed metagenomic studies on the gut microbiome (referring to the genetic information of the gut microbiota) in health and disease. The resulting datasets reveal numerous associations between individual microbial species or communities and specific diseases. However, moving from association to causation through mechanistic insights represents a major challenge due to the complexity of these relationships and the limitations of 'holistic' model systems for human gut-microbe interactions. Mouse models remain the gold standard for modelling and studying mammalian host-microbe interactions at high complexity. Nevertheless, these models have substantial drawbacks with regard to experimental control, scalability and recapitulation of human intestinal interactions with its host-specific commensals and pathogens (Ettayebi et al., 2016; Lamers et al., 2020; Walter et al., 2020). These factors have called into question how human-microbe interactions can be transferred to mouse models (Walter et al., 2020). In recent years, a number of more reductionist *in vitro* approaches have been developed that represent an opportunity for closing the gap between microbial association with disease and mechanistic insight. Human tissue-derived organoids (Kim et al., 2020) and organs-on-chips (Bein et al., 2018) allow clonal expansion (Blokzijl et al., 2016), genetic engineering (Fujii et al., 2015) and modelling of human-specific processes (Yin et al., 2015).

In this review, we introduce intestinal organoids and organ-on-chip platforms and describe how they have been used in the study of host-microbiota interactions (Fig 1). We systematically discuss which aspects of the microbiota and the human intestinal epithelium can be modeled using these new platforms. We compare the two approaches with each other and to related models such as colorectal cancer cell lines and organotypic explant cultures, for which we only discuss individual studies to showcase key differences. An evaluation of each model's suitability for recapitulating the individual interaction processes is provided in Table 1. In the final section, we highlight which features of this complex interplay remain difficult to assess *in vitro* and how future developments may yield more sophisticated co-culture systems.

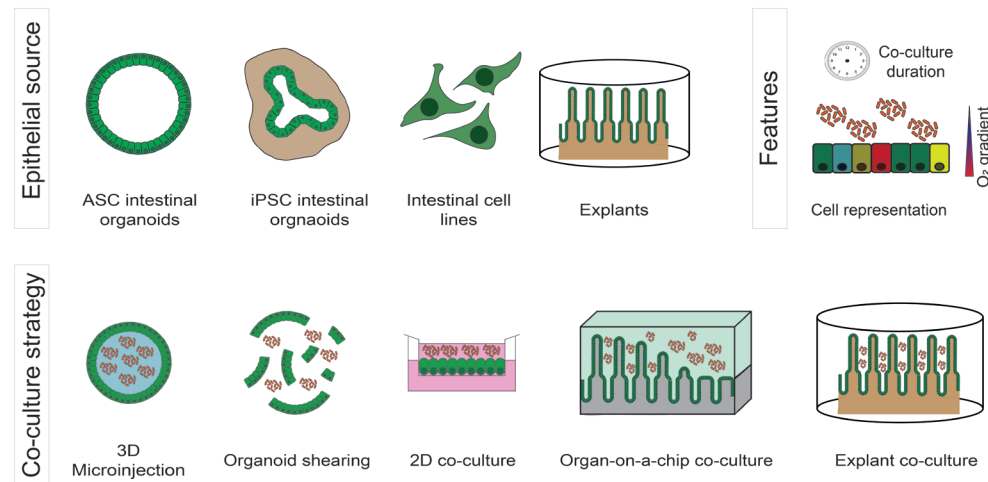


Figure 1. Gut epithelium co-culture models. Top Left: Overview of sources for intestinal epithelial cells. Organoids can be derived from both adult stem cells (ASC) and pluripotent stem cells (PSC). Cancer-derived cell lines and organotypic explants represent alternative sources of epithelial cells. Top Right: Main features of *in vitro* co-culture models. Representation of cell types, generation of an oxygen gradient from epithelium to lumen and co-culture duration are depicted. Bottom: Co-culture strategies for the different models. Microbes can be microinjected into organoids, added during shearing of them or added to organoids, cell lines or explants grown in monolayers. Intestines-on-chip provide an apical chamber for microbe exposure.

THE MODEL SYSTEMS

Cancer cell lines

Since their advent in the 1950s, cell lines derived from tumors and grown as monolayers have become a central workhorse of biomedical research. Their robust growth, often indefinite expansion capacity, ease of use and favorable cost profile have facilitated their wide use to this day. A panoply of colorectal cancer-derived cell lines allow the recapitulation of diverse features of this disease (Wilding and Bodmer, 2014). Caco-2 is the most frequently used cell line for modelling healthy intestinal interactions, as it shares some features with small intestinal enterocytes despite being derived from a colon carcinoma (Sambuy et al., 2005).

Yet, cell lines possess substantial drawbacks. Their transformed character and genomic instability, growth in an unphysiological architecture and failure to recapitulate the cellular heterogeneity of the original organ limit the research questions they can address when co-cultured with microbes. Nevertheless, co-cultures of colorectal cancer cell lines with microbes in monolayer cultures (or more recently in intestine-on-chip formats) recapitulate some aspects of their interactions.

Adult stem cell-derived organoids

Organoids of the human small intestine and colon have recently emerged as tools to study human gut physiology *in vitro* (Sato et al., 2011). Starting from adult stem cells (ASCs), which are located at the bottom of the intestinal crypts, healthy and cancerous intestinal epithelium can be grown in a gelatinous mixture of basement membrane extract (BME, also known as Matrigel®). These reductionist models allow unlimited propagation of all intestinal epithelial cell types in a self-assembling 3D architecture resembling their *in vivo* organization and compositional characteristics of the gut region from which they are derived (Beumer et al., 2020; Kayisoglu et al., 2020).

Human intestinal organoids consist of a polarized monolayer epithelium with a fluid-filled central space representing the original organ's lumen. Because of this, 3D intestinal organoids require microinjection of bacteria into their lumen for an accurate representation of their *in vivo* spatial relationship (Bartfeld, 2016; Heo et al., 2018). As an alternative to microinjections, organoids can be replated as 2D monolayers on transwell plates as used for stomach (Boccellato et al., 2019) and colon (Sasaki et al., 2020) organoids to enable co-cultures including a more mature mucus layer. Different exposure routes have also been used for viral co-cultures, including 2D layers (Ettayebi et al., 2016) and sheared 3D organoids (Fakhiri et al., 2019).

Pluripotent stem cell-derived organoids

Similarly to adult stem cells, pluripotent stem cells (PSCs) can give rise to organoids. Starting from either embryonic stem cells (ESCs) or induced pluripotent stem cells (iPSCs), the differentiation towards a specific organ type is recapitulated over a time frame of weeks to months by sequential exposure to external growth factors guiding tissue-specific developmental routes (Spence et al., 2011). The resulting product is, in contrast to ASC-derived organoids, not limited to intestinal epithelial cell types but can also contain mesenchymal cells. Once the intended organ specification is achieved, the organoids can be expanded further under the conditions defined for ASC-derived intestinal organoids. As for ASC-based organoids, the main co-culture method to date has been microinjection of microbes into the lumen of iPSC-based organoids (Forbester et al., 2015; Holokai et al., 2019).

Organs-on-chip

The term "organ-on-a-chip" describes a microfluidic device containing the cell types of interest in close recapitulation of the original tissue structure, function and physiology (Bein et al., 2018). In comparison with organoids, intestine-on-a-chip platforms offer greater experimental control through multiple connected microfluidic channels. Most intestine-chips today rely on hollow channels with a smooth surface, while recent approaches enable the generation of crypt-villus-like structures through the induction of flow (Kim et al., 2016a) or using a scaffold surface (Nikolaev et al., 2020). The cell

types used to populate chip devices are diverse, ranging from immortalized cell lines (Beaurivage et al., 2019; Kim et al., 2012) to primary tissue (Hinman et al., 2019; Jalili-Firoozinezhad et al., 2019), PSC-derived intestinal organoid cells (Naumovska et al., 2020; Workman et al., 2017) or adult stem cell-derived organoids (Nikolaev et al., 2020). Intestines-on-a-chip can be flushed with liquids to alter luminal versus basal conditions, or to create gradients of growth factors or oxygen (Kim et al., 2019; Shah et al., 2016) allowing to recapitulate the spatial cell type compartmentalization that is typical of the crypt architecture (Hinman et al., 2019). This mediates fine-tuning of the culture environment for bacteria in the intestinal lumen and allows repeated exposure to - and harvesting of - microbes (Grassart et al., 2019; Jalili-Firoozinezhad et al., 2019; Shah et al., 2016). Furthermore, features such as luminal flow and even peristalsis can be incorporated as another advantage of intestines-on-a-chip over static organoids (Kim et al., 2012).

Organotypic explant cultures

Whereas the previously mentioned culture systems are based on recreating the intestinal tissue architecture *in vitro*, organotypic explant cultures rely on transferring intact pieces of the intestinal mucosa to an *ex vivo* culture system. These systems, first described in the 1960s, recapitulate the mucosal architecture, including stromal cells and a mucus layer (Gustafsson et al., 2012). Explants are cultured in medium which does not support the expansion of intestinal stem cells and suffer from decay of the structures within days of culturing. Consequently, they are not suited for longer-term studies or for applications where genetic engineering of tissue components is required. Colonic explant cultures have proven useful for viral diseases such as HIV, where the presence of CD4+ T-cells has enabled infection modelling (Fletcher et al., 2006). As explant models normally retain part of their microbiota, the addition of further bacterial species for defined co-cultures is not routinely performed. However, a protocol for eradicating the endogenous microbiota and repopulating human colonic explants with a donor microbial suspension has been recently described (Sarrabayrouse et al., 2020).

MODEL FEATURES

These *in vitro* models differ in how accurately they can recapitulate crucial features for representative co-culture. Below, we compare their ability to assess distinct host features.

Oxygen gradient

The intestinal vascular network ensures ample oxygen supply for the epithelial cells, but the levels of oxygen steeply drop over one cell-diameter towards the intestinal lumen, reaching a PO₂ below 10 mmHg (Zheng et al., 2015). Most gut microbes inhabit the central gut lumen and are excluded from the mucus layer that covers the villus epithelium, in line with their requirement of low-oxygen conditions. A major hurdle for *in vitro* systems is the recapitulation of this oxygen gradient, providing sufficient oxygen for

epithelial cells to survive while also creating a compartment with low oxygen as required for most intestinal bacterial species.

Classical 2D cultures exhibit homogeneous oxygen levels, allowing merely short-term co-cultures with most gut dwelling bacteria (Rubinstein et al., 2013). Recently, two groups developed co-culture systems with an integrated oxygen gradient as a solution to this challenge (Kim et al., 2019; Sasaki et al., 2020): Human colon organoids can be grown as a monolayer on a transwell insert which is subsequently flushed with an anaerobic gas mix and sealed with a rubber plug. These approaches provide sufficient oxygen supply for epithelial cells from the basolateral medium reservoir while allowing the culture of anaerobic species in the hypoxic apical chamber (Sasaki et al., 2020). 3D organoids can exhibit an oxygen gradient (DiMarco et al., 2014) and in our experience, most anaerobic bacterial species can survive in the hypoxic lumen of human intestinal organoids for up to a week. The precise levels of oxygen within organoids are not known. Novel approaches such as phosphorescent oxygen sensors may facilitate more detailed studies on the microbial niche within organoids in the future (Okkelman et al., 2019). Intestines-on-a-chip represent the most controlled and scalable solution to create this oxygen gradient *in vitro* (Jalili-Firoozinezhad et al., 2019; Marzorati et al., 2014). In a recently developed model, perfusable channels coupled to oxygen sensors offer opportunities to fine-tune oxygen levels at the basolateral and apical side of the epithelial layer and enable extended co-cultures under controlled conditions (Jalili-Firoozinezhad et al., 2019).

Duration of co-culture

The gut microbiota colonizes the intestinal tract from birth and forms a stable mutualistic relationship in the healthy state. Several chronic disease states are linked with a lasting change in microbial composition. Most epithelial co-cultures are performed on a time scale of hours to days and do not model such chronic states well.

Bacterial invasion studies in 2D cell lines are typically performed over a timeframe of hours (Rubinstein et al., 2013). The closed lumen of 3D organoids enables the stable co-culture of most intestinal microbes without bacterial death or overgrowth, but the intrinsic need for organoids to be passaged every 7-14 days prohibits any stable co-culture beyond this time frame. Nevertheless, we have recently demonstrated the feasibility of repeatedly injecting organoids with a single bacterial species over a timeframe of 5 months with mutation accumulation in the epithelial cells as a long-term readout (Pleguezuelos-Manzano et al., 2020). As an alternative, 2D gastric cultures have been shown to allow co-culture of *Helicobacter pylori* for weeks (Boccellato et al., 2019), an approach that should also work for small intestinal and colon organoids. Intestine-on-a-chip systems have enabled co-cultures of complex bacterial communities (Jalili-Firoozinezhad et al., 2019) and individual species (Kim et al., 2016a) for time frames of days to weeks, respectively. The newest generation of intestines-on-a-chip may enable month-long co-cultures on hollow tubes faithfully recapitulating the intestinal cell type composition

(Nikolaev et al., 2020), but the potential of this technology to allow insights into complex long-term relationships between microbes and host cells remains to be demonstrated. For the aerobic eukaryotic parasite *Cryptosporidium parvum*, cultures as long as four weeks could be achieved both in adult stem cell-derived organoids (Heo et al., 2018), monolayer cultures (Wilke et al., 2019) and intestines-on-a-chip (Nikolaev et al., 2020).

Cellular representation

In vitro models based on primary tissue uniquely allow representation of diverse human cell types. Recent years have seen substantial improvements in differentiation strategies, especially for organoids, by the incorporation of new media components and the overexpression of transcription factors (Beumer et al., 2020). Adult stem cell-based organoids offer opportunities to grow tissue of a defined region of the intestinal tract with its specific cellular subtypes (Beumer et al., 2020; Ranganathan et al., 2019). Similarly, intestines-on-a-chip approaches allow to simultaneously obtain populations of proliferating and differentiated cells along engineered crypts (Hinman et al., 2019; Kim et al., 2019). Additionally, a recent study showed promising cell heterogeneity in a murine intestine-on-a-chip setup and the possibility of using human primary cells on the same platform (Nikolaev et al., 2020). Among the most thoroughly characterized intestines-on-a-chip is an iPSC-based model which allows generation of stem cells, paneth cells, transit amplifying cells, enterocytes, goblet cells, and enteroendocrine cells (Workman et al., 2017). Nevertheless, the vast majority of cells on this chip are in a proliferative state and are difficult to control for subspecification along the crypt-villus axis and regional identity, highlighting the need for further developments which are currently being pursued for iPSC-derived organoids (Múnera et al., 2017). These efforts to achieve proper cell type representation are crucial for the modelling of several interaction processes discussed below.

THE PROCESSES

Epithelial consequences of microbial interactions

Microbes interact with the intestinal epithelium in a plethora of ways. Co-cultures model several of these processes, allowing to study the interdependence of multiple host-microbe interactions. Nevertheless, even recapitulating a single feature of microbe-epithelium interaction can make for a useful model system. In this section, we review the numerous ways by which commensal species and pathogens can interact with the human gut epithelium (Fig. 2) and discuss to what extent the aforementioned models allow recapitulation of these processes *in vitro* (Table 1).

DNA damage, mutagenesis and cancer

The ability of pathogenic bacteria to induce epithelial transformation has been subject to much investigation since the first studies on *Helicobacter pylori*'s role in gastric

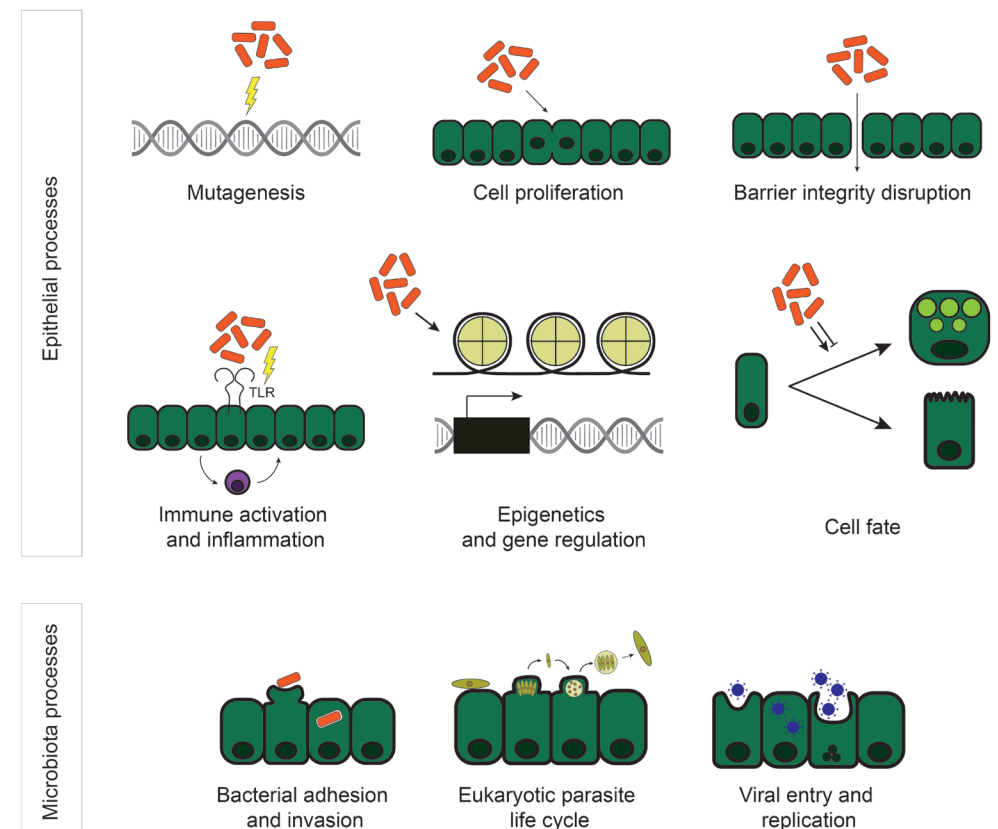


Figure 2. Microbe-epithelium interaction processes. Top: Epithelial processes in response to microbial exposure. Top panel: Epithelial mutation accumulation, proliferation effects and barrier integrity disruption. Middle panel: Sensing of bacterial components by toll like receptors (TLRs) and subsequent cytokine release and immune cell recruitment; epigenetic and gene expression modulation by microbes; cell fate changes induced by microbes. Bottom: Microbial interactions with the epithelium. Bacterial adhesion to and invasion into epithelial cells; completion of complex life cycles of pathogens (such as of eukaryotic parasites) in target cells; viral entry, replication and release in epithelial cells.

tumorigenesis. For colorectal cancer, several large microbiome sequencing studies have revealed associations with species such as *Fusobacterium nucleatum*, Enterotoxigenic *Bacteroides fragilis* and genotoxic *Escherichia coli* (*E. coli*). Despite these numerous associations, few - if any - causal relationships between bacterial species and colorectal cancer have been demonstrated *in vitro*.

One process for which organoids provide an ideally suited model is mutagenesis, as they allow the clonal, long-term expansion of genetically stable epithelium. Recently, a long-term co-culture of genotoxic *E. coli* with human intestinal organoids was employed to identify mutational signatures caused by the bacterial genotoxin colibactin (Pleguezuelos-Manzano et al., 2020). In this study, a month-long co-culture

Table 1. Comparison of *in vitro* gut-microbe co-culture models. Adult stem-cell (ASC)-, pluripotent stem-cell (PSC)-derived organoid, and chip models are compared with monolayer cultures and organotypic explants. *Platform potential, which remains to be demonstrated.

Model comparison	ASC organoids	ASC chips	PSC organoids	2D organoids	Cell line chip	2D cell line	Explant
Features	Oxygen gradient (endogenous)	++	-	++	-	-	-
	Oxygen gradient (engineered)	-	+++	-	++	+++	++*
	Co-culture duration	++	+++	+	++	+++	-
	Flow & Peristalsis	-	+++	-	+	+++	+
	Cell type representation	+++	++	++	++*	-	-
	Regional identity	+++	++	+	+++*	-	-
Processes	Mutagenesis	+++	++*	+	+	+	-
	Epithelial turnover	+++	++	++	++	+	-
	Intestinal cell fate	+++	++	++	+	-	-
	Epigenetics	+++	+++*	++	+++*	+	+
	Epithelial damage & barrier integrity	++	+++	++	+++	+++	+
	Pattern recognition & inflammation	+++	+++	+++	+++	+	+
	Adhesion & Invasion	++	+++	++	++	++	+
	Pathogen replication & life cycle	+++	+++	+++	+++	+	+
Perspectives	Inclusion of microenvironment	++	+++	+++	++	+++	++
	Complex architecture	++	+++	++	-	+	-
	Microbial community dynamics	+	+++	+	+	++	+
	Drug screens	++	++	++	+	+	+

protocol allowed the detection of mutations caused by the DNA damaging activity of colibactin. Of note, colibactin had been described to cause double-strand DNA breaks in studies using cell lines and mouse models (Bossuet-Greif et al., 2018; Dejea et al., 2018; Dziubańska-Kusibab et al., 2020; Nougayrede, 2006). The mutational patterns discovered in the organoids were enriched in samples from CRC origin, indicating the role of genotoxic *E. coli* in colonic mutagenesis (Pleguezuelos-Manzano et al., 2020). More recently, the exposure of mouse small intestinal organoids to genotoxic *E. coli* was linked to epithelial transformation (Iftekhar et al., 2021).

Many studies focus on ways by which bacteria can contribute to colorectal cancer initiation and progression beyond the induction of mutations. Several non-intestinal organoid systems have been used to pinpoint bacterially-driven activation of cancer-

associated pathways, aberrant proliferation and replication stress (Bauer et al., 2020; McCracken et al., 2014; Scanu et al., 2015). We anticipate that applying these methods to colorectal cancer organoids will reveal further causal relationships.

Epithelial cell turnover

Intestinal cell turnover can have important implications in wound healing and colorectal cancer development. It is also one of the features most easily assessed *in vitro*. A seminal study (Kaiko et al., 2016) demonstrated that butyrate, a short chain fatty acid (SCFA) and key metabolite of many gut bacteria, inhibits proliferation of colonic stem cells. Intriguingly, differentiated colonocytes can metabolize butyrate without this inhibiting effect, thereby providing a protected environment for stem cells in the colonic crypts. This study highlights the potential of organoids to disentangle responses of individual cell types to microbial stimuli. Two other studies used murine colon organoids to study the role of lipopolysaccharide (LPS) on proliferation on the intestinal epithelium. Using qPCR (Neal et al., 2012) and flow cytometric (Naito et al., 2017) analysis of the proliferation markers PCNA and Ki67, respectively, a TLR-4 mediated inhibition of proliferation was identified. The co-culture of iPSC-derived intestinal organoids with non-pathogenic strains of *E. coli* helped to investigate epithelial proliferation dynamics upon bacteria challenge (Hill et al., 2017). Following exposure to bacteria, organoids showed an initial wave of increased proliferation at 24h post-exposure followed by a decrease compared to untreated controls. We expect that the recent development of intestines-on-a-chip models with representative crypt-villus architecture and cell type distribution (Jalili-Firoozinezhad et al., 2019; Nikolaev et al., 2020) will enable further representative studies on this topic in the future. For now, the experimental tractability of organoids offers a versatile platform to study the effects of microbes and their metabolites on intestinal cell proliferation.

Cell function and fate

The gut microbiota changes the function and differentiation of host cells in various ways to cater to the microbes' needs. Many of these changes can be detected as altered host cell gene expression. Organoids and organs-on-chips are well-suited to disentangle these interactions, as transcriptomic data can be attributed to either microbe or epithelial cells.

As one example, *Bacteroides thetaiotaomicron* was shown to directly induce *fut2* expression and mucus fucosylation by epithelial cells in organoids and mice, offering an energy source for the bacterium (Engevik et al., 2013). Non-pathogenic *E. coli* co-cultured with iPSC-derived intestinal organoids induce a hypoxic response as a consequence of local oxygen depletion by the bacteria, showcasing another mechanism by which bacteria can change host cell behavior (Hill et al., 2017). The ability of organoids to differentiate into all intestinal epithelial cell types makes them a well-suited model system to study microbial control over epithelial regeneration, nutrient uptake and hormone secretion. Thus, increased goblet cell differentiation has been observed in response to LPS derived

from various bacterial species enriched in colonic crypts (Naito et al., 2017). A challenge to this approach is the difficulty of telling apart changes in differentiated cell number and expression levels in individual cells. Fluorescent reporters for cell type marker genes could overcome this hurdle. Using this approach, *Salmonella* has been shown to reduce the number of Lgr5+ stem cells in adult stem-cell derived mouse intestinal organoids (Zhang et al., 2014). We anticipate that recent work on knock-in reporters for intestinal cell types in human organoids (Beumer et al., 2020) will contribute to larger-scale assessment of cell (sub)type specification by microbes in the future. Another way to assess cell fate and function changes involves single cell RNA sequencing, which allows the detailed characterization of organoid compositions (Grün et al., 2015). While this technique may enable studies at greater detail than the aforementioned approaches, it has not been combined with microbial *in vitro* co-cultures to our knowledge.

Gut microbes may directly modify the epigenetic profile of host cells (Qin and Wade, 2018). The tight experimental control provided by organoids can enable studies of such epigenetic effects of microbe or metabolite exposure. In a pioneering study (Lukovac et al., 2014), the effects of *Akkermansia muciniphila*, *Faecalibacterium prausnitzii* and their short chain fatty acid products were shown to affect, amongst others, histone deacetylases and the consequent epigenetic marks in murine ileal organoids. The observed induction of a marked transcriptional lipid metabolism response by *Akkermansia muciniphila* adds to a growing body of evidence of microbial impact in metabolic diseases. Despite this early promise, modelling the epigenetic effects of microbes *in vitro* is still in its infancy.

Epithelial damage and barrier integrity

The intestinal epithelial and mucus layers constitute the key barrier separating food components and microbiota in the intestinal lumen from the bloodstream. Several diseases such as inflammatory bowel disease (IBD) have been implicated with decreased barrier function of the intestine while a microbial contribution to intestinal barrier integrity is suggested by numerous studies (Martini et al., 2017).

The structure of tight junctions between epithelial cells and bacterial effects on these junctions can readily be visualized in organoids. This has been shown amongst others for pathogenic *Salmonella enterica* serovar Typhimurium (*S. Typhimurium*) by staining for the tight junction protein ZO-1 in mouse small intestinal organoids (Zhang et al., 2014). In another study, the same type of organoids was used to show a protective effect of the probiotic *Lactobacillus acidophilus* against *S. Typhimurium*-induced tissue damage (Lu et al., 2020). Using a different co-culture setup, enterohemorrhagic *E. coli* (EHEC) strains were shown to disrupt the mucus layer, microvilli structure and tight junctions when co-cultured with differentiated human colonocytes on a 2D monolayer setup (In et al., 2016). One straightforward way to assess barrier integrity *in vitro* is the tracking of fluorescently labelled molecules of high molecular weight from the apical to the basolateral side of organoids (Leslie et al., 2015) or organs-on-chips (Jalili-Firoozinezhad et al., 2019).

Organoids can be used to assess barrier integrity effects of individual species and the responsible compounds in a highly controlled way. This has been demonstrated among others using different strains of *Clostridium difficile* and the responsible toxin TcdA (Tao et al., 2016). Even without the use of a fluorescent dye, the induction of pores in an organoid monolayer can be assessed by microscopy. This has recently been demonstrated for *Klebsiella pneumoniae*, which causes such pore formation by inducing Caspase-3-mediated cell death in colon organoid monolayers (Nakamoto et al., 2019). Another often-used method to assess epithelial barrier integrity is the measurement of trans-epithelial electrical resistance (TEER), which can be readily implemented on monolayer cultures and organs-on-chips (Henry et al., 2017; In et al., 2016; Naumovska et al., 2020; Sasaki et al., 2020) (but not easily in 3D organoids). Using intestine-chips, both barrier-protective and -disruptive bacterial effects can be studied in a scalable and robust manner (Kim et al., 2016a; Shin and Kim, 2018). Taken together, these features give intestines-on-a-chip an edge over other *in vitro* models for systematic studies on barrier integrity.

Pattern recognition and inflammation

One of the most intensely studied microbial interactions in the human intestine is the crosstalk with the mucosal immune system (Round and Mazmanian, 2009). The recognition of pathogens by epithelial cells and subsequent induction of an inflammatory response is a crucial step in this process. Basolateral exposure to bacterial components such as lipopolysaccharide (LPS), frequently occurring in case of disrupted barrier function of the epithelium, can trigger the release of pro-inflammatory cytokines by epithelial cells.

Epithelial *in vitro* models are well-suited to uncover the pro- and anti-inflammatory effects of bacterial species and their components in an intact or disrupted gut architecture. Transcriptional read-outs such as qPCR and RNA sequencing are the most accessible means to profile the nature of inflammatory responses in any *in vitro* model system. Especially the comprehensiveness of RNA sequencing can permit detailed insights into the type of immune response which is induced in organoids by triggers such as viral infection (Chang-Graham et al., 2020; Drummond et al., 2017; Lamers et al., 2020).

A key advantage of adult stem cell-derived organoids is their recapitulation of regional identity, which can play an important role in the kind of innate inflammatory response triggered upon bacterial exposure (Kayisoglu et al., 2020). Intestines-on-a-chip have proven well-suited to study inflammatory processes (Naumovska et al., 2020; Shin and Kim, 2018). Thus, the secretion of pro-inflammatory cytokines by a DSS-pretreated intestinal layer in response to *E. coli* and LPS exposure could be measured, as well as the protective effect of a pre-treatment with probiotic bacteria (Shin and Kim, 2018). Human organotypic explant cultures were employed to study the prohibitive effects of initial bacterial load on fecal microbial transplant engraftment in the context

of inflammatory bowel disease (Sarrabayrouse et al., 2020). In this study, the mucosal layer was exposed *ex vivo* to microbial donor material. This setup demonstrated reduced engraftment of anti-inflammatory microbial transplants and consequently higher levels of proinflammatory cytokine secretion in recipients with a high initial mucosal bacterial load. In a separate study, ileal and colonic explants of mice treated with the probiotic *Lactobacillus kefir* showed a decreased inflammatory response upon LPS stimulation, highlighting the utility of explant models to investigate anti-inflammatory effects of *in vivo* treatments using an *ex vivo* system (Carasi et al., 2015).

A recently published virology study showed that the infection of intestinal organoids with rotavirus induced a paracrine ADP/calcium signal through P2Y1 receptors that leads to a deleterious inflammatory response (Chang-Graham et al., 2020). The suitability of an *in vitro* system for inflammation studies is therefore highly context dependent, with an advantage for organs-on-chips where spatial control is important.

MICROBIAL PROCESSES

Adhesion & Invasion

The adhesion to and invasion of epithelial cells by viruses, bacteria and eukaryotic parasites constitutes an important step in the life cycle and pathogenic mechanisms of these microbes. By faithful representation of cellular heterogeneity, entry receptor expression patterns and the possibility to rapidly generate genetically engineered lines, organoids are emerging as a key model to disentangle pathogen invasion mechanisms.

Invasion assays using organoids rely on standard protocols established for 2D cell line invasion studies, most notably the gentamicin protection assay (Koestler et al., 2019; Rubinstein et al., 2013). In this assay, a short-term treatment with the non-permeable antibiotic gentamicin kills extracellular bacteria while intracellular microbes are protected. In elegant studies on 2D cultures of human colon organoids, the invasion processes of pathogenic *Shigella flexneri* could be studied (Koestler et al., 2019). The polarized monolayer allowed detailed studies on the basolateral invasion preference of *Shigella*, as well as apical translocations through disrupted tight junctions. In another study, the importance of M-cell representation and regional identity of human organoid monolayers for *Shigella* infection was demonstrated (Ranganathan et al., 2019). Similarly, the invasion of *EHEC* could be studied in a 2D colonocyte model based on adult stem cells (In et al., 2016). Modified versions of the gentamicin protection assay have been developed for 3D organoid co-culture assays. These include freeing the organoids from BME and the mechanical disruption of their 3D structure, exposing the otherwise protected organoid apical surface before gentamicin treatment (Forbester et al., 2015). As a result, PSC-derived human intestinal organoids enabled studies on the invasion mechanism of *S. Typhimurium* (Forbester et al., 2015). While less commonly applied than organoids, intestines-on-a-chip have also been used for detailed invasion studies. Using fluorescently labeled *Shigella*, apical invasion into the crypt compartment of Caco-2

cells grown on a chip device was detected (Grassart et al., 2019). The dependence on peristalsis of the intestinal layer for this invasion highlights a key advantage of intestines-on-a-chip for host-microbe studies and underlines the potential for further developments of organ-on-chip technology in the area of microbial invasion. A key obstacle for microbes to attach to the epithelium is the mucus layer, a difficult feature to faithfully represent in cell lines and some organoid models. Murine organotypic explants were used to study this process in detail, showing how *S. Typhimurium* can access the caecal epithelium through holes in the mucus layer which are absent in other gut regions (Furter et al., 2019).

Pathogen replication and life cycle

Organoids provide the most faithful recapitulation of intestinal cell types to date and have enabled pioneering studies on *in vitro* propagation and study of several pathogens. Such cell-type representation can be crucial in case of specific tropisms by pathogens. As one example, human noroviruses have been notoriously hard to study as they require enterocytes and bile for entry and replication. Human intestinal organoids, grown as a 2D layer and differentiated towards enterocytes, allowed for the first time to propagate this virus *in vitro*, laying the groundwork for future studies on this virus (Ettayebi et al., 2016). As another example, an adult stem cell-based human small intestinal organoid model exhibited better infection rates of echovirus 11 when differentiation was driven towards cells of the secretory lineage, in particular enteroendocrine cells (Drummond et al., 2017). In case of unknown tropism of a pathogen, the ability to grow organoids from almost every epithelial human tissue enables sophisticated comparative studies. This has been done for example in case of the human bocavirus, which was demonstrated to infect both human airway and intestinal epithelial cells using organoids (Fakhiri et al., 2019). More recently, human intestinal organoids enabled the identification of enterocytes and their progenitors as intestinal target cells of the novel SARS-CoV-2 virus (Lamers et al., 2020). This study highlights the rapid pace at which viral target cells, the epithelial response and other features can be assessed using organoids. For this virus, organoids even enabled comparative studies between species such as bats and humans (Zhou et al., 2020).

PSC-based organoids enabled the detection of both epithelial and non-epithelial target cell types for rotaviruses (Finkbeiner et al., 2012). A comprehensive study on the infection of human small intestinal explants and organoids revealed that the MERS coronavirus can infect several intestinal cell types and replicate in these (Zhou et al., 2017).

Target cell type identification for pathogen propagation is of particular importance for virus infections studies, but not limited to them. Recent work has demonstrated the possibility to recapitulate complex life cycles of the eukaryotic parasites. This is the case for *Cryptosporidium parvum* and *Trichuris muris*, which were studied using adult stem cell-derived human and mouse intestinal organoids, respectively, grown in 3D (Heo et al., 2018; Duque-Correa et al., 2020). *Cryptosporidium parvum* could also be studied on intestinal monolayers at an air-liquid interface (Wilke et al., 2019) and recently transferred to an intestine-on-a-chip device, paving the way for long-term studies (Nikolaev et al., 2020).

CURRENT TRENDS & CHALLENGES

Beyond the significant progress in modelling these numerous interaction processes *in vitro*, important hurdles still need to be overcome to recapitulate gut-microbe relationships at even greater detail. In this section, we discuss recent efforts to add further complexity and highlight outstanding challenges for epithelial co-cultures (Fig. 3).

Other microenvironment components

Despite the many benefits of modelling direct epithelium-microbe interactions *in vitro*, most current approaches are not suited to include additional components of the microenvironment. The immune effects of gut microbiota have especially been the subject of intense study (Round and Mazmanian, 2009) and remain hard to disentangle *in vitro*. Intestinal organoids have proven adequate model systems to study influences of the immune environment on epithelial behavior (Lindemans et al., 2015). The addition of microbes to this equation *in vitro* is still relatively recent but early examples highlight the potential of co-cultures incorporating all three components. For example, the protective effect of the probiotic *Lactobacillus reuteri* on mouse small intestinal organoids challenged with TNF- α could be demonstrated using organoids (Hou et al., 2018), including a role of *Klebsiella pneumoniae* in TH17-mediated inflammatory liver injuries (Nakamoto et al., 2019). Furthermore, gastric organoids were used to assess PD-L1 expression and autologous cytotoxic T lymphocyte activity upon *H. pylori* infection and immune-checkpoint inhibition (Holokai et al., 2019). As an example of viral effects on immune cell interactions, the recruitment of neutrophils in response to Respiratory syncytial virus infection could be studied in airway organoids (Sachs et al., 2019).

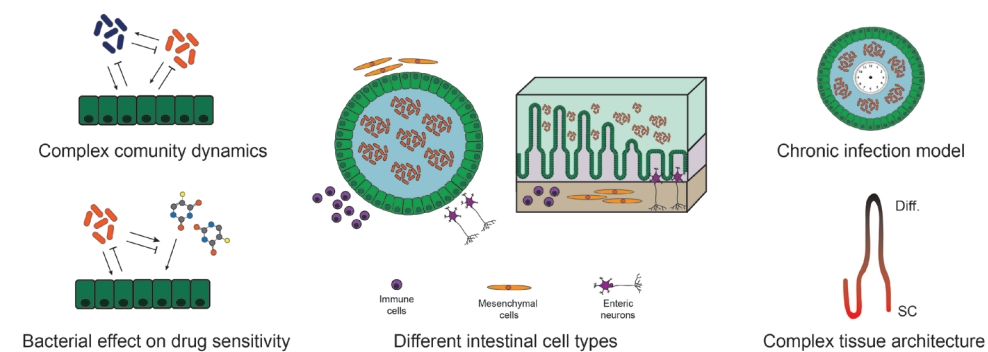


Figure 3. Trends and future perspectives for *in vitro* gut-microbe co-cultures. Top left: Bacterial community interactions with each other and the epithelium. Bottom left: Drug metabolism and epithelial response modulation by microbes. Middle: Incorporation of further microenvironmental components into organoids and intestines-on-chip. Top right: Extended cultures for chronic infection modelling in organoids. Bottom right: Increasing architectural complexity by organizing the relevant cell types in a crypt-villus architecture.

Intestines-on-a-chip are increasingly useful for these studies, as demonstrated by their recent use to study the recruitment of leukocytes upon luminal stimulation with LPS (Maurer et al., 2019), recapitulating a key process of IBD pathogenesis. The role of mesenchymal cell populations in shaping the gut microflora through induction of M-cell differentiation and IgA production has become apparent (Nagashima et al., 2017), and faithful *in vitro* models are wanting to study the precise nature of these interactions. Organoid co-cultures have been successfully established with CD8+ T-cells (Dijkstra et al., 2018), subepithelial myofibroblasts (Greicius et al., 2018) and macrophages (Noel et al., 2017). New generations of intestines-on-a-chips furthermore incorporate blood vessels in a basolateral channel, contributing a controlled oxygen gradient across the epithelial layer (Jalili-Firoozinezhad et al., 2019).

Complex architecture

The intestinal architecture varies greatly along its rostral-caudal axis with regard to crypt-villus unit organization, cell type composition, luminal oxygen levels and protection by heterogeneous mucus layers. Together with other factors, this results in divergent microbiotas inhabiting various niches in each section of the gut (Donaldson et al., 2016). The organization of microbes in biofilms and other spatially-defined communities is another feature not yet represented in current models (Domingue et al., 2020).

The Caco-2 cell line, derived from a colorectal adenocarcinoma and recapitulating some features of enterocytes, has served as a gold-standard for many monolayer and intestine-on-chip studies (Sambuy et al., 2005). While Caco-2 cells can generate crypt-villus-like structures under flow conditions (Kim et al., 2016a), they inevitably have limitations in recapitulating the regional and architectural nuances of epithelium-microbiota interactions. Organoids have enabled culturing all segments of the gastrointestinal tract and contributed to the understanding of microbial effects between the various cell types of crypt and villus compartments (Kaiko et al., 2016).

Microbial community dynamics

The gut microbiota represents an immensely complex ecosystem. Intestinal microbes are intricately connected by resource interdependencies and extensive metabolic networks leading to competitive, mutualistic or symbiotic behaviors (Stubbendieck et al., 2016). In contrast, simplistic models of single microbe effects can easily exaggerate the impact of individual gut microbiota (Walter et al., 2020) underscoring the benefit of investigating microbial communities.

Growing complex intestinal bacterial communities *in vitro* is feasible (Oliphant et al., 2020; Van den Abbeele et al., 2010), but establishing media and oxygen conditions under which both epithelial cells and bacteria with diverse requirements thrive presents a formidable challenge. Consequently, the stable culture of complex microbial communities in the lumen organoids has not been achieved to date. However, different

groups have pioneered the use of intestine-on-a-chip platforms for maintaining defined bacterial communities of several species over the time frame of days to weeks (Kim et al., 2016b; Marzorati et al., 2014). More recent studies on novel chip models demonstrate the possibility to maintain a diverse community of more than 200 operational taxonomic units over several days in culture (Jalili-Firoozinezhad et al., 2019). In this study, an oxygen gradient from epithelium to the lumen of a channel of the chip allowed culture of both aerobes and obligate anaerobes and assessment of parameters such as barrier integrity. These models will likely facilitate future work on microbial relationships in the context of the gut epithelium (Lu et al., 2020). Already now, the protective effect of *Lactobacillus rhamnosus* from *Candida albicans* infections could be modelled on an intestine chip (Maurer et al., 2019).

Drug screens

Organoids and organs-on-chips have reached a scalability which allows screening of therapeutic compounds. The current COVID-19 pandemic underscores the need for rapid development and testing of therapeutics targeted at microbial infection of and replication within host epithelial cells. Recent work highlights the feasibility of these efforts (Lamers et al., 2020; Yin et al., 2015) and we expect that standardized and high throughput (Williamson et al., 2018) organoid-microbe co-culture workflows will enable systematic screens for infectious disease drugs in the near future. In the setting of other diseases such as cancer, the importance of the gut microbiota for drug metabolism (Geller et al., 2017; Zimmermann et al., 2019) and host response to drugs (Yu et al., 2017) have been the subject of pioneering studies. We anticipate that the combination of organoids and microbes will open up new avenues for host-microbe co-metabolism studies and help understand microbially modified treatment responses. Finally, organs-on-chips are being rapidly adopted for drug screenings in diverse settings (Beaurivage et al., 2019), including processes important for microbial interactions such as barrier integrity (Bhatt et al., 2018).

FUTURE OUTLOOK

The important role of the microbiota in the maintenance of intestinal homeostasis and development of disease has become apparent in the last decades. However, it remains difficult to move from the associations uncovered by metagenomic studies to insights into the mechanistic roles of the microbiota. The development of human intestinal organoids and their incorporation into more elaborate organ-on-a-chip setups have led to innovative avenues to evaluate this relationship between the intestinal mucosa and its microbiota. Although still in its infancy, this field has already yielded some key discoveries into how the microbiota contributes to health and disease, recapitulating several human-specific features in processes like viral infection and replication (Ettayebi et al., 2016; Lamers et al., 2020). As a result, several biotechnology companies have developed or adopted organoids and organs-on-a-chip for their preclinical testing. In particular, companies such

as Emulate, MIMETAS or Altis Biosystems have pioneered intestine-on-a-chip models well suited for scalable microbe co-cultures. A comprehensive overview of the commercial activity in the fields of organoids and organs-on-chips can be found in two recent reviews (Allwardt et al., 2020; Choudhury et al., 2020).

Choosing the right *in vitro* model for host-microbe studies depends on the microbe, but even more so on the envisioned readouts. As viruses are dependent on a host cell for replication, generation of the right target cell type(s) is of paramount importance. For bacterial co-cultures, the divergent requirements regarding oxygen levels, nutrients and spatial organization pose main challenges. No current *in vitro* model incorporates all potentially relevant microenvironmental components which would allow a complete recapitulation of the *in vivo* situation, but each of them is suitable for modelling some interactions. The studies highlighted in this review and summarized in Table 1 showcase the advantages of each *in vitro* intestine model. Cell lines remain useful in standardized and scalable assays both as monolayers and on chip architectures. However, the increasing availability of adult stem cell-derived organoids for growth in these formats will likely replace cell lines in many assays. Organotypic explant cultures are the most straightforward way to retain the tissue architecture *ex vivo* for short time frames and can be a crucial technology when this feature is of importance. The lack of experimental control and repeated requirement of biopsy material limit their application. We anticipate a continuous move towards adult stem cell-based systems, both as organoids and intestines-on-a-chip, because of their incorporation of diverse and mature intestinal cell types. Intestines-on-a-chip have improved dramatically in the control of gradients and of cellular representation in recent years, being the model of choice when spatial control of exposure, architecture, flow and movement are of importance. iPSC-derived organoids allow complex mixtures of cells to be cultured and have proven suitable for infection studies and on organ-on-chip devices. ASC-based organoids are most suitable in studies where faithful representation of cell type composition and regional identity is needed, or when inter-individual differences need to be studied with reasonable scalability. Their comparative ease-of-derivation and -use and experimental tractability make them a flexible *in vitro* model for co-culture studies.

The field is rapidly moving from the most reductionist approaches where the effect of a single microbial species on the epithelium is studied to more elaborate setups. These will include complex bacterial communities from healthy or diseased individuals and as well as other components of the intestinal mucosa like immune cells, the mesenchyme or enteric neurons. We anticipate that these approaches will allow the establishment of chronic models of microbial co-cultures to study diseases like IBD or colorectal cancer.

Finally, the intestinal microenvironment is an immensely complex system, and *in vivo* models remain the only option to study systemic effects at this moment. Nevertheless, there is no conceptual boundary which would prevent the stepwise reassembly of this system based on a growing understanding of cell types' requirements and their interplay.

As a result, organoids and organs-on-chips are set to play a growing role in disentangling host-microbe interactions *in vitro*.

ACKNOWLEDGEMENTS

This work was supported by CRUK grant OPTIMISTIC [C10674/A27140], the Netherlands Organ-on-Chip Initiative (024.003.001) from the Netherlands Organisation for Scientific Research (NWO) funded by the Ministry of Education, Culture and Science of the government of the Netherlands, the Onco Institute (partly financed by the Dutch Cancer Society) the European Research Council under ERC Advanced Grant Agreement no. 67013.

DECLARATION OF INTERESTS

H.C. is inventor on multiple patents held by the Dutch Royal Netherlands Academy of Arts and Sciences that cover organoid technology. H.C. is member of the board of directors of Roche. H.C.'s full disclosure is given at <https://www.uu.nl/staff/JCClevers/>.

REFERENCES

- Allwardt, V., Ainscough, A.J., Viswanathan, P., Sherrod, S.D., McLean, J.A., Haddrick, M., and Pensabene, V. (2020). Translational Roadmap for the Organs-on-a-Chip Industry toward Broad Adoption. *Bioengineering* 7.
- Bartfeld, S. (2016). Modeling infectious diseases and host-microbe interactions in gastrointestinal organoids. *Dev. Biol.* 420, 262–270.
- Bauer, M., Nascakova, Z., Mihai, A.-I., Cheng, P.F., Levesque, M.P., Lampart, S., Hurwitz, R., Pfannkuch, L., Dobrovolna, J., Jacobs, M., et al. (2020). The ALPK1/TIFA/NF- κ B axis links a bacterial carcinogen to R-loop-induced replication stress. *Nat. Commun.* 11, 5117.
- Beurivage, C., Naumovska, E., Chang, Y.X., Elstak, E.D., Nicolas, A., Wouters, H., van Moolenbroek, G., Lanz, H.L., Trietsch, S.J., Joore, J., et al. (2019). Development of a Gut-on-a-Chip Model for High Throughput Disease Modeling and Drug Discovery. *Int. J. Mol. Sci.* 20.
- Bein, A., Shin, W., Jalili-Firoozinezhad, S., Park, M.H., Sontheimer-Phelps, A., Tovaglieri, A., Chalkiadaki, A., Kim, H.J., and Ingber, D.E. (2018). Microfluidic Organ-on-a-Chip Models of Human Intestine. *Cell. Mol. Gastroenterol. Hepatol.* 5, 659–668.
- Beumer, J., Puschhof, J., Bauzá-Martinez, J., Martínez-Silgado, A., Elmentaite, R., James, K.R., Ross, A., Hendriks, D., Artegiani, B., Busslinger, G.A., et al. (2020). High-Resolution mRNA and Secretome Atlas of Human Enteroendocrine Cells. *Cell* 181, 1291–1306.e19.
- Bhatt, A.P., Gunasekara, D.B., Speer, J., Reed, M.I., Peña, A.N., Midkiff, B.R., Magness, S.T., Bultman, S.J., Allbritton, N.L., and Redinbo, M.R. (2018). NSAID-Induced Leaky Gut Modeled Using Polarized Monolayers of Primary Human Intestinal Epithelial Cells. *ACS Infect. Dis.* 4, 46–52.
- Blokzijl, F., de Ligt, J., Jager, M., Sasselli, V., Roerink, S., Sasaki, N., Huch, M., Boymans, S., Kuijk, E., Prins, P., et al. (2016). Tissue-specific mutation accumulation in human adult stem cells during life. *Nature* 538, 260–264.
- Boccellato, F., Woelffling, S., Imai-Matsushima, A., Sanchez, G., Goosmann, C., Schmid, M., Berger, H., Morey, P., Denecke, C., Ordemann, J., et al. (2019). Polarised epithelial monolayers of the gastric mucosa reveal insights into mucosal homeostasis and defence against infection. *Gut* 68, 400–413.
- Bossuet-Greif, N., Vignard, J., Taieb, F., Mirey, G., Dubois, D., Petit, C., Oswald, E., and Nougayrède, J.-P. (2018). The Colibactin Genotoxin Generates DNA Interstrand Cross-Links in Infected Cells. *MBio* 9.
- Carasi, P., Racedo, S.M., Jacquot, C., Romanin, D.E., Serradell, M.A., and Urdaci, M.C. (2015). Impact of Kefir Derived Lactobacillus kefiri on the Mucosal Immune Response and Gut Microbiota. *J. Immunol. Res.* 2015.
- Chang-Graham, A.L., Perry, J.L., Engevik, M.A., Engevik, K.A., Scribano, F.J., Gebert, J.T., Danhof, H.A., Nelson, J.C., Kellen, J.S., Strtak, A.C., et al. (2020). Rotavirus induces intercellular calcium waves through ADP signaling. *Science* 370.
- Choudhury, D., Ashok, A., and Naing, M.W. (2020). Commercialization of Organoids. *Trends Mol. Med.* 26, 245–249.
- Dejea, C.M., Fathi, P., Craig, J.M., Boleij, A., Taddese, R., Geis, A.L., Wu, X., DeStefano Shields, C.E., Hechenbleikner, E.M., Huso, D.L., et al. (2018). Patients with familial adenomatous polyposis harbor colonic biofilms containing tumorigenic bacteria. *Science* 359, 592–597.
- Dijkstra, K.K., Cattaneo, C.M., Weeber, F., Chalabi, M., van de Haar, J., Fanchi, L.F., Slagter, M., van der Velden, D.L., Kaing, S., Kelderman, S., et al. (2018). Generation of Tumor-Reactive T Cells by Co-culture of Peripheral Blood Lymphocytes and Tumor Organoids. *Cell* 174, 1586–1598.e12.
- DiMarco, R.L., Su, J., Yan, K.S., Dewi, R., Kuo, C.J., and Heilshorn, S.C. (2014). Engineering of Three-Dimensional Microenvironments to Promote Contractile Behavior in Primary

- Intestinal Organoids. *Integr. Biol. Quant. Biosci. Nano Macro* 6, 127–142.
17. Domingue, J.C., Drewes, J.L., Merlo, C.A., Housseau, F., and Sears, C.L. (2020). Host responses to mucosal biofilms in the lung and gut. *Mucosal Immunol.* 13, 413–422.
 18. Donaldson, G.P., Lee, S.M., and Mazmanian, S.K. (2016). Gut biogeography of the bacterial microbiota. *Nat. Rev. Microbiol.* 14, 20–32.
 19. Drummond, C.G., Bolock, A.M., Ma, C., Luke, C.J., Good, M., and Coyne, C.B. (2017). Enteroviruses infect human enteroids and induce antiviral signaling in a cell lineage-specific manner. *Proc. Natl. Acad. Sci. U. S. A.* 114, 1672–1677.
 20. Duque-Correa, M.A., Schreiber, F., Rodgers, F.H., Goulding, D., Forrest, S., White, R., Buck, A., Grecis, R.K., and Berriman, M. (2020). Development of caecaloids to study host-pathogen interactions: new insights into immunoregulatory functions of *Trichuris muris* extracellular vesicles in the caecum. *Int. J. Parasitol.* 50, 707–718.
 21. Dziubańska-Kusibab, P.J., Berger, H., Battistini, F., Bouwman, B.A.M., Iftekhar, A., Katainen, R., Cajuso, T., Crosetto, N., Orozco, M., Aaltonen, L.A., et al. (2020). Colibactin DNA-damage signature indicates mutational impact in colorectal cancer. *Nat. Med.* 26, 1063–1069.
 22. Engevik, M.A., Aihara, E., Montrose, M.H., Shull, G.E., Hassett, D.J., and Worrell, R.T. (2013). Loss of NHE3 alters gut microbiota composition and influences *Bacteroides thetaiotaomicron* growth. *Am. J. Physiol. - Gastrointest. Liver Physiol.* 305, G697–G711.
 23. Ettayebi, K., Crawford, S.E., Murakami, K., Broughman, J.R., Karandikar, U., Tenge, V.R., Neill, F.H., Blutt, S.E., Zeng, X.-L., Qu, L., et al. (2016). Replication of Human Noroviruses in Stem Cell-Derived Human Enteroids. *Science* 353, 1387–1393.
 24. Fakhiri, J., Schneider, M.A., Puschhof, J., Stanifer, M., Schildgen, V., Holderbach, S., Voss, Y., El Andari, J., Schildgen, O., Boulant, S., et al. (2019). Novel Chimeric Gene Therapy Vectors Based on Adeno-Associated Virus and Four Different Mammalian Bocaviruses. *Mol. Ther. Methods Clin. Dev.* 12, 202–222.
 25. Finkbeiner, S.R., Zeng, X.-L., Utama, B., Atmar, R.L., Shroyer, N.F., and Estes, M.K. (2012). Stem Cell-Derived Human Intestinal Organoids as an Infection Model for Rotaviruses. *MBio* 3.
 26. Fletcher, P.S., Elliott, J., Grivel, J.-C., Margolis, L., Anton, P., McGowan, I., and Shattock, R.J. (2006). Ex vivo culture of human colorectal tissue for the evaluation of candidate microbicides. *AIDS Lond. Engl.* 20, 1237–1245.
 27. Forbester, J.L., Goulding, D., Vallier, L., Hannan, N., Hale, C., Pickard, D., Mukhopadhyay, S., and Dougan, G. (2015). Interaction of *Salmonella enterica* Serovar Typhimurium with Intestinal Organoids Derived from Human Induced Pluripotent Stem Cells. *Infect. Immun.* 83, 2926–2934.
 28. Fujii, M., Matano, M., Nanki, K., and Sato, T. (2015). Efficient genetic engineering of human intestinal organoids using electroporation. *Nat. Protoc.* 10, 1474–1485.
 29. Furter, M., Sellin, M.E., Hansson, G.C., and Hardt, W.-D. (2019). Mucus Architecture and Near-Surface Swimming Affect Distinct *Salmonella* Typhimurium Infection Patterns along the Murine Intestinal Tract. *Cell Rep.* 27, 2665–2678.e3.
 30. Geller, L.T., Barzily-Rokni, M., Danino, T., Jonas, O.H., Shental, N., Nejman, D., Gavert, N., Zwang, Y., Cooper, Z.A., Shee, K., et al. (2017). Potential role of intratumor bacteria in mediating tumor resistance to the chemotherapeutic drug gemcitabine. *Science* 357, 1156–1160.
 31. Grassart, A., Malardé, V., Gobaa, S., Sartori-Rupp, A., Kerns, J., Karalis, K., Marteyn, B., Sansonetti, P., and Sauvonnnet, N. (2019). Bioengineered Human Organ-on-Chip Reveals Intestinal Microenvironment and Mechanical Forces Impacting *Shigella* Infection. *Cell Host Microbe* 26, 565.
 32. Greicius, G., Kabiri, Z., Sigmundsson, K., Liang, C., Bunte, R., Singh, M.K., and Virshup, D.M. (2018). PDGFR α pericyptal stromal cells are the critical source of Wnts and RSPO3 for murine intestinal stem cells in vivo. *Proc. Natl. Acad. Sci. U. S. A.* 115, E3173–E3181.
 33. Grün, D., Lyubimova, A., Kester, L., Wiebrands, K., Basak, O., Sasaki, N., Clevers, H., and van Oudenaarden, A. (2015). Single-cell messenger RNA sequencing reveals rare intestinal cell types. *Nature* 525, 251–255.
 34. Gustafsson, J.K., Ermund, A., Johansson, M.E.V., Schütte, A., Hansson, G.C., and Sjövall, H. (2012). An ex vivo method for studying mucus formation, properties, and thickness in human colonic biopsies and mouse small and large intestinal explants. *Am. J. Physiol. - Gastrointest. Liver Physiol.* 302, G430–G438.
 35. Henry, O.Y.F., Villenave, R., Crouce, M., Leineweber, W., Benz, M., and Ingber, D.E. (2017). Organs-on-Chips with integrated electrodes for Trans-Epithelial Electrical Resistance (TEER) measurements of human epithelial barrier function. *Lab. Chip* 17, 2264–2271.
 36. Heo, I., Dutta, D., Schaefer, D.A., Iakobachvili, N., Artegiani, B., Sachs, N., Boonekamp, K.E., Bowden, G., Hendrickx, A.P.A., Willems, R.J.R., et al. (2018). Modeling *Cryptosporidium* infection in human small intestinal and lung organoids. *Nat. Microbiol.* 3, 814–823.
 37. Hill, D.R., Huang, S., Nagy, M.S., Yadagiri, V.K., Fields, C., Mukherjee, D., Bons, B., Dedhia, P.H., Chin, A.M., Tsai, Y.-H., et al. (2017). Bacterial colonization stimulates a complex physiological response in the immature human intestinal epithelium. *ELife* 6, e29132.
 38. Hinman, S.S., Wang, Y., and Allbritton, N.L. (2019). Photopatterned Membranes and Chemical Gradients Enable Scalable Phenotypic Organization of Primary Human Colon Epithelial Models. *Anal. Chem.* 91, 15240–15247.
 39. Holokai, L., Chakrabarti, J., Broda, T., Chang, J., Hawkins, J.A., Sundaram, N., Wroblewski, L.E., Peek, R.M., Wang, J., Helmuth, M., et al. (2019). Increased Programmed Death-Ligand 1 is an Early Epithelial Cell Response to *Helicobacter pylori* Infection. *PLoS Pathog.* 15.
 40. Hou, Q., Ye, L., Liu, H., Huang, L., Yang, Q., Turner, J., and Yu, Q. (2018). *Lactobacillus* accelerates ISCs regeneration to protect the integrity of intestinal mucosa through activation of STAT3 signaling pathway induced by LPLs secretion of IL-22. *Cell Death Differ.* 25, 1657–1670.
 41. Iftekhar, A., Berger, H., Bouznad, N., Heuberger, J., Boccellato, F., Dobrindt, U., Hermeking, H., Sigal, M., and Meyer, T.F. (2021). Genomic aberrations after short-term exposure to colibactin-producing *E. coli* transform primary colon epithelial cells. *Nat. Commun.* 12, 1003.
 42. In, J., Foulke-Abel, J., Zachos, N.C., Hansen, A.-M., Kaper, J.B., Bernstein, H.D., Halushka, M., Blutt, S., Estes, M.K., Donowitz, M., et al. (2016). Enterohemorrhagic *Escherichia coli* Reduces Mucus and Intermicrovillar Bridges in Human Stem Cell-Derived Colonoids. *Cell. Mol. Gastroenterol. Hepatol.* 2, 48–62.e3.
 43. Jalili-Firoozinezhad, S., Gazzaniga, F.S., Calamari, E.L., Camacho, D.M., Fadel, C.W., Bein, A., Swenor, B., Nestor, B., Crouce, M.J., Tovaglieri, A., et al. (2019). A complex human gut microbiome cultured in an anaerobic intestine-on-a-chip. *Nat. Biomed. Eng.* 3, 520–531.
 44. Kaiko, G.E., Ryu, S.H., Koues, O.I., Collins, P.L., Solnica-Krezel, L., Pearce, E.J., Pearce, E.L., Oltz, E.M., and Stappenbeck, T.S. (2016). The Colonic Crypt Protects Stem Cells from Microbiota-Derived Metabolites. *Cell* 165, 1708–1720.
 45. Kayisoglu, O., Weiss, F., Niklas, C., Pierotti, I., Pompaiah, M., Wallaschek, N., Germer, C.-T., Wiegner, A., and Bartfeld, S. (2020). Location-specific cell identity rather than exposure to GI microbiota defines many innate immune signalling cascades in the gut epithelium. *Gut*.
 46. Kim, H.J., Huh, D., Hamilton, G., and Ingber, D.E. (2012). Human gut-on-a-chip inhabited by microbial flora that experiences intestinal peristalsis-like motions and flow. *Lab. Chip* 12, 2165–2174.
 47. Kim, H.J., Li, H., Collins, J.J., and Ingber, D.E. (2016a). Contributions of microbiome and mechanical deformation to intestinal bacterial overgrowth and inflammation in a human gut-on-a-chip. *Proc. Natl. Acad. Sci. U. S. A.* 113, E7–E15.

48. Kim, H.J., Li, H., Collins, J.J., and Ingber, D.E. (2016b). Contributions of microbiome and mechanical deformation to intestinal bacterial overgrowth and inflammation in a human gut-on-a-chip. *Proc. Natl. Acad. Sci. U. S. A.* 113, E7–E15.
49. Kim, J., Koo, B.-K., and Knoblich, J.A. (2020). Human organoids: model systems for human biology and medicine. *Nat. Rev. Mol. Cell Biol.* 1–14.
50. Kim, R., Attayek, P.J., Wang, Y., Furtado, K.L., Tamayo, R., Sims, C.E., and Allbritton, N.L. (2019). An in vitro intestinal platform with a self-sustaining oxygen gradient to study the human gut/microbiome interface. *Biofabrication* 12, 015006.
51. Koestler, B.J., Ward, C.M., Fisher, C.R., Rajan, A., Maresso, A.W., and Payne, S.M. (2019). Human Intestinal Enteroids as a Model System of Shigella Pathogenesis. *Infect. Immun.* 87.
52. Lamers, M.M., Beumer, J., Vaart, J. van der, Knoop, K., Puschhof, J., Breugem, T.I., Ravelli, R.B.G., Schayck, J.P. van, Mykytyn, A.Z., Duimel, H.Q., et al. (2020). SARS-CoV-2 productively infects human gut enterocytes. *Science* 369, 50–54.
53. Leslie, J.L., Huang, S., Opp, J.S., Nagy, M.S., Kobayashi, M., Young, V.B., and Spence, J.R. (2015). Persistence and Toxin Production by Clostridium difficile within Human Intestinal Organoids Result in Disruption of Epithelial Paracellular Barrier Function. *Infect. Immun.* 83, 138–145.
54. Lindemans, C.A., Calafiore, M., Mertelmann, A.M., O'Connor, M.H., Dudakov, J.A., Jenq, R.R., Velardi, E., Young, L.F., Smith, O.M., Lawrence, G., et al. (2015). Interleukin-22 promotes intestinal-stem-cell-mediated epithelial regeneration. *Nature* 528, 560–564.
55. Lu, X., Xie, S., Ye, L., Zhu, L., and Yu, Q. (2020). Lactobacillus Protects Against S. Typhimurium-Induced Intestinal Inflammation by Determining the Fate of Epithelial Proliferation and Differentiation. *Mol. Nutr. Food Res.* 64, 1900655.
56. Lukovac, S., Belzer, C., Pellis, L., Keijser, B.J., de Vos, W.M., Montijn, R.C., and Roeselers, G. (2014). Differential Modulation by Akkermansia muciniphila and Faecalibacterium prausnitzii of Host Peripheral Lipid Metabolism and Histone Acetylation in Mouse Gut Organoids. *MBio* 5.
57. Martini, E., Krug, S.M., Siegmund, B., Neurath, M.F., and Becker, C. (2017). Mend Your Fences: The Epithelial Barrier and its Relationship With Mucosal Immunity in Inflammatory Bowel Disease. *Cell. Mol. Gastroenterol. Hepatol.* 4, 33–46.
58. Marzorati, M., Vanhoecke, B., De Ryck, T., Sadaghian Sadabad, M., Pinheiro, I., Possemiers, S., Van den Abbeele, P., Derycke, L., Bracke, M., Pieters, J., et al. (2014). The HMITM module: a new tool to study the Host-Microbiota Interaction in the human gastrointestinal tract in vitro. *BMC Microbiol.* 14, 133.
59. Maurer, M., Gresnigt, M.S., Last, A., Wollny, T., Berlinghof, F., Pospich, R., Cseresnyes, Z., Medyukhina, A., Graf, K., Gröger, M., et al. (2019). A three-dimensional immunocompetent intestine-on-chip model as in vitro platform for functional and microbial interaction studies. *Biomaterials* 220, 119396.
60. McCracken, K.W., Catá, E.M., Crawford, C.M., Sinagoga, K.L., Schumacher, M., Rockich, B.E., Tsai, Y.-H., Mayhew, C.N., Spence, J.R., Zavros, Y., et al. (2014). Modelling human development and disease in pluripotent stem-cell-derived gastric organoids. *Nature* 516, 400–404.
61. Múnera, J.O., Sundaram, N., Rankin, S.A., Hill, D., Watson, C., Mahe, M., Vallance, J.E., Shroyer, N.F., Sinagoga, K.L., Zarzoso-Lacoste, A., et al. (2017). Differentiation of Human Pluripotent Stem Cells into Colonic Organoids via Transient Activation of BMP Signaling. *Cell Stem Cell* 21, 51–64.e6.
62. Nagashima, K., Sawa, S., Nitta, T., Tsutsumi, M., Okamura, T., Penninger, J.M., Nakashima, T., and Takayanagi, H. (2017). Identification of subepithelial mesenchymal cells that induce IgA and diversify gut microbiota. *Nat. Immunol.* 18, 675–682.
63. Naito, T., Mulet, C., Castro, C.D., Molinaro, A., Saffarian, A., Nigro, G., Bérard, M., Clerc, M., Pedersen, A.B., Sansonetti, P.J., et al. (2017). Lipopolysaccharide from Crypt-Specific Core Microbiota Modulates the Colonic Epithelial Proliferation-to-Differentiation Balance. *MBio* 8.
64. Nakamoto, N., Sasaki, N., Aoki, R., Miyamoto, K., Suda, W., Teratani, T., Suzuki, T., Koda, Y., Chu, P.-S., Taniki, N., et al. (2019). Gut pathobionts underlie intestinal barrier dysfunction and liver T helper 17 cell immune response in primary sclerosing cholangitis. *Nat. Microbiol.* 4, 492–503.
65. Naumovska, E., Aalderink, G., Wong Valencia, C., Kosim, K., Nicolas, A., Brown, S., Vulto, P., Erdmann, K.S., and Kurek, D. (2020). Direct On-Chip Differentiation of Intestinal Tubules from Induced Pluripotent Stem Cells. *Int. J. Mol. Sci.* 21.
66. Neal, M.D., Sodhi, C.P., Jia, H., Dyer, M., Egan, C.E., Yazji, I., Good, M., Afrazi, A., Marino, R., Slagle, D., et al. (2012). Toll-like Receptor 4 Is Expressed on Intestinal Stem Cells and Regulates Their Proliferation and Apoptosis via the p53 Up-regulated Modulator of Apoptosis. *J. Biol. Chem.* 287, 37296–37308.
67. Nikolaev, M., Mitrofanova, O., Brogiere, N., Geraldo, S., Dutta, D., Tabata, Y., Elci, B., Brandenburg, N., Kolotuev, I., Gjorevski, N., et al. (2020). Homeostatic mini-intestines through scaffold-guided organoid morphogenesis. *Nature* 585, 574–578.
68. Noel, G., Baetz, N.W., Staab, J.F., Donowitz, M., Kovbasnjuk, O., Pasetti, M.F., and Zchos, N.C. (2017). A primary human macrophage-enteroid co-culture model to investigate mucosal gut physiology and host-pathogen interactions. *Sci. Rep.* 7.
69. Nougayrede, J.-P. (2006). Escherichia coli Induces DNA Double-Strand Breaks in Eukaryotic Cells. *Science* 313, 848–851.
70. Okkelman, I.A., Neto, N., Papkovsky, D.B., Monaghan, M.G., and Dmitriev, R.I. (2019). A deeper understanding of intestinal organoid metabolism revealed by combining fluorescence lifetime imaging microscopy (FLIM) and extracellular flux analyses. *Redox Biol.* 30.
71. Oliphant, K., Cochrane, K., Schroeter, K., Daigneault, M.C., Yen, S., Verdu, E.F., and Allen-Vercoe, E. (2020). Effects of Antibiotic Pretreatment of an Ulcerative Colitis-Derived Fecal Microbial Community on the Integration of Therapeutic Bacteria In Vitro. *MSystems* 5.
72. Pleguezuelos-Manzano, C., Puschhof, J., Rosendahl Huber, A., van Hoeck, A., Wood, H.M., Nomburg, J., Gurjao, C., Manders, F., Dalmasso, G., Stege, P.B., et al. (2020). Mutational signature in colorectal cancer caused by genotoxic pks+ E. coli. *Nature* 580, 269–273.
73. Qin, Y., and Wade, P.A. (2018). Crosstalk between the microbiome and epigenome: messages from bugs. *J. Biochem. (Tokyo)* 163, 105–112.
74. Ranganathan, S., Doucet, M., Grassel, C.L., Delaine-Elias, B., Zachos, N.C., and Barry, E.M. (2019). Evaluating Shigella flexneri Pathogenesis in the Human Enteroid Model. *Infect. Immun.* 87.
75. Round, J.L., and Mazmanian, S.K. (2009). The gut microbiome shapes intestinal immune responses during health and disease. *Nat. Rev. Immunol.* 9, 313–323.
76. Rubinstein, M.R., Wang, X., Liu, W., Hao, Y., Cai, G., and Han, Y.W. (2013). Fusobacterium nucleatum Promotes Colorectal Carcinogenesis by Modulating E-Cadherin/Catenin Signaling via its FadA Adhesin. *Cell Host Microbe* 14, 195–206.
77. Sachs, N., Pappasypoulos, A., Zomer-van Ommen, D.D., Heo, I., Böttinger, L., Klay, D., Weeber, F., Huelsz-Prince, G., Iakobachvili, N., Amatngalim, G.D., et al. (2019). Long-term expanding human airway organoids for disease modeling. *EMBO J.* 38.
78. Sambuy, Y., De Angelis, I., Ranaldi, G., Scarino, M.L., Stammati, A., and Zucco, F. (2005). The Caco-2 cell line as a model of the intestinal barrier: influence of cell and culture-related factors on Caco-2 cell functional characteristics. *Cell Biol. Toxicol.* 21, 1–26.
79. Sarrabayrouse, G., Landolfi, S., Pozuelo, M., Willamil, J., Varela, E., Clark, A., Campos, D., Herrera, C., Santiago, A., Machiels, K., et al. (2020). Mucosal microbial load in Crohn's disease: A potential predictor of response to faecal microbiota transplantation. *EBioMedicine* 51.
80. Sasaki, N., Miyamoto, K., Maslowski, K.M., Ohno, H., Kanai, T., and Sato, T. (2020). Development of a Scalable Coculture System for Gut Anaerobes and Human Colon Epithelium. *Gastroenterology* 159, 388–390.e5.

81. Sato, T., Stange, D.E., Ferrante, M., Vries, R.G.J., Van Es, J.H., Van Den Brink, S., Van Houdt, W.J., Pronk, A., Van Gorp, J., Siersema, P.D., et al. (2011). Long-term expansion of epithelial organoids from human colon, adenoma, adenocarcinoma, and Barrett's epithelium. *Gastroenterology* 141, 1762–1772.
82. Scanu, T., Spaapen, R.M., Bakker, J.M., Pratap, C.B., Wu, L., Hofland, I., Broeks, A., Shukla, V.K., Kumar, M., Janssen, H., et al. (2015). Salmonella Manipulation of Host Signaling Pathways Provokes Cellular Transformation Associated with Gallbladder Carcinoma. *Cell Host Microbe* 17, 763–774.
83. Shah, P., Fritz, J.V., Glaab, E., Desai, M.S., Greenhalgh, K., Frachet, A., Niegowska, M., Estes, M., Jäger, C., Seguin-Devaux, C., et al. (2016). A microfluidics-based in vitro model of the gastrointestinal human-microbe interface. *Nat. Commun.* 7, 11535.
84. Shin, W., and Kim, H.J. (2018). Intestinal barrier dysfunction orchestrates the onset of inflammatory host-microbiome crosstalk in a human gut inflammation-on-a-chip. *Proc. Natl. Acad. Sci. U. S. A.* 115, E10539–E10547.
85. Spence, J.R., Mayhew, C.N., Rankin, S.A., Kuhar, M., Vallance, J.E., Tolle, K., Hoskins, E.E., Kalinichenko, V.V., Wells, S.I., Zorn, A.M., et al. (2011). Directed differentiation of human pluripotent stem cells into intestinal tissue in vitro. *Nature* 470, 105–109.
86. Stubbendieck, R.M., Vargas-Bautista, C., and Straight, P.D. (2016). Bacterial Communities: Interactions to Scale. *Front. Microbiol.* 7.
87. Tao, L., Zhang, J., Meraner, P., Tovaglieri, A., Wu, X., Gerhard, R., Zhang, X., Stallcup, W.B., Miao, J., He, X., et al. (2016). Frizzled are colonic epithelial receptors for *Clostridium difficile* toxin B. *Nature* 538, 350–355.
88. Van den Abbeele, P., Grootaert, C., Marzorati, M., Possemiers, S., Verstraete, W., Gérard, P., Rabot, S., Bruneau, A., El Aidy, S., Derrien, M., et al. (2010). Microbial Community Development in a Dynamic Gut Model Is Reproducible, Colon Region Specific, and Selective for Bacteroidetes and *Clostridium* Cluster IX. *Appl. Environ. Microbiol.* 76, 5237–5246.
89. Walter, J., Armet, A.M., Finlay, B.B., and Shanahan, F. (2020). Establishing or Exaggerating Causality for the Gut Microbiome: Lessons from Human Microbiota-Associated Rodents. *Cell* 180, 221–232.
90. Wilding, J.L., and Bodmer, W.F. (2014). Cancer cell lines for drug discovery and development. *Cancer Res.* 74, 2377–2384.
91. Wilke, G., Funkhouser-Jones, L.J., Wang, Y., Ravindran, S., Wang, Q., Beatty, W.L., Baldridge, M.T., VanDussen, K.L., Shen, B., Kuhlenschmidt, M.S., et al. (2019). A Stem-Cell-Derived Platform Enables Complete *Cryptosporidium* Development In Vitro and Genetic Tractability. *Cell Host Microbe* 26, 123–134.e8.
92. Williamson, I.A., Arnold, J.W., Samsa, L.A., Gaynor, L., DiSalvo, M., Cocchiari, J.L., Carroll, I., Azcarate-Peril, M.A., Rawls, J.F., Allbritton, N.L., et al. (2018). A High-Throughput Organoid Microinjection Platform to Study Gastrointestinal Microbiota and Luminal Physiology. *Cell. Mol. Gastroenterol. Hepatol.* 6, 301–319.
93. Workman, M.J., Gleeson, J.P., Troisi, E.J., Estrada, H.Q., Kerns, S.J., Hinojosa, C.D., Hamilton, G.A., Targan, S.R., Svendsen, C.N., and Barrett, R.J. (2017). Enhanced Utilization of Induced Pluripotent Stem Cell-Derived Human Intestinal Organoids Using Microengineered Chips. *Cell. Mol. Gastroenterol. Hepatol.* 5, 669–677.e2.
94. Yin, Y., Bijvelds, M., Dang, W., Xu, L., van der Eijk, A.A., Knipping, K., Tuysuz, N., Dekkers, J.F., Wang, Y., de Jonge, J., et al. (2015). Modeling rotavirus infection and antiviral therapy using primary intestinal organoids. *Antiviral Res.* 123, 120–131.
95. Yu, T.C., Guo, F., Yu, Y., Sun, T., Ma, D., Han, J., Qian, Y., Kryczek, I., Sun, D., Nagarsheth, N., et al. (2017). *Fusobacterium nucleatum* Promotes Chemoresistance to Colorectal Cancer by Modulating Autophagy. *Cell* 170, 548–563.e16.
96. Zhang, Y., Wu, S., Xia, Y., and Sun, J. (2014). Salmonella-infected crypt-derived intestinal organoid culture system for host-bacterial interactions. *Physiol. Rep.* 2.
97. Zheng, L., Kelly, C.J., and Colgan, S.P. (2015). Physiologic hypoxia and oxygen homeostasis in the healthy intestine. A Review in the Theme: Cellular Responses to Hypoxia. *Am. J. Physiol. - Cell Physiol.* 309, C350–C360.
98. Zhou, J., Li, C., Zhao, G., Chu, H., Wang, D., Yan, H.H.-N., Poon, V.K.-M., Wen, L., Wong, B.H.-Y., Zhao, X., et al. (2017). Human intestinal tract serves as an alternative infection route for Middle East respiratory syndrome coronavirus. *Sci. Adv.* 3.
99. Zhou, J., Li, C., Liu, X., Chiu, M.C., Zhao, X., Wang, D., Wei, Y., Lee, A., Zhang, A.J., Chu, H., et al. (2020). Infection of bat and human intestinal organoids by SARS-CoV-2. *Nat. Med.* 26, 1077–1083.
100. Zimmermann, M., Zimmermann-Kogadeeva, M., Wegmann, R., and Goodman, A.L. (2019). Mapping human microbiome drug metabolism by gut bacteria and their genes. *Nature* 570, 462–467.

3

ESTABLISHMENT AND CULTURE OF HUMAN INTESTINAL ORGANOIDS DERIVED FROM ADULT STEM CELLS

Cayetano Pleguezuelos-Manzano^{1,2,4}, Jens Puschhof^{1,2,4}, Stieneke van den Brink^{1,2},
Veerle Geurts^{1,2}, Joep Beumer^{1,2}, Hans Clevers^{1,2,3}

¹Hubrecht Institute, Royal Netherlands Academy of Arts and Sciences (KNAW) and UMC Utrecht,
Utrecht, The Netherlands. ²Oncode Institute, Utrecht, The Netherlands. ³The Princess Maxima
Center for Pediatric Oncology, Utrecht, The Netherlands.
⁴These authors contributed equally to this work.

ABSTRACT

Human intestinal organoids derived from adult stem cells (ASC) are miniature *ex vivo* versions of the human intestinal epithelium. Intestinal organoids are useful tools for the study of intestinal physiology as well as many disease conditions. Human ASC-derived organoids present numerous advantages compared to the use of immortalized cell lines; however, working with organoids requires the use of dedicated techniques. The protocols described in this unit provide a basic guide to the establishment and maintenance of human intestinal organoids derived from small intestine and colon biopsies. Additionally, we provide an overview on several downstream applications of human intestinal organoids.

KEYWORDS

Adult stem cells, human intestinal organoids, organoid culture establishment, organoid passage, organoid cryopreservation, organoid immunofluorescence, organoid differentiation, specialized organoid reagents, single-cell clonal organoid culture.

INTRODUCTION

Adult stem cell-derived organoids are miniature versions of epithelia that grow in 3D and can be expanded *ex vivo*. These mini-organs are derived from tissue biopsies and are entirely composed of primary epithelial cells, relying on the ability of the adult stem cells to expand indefinitely. They permit studying epithelial physiology in a setup that closely resembles the *in vivo* situation. In contrast to animal models, adult stem cell organoids allow to examine direct interactions between different cell types in a reductionist approach. Since they can also be derived from humans, adult stem cell organoids capture the specific characteristics of human tissues. All these characteristics make them a powerful tool (Clevers, 2016).

Since organoids retain the characteristics of the native tissue they are derived from, human intestinal organoids have been useful in the study of intestinal epithelial physiology and stem cell differentiation dynamics (Farin et al., 2016 (mouse), Beumer et al., 2020 (human)). Additionally, human intestinal organoids have been used to study human disease (Fujii et al., 2019), usually following three approaches: 1) disease modeling by establishing organoid lines from monogenic disease patients, e.g., from cystic fibrosis (*CFTR*; Dekkers et al., 2013), multiple intestinal atresia (*TTC7A*, Bigorgne et al., 2014), congenital diarrheal disorders (*DGAT1*; van Rijn et al., 2018). By repairing these mutations using CRISPR/Cas9-based genetic engineering in the patient-derived organoids, this technology might be used in future regenerative medicine approaches (Schwank et al., 2013; Geurts et al., 2020). 2) The introduction of mutations, again using CRISPR/Cas9 technologies, in healthy organoids allows molecular studies of different diseases such as cancer (Drost et al., 2015). 3) Establishment of tumor and matched healthy organoid lines from colorectal cancer patients for treatment response and tumor heterogeneity studies (van de Wetering et al., 2015, Drost & Clevers, 2018). Furthermore, organoids have proven to be valuable tools to study mutagenic processes in human physiology and disease (Blokzijl et al., 2016; Christensen et al., 2019; Pleguezuelos-Manzano et al., 2020).

The human intestinal epithelium functions as a physical barrier that separates the internal and the external face of the intestinal tract. Because of this, the intestinal epithelium is in constant interplay with the immune environment. This interplay is of high importance for the maintenance of a homeostatic state and its imbalance is often linked to disease. For this reason, human intestinal organoids have emerged as a great tool to study the functioning of this epithelium and its relations with the immune component in disease (Bar-Ephraim et al., 2019), like celiac disease (Freire et al., 2019; Dieterich et al., 2020) and ulcerative colitis (Nanki et al., 2020) among others. Besides, human intestinal organoids can be useful in cancer immunotherapy research (Dijkstra et al., 2018).

This article describes how to establish human organoid cultures from human small intestine or colon biopsies (Basic Protocol 1) and the methods for their subsequent expansion *ex vivo* (Basic Protocol 2). Alternate Protocol 1 focuses on how to differentiate expanding intestinal organoids, predominantly composed of stem and transit amplifying

cells, towards a more mature cell type composition (enterocytes, enteroendocrine cells (EECs) or goblet cells). The production of some essential medium components (Wnt3A- and Rspo1-conditioned media (CM)) is detailed in Support protocols 1 and 2. Organoid cryopreservation and thawing is discussed in Basic Protocol 3. Then, several methods are included exemplifying how to perform some of the most common downstream applications/readouts with organoids. Basic Protocol 4 describes how to perform the basic steps immunofluorescence staining for fluorescence/confocal imaging. In light of the increasing importance of CRISPR/Cas9 engineered organoids and whole-genome sequencing (WGS) of organoid lines, a protocol for single-cell clonal outgrowth of intestinal organoids, which is of key importance for both applications, is described (Basic Protocol 5). These protocols are supplemented by a method to extract organoid RNA that can be used for gene expression readouts like quantitative real-time PCR or RNA sequencing (Support Protocol 3).

STRATEGIC PLANNING

Organoid lines can be either established from biopsies (Basic Protocol 1) or obtained from a biobank or the research community. From biopsies, organoids can normally be derived in sufficient quantities for extensive experimentation and storage within a month. Established lines can be shipped on dry ice and can be used for experiments 1-2 weeks after thawing. Single nucleotide polymorphism fingerprinting or comparable methods should be used to confirm line identity over time. Mycoplasma tests should be performed regularly analogous to cell lines. The use of patient-derived material should in all cases comply with the ethical regulations and guidelines of the relevant institutional boards. Written informed consent is required from all donors.

General Considerations

Human organoid lines present some degree of heterogeneity due to inter and intra donor variability. Particularly, the expansion ability or stemness of some lines is higher than others and this usually inversely correlates with their ability to achieve full differentiation. This should be taken into consideration when selecting a pre-established organoid line for an experiment or when characterizing a newly established organoid line. Furthermore, there are also some differences in organoids derived from different regions of the intestinal tract, reflecting the intrinsic differences between these epithelial regions *in vivo*. Generally, duodenum organoids are showing a higher stemness *ex vivo* compared to the other regions and therefore are easier to expand. A key factor to organoid culture expansion is activation of the Wnt pathway. To achieve this, two different Wnt sources (Wnt3A-CM (Support Protocol 1 and Reagents and Solutions) and Wnt Surrogate molecules (Reagents and Solutions) have been successfully applied. Wnt3A-CM is a more economical source of Wnt ligands; however, it shows a lower level of Wnt activation and may suffer from batch-to-batch variability. In contrast, synthetic Wnt surrogate can achieve a high activation of

the Wnt pathway fueling faster organoid expansion in some organoid systems. The use of Wnt surrogate is recommended especially for human colon organoid cultures and when growing single-cell clonal cultures.

Preparations and considerations before starting the organoid work

Basement membrane extract (BME) should be thawed overnight at 4°C before starting any of the protocols described. Subsequently, BME should be kept at 4°C at every moment. Freeze-thaw cycles of BME are not recommended. Multiwell cell culture plates should be prewarmed at 37°C for several hours before using them for organoid culture. This will help the liquid BME-organoid solution to solidify on the culture plate.

General consumable and equipment used for organoid culture

General consumables include sterile 1.5, 15 and 50 mL plastic tubes, Cell Culture Multiwell Plates, suspension culture quality, different well formats (Greiner bio-one, cat. no. 657 185 (6 wells), 665 102 (12 wells), 662 102 (24 wells), 677 102 (48 wells)). P1000, P200 and P20 micropipettes and serological pipettes. General equipment includes a Class II biosafety cabinet, centrifuge, microcentrifuge, inverted light microscope and 5% CO₂ incubator at 37°C.

BASIC PROTOCOL 1

Establishment of human small intestine and colon organoid cultures from fresh biopsies

INTRODUCTION

This protocol describes a method for the establishment of human intestinal adult stem cell-derived organoids cultures from healthy small intestine or colon fresh biopsies. Tissue is dissociated into small epithelial fragments that are embedded into extracellular matrix domes and supplemented with medium containing growth factors for organoid expansion.

MATERIALS

- Fresh tissue biopsy from human small intestine or colon, healthy or tumor tissue (use 30 mg of tissue for optimal organoid line establishment)
- AdvDMEM+++ (See Reagents and Solutions)
- Intestinal expansion medium (See Reagents and Solutions)
- Cultrex reduced growth factor basement membrane extract (BME), type 2, Pathclear (R&D Systems / Bio-techne, cat. no. 3533-001)
- Digestion Medium (See Reagents and Solutions)
- Y-27632 Rho kinase inhibitor (RhoKi) (Abmole, cat. no. Y-27632)
- Red blood cell lysis solution (Gibco cat. no. A1049201)

- Primocin (InvivoGen, cat. no. ant-pm-1)
- Collagenase type II (Sigma Aldrich, cat. no. C9407-1)
- Sterile glass Pasteur pipettes (VWR, cat. no. 14673-010)
- Disposable scalpels (VWR, cat. no. HERE1110810)
- Cell strainer 100 μm (Green Bioresearch, cat. no. 542000)
- Parafilm (Sigma Aldrich, cat. no. P7793-1EA)
- Orbital shaker
- Vortex mixer

PROTOCOL

1. Collect the tissue sample from the tissue sample source site. The tissue should be collected in a 50 mL Falcon tube containing 25 mL AdvDMEM+++ and 100 $\mu\text{g}/\text{mL}$ Primocin. Keep the tissue at 4°C until further use.
Small intestine and colon biopsies are both suited organoid culture sources. Organoids maintain region-specific characteristics and it is not recommended to pool biopsies from different intestinal regions or donors. In the case of CRC biopsies, it is recommended to collect a paired normal sample from surrounding healthy tissue.
It is recommended to isolate the tissue within 24 h after surgery for increased efficiency. Avoid freezing of tissue, as this will result in cell death.
2. Start-up the biosafety cabinet, disinfect the work area surface and pipets by spraying with 70% ethanol and allow to air dry.
3. Prepare fresh digestion medium for each tissue sample. Aliquot 5 mL AdvDMEM+++ into a 15 mL plastic tube and add 5 mg/mL collagenase Type II and 10 μM RhoKi. Mix by inverting and store on ice until further use.
4. Transfer the tissue to a 10 cm Petri dish.
Optionally, excise out a tissue piece and place it into a cryovial. Snap-freeze and store in liquid nitrogen for additional DNA/RNA analysis and/or fix the tissue for histology.
5. Mince the tissue using two scalpels, into small pieces of approximately 1 mm³. Add 5 mL of digestion medium and mix the tissue pieces by pipetting. Transfer digestion medium with tissue into a 15 mL plastic tube. Rinse with digestion medium from the same Falcon tube and transfer all the tissue pieces into the 1.5 mL plastic tube.
6. Seal the lid of the plastic tube with parafilm.
7. Place the Falcon tube under with a low angle on an orbital shaker. Digest the tissue for 30 to 45 min at 37°C and 140 rpm.
Check the turbidity of the solution regularly. If the tissue is dissociated (typically after ~30 min of incubation) the solution will look turbid without any large clumps.
8. Place a 100 μm cell strainer into a 50 mL plastic tube.

9. Pipet the digested tissue onto the 100 μm filter. With the help of a 5 mL pipet, pass the cell suspension through the filter. Large tissue pieces will be retained on the filter.
10. Rinse the strainer with 5 mL AdvDMEM+++ and collect the washing in the 50 mL plastic tube.
11. Transfer the solution (a total of 10 mL) back to a 15 mL plastic tube.
12. Centrifuge at 450xg for 5 min, 4°C. Aspirate the supernatant.
If red blood cells are present (observed as a dark red pellet), resuspend the pellet in 3 ml of red blood cell lysis buffer and incubate it for 5 min at room temperature. After incubation, add 5 ml AdvDMEM+++ to the cell solution and centrifuge at 450xg for 5 min, 4°C. Aspirate the supernatant.
13. Wash the cell pellet 3 times by adding 10 mL of AdvDMEM+++ , each time spinning at 450xg for 5 min, 4°C. Aspirate the supernatant.
14. Resuspend the cell pellet in undiluted BME.
The volume of BME depends on the pellet size. Usually, a cell pellet obtained from approximately 30 mg of primary tissue is plated in 300 μL BME. Cells plated at the right density have enhanced efficiency of organoid culture establishment, while too dense plating will result in increased cell death at the core of the dome.
15. Plate 50 μL BME with cells as multiple droplets of ~15 μL in a pre-warmed 24-well cell culture plate.
16. Turn the plate upside-down and place it in the 37°C cell culture incubator. Allow the droplets to solidify for 20 min.
17. Add 500 μL organoid medium supplemented with 10 μM RhoKi carefully to each well and put the plate back into the incubator (Fig. 1).
If establishing tumor lines, use organoid medium depleted of Wnt3A-CM or Wnt surrogate. In this way, tumor cells with acquired Wnt pathway independence will be selected in culture. Organoids should be incubated for approximately one week before they grow out and can be expanded following Basic Protocol 2. Because of the inherent donor-to-donor variability of organoid cultures this time frame should be adjusted accordingly. Use Figure 1 as a reference for estimating the adequate moment to perform the first split and expansion of the organoids.

BASIC PROTOCOL 2

Human intestinal organoids mechanical split, passage and culture expansion

INTRODUCTION

This protocol illustrates the process of mechanical split and passage of human small intestinal and colon organoids. Due to the high similarity of these two organoid types the protocol is similar in both cases. In short, organoids are recovered from the basement membrane matrix and broken mechanically into smaller fragments. These fragments

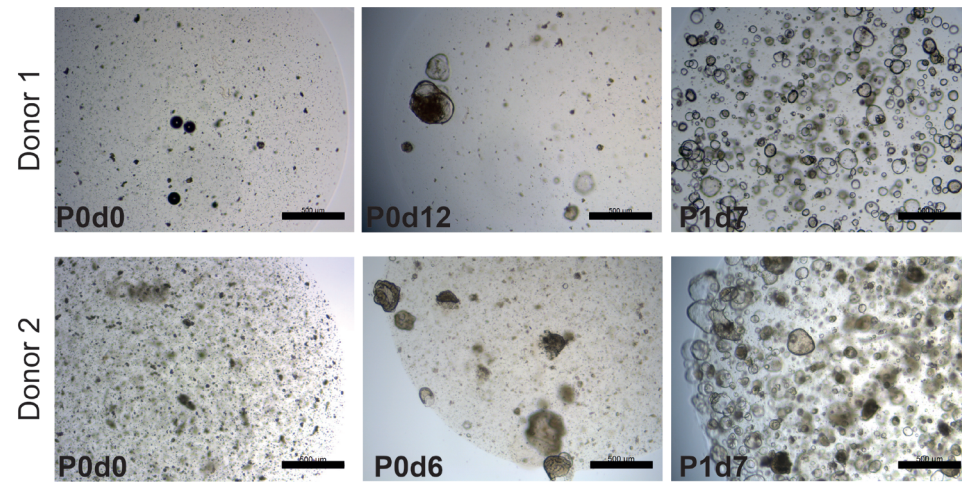


Figure 1. Establishment of human colon organoid lines from fresh biopsy of normal tissue. Representative images from two organoid lines. Cells are shown after establishment of cultures (left), before the first split (middle), and after the first split (right). P indicates passage number; d indicates days after seeding or passage; scale bars, 0.5 mm.

are resuspended in fresh BME and replated in culture plates. They will self-assemble as new organoids and the stem cells and transit amplifying present in them will continue to proliferate, giving rise to a fully grown expanded organoid culture (Fig. 2a).

MATERIALS

- Established human intestinal organoid culture; 1 well of a 12-well culture plate (From Basic Protocol 1, step 17 if first passage, or from Basic Protocol 2, step 8 if later passage)
- AdvDMEM+++ (see recipe in Reagents and Solutions)
- Cultrex reduced growth factor basement membrane extract (BME), type 2, Pathclear (R&D Systems / Bio-technie, cat. no. 3533-001)
- Intestinal organoid medium (see Reagents and Solutions)
- Sterile plugged Pasteur glass pipette (VWR®, cat. no. 14672-400)
- Sterile 10 μ L pipette tips
- Bunsen burner

PROTOCOL

1. Starting with 1 well of a 12-well plate culture of established human intestinal organoid culture, remove the medium from the culture well.
The process can be scaled up or down using different cell culture plate formats. For a guide to other formats see Table 1.

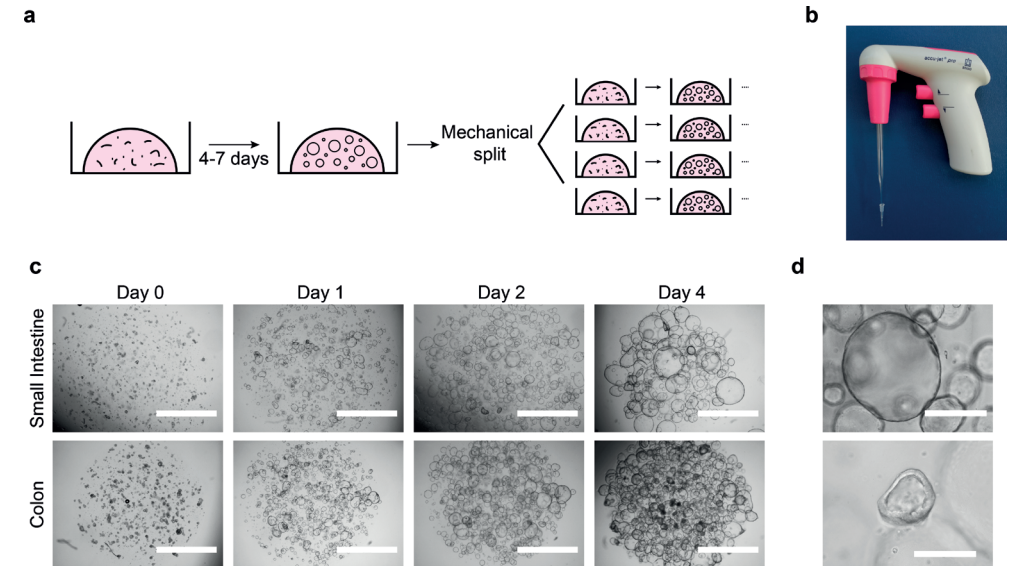


Figure 2. Mechanical splitting and expansion of human intestinal organoids. **a**, Schematic of culture procedure. **b**, Glass Pasteur pipette connected to a 10- μ l tip used for mechanical disruption of organoids. **c**, Representative bright-field microscopy images of organoid cultures at days 0, 1, 2, and 4 after mechanical split. Scale bars, 2 mm. **d**, Examples of a healthy organoid (top), composed mostly of stem/transit amplifying cells, and a suboptimal organoid (bottom), with signs of differentiation (thickening of wall). Scale bars, 0.4 mm.

Table 1. Reference BME volume used in different well-plate formats

Plate format	BME volume/well (μ L)	Domes/well	Culture medium/well (mL)
6-well plate	200	10-15	2
12-well plate	100	5-7	1
24-well plate	50	1-3	0.5
48-well plate	25	1	0.25
96-well plate	5-10	1	0.1

2. Flush and collect the organoids from the well with 1 mL of ice-cold AdvDMEM+++ in order to disrupt the BME droplets using a P1000 pipette. Collect the organoids in a 15 mL plastic tube containing 4 mL of ice-cold AdvDMEM+++.
3. Spin down the organoids 5 min at 450xg, 4°C
4. Remove supernatant.
Often in this step, undissolved BME accumulates over the organoid pellet as a cloudy mesh. It is important to remove as much BME as possible without taking the organoids. If organoids did not separate from the BME, resuspend the pellet

with the BME mesh in the AdvDMEM+++ and incubate in ice for 10 min to help for BME dissociation. Then repeat step 3.

- Resuspend the pellet in 1 mL of ice-cold AdvDMEM+++ with a P1000 pipette. Subsequently, take a glass pipette and plug to its tip a sterile 10 μ L pipette tip (Fig. 2b). Pass the organoids through the pipette opening for 5-10 times until large clumps are no longer visible. Add 4 mL of ice-cold AdvDMEM+++ and spin down 5 min at 450xg, 4°C. Remove supernatant.

Foam formation at this step usually leads to loss of cells in the process. To avoid this, pipette the cell solution against the middle part of the tube wall.

Alternatively, mechanical disruption can be done with a fire-polished glass pipette, with the tip narrowed down to a diameter of ~0.5-1 mm using a Bunsen burner.

- Resuspend the cell pellet in 300-400 μ L BME using a P1000 pipette. Dispense ~15 μ L per dome, 100 μ L per well of a 12-well cell culture suspension plate (Fig. 2c). See Table 1 for detailed BME dome number and volume per well in different plate formats

Some residual AdvDMEM+++ is acceptable in the resuspension step, but the final BME concentration should be 75-100%.

Usually, the split ratio of a fully grown culture is 1:3-1:4 (of BME volume). Volume and domes per well are indicated in Table 1.

Avoid bubble formation when resuspending the cell pellet in BME as this will render the BME droplet unstable and lead to its disruption before splitting time.

- Flip the plate upside down, and let the domes solidify by placing the plate in the incubator for 20 min.

By doing this, organoids spread over the volume of the BME, locating closer to the dome surface. In this way, nutrients exchange is maximized and organoid attachment to the plate surface is minimized.

- Add complete intestinal organoid medium and keep in the incubator at 37°C and 5% CO₂. Refresh the medium every 2-3 days. After 7 days, organoids can be further expanded by repeating this protocol (Fig. 2a, c).

Under these conditions, organoids containing proliferating stem cells should look cystic with a thin wall (Fig. 2d, upper panel). If organoids in culture look dense and with a thick wall, they show signs of cell differentiation (Fig. 2d, lower panel) which will lead to loss of the cultures.

Due to donor-to-donor variability, the time required for a human intestinal organoid culture to reach confluence varies among organoid lines. 7 days is a standard estimation, and the definite expansion time should be empirically determined for each individual line. Too early passage will result in increased materials cost and suboptimal expansion speed. Too late passage may result in spontaneously differentiating organoids, decreased cell viability and suboptimal expansion.

ALTERNATE PROTOCOL 1

Human intestinal organoid differentiation protocol

INTRODUCTION

This protocol describes ways to differentiate organoids to the various cell types of the small intestinal and colonic epithelium. By withdrawing growth factors, which enforce a stem cell state in the expansion medium, and adding components, which skew differentiation trajectories, different types and ratios of mature can be obtained within 5 days. These mature cell types can be used for functional studies of the human gut epithelium.

ADDITIONAL MATERIALS

- Established human intestinal organoid culture; 1 well of a 12-well culture plate (From Basic Protocol 2, step 8)
- AdvDMEM+++ (see recipe in Reagents and Solutions)
- Cultrex reduced growth factor basement membrane extract (BME), type 2, Pathclear (R&D Systems / Bio-techne, cat. no. 3533-001)
- Intestinal differentiation medium (see Reagents and Solutions)
- Sterile plugged Pasteur glass pipette (VWR®, cat. no. 14672-400)
- Sterile 10 μ L pipette tips
- Bunsen burner

PROTOCOL

- Starting with established organoid culture, aspirate the medium from the culture well. Let organoids grow until an average size of 100 μ m, usually 5 days after mechanical split. Smaller organoids are sensitive to some of the small molecules used for differentiation at later steps.
- Add 1 mL of pre-warmed AdvDMEM+++ to the culture well. Incubate for at least 15 min in a 37°C incubator at 5% CO₂ to allow for diffusion of growth factors from the BME domes. If larger domes than 15 μ L are used, the incubation time has to be extended to allow proper diffusion of growth factors.
- Aspirate AdvDMEM+++ from the culture well.
- Add 1 mL of pre-warmed differentiation medium (see Table 2 for different differentiation media and expected cell type composition) per well of a 12-well plate. Move to a 37°C incubator at 5% CO₂.
- Refresh differentiation medium the next day to wash away any growth factors which may have been carried over inside the BME domes.
- Refresh differentiation medium every 2-3 days. As organoids differentiate, some cells undergo apoptosis and are shed to the organoid lumen. Together with more granular differentiated cells, this

results in a darker appearance of the organoids, with thicker organoid walls and debris accumulation in the organoid lumen. This can be used as an indicator of differentiation progress (Fig. 3a, b).

- After 5-7 days, fully differentiated cells will be present in the organoids and at this point organoids should be used for downstream assays.

Organoid viability can decrease substantially within days after terminal differentiation, so assays should be performed as early as possible for optimal results.

BASIC PROTOCOL 3

Human intestinal organoids cryopreservation and thawing protocol INTRODUCTION

This protocol details the steps for cryopreservation and thawing of intestinal and colon organoids. Cryopreservation is especially advisable to store organoids for years in liquid

Table 2. Intestinal differentiation media and their expected cell type compositions^{a,b}.

Medium	Reference	Expected outcome	Special considerations
ENR	(Sato et al., 2011)	Enterocytes; EECs, TACs, goblet cells	Generic differentiation medium for broad coverage of differentiated cell types, with a particular enrichment of enterocytes
ENR+Notchi	(Beumer et al., 2018)	Goblet cells	Goblet cell differentiation
ENR+MEKi+Notchi		EECs (crypt / lower villus state)	Enteroendocrine cell differentiation inducing a crypt hormone profile
ER+MEKi+Notchi+ BMP4+BMP2	(Beumer et al., 2018)	EECs (upper villus state)	Enteroendocrine cell differentiation inducing an upper villus hormone profile

^a For full media composition see Reagents and Solutions.

^b Abbreviations: BMP, bone morphogenic protein; EEC, enteroendocrine cell; ENR, EGF-Noggin-Rspo1; MEK, p38 MAP kinase; TAC, transit amplifying cell.

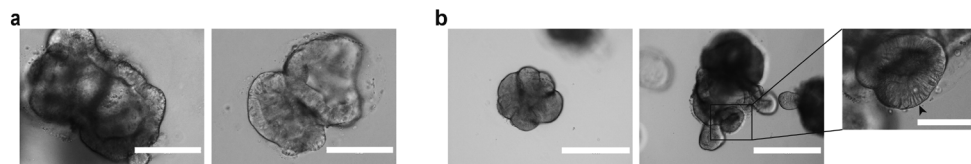


Figure 3. Differentiation of human intestinal organoids. **a**, Representative images of organoids differentiated towards the enteroendocrine cell lineage as in Beumer et al. (2020). Scale bars, 0.2 mm. **b**, Representative images of organoids differentiated towards the enterocyte lineage. Scale bars, 0.4 mm. Inset: Detail of differentiated organoid with enterocytes (elongated cells, arrowhead). Scale bar, 0.1 mm.

nitrogen, but also to ship organoid lines on dry ice. In brief, organoids are freed from the BME and resuspended in the freezing medium for cryopreservation. For re-starting the cultures, organoids are carefully thawed, washed and placed back into BME domes. Thawed organoids are anticipated to be ready for mechanical passage according to Basic Protocol 2. After one passage, organoids should have normal growth characteristics and can be used for any downstream assay.

MATERIALS

- Established human intestinal organoid culture (Basic Protocol 2, step 8); 1 well of a 12-well culture plate
- AdvDMEM+++ (see recipe in Reagents and Solutions)
- 2x freezing medium (see recipe in Reagents and Solutions)
- Cultrex reduced growth factor basement membrane extract (BME), type 2, Pathclear (R&D Systems / Bio-techne, cat. no. 3533-001)
- Intestinal expansion medium (see Reagents and Solutions)
- Cryopreservation tubes
- Freezing container
- Water bath

PROTOCOL

Freezing organoids

- For optimal recovery, small organoids in exponential growth phase should be frozen. Ideally passage organoids with thorough mechanical shearing as described in Basic Protocol 2, 2-3 days before cryopreservation.
- Starting with 1 well of a 12-well plate culture of established human intestinal organoid culture, remove the medium from the culture well.
The process can be scaled up or down using different cell culture plate formats. For a guide to other formats see Table 1.
- Flush and collect the organoids from the well with 1 mL of ice-cold AdvDMEM+++ in order to disrupt the BME droplets using a P1000 pipette. Collect the organoids in a 15 mL centrifuge tube containing 4 mL of ice-cold AdvDMEM+++.
- Spin down the organoids 5 min at 450xg, 4°C. Remove supernatant.
Often in this step, undissolved BME accumulates over the organoid pellet as a cloudy mesh. It is important to remove as much BME as possible without taking the organoids. If this is not possible, resuspend the pellet in 10 mL of ice-cold AdvDMEM+++ and incubate in ice for 10 min. Then repeat step 3.
- Resuspend the pellet in 1 volume of ice-cold AdvDMEM+++ with a P1000 pipette. Dropwise add 1 volume of 2x freezing medium under constant shaking.
Ensure slow addition of freezing medium to avoid an osmotic shock to the cells. The volumes used in this step depend on the number cryopreservation tubes to be

prepared and the organoid number per vial. For 1 densely plated well of a 12-well plate, 500 μ L AdvDMEM+++ and 500 μ L of 2x freezing medium is recommended.

6. Transfer the organoid suspension into properly labelled cryopreservation tubes. 1 mL of suspension per cryopreservation tube is recommended.
7. Place cryopreservation tubes in a freezing container and freeze at -80°C overnight. After one day, the tubes should be transferred to a liquid nitrogen container. Organoids can be stored at -80°C for several weeks and in liquid nitrogen for years without major impairments in cell viability.

Thawing organoid cryostocks

8. Starting with a cryovial containing organoids from a well of a 12-well plate, retrieve cryopreservation tubes of organoids from the liquid nitrogen and transport it to a flow cabinet on dry ice. Prepare AdvDMEM+++ and labeled 15 mL tubes while the organoids are still frozen to minimize the thawing and processing times. Delays will lead to a decreased recovery rate.
9. Thaw cryopreservation tubes in a water bath at 37°C .
10. Transfer thawed organoid suspension into a 15 mL falcon tube and dropwise add 10 mL of AdvDMEM+++ under constant shaking. Ensure slow addition of AdvDMEM+++ to avoid an osmotic shock to the cells.
11. Spin down 5 min at 450xg, 4°C . Remove supernatant.
12. Resuspend the cell pellet in 100 μ L BME per cryovial using a P200 pipette. Dispense as drops of ~ 15 μ L in a well of a 12-well cell culture suspension plate. Avoid bubble formation when resuspending the cell pellet in BME.
13. Flip the plate upside down, and let the domes solidify by placing the plate in the incubator for 20 min.
14. Add complete intestinal organoid medium and keep in the incubator at 37°C and 5% CO_2 . Refresh the medium every 2-3 days. After 7 days, organoids can be further expanded by repeating this protocol.

BASIC PROTOCOL 4

Organoid immunofluorescence staining

INTRODUCTION

This protocol describes a way to perform immunofluorescence staining compatible with fluorescence and confocal microscopy. In order to achieve this, organoids need to be released from the BME without disruption of their 3D architecture. Subsequent steps including fixation, permeabilization, blocking, staining and washes are performed with the organoids in suspension.

MATERIALS

- Established human intestinal organoid culture; 1 well of a 24-well plate (Basic Protocol 2, step 8; or after subjecting organoids to experimental conditions)
- Cell Recovery Solution (Corning, cat. no. 354253)
- Dispase (StemCell Technologies, cat. no. 07923)
- 4% Formaldehyde (v/v) in aqueous solution, buffered
- Permeabilization solution (See Reagents and Solutions)
- Blocking solution (See Reagents and Solutions)
- Mouse anti-human KI67 primary antibody (BD Pharmigen, cat. no. 550609)
- PBS
- Alexa Fluor 488 donkey anti-mouse secondary antibody (Invitrogen, cat. no. A-21202)
- Phalloidin-Atto 647N (Sigma-Aldrich, cat. no. 65906-10NMOL)
- DAPI
- Fetal Bovine Serum (FBS, Sigma-Aldrich, cat. no. F7524)
- ProLong™ Gold Antifade Mounting solution (ThermoFisher cat. no. P36934)
- Petroleum Jelly (Vaseline)
- Nail polish
- Sterile Scissors
- 1.5 mL microcentrifuge plastic tubes
- Tube roller
- Low retention 300 μ L filter tips (Greiner Bio-One, cat. no. 738 265)
- Glass bottom 96-well black plate (Greiner bio-one, cat. No. 655892)
- Microscope slides and cover slips

PROTOCOL

1. Remove and discard medium from organoid culture.
2. With sterile scissors, cut the opening of a 1000 μ L tip 2-3 mm from its end. *This is required to avoid the disruption of organoid structure while pipetting.*
3. First, coat this tip with FBS. Then, pipette 1 mL of Cell Recovery Solution to the well and collect the organoids in a 1.5 mL microcentrifuge plastic tube pre-coated with FBS.
4. Incubate on ice for 20-30 min. Invert regularly to avoid clumping and heterogeneous BME dissociation. Let the organoids sediment by gravity at the bottom of the tube and remove supernatant. *The cell recovery solution dissolves the BME, freeing the organoids without disrupting their structure. Efficient dissolution of BME is a key factor to achieve an efficient staining. Alternatively, the culture can be (pre-)incubated with dispase for 30 min at 37°C . In both cases, check regularly under the microscope for BME dissociation, and stop when BME is sufficiently dissolved. Remaining BME can result in poor staining and background signal when performing imaging of the immunostained organoids.*

5. Add 1 mL of 4% formaldehyde and incubate 16 h at 4°C under constant rolling of the tube to ensure homogeneous fixation. After this time period, let the organoids sediment by gravity and remove supernatant.
Alternatively, incubate 2h at room temperature.
Caution: Formaldehyde is a toxic compound. Avoid contact with skin and dispose of it according to the safety rules.
6. Add 1 mL of permeabilization solution and incubate under constant rolling for 30 min at 4°C. Let the organoids sediment by gravity and remove supernatant.
Permeabilization time and temperature might be optimized for particular staining.
7. Add 1 mL of blocking solution and incubate for 15 min at room temperature under constant rolling. Let the organoids sediment by gravity and remove supernatant.
8. Add 200 µL of 500 ng/mL mouse anti-human KI67 primary antibody dissolved in blocking solution and incubate for 16 h at 4°C under constant rolling of the tube to ensure homogeneous staining. Let the organoids sediment by gravity and remove the supernatant.
Important: If using a different primary antibody, optimization of the final concentration will be required.
9. Washing step. Resuspend the pellet in 1 mL of PBS. Incubate 10 min at room temperature while rolling. Let the organoids sediment by gravity and remove supernatant.
10. Repeat step 9 another 2 times.
11. Add 200 µL of 4 µg/mL Alexa Fluor 488 donkey anti-mouse secondary antibody, 10 nM of Phalloidin-Atto 647N and 2 µg/mL DAPI dissolved in blocking solution. Incubate 1-2h at room temperature while rolling, placing the samples in a dark environment to protect the fluorophores from bleaching.
Important: If using a different secondary antibody, optimization of the final concentration will be required.
12. Washing step. Resuspend the pellet in 1 mL of PBS. Incubate 10 min at room temperature while rolling. Let the organoids sediment by gravity and remove supernatant.
13. Repeat step 12 another 2 times.
14. Wash with MilliQ once to avoid crystal formation.
15. With scissors, cut the tip of a low retention 300 µL tip 2-3 mm from its end. Using this tip on a P200 pipette, coat the tip in FBS by pipetting 200 µL up and down once.
CRITICAL. The FBS coating and low binding tips minimizes the number of organoids lost due to adhesion to the plastic surface in the next step.
16. Using the coated tip, resuspend the organoids in 150-200 µL of PBS and transfer them to one well of a glass bottom 96-well black plate (Fig. 4).
It is recommended to image the samples immediately after staining procedure for optimal results.
17. *As an alternative, resuspend the organoids in 50 µL ProLong Gold mounting solution and transfer them to a microscope slide. Apply vaseline at the edges of the slide so that the cover slip doesn't disrupt organoid structure after mounting.*

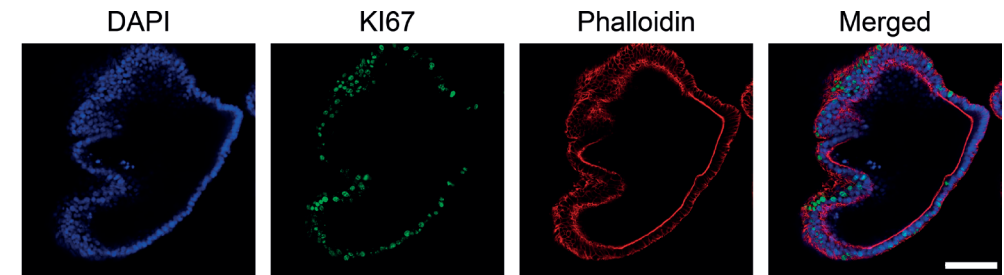


Figure 4. Confocal immunofluorescence images of human intestinal organoids cultured under expansion conditions. DAPI, nuclei; KI67, proliferation marker; phalloidin, F-actin staining. Scale bar, 0.1 mm.

Seal the slide using nail polish. This alternative mounting method allows to store the samples at 4°C, maintaining fluorescence signal for a longer period of time. Starting with small organoids will help to keep their structure intact. When starting with large and cystic organoids, organoids will more likely be disrupted during the process.

BASIC PROTOCOL 5

Single-cell clonal intestinal organoid culture generation

INTRODUCTION

Many downstream applications of organoid cultures (e.g., CRISPR/Cas9 genetic engineering, or WGS) require the generation of single cell-derived organoid clonal cultures. This protocol describes a method to efficiently generate such cultures. Initially, organoids are dissociated to single cells and seeded sparsely. After 10-15 days organoids emerge. At this point individual organoids are picked using the P20 pipette and gently disrupted by enzymatic means and reseeded. After this step grown organoids can be mechanically split following Basic Protocol 2. For a general overview see Fig. 5a.

MATERIALS

- Established human intestinal organoids culture; 1 well of a 12-well (Start with organoids from Basic Protocol 2, step 8 or after experimental conditions like genetic engineering, treatment with mutagens or other experimental set up requiring WGS)
- AdvDMEM+++ (see Reagents and Solutions)
- TrypLE Express Enzyme (1X), phenol red (TrpLE) (Gibco, cat. no. 12605036)
- Y-27632 Rho kinase inhibitor (RhoKi) (Abmole, cat. no. Y-27632)
- DAPI
- Cultrex reduced growth factor basement membrane extract, type 2, Pathclear (BME) (R&D Systems / Bio-technie, cat. no. 3533-001)

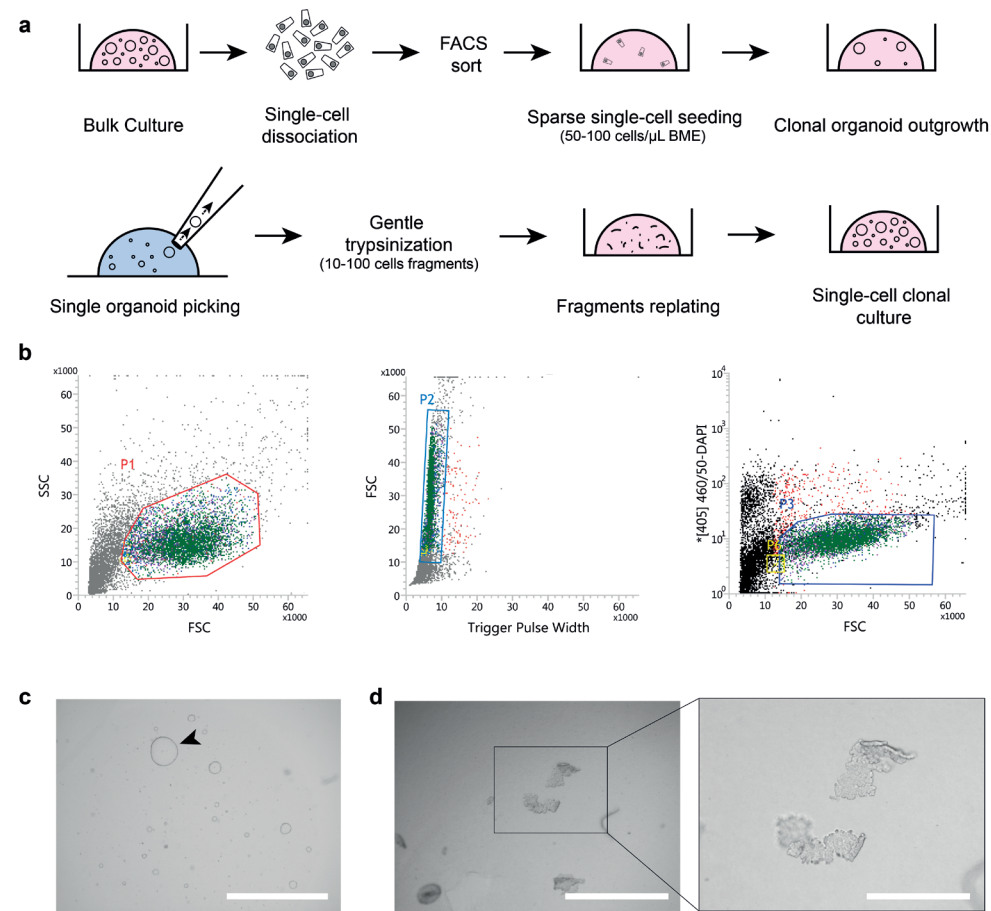


Figure 5. Clonal expansion of human intestinal organoid cultures. **a**, Schematic of process. **b**, Gating strategy for sorting of living cells used for clonal organoid outgrowth. Cells in P3 gate were sorted and seeded. **c**, Single-cell organoid outgrowth after 10 days. Arrowhead indicates organoid of proper size for picking. Scale bar, 2 mm. **d**, Organoid fragments after trypsinization of a single picked organoid. Scale bars, 1 mm (left) and 0.4 mm (inset at right).

- Intestinal expansion medium
- Cell Recovery Solution (Corning, cat. no. 354253)
- Primocin (InvivoGen, cat no. ant-pm-1)
- Water Bath 37°C
- Sterile plugged Pasteur glass pipette
- Sterile 10 μ L pipette tips
- Flow cytometry tube with 35 μ m strainer cup (Corning, cat. no. 08-771-23)
- Flow cytometer
- 40 μ m cell strainer (VWR cat. no. 89508-342)
- Sterile 100 mm cell culture dish

PROTOCOL

Organoid preparation

- Starting with 1 well of a 12-well plate culture of established human intestinal organoid culture, remove the medium from the culture well.
The process can be scaled up or down using different cell culture plate formats. For a guide to other formats see Table 1.
- Flush and collect the organoids from the well with 1 mL of ice-cold AdvDMEM+++ in order to disrupt the BME droplets using a P1000 pipette. Collect the organoids in a 15 mL centrifuge tube containing 4 mL of ice-cold AdvDMEM+++.
- Spin down the organoids 5 min at 450xg, 4°C. Remove supernatant.
Often in this step, undissolved BME accumulates over the organoid pellet as a cloudy mesh. It is important to remove as much BME as possible without taking the organoids. If this is not possible, resuspend the pellet in the AdvDMEM+++ and incubate in ice for 10 min. Then repeat step 3.
- Resuspend the cell pellet in 1 mL of TrpLE prewarmed at 37°C.
- Incubate the cells in a water bath 5 min at 37°C. Regularly check dissociation progress and stop once the majority of fragments consists of single cells. Vortex to increase dissociation speed at regular intervals.
- After this incubation time, use a plugged Pasteur glass pipette, coated with FBS to avoid cells sticking to the glass, connected to a sterile 10 μ L tip to mechanically disrupt the organoid fragments to obtain single cells (as in Basic Protocol 2, step 4).
IMPORTANT. After this, check cell suspension under the microscope. If organoids are not dissociated enough into single cells, repeat steps 5 and 6 of this protocol. Long incubation times with TrpLE will lead to increased cell death. It is important to maximize the number of single cells while minimizing the cell death rate.
- Add 4 mL ice-cold AdvDMEM+++ with 10 μ M RhoKi to the cells. Centrifuge cells for 5 min at 450xg, 4°C. Remove supernatant.
Move a small fraction of cells to another tube for parallel processing without DAPI in the next step. This is later used as a DAPI-negative control in the FACS gating.
- Resuspend cells in 0.5 mL of ice-cold AdvDMEM+++ supplemented with 10 μ M RhoKi and 2 μ g/mL DAPI, pass them through the strainer of a 35 μ m mesh-cupped flow cytometry tube. Transport cells to the flow cytometer incubated on ice and protected from light.
DAPI will only stain apoptotic cells with disrupted cell membrane integrity

Live-cell sort and single-cell clonal organoids outgrowth

- Sort living cells (DAPI-negative) into a 1.5 mL tube containing 0.5 mL of AdvDMEM+++ supplemented with 10 μ M RhoKi (Fig. 5b).
First, use FSC and SSC to gate intact epithelial cells with intact morphology (Fig. 5b, left panel, P1), then on the gated population use FSC and Trigger Pulse Width to

select single cells and deplete cell duplets or triplets (Fig 5b, middle panel, P2), and subsequently use the [405]460/50-DAPI channel to gate and sort living DAPI negative cells (Fig 5b, right panel, P3).

The fraction of cells, processed in parallel, not treated with DAPI can be used as negative control in the FACS gating strategy (Fig. 5b).

At this step note the number of cells sorted in the tube in order to calculate seeding cell density in the following steps.

IMPORTANT: Sorting is important to make sure that cells are single cell dissociated in order to grow clonal cultures later on. It is very important if WGS will be performed at later stages, as loss of clonality prevents interpretation of WGS data. Alternatively, if cells have been subjected to CRISPR/Cas9 gene editing, cells can be passed through a 40 µm cell strainer to increase the likelihood dissociated single cells are seeded. After this, count living cells using a hemocytometer seeding so that the seeding density can be estimated. While this approach is less stringent than sorting, it may enhance outgrowth efficiency and is acceptable if many clonal lines which can be screened later are generated. Double picking strategies can be applied in order to increase the likelihood of having clonal cultures.

10. Spin down cells for 5 min at 450xg, 4°C. Remove supernatant.

CAUTION: Pellet might not be visible due to a low number of sorted cells. Be extremely careful when removing the supernatant, do not touch tube walls with the pipette tip.

It is important that the BME drops are solid after seeding in order not to dissociate before picking time and to avoid loss of organoid clones. For this, make sure to remove as much supernatant as possible to increase BME concentration.

11. Resuspend cells homogeneously in BME to a density of 50-100 cells/µL of BME. Pipette the cells in ~15 µL domes in a 12-well plate.
IMPORTANT: Final cell concentration should be between 50 and 100 cells per µL of BME in order to maximize organoid outgrowth and minimize organoid fusion afterwards. Too sparse seeding will impair organoid outgrowth, while too dense could lead to organoid fusion and loss of clonality of the future culture.
12. Flip the plate upside down, and let the domes solidify by placing the plate in the incubator for 20 minutes.
13. Add complete organoid culture medium supplemented with 10 µM RhoKi and keep in the incubator at 37°C and 5% CO₂. Refresh the medium every 2-3 days, keeping RhoKi in the medium.

Clonal organoid isolation and expansion

14. After 7-14 days single cells should have formed organoids (Fig. 5c).
Due to donor-to-donor variability some donors will take longer. If this is the case keep the organoids expanding for an extra week before continuing with the next step.

15. Remove medium from the organoid well and collect them in cell recovery solution and incubate them on ice for 30 min.
In this way organoids should be liberated from the BME which makes them easier to be picked in the next step.
16. Pipette the solution containing the organoids in drops of ~500 µL into a sterile 100 mm cell culture dish.
It is important that the drop does not touch the dish walls, otherwise organoids will not be visible under the microscope.
17. Place the plate under a brightfield microscope and open the lid.
Avoid moving and speaking above the opened plate. Make sure to add primocin in the culture medium after this step.
18. Using a P20 pipette pick individual organoids from the drop. Transfer them to a 1.5 mL plastic tube containing 300 µL of TrypLE at 4°C.
It is recommended to pick a high number of clonal organoids because the outgrowth efficiency is not 100%. We recommend picking around 20 organoids per condition under optimal growth conditions.
19. Incubate at 37°C in the water bath for one minute. Add 700 µL of AdvDMEM+++ containing 10 µM RhoKi. Pipette up and down 3-5 times using a P1000 pipette.
20. Centrifuge 5 min at 500xg, 4°C. Remove supernatant.
CAUTION: Pellet might not be visible due to the low number of cells in the organoid. Be extremely careful when removing the supernatant, do not touch tube walls with the pipette tip.
21. Resuspend in 20 µL BME and seed in a well of a 48-well plate (Fig 4d).
22. Add complete intestinal organoid expansion medium supplemented with 100 µg/mL primocin.
23. After organoids grow out in this step, pass them as in Basic Protocol 2.

SUPPORT PROTOCOL 1

Wnt3A-conditioned medium (CM) production

MATERIALS

- L-Wnt-3A cells frozen cryovial (from a T25 flask cultured to 95-100% confluence) (in house; provided upon request and after material transfer agreement)
- DMEM++ (See Reagents and Solutions)
- Zeocin (Gibco, cat.no R25001)
- TrypLE Express Enzyme (1X), phenol red (Gibco, cat. no.12605036)
- PBS0
- HEK 293-STF (ATCC CRL-3249)
- T175 cell culture flask (Greiner Bio-one, cat. no. 661160)
- 145 mm cell culture dish (Greiner Bio-one, cat no 639160)

- Stericup-GP, 0.22 µm, polyethersulfone, 500 mL, radio-sterilized (Millipore, cat. no. SCGPU05RE)

PROTOCOL

Start L-Wnt-3A cell culture from frozen cryovial. Seed cells in a T175 flask with 20 mL of DMEM++ supplemented with 125 µg/mL zeocin at 37°C and 5% CO₂ until it reaches 90-100% confluence.

A key component of DMEM++ medium is FBS. L cells are very sensitive to it. Test different batches of FBS to find one supporting L cells and organoids growth efficiently.

1. Split cells into two T175 flasks using TrypLE and grow the cells in DMEM++ with 125 µg/mL zeocin at 37°C and 5% CO₂ until they reach 90-100% confluence.
2. Split the cultures into 12 T175 flasks. Add DMEM++ supplemented with 125 µg/mL zeocin to two flasks and use them for a new round of Wnt3A-CM production (Step 2). Add DMEM++ without zeocin to the rest of the flasks (10) and use these to continue with step 4.

Use L-Wnt-3A cells only until passage 10-12.

3. After cells have reached confluence, trypsinize the cultures, pool and seed them into 60 140 cm² dishes in 20 mL of DMEM++ without zeocin per plate. Incubate cells at 37°C and 5% CO₂.
4. After one week, harvest the medium and spin down for 5 min at 450xg, 4°C.
5. Collect the supernatant and pass it through a Stericup-GP 0.22 µm filter.

CRITICAL STEP. *It is important to remove all cells from the conditioned medium as otherwise they would overgrow the organoids once the Wnt3A-CM is used for organoid culture.*

IMPORTANT. *Test the quality of Wnt3A-CM for every batch using HEK 293T-STF Wnt reporter cell line luciferase-based assay. An optimal batch induces 300-fold and 15-fold signal increase when used at concentrations of 50% v/v and 12.5% v/v respectively. Using 1-2% v/v of Wnt3A-CM should give a signal similar to background levels. Use these criteria as a reference for the quality of the Wnt3A-CM batch.*

Freshly prepared Wnt3A-CM can be stored at 4°C for long periods of time >6 months.

SUPPORT PROTOCOL 2

Rspo1-CM production

MATERIALS

- 293T-HA-Rspol Fc cell line frozen cryovial (from a T25 flask cultured to 95-100% confluence) (R&D Systems, cat. no. 3710-001-01)
- DMEM++ (see Reagents and Solutions)
- Zeocin (Gibco, cat. no. R25001)

- TrypLE Express Enzyme (1X), phenol red (Gibco, cat. no.12605036)
- PBS0
- AdvDMEM+++ (see Reagents and Solutions)
- HEK 293-STF (ATCC CRL-3249)
- T75 cell culture flask (Greiner Bio-one, cat. no. 658170)
- T175 tissue flask (Greiner Bio-one, cat. no. 661160)
- Stericup-GP, 0.22 µm, polyethersulfone, 500 mL, radio-sterilized (Millipore, cat. no. SCGPU05RE)

PROTOCOL

1. Start 293T-HA-Rspol Fc cell culture from frozen cryovial. Seed cells in a T75 flask with 20 mL of DMEM++ supplemented with 300 µg/mL zeocin at 37°C and 5% CO₂ until it reaches 90%-100% confluence.
2. Split cells into two T175 flasks using TrypLE and grow the cells in DMEM++ with 300 µg/mL zeocin at 37°C and 5% CO₂ until they reach 90-100% confluence.
3. Split the cultures into 12 T175 flasks. Add DMEM++ supplemented with 300 µg/mL zeocin to 2 flasks and use them for a new round of Rspo1 CM production (Step 2). Add DMEM++ without zeocin to the rest of the flasks (10) and use these to continue with step 4.

Culture 293T-HA-Rspol Fc cells only until passage 10-12.

4. After 2-3 days cells growing in medium without Zeocin should have reached 75% confluence. Remove DMEM++ from the culture. Add 50 mL serum free AdvDMEM+++ without zeocin per flask. Incubate cells 1 week at 37°C and 5% CO₂. *During the week, culture medium will acquire a yellow coloring but do not refresh the medium because Rspo1 is being secreted during the culture time span.*
5. After 1 week, harvest the medium and spin down for 5 min at 450xg, 4°C.
6. Collect the supernatant and pass it through a Stericup-GP 0.22 µm filter.

CRITICAL. *It is important to remove all 293T cells from the conditioned medium as otherwise they would overgrow once the Rspo1-CM is used in organoids*

CRITICAL. *Test the quality of Rspo1-CM for every batch using HEK 293T-STF Wnt reporter cell line luciferase-based assay. Different concentrations of Rspo1-CM are tested. An optimal batch induces a 600-fold and 100-fold signal increase over background levels, when used at concentrations of 2.5% v/v and 0.25% v/v respectively, when used in combination in combination with 12.5% v/v Wnt3A-CM. Use these criteria as a reference for the quality of the Rspo1-CM batch.*

The process can be scaled-up if larger volumes of Rspo1-CM are required. The medium volume:Culture surface ratio should be maintained.

Freshly prepared Rspo1-CM can be stored at -20°C for 6 months. Prepare aliquots adequate to your needs before freezing. Once thawed, store at 4°C and use preferentially within 4 weeks. Avoid repeated freeze-thaw cycles.

SUPPORT PROTOCOL 3

RNA extraction from intestinal organoid cultures

MATERIALS

- Established human intestinal organoid culture (From Basic protocol 2, step 8, or after subjecting organoids to experimental conditions)
- Column-based extraction kit: RNeasy Mini Kit (Qiagen, cat. no. 74104)
- Freshly prepared 70% ethanol
- RNase-free DNase set (Qiagen, cat.no. 79254)
- RNase-free 1.5 mL microcentrifuge plastic tubes

PROTOCOL

1. Remove medium from organoid well, and dissolve the BME drop containing the organoids directly in 350 μ L of RLT buffer from RNeasy Mini Kit, pipetting several times up and down. Collect it in a 15 mL plastic tube.
Starting material should be at least a full well of a 24-well culture plate. To ensure enough RNA material is preferable to use 1 full well of a 12-well plate. If organoids are cultured in differentiation conditions, expect the yield to decrease and use increased amounts of organoids for RNA assessments.
2. Mix the resulting solution 1:1 v/v with freshly prepared 70% ethanol and vortex.
3. To continue RNA isolation from organoids, continue with step 4, from the section titled "Protocol: Purification of Total RNA from Animal Cells Using Spin Technology" of the *Qiagen RNeasy Handbook guide* (Available at: <https://www.qiagen.com/ie/resources/resourcedetail?id=14e7cf6e-521a-4cf7-8cbc-bf9f6fa33e24&lang=en>)
Perform optional DNase digestion after step 5 of the protocol, as indicated in "Appendix D: Optional On-Column DNase Digestion with the RNase-Free DNase Set" of the Qiagen RNeasy Handbook guide.
4. Elute in 30 μ L of RNase-free water.
Elution volume depends on the amount of starting material, adjust accordingly.

REAGENTS AND SOLUTIONS

AdvDMEM+++

- Advanced Dulbecco's Modified Eagle Medium/F12 (Gibco, cat. no. 12634-010)
- 10 mM HEPES (Gibco, cat. no. 15630-056)
- 1 \times GlutaMAX Supplement (Gibco, cat. no. 35050-038)
- 100 U/ml penicillin-streptomycin (Gibco, cat. no. 15140163)
Store up to 1 month at 4°C

Blocking solution

- Phosphate-buffered saline (PBS)

- 0.1% (v/v) Tween-20
- 2% (v/v) donkey serum
- *Prepare fresh before use*

Differentiation medium

For base ENR medium:

- AdvDMEM+++ (see recipe)
- 1 \times B-27 Supplement (50 \times , serum free, Life Technologies, 17504-044)
- 20% (v/v) Rspo1-CM (see Support Protocol 2)
- 2% (v/v) Noggin conditioned medium (U-Protein Express, N002)
- 1.25 mM N-acetylcysteine (Sigma-Aldrich, A9165)
- 50 ng/ml epidermal growth factor (EGF, Peprotech, AF-100-15)
- *Store up to 1 month at 4°C*

Before use, add differentiation components:

- 10 μ M Notch inhibitor DAPT (Sigma-Aldrich, D5942)
- 0.1-1 μ M MEK inhibitor PD0325901 (Sigma-Aldrich, PZ0162)
- 50 ng/ml BMP2 (Peprotech, 120-02C)
- 50 ng/ml BMP4 (Peprotech, 120-05ET)

See Table 1 for selection of appropriate medium. For ENR+Notchi, add DAPT to base medium. For ENR+MEKi+Notchi, add PD0325901 and DAPT to base medium. For ER+MEKi+Notchi+BMP2+BMP4, add all four components and omit Noggin CM. Additional differentiation components should be added fresh to the medium prior use.

DMEM++

- 1 \times DMEM + GlutaMAX-I (Gibco, cat. no. 31966-021)
- 100 U/ml penicillin-streptomycin (Gibco, cat. no. 15140163)
- 10% (v/v) fetal bovine serum (FBS; Sigma-Aldrich, cat. no. F7524)
Store up to 1 month at 4°C

Expansion medium

- AdvDMEM+++ (see recipe)
- 1 \times B-27 Supplement (50 \times , serum free, Life Technologies, 17504-044)
- 50% (v/v) Wnt3A-CM (see Support Protocol 1) or 0.5 nM Wnt surrogate (U-Protein Express, N001)
- 20% (v/v) Rspo1-CM (see Support Protocol 2)
- 2% (v/v) Noggin conditioned medium (U-Protein Express, N002)
- 1.25 mM N-acetylcysteine (Sigma-Aldrich, A9165)
- 10 mM nicotinamide (Sigma-Aldrich, N0636)
- 10 μ M p38 inhibitor SB202190 (Sigma-Aldrich, S7076)

- 50 ng/ml epidermal growth factor (EGF, Peprotech, AF-100-15)
- 0.5 μ M ALK5 inhibitor A83-01 (Tocris/Bio-Techne, 2939)
- 1 μ M prostaglandin E2 (PGE2, Tocris/Bio-Techne, 2296)

Store up to 1 month at 4°C

See *Strategic Planning and Critical Parameters for discussions on the use of Wnt ligands. Omit Wnt ligands when culturing CRC-derived organoids.*

Freezing medium 2x

- 10 ml DMSO (Sigma-Aldrich, cat. no. D2650)
- 40 ml FBS (Sigma-Aldrich, cat. no. F7524)

Store up to 1 month at 4°C

Permeabilization solution

- Phosphate-buffered saline (PBS)
- 0.5% (v/v) Triton X-100
- 2% (v/v) donkey serum (Bio-Rad, C06SB)

Prepare fresh before use.

COMMENTARY

Background information

The initial development of ASC-derived organoids occurred hand-in-hand with the knowledge obtained on the signaling pathways governing the adult intestinal epithelium development. The intestinal crypt-villus (small intestine) or crypt (colon) structural units are hallmarks of the adult stem cell functioning. Intestinal stem cells - marked by expression of the G-protein coupled receptor Lgr5 - reside at the bottom of the crypts and are able to replenish the entire intestinal epithelium within a short turnover of time of ~5 days. Lgr5⁺ cells that reside at the bottom of the crypts actively divide, generating transit amplifying (TA) cells. These TA cells proliferate and give rise to all the functional epithelial cell types that carry out the essential intestinal functions (e.g. enterocytes, Paneth cells, enteroendocrine cells, goblet cells, tuft cells and - at the Peyer's patches - M cells). These cell population dynamics are tightly governed by the action of four signaling pathways, namely Wnt, Epidermal Growth Factor (EGF), Notch and Bone Morphogenetic Protein (BMP) (Clevers, 2013).

ASC-derived intestinal organoids rely on the infinite ability of epithelial Lgr5⁺ stem cells to divide and repopulate the entire intestinal epithelium. The initial development of the technology was guided by the knowledge on the niche factors that promote the stem cell state at the bottom of the crypt (Sato et al., 2009, 2011). By providing Wnt and EGF agonists and BMP inhibitors in the medium cocktail, these stem cells can be maintained and expanded in culture indefinitely. In the case of mouse small intestinal organoids, Paneth cells are a source of Wnt ligands which allow to culture them in the absence of an

exogenous Wnt source. This inherently creates a local Wnt gradient around Paneth cells, giving rise to the characteristic budding structures of mouse small intestinal organoids. For human intestinal organoids, ectopic Wnt ligands need to be added to the medium as Paneth cells do not produce as much Wnt as in the case of mouse. In turn, this leads to the characteristic cystic structures of human small intestine and colon organoids.

Critical parameters and troubleshooting

It is essential to establish organoid cultures from fresh biopsies after surgery and avoid freezing of the tissue. Both a substantial delay after surgery and freezing of the tissue may result in failure to obtain organoids. Additionally, the quality (e.g. High proportion of muscle cells) of the tissue biopsies influences the efficiency of organoid outgrowth.

One of the most critical parameters regarding the culture of human intestinal organoids is the source of Wnt pathway agonists used and the level of Wnt pathway activation that they achieve. High levels of Wnt activation will result in cystic organoids that maintain most of their cells in a stem cell or transit amplifying state, allowing indefinite expansion of the culture. However, if a suboptimal Wnt agonist source is used, stem cells will start to differentiate, leading to a loss of the organoid culture after some passages. A protocol for Wnt3A-CM production is provided in Support protocol 1. Wnt3A-CM is the most established source of Wnt agonist. However, batch to batch variability in the Wnt activation activity mandates regular quality controls of this reagent. In order to overcome this problem, combination of different Wnt3A-CM batches is recommended, as well as performing Wnt activity assays using reporter cell lines (ATCC® CRL-3249™). Additionally, the recent development of synthetic Wnt agonists (Janda et al., 2017) has improved and facilitated the culture of human intestinal organoids, particularly for growing human colon organoids derived from single cells.

When using organoids for experiments, it is crucial to consider the cell type composition. Organoids cultured in expansion medium will predominantly consist of stem and transit amplifying cells. Whereas these are useful in stem cell and cancer studies, many experiments on healthy gut physiology require mature cell types. These can be obtained within 5 days using tailored differentiation media for all major mature cell types. It is crucial to validate differentiation success by quantitative real-time PCR for cell type marker genes or antibody-based staining. Beyond the media recipes provided here, other differentiation strategies can be applied (Fujii et al., 2018, Beumer et al., 2020) but are beyond the scope of this protocol.

Another matter of high importance is the effect of cell density on the ability to expand the organoid culture. The right seeding density enables paracrine signaling support for organoid growth while it also leaves space for organoids to grow and avoids excessive media component consumption and impaired diffusion of growth factors to the core of BME domes. The seeding density has a crucial effect especially in the single cell clonal expansion step. Too sparse seeding may greatly reduce outgrowth efficiency, whereas

too high density increases the risk of organoid fusion and thereby loss of clonality. This is especially relevant in experiments involving whole genome sequencing due to the high cost per genome. It is recommended to maintain organoids seeded at the suggested density as it can be observed in Fig 3. There is considerable inter-donor variability observable in organoid line density preference and tolerance. Some lines display expansion potential even at suboptimal density, others tend to differentiate in too sparse seeding and lose viability if plated too densely.

An important factor to consider when working with organoids is the addition of Rho kinase inhibitor in all the steps at which organoids are dissociated to single cells, both during passage and once seeded. This will block anoikis, which otherwise occurs due to the loss of cell-cell contact.

Using low attachment pipette tips and coating with FBS prior to pipetting avoids organoid attaching to the pipette tip and the subsequent material loss. This is particularly important in the first and last steps of the whole mount staining immunofluorescence staining (Basic Protocol 4), when organoids are transferred, but can also be advisable when establishing organoid lines from limited material.

Troubleshooting Guide

Troubleshooting

Time considerations

The amount of hands-on time dedicated to these techniques is not extensive, although organoid work is more dedicated and requires more attention than that of cell lines. Additionally, organoids grow considerably slower than other standard cell lines. The time required to perform all these techniques depends on the number of lines that are being processed in parallel.

Typically, establishing 1 organoid line from a biopsy takes around 3 h with 1.5 h hands-on time. It normally takes an additional 2-4 weeks and 2 passages until enough biomass for cryopreservation and experiments is generated. Performing mechanical passage of a single organoid line could take approximately 1 h with 15 min hands-on time. In general, the time required for organoids to expand after passage is 1 week, although donor-to-donor variability should be taken into consideration. Differentiation of organoids takes ~30 min hands-on time and 5 days of incubation. The staining protocol for organoid immunofluorescence usually takes 2 days to complete if fixation is performed overnight. If fixation is performed 2 h at room temperature it can be achieved within 1 day. Establishing single cell clonal organoid lines is a long process that in some cases can take 2 months before a fully clonal culture is established (1 full well of a 12-well plate, which depending on the donor can take longer). Hands-on time required for the initial step of single cell culture establishment is around 2 h. Single-cell outgrowth to organoids can take 2 or 3 weeks depending on the organoid line. The time required in the picking of the organoids highly depends on the number of clones to be picked. Usually, picking and

passing 24 clones from a single condition would take between 30 and 60 mins. Expansion of these clones in 48-well plates will require 1-2 weeks after which another passage (1-2 weeks) will be required to reach 1 full well of a 12-well plate per clonal culture. RNA extraction from organoids takes 30-60 minutes. DNA extraction from organoids takes around 3 h total time. The production of Wnt and R-Spondin conditioned medium takes 12 days for one batch. If more batches are produced in parallel, production time will increase to around 20 days.

ACKNOWLEDGEMENTS

We thank M. Bannier-Hélaouët for critical reading of the manuscript. This protocol was supported by CRUK grant OPTIMISTIC (C10674/A27140) (C.P.-M., J.P.), the Gravitation projects CancerGenomiCs.nl and the Netherlands Organ-on-Chip Initiative (024.003.001) from the Netherlands Organisation for Scientific Research (NWO) funded by the Ministry of Education, Culture and Science of the government of the Netherlands (C.P.-M., J.P.), the Oncode Institute (partly financed by the Dutch Cancer Society), the European Research Council under ERC Advanced Grant Agreement no. 67013 (J.P., H.C.) and NERF/Petersen Accelerator (J.B.).

CONFLICT OF INTEREST

H.C. is inventor on several patents related to organoid technology; his full disclosure is given at <https://www.uu.nl/staff/JCClevers/>.

REFERENCES

- Bar-Ephraim, Y. E., Kretschmar, K., & Clevers, H. (2019). Organoids in immunological research. *Nature Reviews Immunology*, 1–15. <https://doi.org/10.1038/s41577-019-0248-y>
- Beumer, J., Artegiani, B., Post, Y., Reimann, F., Gribble, F., Nguyen, T. N., Zeng, H., Born, M. V. den, Es, J. H. V., & Clevers, H. (2018). Enteroendocrine cells switch hormone expression along the crypt-to-villus BMP signalling gradient. *Nature Cell Biology*, 20(8), 909–916. <https://doi.org/10.1038/s41556-018-0143-y>
- Beumer, J., Puschhof, J., Bauzá-Martinez, J., Martínez-Silgado, A., Elmentaite, R., James, K. R., Ross, A., Hendriks, D., Artegiani, B., Busslinger, G. A., Ponsoen, B., Andersson-Rolf, A., Saftien, A., Boot, C., Kretschmar, K., Geurts, M. H., Bar-Ephraim, Y. E., Pleguezuelos-Manzano, C., Post, Y., ... Clevers, H. (2020). High-Resolution mRNA and Secretome Atlas of Human Enteroendocrine Cells. *Cell*, 0(0). <https://doi.org/10.1016/j.cell.2020.04.036>
- Bigorgne, A. E., Farin, H. F., Lemoine, R., Mahlaoui, N., Lambert, N., Gil, M., Schulz, A., Philippet, P., Schlessner, P., Abrahamsen, T. G., Oymar, K., Davies, E. G., Ellingsen, C. L., Leteurtre, E., Moreau-Massart, B., Berrebi, D., Bole-Feysot, C., Nischke, P., Brousse, N., ... Basile, G. de S. (2014). *TTC7A* mutations disrupt intestinal epithelial apicobasal polarity. *The Journal of Clinical Investigation*, 124(1), 328–337. <https://doi.org/10.1172/JCI71471>
- Blokzijl, F., de Ligt, J., Jager, M., Sasselli, V., Roerink, S., Sasaki, N., Huch, M., Boymans, S., Kuijk, E., Prins, P., Nijman, I. J., Martincorena, I., Mokry, M., Wiegerinck, C. L., Middendorp, S., Sato, T., Schwank, G., Nieuwenhuis, E. E. S., Verstegen, M. M. A., ... van Boxtel, R. (2016). Tissue-specific mutation accumulation in human adult stem cells during life. *Nature*, 538(7624), 260–264. <https://doi.org/10.1038/nature19768>
- Christensen, S., Van der Roest, B., Besselink, N., Janssen, R., Boymans, S., Martens, J. W. M., Yaspo, M.-L., Priestley, P., Kuijk, E., Cuppen, E., & Van Hoeck, A. (2019). 5-Fluorouracil treatment induces characteristic T>G mutations in human cancer. *Nature Communications*, 10(1), 1–11. <https://doi.org/10.1038/s41467-019-12594-8>
- Clevers, H. (2013). The Intestinal Crypt, A Prototype Stem Cell Compartment. *Cell*, 154(2), 274–284. <https://doi.org/10.1016/j.cell.2013.07.004>
- Clevers, H. (2016). Modeling Development and Disease with Organoids. *Cell*, 165(7), 1586–1597. <https://doi.org/10.1016/j.cell.2016.05.082>
- Dekkers, J. F., Wiegerinck, C. L., de Jonge, H. R., Bronsveld, I., Janssens, H. M., de Winter-de Groot, K. M., Brandsma, A. M., de Jong, N. W. M., Bijvelds, M. J. C., Scholte, B. J., Nieuwenhuis, E. E. S., van den Brink, S., Clevers, H., van der Ent, C. K., Middendorp, S., & Beekman, J. M. (2013). A functional CFTR assay using primary cystic fibrosis intestinal organoids. *Nature Medicine*, 19(7), 939–945. <https://doi.org/10.1038/nm.3201>
- Dieterich, W., Neurath, M. F., & Zopf, Y. (2020). Intestinal ex vivo organoid culture reveals altered programmed crypt stem cells in patients with celiac disease. *Scientific Reports*, 10(1), 1–10. <https://doi.org/10.1038/s41598-020-60521-5>
- Dijkstra, K. K., Cattaneo, C. M., Weeber, F., Chalabi, M., van de Haar, J., Fanchi, L. F., Slagter, M., van der Velden, D. L., Kaing, S., Kelderman, S., van Rooij, N., van Leerdam, M. E., Depla, A., Smit, E. F., Hartemink, K. J., de Groot, R., Wolkers, M. C., Sachs, N., Snaebjornsson, P., ... Voest, E. E. (2018). Generation of Tumor-Reactive T Cells by Co-culture of Peripheral Blood Lymphocytes and Tumor Organoids. *Cell*, 174(6), 1586–1598.e12. <https://doi.org/10.1016/j.cell.2018.07.009>
- Drost, J., & Clevers, H. (2018). Organoids in cancer research. *Nature Reviews Cancer*, 18(7), 407–418. <https://doi.org/10.1038/s41568-018-0007-6>
- Drost, J., van Jaarsveld, R. H., Ponsoen, B., Zimmerlin, C., van Boxtel, R., Buijs, A., Sachs, N., Overmeer, R. M., Offerhaus, G. J., Begthel, H., Korving, J., van de Wetering, M., Schwank, G., Logtenberg, M., Cuppen, E., Snippert, H. J., Medema, J. P., Kops, G. J. P. L., & Clevers, H. (2015). Sequential cancer mutations in cultured human intestinal stem cells. *Nature*, 521(7550), 43–47. <https://doi.org/10.1038/nature14415>
- Farin, H. F., Jordens, I., Mosa, M. H., Basak, O., Korving, J., Tauriello, D. V. F., de Punder, K., Angers, S., Peters, P. J., Maurice, M. M., & Clevers, H. (2016). Visualization of a short-range Wnt gradient in the intestinal stem-cell niche. *Nature*, 530(7590), 340–343. <https://doi.org/10.1038/nature16937>
- Freire, R., Ingano, L., Serena, G., Cetinbas, M., Anselmo, A., Sapone, A., Sadreyev, R. I., Fasano, A., & Senger, S. (2019). Human gut derived-organoids provide model to study gluten response and effects of microbiota-derived molecules in celiac disease. *Scientific Reports*, 9(1), 1–15. <https://doi.org/10.1038/s41598-019-43426-w>
- Fujii, M., Clevers, H., & Sato, T. (2019). Modeling Human Digestive Diseases With CRISPR-Cas9–Modified Organoids. *Gastroenterology*, 156(3), 562–576. <https://doi.org/10.1053/j.gastro.2018.11.048>
- Fujii, M., Matano, M., Nanki, K., & Sato, T. (2015). Efficient genetic engineering of human intestinal organoids using electroporation. *Nature Protocols*, 10(10), 1474–1485. <https://doi.org/10.1038/nprot.2015.088>
- Fujii, M., Matano, M., Toshimitsu, K., Takano, A., Mikami, Y., Nishikori, S., Sugimoto, S., & Sato, T. (2018). Human Intestinal Organoids Maintain Self-Renewal Capacity and Cellular Diversity in Niche-Inspired Culture Condition. *Cell Stem Cell*, 23(6), 787–793.e6. <https://doi.org/10.1016/j.stem.2018.11.016>
- Geurts, M. H., de Poel, E., Amatngalim, G. D., Oka, R., Meijers, F. M., Kruijselbrink, E., van Mourik, P., Berkens, G., de Winter-de Groot, K. M., Michel, S., Muilwijk, D., Aalbers, B. L., Mullenders, J., Boj, S. F., Suen, S. W. F., Brunsveld, J. E., Janssens, H. M., Mall, M. A., Graeber, S. Y., ... Clevers, H. (2020). CRISPR-Based Adenine Editors Correct Nonsense Mutations in a Cystic Fibrosis Organoid Biobank. *Cell Stem Cell*, 26(4), 503–510.e7. <https://doi.org/10.1016/j.stem.2020.01.019>
- Janda, C. Y., Dang, L. T., You, C., Chang, J., Lau, W. de, Zhong, Z. A., Yan, K. S., Marecic, O., Siepe, D., Li, X., Moody, J. D., Williams, B. O., Clevers, H., Piehler, J., Baker, D., Kuo, C. J., & Garcia, K. C. (2017). Surrogate Wnt agonists that phenocopy canonical Wnt and β -catenin signalling. *Nature*, 545(7653), 234–237. <https://doi.org/10.1038/nature22306>
- Nanki, K., Fujii, M., Shimokawa, M., Matano, M., Nishikori, S., Date, S., Takano, A., Toshimitsu, K., Ohta, Y., Takahashi, S., Sugimoto, S., Ishimaru, K., Kawasaki, K., Nagai, Y., Ishii, R., Yoshida, K., Sasaki, N., Hibi, T., Ishihara, S., ... Sato, T. (2020). Somatic inflammatory gene mutations in human ulcerative colitis epithelium. *Nature*, 577(7789), 254–259. <https://doi.org/10.1038/s41586-019-1844-5>
- Pleguezuelos-Manzano, C., Puschhof, J., Rosendahl Huber, A., van Hoeck, A., Wood, H. M., Nomburg, J., Gurjao, C., Manders, F., Dalmasso, G., Stege, P. B., Paganelli, F. L., Geurts, M. H., Beumer, J., Mizutani, T., Miao, Y., van der Linden, R., van der Elst, S., Garcia, K. C., Top, J., ... Clevers, H. (2020). Mutational signature in colorectal cancer caused by genotoxic pks + *E. coli*. *Nature*, 580(7802), 269–273. <https://doi.org/10.1038/s41586-020-2080-8>
- Sato, T., Stange, D. E., Ferrante, M., Vries, R. G. J., Es, J. H. van, Brink, S. van den, Houdt, W. J. van, Pronk, A., Gorp, J. van, Siersema, P. D., & Clevers, H. (2011). Long-term Expansion of Epithelial Organoids From Human Colon, Adenoma, Adenocarcinoma, and Barrett's Epithelium. *Gastroenterology*, 141(5), 1762–1772. <https://doi.org/10.1053/j.gastro.2011.07.050>
- Sato, T., Vries, R. G., Snippert, H. J., van de Wetering, M., Barker, N., Stange, D. E., van Es, J. H., Abo, A., Kujala, P., Peters, P. J., & Clevers, H. (2009). Single Lgr5 stem cells build crypt-villus structures in vitro without a mesenchymal niche. *Nature*, 459(7244), 262–265. <https://doi.org/10.1038/nature07935>
- Schwank, G., Koo, B.-K., Sasselli, V., Dekkers, J. F., Heo, I., Demircan, T., Sasaki, N., Boymans, S., Cuppen, E., van der Ent, C. K., Nieuwenhuis, E. E. S., Beekman, J. M., & Clevers, H. (2013). Functional Repair of CFTR by CRISPR/Cas9 in Intestinal Stem Cell Organoids of Cystic Fibrosis Patients. *Cell Stem Cell*, 13(6), 653–658. <https://doi.org/10.1016/j.stem.2013.11.002>

26. van de Wetering, M., Francies, H. E., Francis, J. M., Bounova, G., Iorio, F., Pronk, A., van Houdt, W., van Gorp, J., Taylor-Weiner, A., Kester, L., McLaren-Douglas, A., Blokker, J., Jaksani, S., Bartfeld, S., Volckman, R., van Sluis, P., Li, V. S. W., Seepo, S., Sekhar Pedomallu, C., ... Clevers, H. (2015). Prospective Derivation of a Living Organoid Biobank of Colorectal Cancer Patients. *Cell*, 161(4), 933–945. <https://doi.org/10.1016/j.cell.2015.03.053>
27. van Rijn, J. M., Ardy, R. C., Kuloğlu, Z., Härter, B., van Haften-Visser, D. Y., van der Doef, H. P. J., van Hoesel, M., Kansu, A., van Vugt, A. H. M., Thian, M., Kokke, F. T. M., Krolo, A., Başaran, M. K., Kaya, N. G., Aksu, A. Ü., Dalgıç, B., Ozcay, F., Baris, Z., Kain, R., ... Boztug, K. (2018). Intestinal Failure and Aberrant Lipid Metabolism in Patients With DGAT1 Deficiency. *Gastroenterology*, 155(1), 130-143.e15. <https://doi.org/10.1053/j.gastro.2018.03.040>

4

INTESTINAL ORGANOID CO-CULTURES WITH MICROBES

Jens Puschhof^{1,2,*}, Cayetano Pleguezuelos-Manzano^{1,2,*}, Adriana Martinez-Silgado^{1,2},
Ninouk Akkerman^{1,2}, Aurelia Sftien^{1,2}, Charelle Boot^{1,2}, Amy de Waal^{1,2}, Joep Beumer^{1,2},
Devanjali Dutta^{1,2}, Inha Heo^{1,2}, Hans Clevers^{1,2}

¹Hubrecht Institute, Royal Netherlands Academy of Arts and Sciences (KNAW) and UMC Utrecht, 3584 CT Utrecht, the Netherlands. ²Oncode Institute, Hubrecht Institute, 3584 CT Utrecht, the Netherlands.

*Co-first author

ABSTRACT

Adult-stem-cell-derived organoids model human epithelial tissues *ex vivo*, which enables the study of host–microbe interactions with great experimental control. This protocol comprises methods to coculture organoids with microbes, particularly focusing on human small intestinal and colon organoids exposed to individual bacterial species. Microinjection into the lumen and periphery of 3D organoids is discussed, as well as exposure of organoids to microbes in a 2D layer. We provide detailed protocols for characterizing the coculture with regard to bacterial and organoid cell viability and growth kinetics. Spatial relationships can be studied by fluorescence live microscopy, as well as scanning electron microscopy. Finally, we discuss considerations for assessing the impact of bacteria on gene expression and mutations through RNA and DNA sequencing. This protocol requires equipment for standard mammalian tissue culture, or bacterial or viral culture, as well as a microinjection device.

INTRODUCTION

Since they were first reported in 2009 (ref.¹), adult-stem-cell-derived organoids have vastly expanded the possibilities to grow healthy epithelial cell types. In recent years, these near-physiological models have led to substantial advances in stem cell biology, disease modeling and the study of host–microbe interactions. Amongst others^{2–4}, adult-stem-cell-derived organoids have been harnessed to study *Cryptosporidium parvum*⁵, *Helicobacter pylori*⁶, norovirus⁷, severe acute respiratory syndrome coronavirus 2 (refs.^{8,9}) and genotoxic *Escherichia coli*¹⁰ infections. The important role of the intestinal microbiota in healthy organ function and diseased states is increasingly recognized. Nevertheless, many links of microbes to diseases remain correlative owing to the difficulty of modeling host–microbe relationships in a reductionist yet meaningful way. This underlines the importance of sophisticated *in vitro* model systems to gain mechanistic insights into microbial effects on the epithelium and enable the development of therapeutics targeted at microbial–epithelial interaction processes. In this protocol, we lay out a broadly applicable procedure for the injection of microbes into the organoid lumen, as employed in recent studies^{5,10}. Furthermore, we present protocols for 3D and 2D apical and basal exposure to microbes for medium-throughput studies and for pathogens with a non-apical infection route. While these protocols mostly entail bacterial cocultures, dedicated protocols for viral¹¹ and parasitic^{12,13} organoid exposure have recently been published and can be directly coupled to the methods described here.

DEVELOPMENT OF THE PROTOCOL

The protocols for microbe–epithelium cocultures presented here are based on human adult-stem-cell-derived organoids, which have been described previously¹⁴. The polarization of human small intestinal and colonic organoids results in a cystic shape with the inside corresponding to the gut lumen. This necessitates microinjection of gut microbiota into the lumen of organoids for a faithful representation of epithelium–microbe orientation. Based on the development of microinjection procedures for various organoid systems and pathogens in our group, we here provide a comprehensive protocol for the preparation and microbe coculture of human intestinal organoids (Fig. 1). We also describe deviations from this coculture protocol that can be performed without the need for microinjections, such as viral exposure^{8,15} or 2D cocultures in Transwell plates (Box 1).

APPLICATIONS

The protocols outlined below have broad applications in the study of microbe–epithelium interactions in cancer, infectious diseases and homeostasis. They are suitable for the investigation of single microbial species effects but could also be amended for combinations of different microorganisms. The use of adult-stem-cell-derived organoids makes the protocols ideally suited for applications where faithful recapitulation of wild-type epithelial cell types is of importance and where other microenvironmental

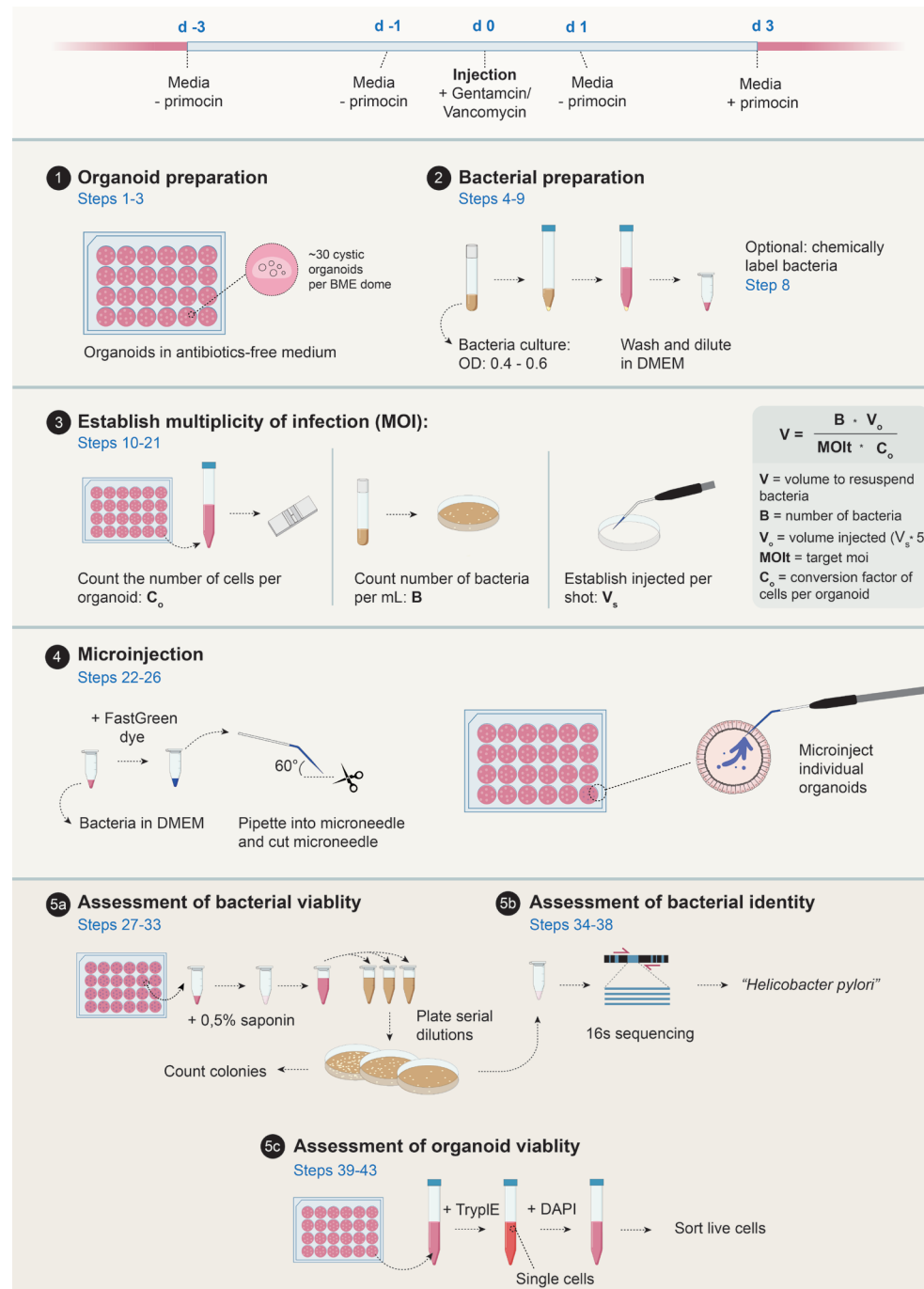


Figure 1. Overview of the protocol steps. First row: timeline of medium modifications for a typical bacterial coculture. Second row: preparation of bacteria and organoids. Third row: calculation of the MOI for organoid injections. Fourth row: organoid microinjections. Fifth row: assays for characterizing the coculture success.

influences need to be excluded. In particular, target cells for viral or bacterial infection can be characterized in great detail and with tight experimental control.

LIMITATIONS

There are limitations that need to be addressed in the future regarding the coculture of organoids with microbes. Particularly, the manual nature of the microinjection procedure makes it difficult to scale it up to higher-throughput experimental setups. Additionally, this protocol describes a reductionist approach to organoid–microbe coculture, using single microbial species. This strategy does not take into account the whole complexity of the intestinal microbiota ecosystem, such as complex interactions with the immune compartment. Furthermore, this system does not fully recapitulate other aspects of the intestinal tract such as the crypt–villus structure, a fully mature mucus layer or the incorporation of flow. Finally, the manipulation of important factors such as oxygen and nutrient levels during the coculture process is still in its infancy. Therefore, some aspects might be modeled in a more reliable way using alternative systems that are briefly discussed below.

CRITICAL Injection of intestinal organoids allows coculture under the most physiological conditions, but standardization and scalability of this protocol is difficult to achieve. Below, we provide a protocol to grow and differentiate organoids in monolayers for cocultures.

1. Coat the bottom of a 96-well plate or a 24-well plate Transwell insert with 5% (vol/vol) BME in DMEM for 30 min at 37 °C. Transwell inserts grant apical and basal access to the cell layer, whereas standard cell culture plates allow for the greatest scalability.
2. After the coating process, remove the supernatant and allow the BME coating to dry in the incubator for another 15–30 min.
3. Harvest organoids from the culture in 1 mL of cold DMEM, and transfer to a 15 mL Falcon tube. Top up to 10 mL with cold DMEM.
4. Spin for 5 min at 300g, and discard supernatant.
5. Dissociate the organoids to single cells as described previously¹⁶ (basic protocol 5).
6. Resuspend in expansion medium with 10 μM RhoKi at a density of 1,000,000 cells per 1 mL.
7. Seed 100,000 cells in 100 μL per well of a tissue-culture-treated 96-well plate or a Transwell insert of 6.5 mm diameter.
8. Allow cells to settle for 2 d.
9. After 3 d or when the layer is close to confluence, switch to any differentiation medium if needed.
10. Upon reaching confluence, add microbes to the apical or basal side in a medium suitable for exposure. For MOI calculations, a representative well can be harvested and cells counted as described above.
11. Perform read-outs in analogy to 3D coculture.

Box 1. Organoid monolayer cocultures • Timing 1.5 h hands-on time, 3–5 d in total

COMPARISON WITH ALTERNATIVE HOST-MICROBE INTERACTION MODEL SYSTEMS

Adult-stem-cell-derived organoids provide a faithful representation of fully differentiated and progenitor epithelial cell types, making them ideally suited for studies on direct microbe–epithelium interactions^{16,17}. The organoid lumen, which mimics the microbiota's habitat, can be exposed to the microbe of interest via microinjection. The cystic nature of organoids allows bacterial species with low oxygen tolerance to survive and prevents bacterial overgrowth. Furthermore, organoid cocultures offer experimental control over the timeframe of exposure and the types of host cells that are involved. This can be tuned through differentiation in tailored organoid media¹⁸, yielding a faithful representation of the cell types required to answer the research question at hand. This reductionist, highly controlled approach allows detailed studies and exclusion of confounding factors, but it comes at the cost of reduced complexity of the model system. While the inclusion of further cell types from the stromal and immune compartment into organoid models is rapidly progressing^{19–22}, no *in vitro* model represents the entire microenvironment faithfully to date.

Mouse models remain more suited to capture the full complexity of host–microbiota interactions, allowing simultaneous assessment of immune cell interactions and systemic effects of changes of the gut microflora, for instance²³. They furthermore enable long-term experiments and the simultaneous study of different gut regions. Nevertheless, the complexity of the intestinal microenvironment and challenges with assessing parameters in real time complicates the derivation of direct causation. Crucially, human-specific microbe interactions cannot be modeled with mouse models.

Pluripotent-stem-cell-based organoids allow easy addition of stromal cell types to the organoids using dedicated differentiation protocols and therefore enable the investigation of more complex relationships^{24,25}. Consequently, pluripotent-stem-cell-derived organoids have enabled pioneering work on bacterial and viral infections of intestinal cells^{26–28}. However, handling of these organoids is more time-consuming and may prove restrictive for studies involving repeated genetic manipulation of organoids and clonal outgrowth after exposure to a pathogen.

Intestines-on-chip approaches have seen remarkable progress in the past years and have started to enable long-term cocultures with single microbial species²⁹ or even complex communities³⁰. We anticipate that intestines-on-chip will facilitate many host–microbe studies in the future with regard to scalability, experimental control and easy readouts such as barrier integrity of the epithelium. At this moment, many models still rely on seeding of immortalized cell lines³¹; culturing primary or organoid-derived cells on chip devices is in its infancy^{30,32}. Therefore, proper representation of mature cell types remains a challenge, and detailed chip-based studies on host–microbe interactions are still scarce.

EXPERIMENTAL DESIGN

When setting up an organoid coculture, both the microbes' and epithelial cells' growth requirements demand close attention. Optimal medium compositions are likely to differ; hence, a dedicated medium recipe has to be found that addresses the needs of both. This is a vital step to ensure that the essential prerequisites to address the research question (such as viability and metabolic activity) are maintained. For viruses, these considerations are less pressing, as they can generally be cocultured using standard organoid media.

Another key consideration is the architecture of the coculture. Injections into the lumen of organoids have major advantages such as the physiologically relevant localization of bacteria and 3D recapitulation of the organ. Nevertheless, cocultures can also be set up using sheared organoids (Steps 77–87) and monolayers grown on Transwells (Box 1, Steps 1–11). A main advantage of these alternative protocols is the enhanced scalability and more homogeneous exposure of individual cells to microbes. A main drawback is the lack of a spatially and environmentally protected bacterial compartment, resulting in poor survival of obligate anaerobes or uncontrolled growth of other bacterial species. Furthermore, monolayer cultures lose the original 3D structure of the organ, and basal exposure to bacteria can be hampered by sedimentation of microorganisms. Exposure of sheared organoids also precludes any control over apical or basal exposure, which can be important in the case of luminal bacteria, for instance. For these reasons, the protocols below focus on microinjections into the lumen of cystic organoids unless stated otherwise.

A key consideration for organoid–microbe cocultures is synchronization of both components in the right growth state. Organoids should be grown as cysts of >200 μm in diameter for ideal injection success rate. Furthermore, organoids should be seeded sparsely before injection to ensure that the majority of organoids can be injected (Fig. 2g). For these reasons, organoids should be grown until spanning >200 μm in average diameter before being passed gently to avoid excessive shearing of organoids and seeded sparsely into a new plate (see Steps 1–3). Within 7 d after passage, organoids should regain their cystic shape and be ready for injection. Depending on bacterial growth speed, they should be inoculated 6–48 h before the planned injection to reach the optimal growth phase and numbers for coculture. This timing has to be optimized for each organoid line and microbe species to ensure synchronization and coculture success.

In the case of studies on microbe interactions with terminally differentiated cell types, the timing of differentiation has to be optimized. Intestinal cells typically reach a mature state 5 d after induction of differentiation through a tailored culture medium or genetic induction¹⁷. Organoids become harder to inject in the process of differentiation, primarily due to a decrease in lumen size and increased thickness of the epithelial layer (Fig. 2j). In our experience, injecting within the first 2 d after differentiation induction enables the best coculture results unless terminally differentiated cells are required from the beginning of the exposure.

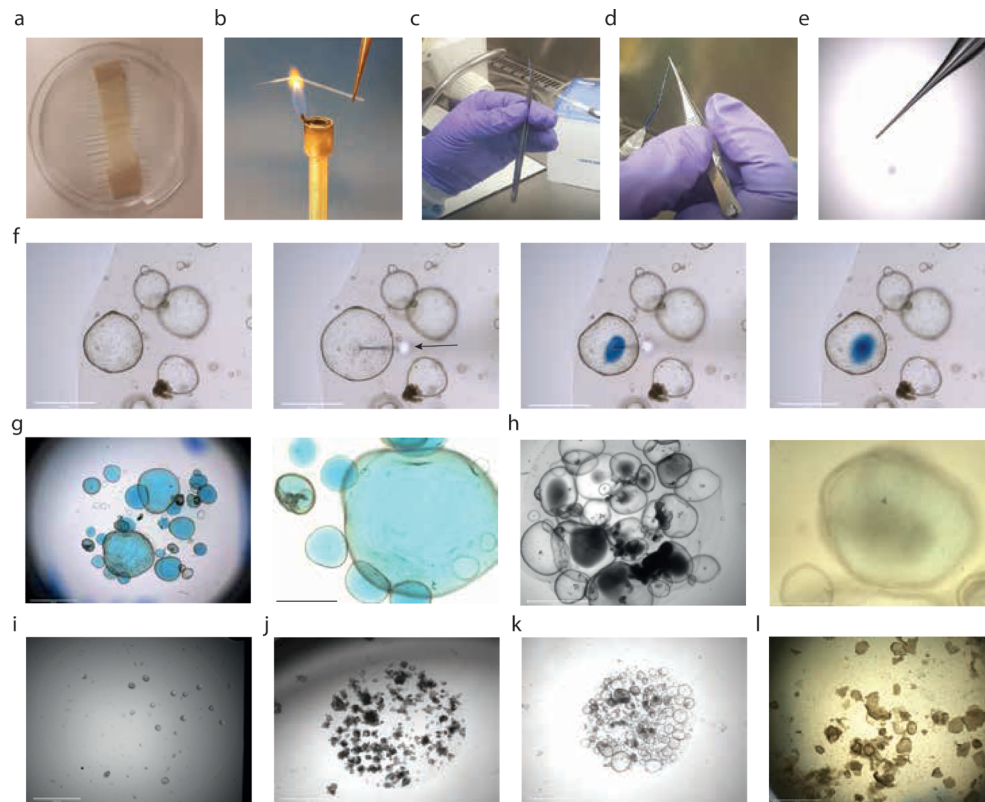


Figure 2. Organoid microinjections. **a**, Double-sided tape holder for storage of injection needles. **b**, Bending of an injection needle. **c**, Transfer of bacteria suspension to an injection needle. **d**, Cutting of a needle under an appropriate angle. **e**, Representative image of a cut needle. **f**, Process of injecting an organoid with FastGreen dye. **g**, Overview images of a dome with injected organoids (scale bars, 2.5 mm and 0.5 mm, respectively). **h**, Bacteria clouds in injected organoids (scale bars, 2.5 mm and 0.5 mm, respectively). **i**, Organoids too small for injection (scale bar, 0.5 mm). **j**, Organoids too differentiated for injection (scale bar, 2 mm). **k**, Organoids too dense for efficient injection (scale bar, 2 mm). **l**, Bacterial overgrowth with marked organoid damage (scale bar, 2.5 mm).

Since the size of organoids to be injected is heterogeneous, the number of injection shots per organoid should be adjusted depending on organoid size to keep the multiplicity of infection (MOI) similar between organoids. Calculating with five injection shots for an average-sized organoid is most practical to limit the number of injection shots while maintaining enough flexibility to adjust for smaller and larger organoids by changing the number of shots per organoid depending on size.

It is important to consider the intended readout of the coculture experiment. The protocols described here have proven useful in a variety of assays, ranging from modeling pathogen life cycles⁵ and immediate epithelial responses⁸ to long-term carcinogenic effects of bacterial exposure¹⁰. Studies on immediate effects of microbial exposure require consideration of the number of organoids that are necessary for each

assay. Depending on this, the timing and numbers of injection can be carefully planned to allow controlled experiments without unnecessary delays. For long-term studies, the choice of a rapidly and cystically growing organoid line is advisable to enable repeated injections at high efficiency. Ideally, several organoid lines from independent donors with comparable growth characteristics should be used. In contrast to short-term experiments, the number of injected organoids becomes less important if the exposure is followed by a clonal expansion step to assess genomic effects in individual cells (Steps 65–76).

During cDNA synthesis for qPCR or library preparation, epithelial and bacterial RNA has different requirements. If epithelial RNA enrichment is required, use polyA primers. If synthesizing bacterial cDNA alone or together with epithelial cDNA, use random hexamer primers.

RNA derived from organoid–bacteria cocultures is amenable to several techniques that allow for the simultaneous analysis of both interacting partners’ transcripts^{33–35}. For all of these approaches, a high proportion of harvested organoids should be injected to allow faithful detection of expression changes.

When setting up an organoid co-culture, both the microbes’ and epithelial cells’ growth requirements demand close attention. Optimal media compositions are likely to differ, hence a dedicated media recipe has to be found which addresses the needs of both. This is a vital step to ensure that the essential prerequisites to address the research question (such as viability and metabolic activity) are maintained. For viruses, these considerations are less pressing, as they can generally be co-cultured using standard organoid media.

Another key consideration is the architecture of the co-culture. Injections into the lumen of organoids remain the gold-standard due to the physiologically relevant localization of bacteria and 3D recapitulation of the organ. Nevertheless, co-cultures can also be set up using sheared organoids (Protocol 6) and monolayers grown on transwells (Protocol 7). A main upside of both alternative protocols is the enhanced scalability and more homogenous exposure of individual cells to microbes. A main drawback is the lack of a spatially and environmentally protected bacterial compartment, resulting in poor survival of obligate anaerobes or uncontrolled growth of other bacterial species. Furthermore, monolayer cultures lose the original 3D structure of the organ and basal exposure to bacteria can be hampered by sedimentation of microorganisms. Exposure of sheared organoids also prevents any control over apical or basal exposure which can be important in case of luminal bacteria, for instance. For these reasons the protocols below focus on microinjections into the lumen of cystic organoids unless stated otherwise.

A key consideration for organoid-microbe co-cultures is synchronization of both components in the right growth state. Organoids should be grown as cysts of >200 μm in diameter for ideal injection success rate. Furthermore, organoids should be seeded sparsely before injection to ensure that the majority of organoids can be injected (see Fig. 2f). For these reasons, organoids should be grown until spanning >200 μm in average diameter before being passed gently to avoid excessive shearing of organoids and seeded sparsely into a new plate (see Protocol 1: Organoid preparation). Within 2

days after passage, organoids should regain their cystic shape and be ready for injection. Depending on bacterial growth speed, they should be inoculated 6 - 48h before the planned injection to reach the optimal growth phase and number for co-culture. This timing has to be optimized for each organoid line and microbe species to ensure optimal synchronization and co-culture success.

In case of studies on microbe interactions with terminally differentiated cell types, the timing of differentiation has to be optimized. Intestinal cells typically reach a mature state 5 days after induction of differentiation through a tailored culture medium or genetic induction¹⁶. Organoids become harder to inject in the process of differentiation, primarily due to a decrease in lumen size and increased thickness of the epithelial layer (see Fig. 2i). In our experience, injecting within the first 2 days after differentiation induction enables the best co-culture results unless terminally differentiated cells are required from the beginning of the exposure.

It is important to take into account the intended readout of the co-culture experiment. The protocols described here have proven useful in a variety of assays, ranging from modelling pathogen life cycles⁵ and immediate epithelial responses⁹ to long-term carcinogenic effects of bacterial exposure¹⁰. Studies on immediate effects of microbial exposure require experience with the number of organoids which are necessary for each assay. Depending on this, the timing and numbers of injection can be carefully planned to allow controlled experiments without unnecessary delays. For long-term studies, the choice of a rapidly and cystically growing organoid line is advisable to enable repeated injections at high efficiency. In contrast to short-term experiments, the number of injected organoids becomes less important if the exposure is followed by a clonal expansion step to assess genomic effects in individual cells (Protocol 5H).

MATERIALS

Reagents

- Dulbecco's Modified Eagle Medium (DMEM; Thermo Scientific, cat. no. 11965-092)
- Advanced DMEM/F12 (Thermo Scientific, cat. no. 12634-010)
- B-27 Supplement (Thermo Scientific, cat. no. 17504044)
- GlutaMAX (Thermo Scientific, cat. no. 35050061)
- HEPES (Thermo Scientific, cat. no. 15630080)
- Penicillin–streptomycin (Thermo Scientific, cat. no. 15140122)
- Primocin (Invivogen, cat. no. ant-pm-2)
- Gentamicin (Sigma-Aldrich, cat. no. G1397)
- Vancomycin (Sigma-Aldrich, cat. no. SBR00001)
- *N*-acetyl-L-cysteine (Sigma-Aldrich, cat. no. A9165)
- Nicotinamide (Sigma-Aldrich, cat. no. N0636)
- Wnt surrogate (U-Protein Express, cat. no. N001)
- Noggin conditioned medium (U-Protein Express, custom order)

- R-spondin conditioned medium (U-Protein Express, custom order)
- Human epidermal growth factor (Peprotech, cat. no. AF-100-15)
- A83-01 (Tocris, cat. no. 2939)
- SB202190 (Sigma Aldrich, cat. no. S7076)
- Prostaglandin E2 (Tocris, cat. no. 2296)
- Glutaraldehyde solution (Sigma-Aldrich, cat. no. G5882)
- PBS (Thermo Scientific, cat. no. AM9624AM9624)
- FBS (Thermo Scientific, cat. no. 16140-071)
- Basement membrane extract (BME), growth factor reduced, type 2 (R&D Systems/Bio-Techne, cat. no.3533-001-02)
- Cell Recovery Solution (Corning, cat. no. Z317047)
- DAPI (Thermo Scientific, cat. no. D1306)
- TRIzol (Thermo Scientific, cat. no. 15596026)
- RNeasy Mini Kit (Qiagen, cat. no. 74104)
- CD326 (EpCAM) monoclonal antibody (MH99) (Alexa Fluor 488, eBioscience/Thermo Scientific, cat. no. 53-8326-42)
- Fast Green FCF (Sigma-Aldrich, cat. no. F7252)
- Brain heart infusion broth (Merck, cat. no. 53286)
- eBioscience Cell Proliferation Dye eFluor 450 (Thermo Scientific, cat. no. 65-0842-85)
- 5(6)-CFDA, SE; CFSE (5-(and-6)-carboxyfluorescein diacetate, succinimidyl ester), mixed isomers (Thermo Scientific, cat. no. C1157)
- CellTracker Orange CMTMR Dye (Thermo Scientific, cat. no. C2927)
- CellTracker Red CMTPX Dye (Thermo Scientific, cat. no. C34552)
- Y-27632 Rho kinase inhibitor (RhoKi; Abmole, cat. no. Y-27632)
- TrypLE (Thermo Fisher Scientific, cat. no. 12605010)
- SB 202190 (Sigma-Aldrich, cat. no. S7076)

EQUIPMENT

- Falcon tubes, 15 mL (Corning, cat. no. CLS430053)
- 5 mL polystyrene round-bottom tube with cell-strainer caps (Corning, cat. no. 352235)
- Microcentrifuge tubes, 1.5 mL (Eppendorf, cat. no. 0030 120.0860030 120.086)
- Plates, six-well (Greiner Bio-One, cat. no. 657 160)
- Plates, 12-well (Greiner Bio-One, cat. no. 665 180)
- Plates, 24-well (Greiner Bio-One, cat. no. 662 160)
- Plates, 48-well (Greiner Bio-One, cat. no. 677 180)
- Cell culture dishes, 100 × 20 mm (Greiner Bio-One, cat. no. 664 160)
- Glass pasteur pipettes (VWR, cat. no. 612-1701)
- EVOS Cell Imaging System (Thermo Fisher, cat. no. M5000)
- Overhead microscope in ML-2 biosafety cabinet (Leica, cat. no. MZ75)

- Centrifuge (Eppendorf, cat. no. 5810R)
- Centrifuge (Eppendorf, cat. no. 5424)
- 24-well plate Transwell inset (Corning HTS Transwell-24 well permeable; 0.4 µm pore polycarbonate membrane; cat. no. CLS3396)
- Eppendorf Microloader (Sigma-Aldrich, cat. no. EP5242956003)
- Corning BioCoat poly-L-lysine, 12 mm (Corning, cat. no. 354085)
- Hexamethyldisilazane (Sigma, cat. no. 440191)
- Scanning electron microscopy (SEM) pin stubs, 12.5 mm (Agar Scientific, cat. no. AGG301-S-50)
- Q150R sputter coater (Quorum Technologies, cat. no. Q150R)
- Phenom PRO table-top scanning electron microscope (Phenom-World)
- FemtoJet 4i microinjector (Eppendorf, cat. no. 5252 000.013)
- Thin-wall glass capillaries (World Precision Instruments, cat. no. TW100F-4)
- Needle puller model P-80/PC (Sutter Instrument Company)

REAGENT SETUP

Organoid expansion medium

Organoid injections are performed in a medium that supports viability of both epithelium and a variety of bacterial strains. To make this expansion medium, supplement AdDMEM/F12 with B-27 Supplement (1×), Glutamax (1×), HEPES (1×), 1.25 mM *N*-acetylcysteine and 10 mM nicotinamide. The following growth factors should be added: 2% Noggin conditioned medium, 20% RSpondin I conditioned medium, 50 ng/mL epidermal growth factor, 0.5 mM A83-01, 1 µM PGE2, 10 µM SB202190 and 0.5 nM Wnt surrogate.

Some bacteria may be inhibited by *N*-acetylcysteine. For cocultures with these, the compound may be left out for the coculture period (make sure to also withdraw it in a control well for comparisons).

The organoid medium should be used within 1 month after preparation and stored at 4 °C. It can be stored frozen or as a liquid and used within the same timeframe after thawing. Avoid freeze–thaw cycles.

Antibiotics additions

To avoid contaminations in monoculture of organoids, add either 100 U/mL penicillin–streptomycin (stable at 4 °C for 2 weeks) or 100 mg/mL primocin (stable at 4 °C for 3 months) to the expansion medium and store at 4 °C.

After injection in antibiotics-free medium, the medium may be replaced with expansion medium containing 5 µg/mL of the non-permeant antibiotic gentamicin (stable at 4 °C for 1 month) or 500 ng/mL vancomycin (stable at 4 °C for 1 week), when working with Gram-positive bacteria. This will prevent growth of bacteria outside of the organoid lumen, while also preserving viability of bacteria inside the organoids. To terminate a coculture without splitting the organoids, 100 mg/mL of the antibiotics mix primocin is added to the culture.

Needle preparation

Pull glass cuvettes using a glass needle puller (we routinely use a P-80/PC (Sutter) needle puller at the following settings: Heat 645; Pull 100; Vel 200, Time 40). Pulled needles can be stored on a strip of tape in a Petri dish (Fig. 2a) and should be exposed to 10 min of UV irradiation in a tissue culture cabinet before their first use to minimize contamination. Pulled needles can be stored in the Petri dish inside a biosafety cabinet for more than a year. For injections into wells of 24-, 48- and 96-well plates, needles should be bent by flaming their center part with a Bunsen burner until an angle of ~45° is reached (Fig. 2b).

Chemical labelling of bacteria

Staining bacteria with fluorescent dyes before injection allows their behavior in coculture to be traced for up to 1 week. The following dye mixes (presented in the table below) can be used for labeling a variety of bacterial species (we have validated their use for strains of *Fusobacterium nucleatum*, *Escherichia coli*, *Akkermansia muciniphila*, *Bacteroides fragilis*, *Bacteroides thetaiotaomicron*, *Bifidobacterium brevis*, *Bifidobacterium longum*, *Clostridium scindens* and *Lactobacillus reuteri*).

Organoid preparation for microinjection • Timing 3 h hands-on time, ~1 week in total

1. ~10 d before injection: starting from one densely plated well of a 24-well plate (~300,000 cells or 150 organoids with a diameter of ~300 µm), shear organoids mechanically as described before¹⁷. Ensure homogeneous size distribution using extensive passage through a narrowed glass pipette. Seed organoids sparsely (~30 organoid fragments per dome of ~20 µL) with one dome per well of a 24-well plate. Alternatively, to 3D coculture, organoids can be seeded in Transwells for exposure of monolayers (Box 1).

CRITICAL STEP The seeding density is dependent on the downstream application. As a rule of thumb, a seeding density approximately tenfold lower than for standard organoid culture is advantageous to ensure that most organoids can be injected.

Fluorescent dyes for labeling bacteria

Color	Dye	Final concentration	Excitation	Emission
Blue	eBioscience™ Cell Proliferation Dye eFluor™ 450	20 µM	405	450
Green	5(6)-CFDA, SE; CFSE (5-(and-6)-Carboxyfluorescein Diacetate, Succinimidyl Ester), mixed isomers	20 µM	492	517
Orange	CellTracker™ Orange CMTMR Dye	20 µM	541	565
Red	CellTracker™ Red CMTMX Dye	20 µM	577	602

A good density is shown in Fig. 2g, whereas a common organoid seeding that is too dense for efficient injections is depicted in Fig. 2k.

- Let organoids grow until they have reached an average diameter of $>200\ \mu\text{m}$ (normally within 5–10 d after mechanical shearing). If the organoids are seeded too densely, they can be carefully reseeded in a new plate using a cut P1000 tip in a higher dilution ~ 3 d before the planned injection.

CRITICAL STEP Cystic organoids are essential for injection efficiency. Organoid lines with cystic growth behavior and optimal medium conditions¹⁶ should be used for injection experiments. Examples of unsuitable organoid states are depicted in Fig. 2i-k.

- Three days before injection: change the medium to antibiotics-free medium to allow enough time for the antibiotics to diffuse from the BME domes. One day before injection, refresh the medium once more with antibiotic-free medium.

Bacteria preparation • Timing 1.5 h hands-on time, 1–2 d in total

- Inoculate bacteria from cryostock into their optimal culture medium, and incubate overnight at $37\ ^\circ\text{C}$ and 180 rpm.
- Resuspend grown bacteria 1:10 in fresh optimal culture medium, and incubate until they have reached exponential growth phase and sufficient quantity for injection (an OD of ~ 0.4 – 0.6 in 1 mL medium is sufficient for most bacterial strains).

CRITICAL STEP For obligate anaerobic bacteria, an anaerobic chamber or comparable equipment should be used to grow the bacteria. Make sure to use anoxic media and maintain an anoxic environment for all steps until injection.

- Spin bacteria for 10 min at $3,000g$, and discard supernatant.
- Wash with 10 mL of DMEM, and repeat Step 5.
- Optional steps: if identification of the bacteria in a coculture by fluorescence microscopy (Steps 43–45) is desired, perform chemical labeling of bacteria by the following instructions (Fig. 3a,b):

- Wash bacteria pellet twice with 10 mL of PBS to remove protein remainder
- CRITICAL STEP** Improper washing will prevent the dye from entering the cells in the next step.
- Incubate for 45 min with $20\ \mu\text{M}$ freshly prepared fluorescent dye (see table in 'Reagent setup' for suitable dye options)
- Wash once with 10 mL of PBS

- Resuspend the pellet in a volume (V) of DMEM (typically 0.250 mL, see 'Experimental design') to achieve an optimal concentration for injections (see Steps 10–21).

Establish MOI • Timing 3 h hands-on time, 2 d in total

CRITICAL To calculate the MOI, both bacterial and organoid cell numbers need to be estimated. Owing to the heterogeneity of organoids, a target MOI is calculated assuming

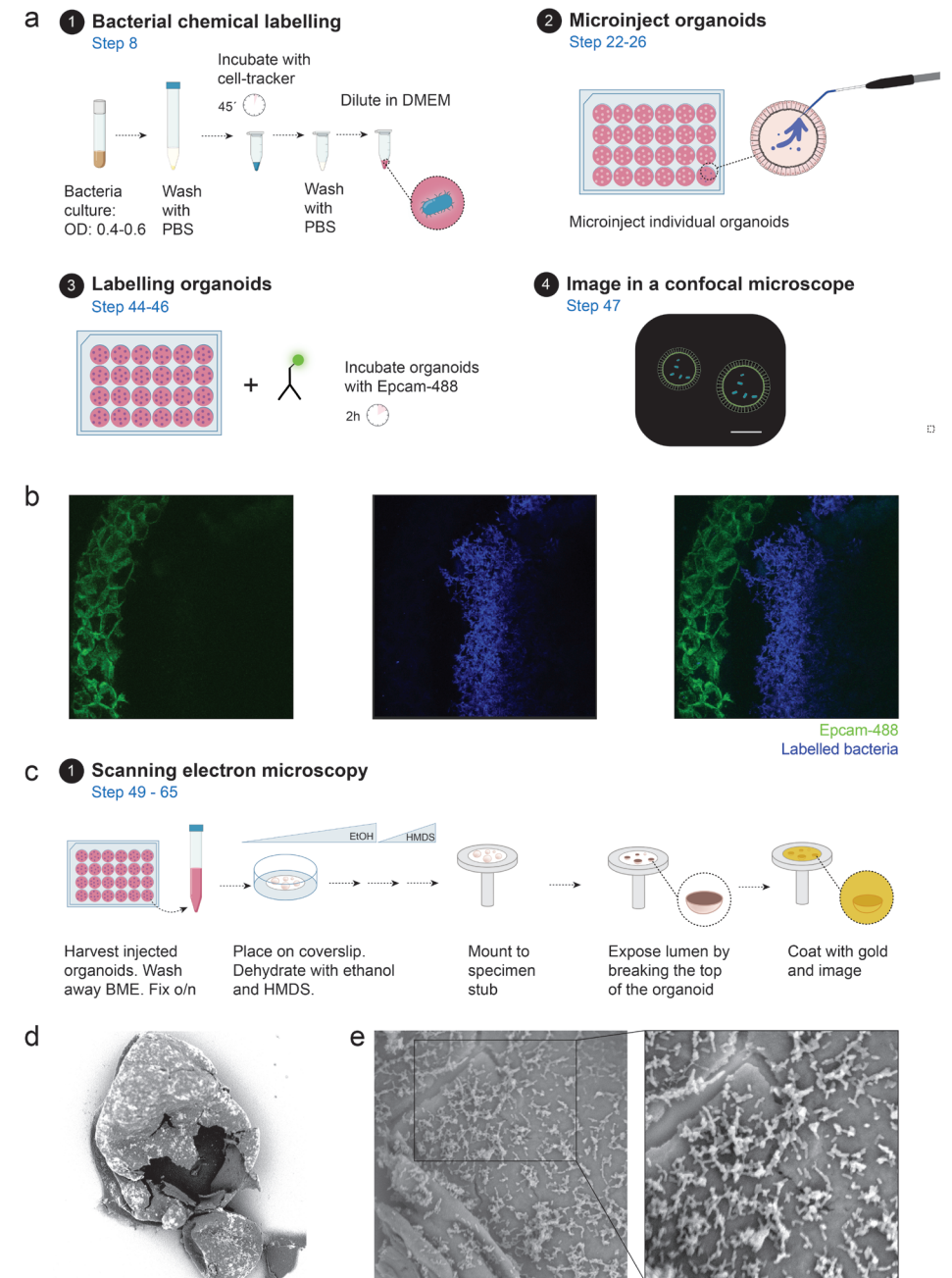


Figure 3. Visualizing organoid cocultures. **a**, Fluorescent labeling of bacteria and organoids. **b**, Coculture of fluorescently labeled organoid (CD326 (EpCAM) Alexa Fluor 488, green, left panel) and bacteria (*Fusobacterium nucleatum* subsp. *animalis* strain B7_1 labeled with Cell Proliferation Dye eFluor 450, blue, middle) (merged on the right panel) after 24 h of coculture (scale bar, $150\ \mu\text{m}$). **c**, SEM for visualizing bacteria in the lumen of organoids. **d**, Organoid broken with a tungsten needle to expose bacteria on the inside (scale bar, $300\ \mu\text{m}$). **e**, Close-up images of bacteria on the apical surface of an organoid (scale bar, $10\ \mu\text{m}$).

an average-sized organoid, and the exact MOI for any individual organoid will vary slightly from this value.

Establishing the cells per organoid conversion factor

10. Count the organoids in one representative dome of BME under a brightfield microscope.
11. Harvest this dome with a P1000 pipette, and dissociate the organoids to single cells as described in ref.¹⁶ (basic protocol 5).
12. Count the single cells derived from the dome using a standard hemocytometer.
13. Calculate the cells per organoid conversion factor (C_o) by dividing the number of cells (Step 12) by the number of organoids (Step 10) in the dome.

The value of C_o is typically ~1,000 cells/organoid for organoids in optimal injection state.

Establishing the bacterial cell number

For some bacterial species, the optical density at a wavelength of 600 nm (OD_{600}) to bacterial number conversion factor is well established (e.g., for *Escherichia coli*³⁶) and can be used as OD_c . Nevertheless, due to instrument and strain variations, it is recommended to generate a bacterial OD_{600} to cell number conversion factor as described below and use the conversion factor only in the linear OD_{600} to bacterial number conversion range.

To establish the bacterial cell number per optical density (OD_c), a liquid culture of bacteria is grown and its OD_{600} is measured (OD). After dilution and plating, the colony count C_b is used to calculate the conversion factor.

14. Grow bacteria to OD_{600} values of 0.1–1.0, plate in dilutions and count colonies after 1–2 d of growth to establish a conversion factor between OD and bacterial number:

$$OD_c = \frac{C_b}{OD_l * D * V_p}$$

OD_c = OD_{600} to bacterial count conversion factor

C_b = observed colony count

OD_l = OD_{600} of original liquid culture

D = dilution factor from original culture (e.g., 0.1 for a tenfold dilution)

V_p = plated volume

15. After establishing the conversion factor OD_c , the bacterial count in any liquid culture harvested at density of OD_m can be calculated to determine the required dilution for injection into organoids. Multiply the harvested volume and measure OD_m with the conversion factor OD_c to yield the total number of harvested bacteria (B):

$$B = OD_c * OD_m * V_h$$

where B is bacterial number, OD_c is OD to bacterial count conversion factor, OD_m is measured OD value and V_h is harvested volume.

Establishing the injected volume

16. To establish the volume per injection, transfer 1 μ L of 0.05% (wt/vol) Fast Green Dye in DMEM to a microinjection needle using a microloader tip, and insert it in the microinjector (Fig. 2c).
17. Cut open the needle at a $\sim 60^\circ$ angle to ensure later optimal organoid penetration and bacteria release later in the procedure (Fig. 2d).
18. Repeatedly inject into a Petri dish filled with PBS until the volume is completely ejected.
19. By dividing the ejected volume by the number of shots needed to empty the needle, derive the injected volume per shot (V_s). In our experience, a V_s value of 2–20 nL is ideal for injecting organoids of various sizes. Adjust pressure or needle cutting if V_s deviates from this target range.
20. Calculate the planned injection volume (V_o) for an average organoid that received five injection shots as $V_s \times 5$.

Diluting bacteria for injection at desired MOI

21. Resuspend a pellet containing a number of bacteria (B) in the volume V of DMEM with 0.05% (wt/vol) Fast Green Dye to visualize injections. To reach the appropriate target MOI (MOI_t) for coculture, V is calculated as:

$$V = \frac{B * V_o}{MOI_t * C_o}$$

where V is volume for resuspending the bacterial pellet, B is number of bacteria in pellet, V_o is volume injected into an average organoid, MOI_t = target MOI and C_o is conversion factor of cells per average organoid.

Microinjection • Timing hands-on and total time depend on number of organoids to be injected; ~5 min per dome

22. Take up 10 μ L of the bacteria injection mix with a microloader tip, transfer it to the microinjection needle and insert it in the microinjector.

23. Cut the needle open at a ~60° angle to ensure optimal organoid penetration and bacteria release (see Step 17 and Fig. 2d,e).
24. Place the plate with organoids under a stereomicroscope in a flow cabinet.
25. Penetrate individual organoids with the needle, and inject a defined amount of bacteria–dye mix into the lumen (Fig. 2f). Surplus wells should be injected and discarded in the case of excessive leakage outside the organoids.
26. Track the fraction of injected organoids by brightfield microscopy of the injection dye (Fig. 2g) and bacteria at higher magnification immediately after injection and over the next days. The injection dye is normally lost within a few days owing to diffusion, but bacteria will remain visible as opaque clouds in the organoid lumen (Fig. 2h).

(Optional) Characterizing the coculture

(Optional) Assessment of bacterial viability • Timing 30 min hands-on time, 1–2 d in total

CRITICAL Growth media, oxygen levels, spatial restriction within organoids and cellular interactions may influence bacterial growth in the coculture. To gain an understanding of the coculture dynamics, the number of viable bacteria should be checked regularly.

27. Harvest a defined number of organoids from the culture (e.g., one representative dome) in 1 mL of cold DMEM, and transfer to an Eppendorf tube.
28. Spin for 5 min at 3,000g, and discard the supernatant. In the case of anaerobic bacteria, transfer to an anoxic environment at this step and make sure all reagents are anoxic from here onwards.
29. Incubate with 200 µL 0.5% saponin for 10 min to lyse the organoid cells and free luminal and intracellular bacteria.
30. Top up to 1 mL with PBS, spin for 5 min at 3,000g and discard the supernatant.
31. Resuspend in PBS, and make serial dilutions.
32. Plate a defined volume of liquid of each dilution step on the appropriate agar plates.
33. Incubate at 37 °C overnight, and count colonies within the next 3 days, depending on the growth speed of the colonies. The number of live bacteria per organoid can be calculated and compared with the initially injected number of bacteria (Steps 14–21).

(Optional) Assessment of bacterial identity • Timing 30 min hands-on time, 1 d in total

CRITICAL A universal 16S locus primer pair 357F/926R (375F 5'-CCTACG GGAGGCAGCAG-3', 926R 5'-CCGTCAATTCMTTTRAGT-3') can be used to amplify the 16S rRNA V3–V5 regions of bacteria³⁷.

34. Pick a colony, wash in PBS and discard the supernatant. Resuspend in 10 µL PBS, and add 1 µL directly to the PCR mix (for a total volume of 30 µL). Use 4 µL 16S forward and reverse primers (both 5 µM). Proceed to run a 16S PCR. Run the following program:
 - 94 °C 10 min
 - [94 °C 1 min, 50 °C 30 s, 72 °C 30 s] × 30 cycles
 - 72 °C 5 min
 - 4 °C∞
35. (Optional) In the case of Gram-positive bacteria, enzymatic DNA isolation may be required prior to PCR amplification. If so, pick a colony, resuspend in the appropriate liquid medium and grow overnight. Harvest 1 mL of overnight culture, spin for 5 min at 13,000g and discard the supernatant. Isolate the DNA according to the manufacturer's protocol, and run the 16S PCR.
36. Perform gel electrophoresis of the PCR product on a 1% agarose gel with ethidium bromide, excise the band corresponding to the 16S amplicon (569 bp if using the universal 16S primers indicated above) and isolate the DNA. In the case of a clean PCR product (single, well-defined band), the PCR product can be purified instead.
37. Sequence the DNA to assess the identity of the bacteria.

(Optional) Assessment of organoid viability • Timing 1.5 h hands-on time, 1–2 d in total

38. Harvest organoids from the culture in 1 mL of ice cold (4 °C) DMEM, and transfer to a 15 mL Falcon tube. Top up to 10 mL with DMEM (4°C).
39. Spin for 5 min at 300g, and discard supernatant.
40. Dissociate the organoids to single cells as described previously¹⁶ (basic protocol 5).
41. Resuspend cells in DMEM with 2 µg/mL DAPI, and pass through the cap of a cell strainer FACS tube.
42. Run on an analytical flow sorter, and assess ratio of DAPI negative to total cells to establish viability as described previously^{10,16} (basic protocol 5).

(Optional) Staining for live microscopy • Timing 15 min hands-on time, ~2 h in total

CRITICAL The interactions in organoid–bacteria cocultures can be characterized by live microscopy (Fig. 3a). Ideally, distinct fluorescent dyes should be used to mark epithelial and bacterial cells. For visualizing bacteria with fluorescent dyes before injection, refer to Step 8.

43. Add a fluorescently conjugated cell surface marker antibody (e.g., EpCAM Alexa Fluor 488 antibody) to the medium of a well with organoids in BME domes. For live

staining in BME domes, high (1 µg/mL) concentrations of antibodies may need to be used.

44. Incubate for 2 h to allow the antibody to penetrate the BME and mark epithelial cell surfaces.
45. Image cocultures by fluorescence live microscopy (example shown in Fig. 3b).

(Optional) Scanning electron microscopy • Timing 2 h hands-on time, 2 d in total

CRITICAL SEM allows detailed insights into the bacterial organization at the cell surface (Fig. 3c).

46. Cut the front end of a P1000 tip to avoid mechanical shearing of organoids.
47. Harvest organoids from the culture in 1 mL of cold Cell Recovery solution, and transfer to a 15 mL Falcon tube.
48. Incubate for 2 h at 4 °C under regular rocking to facilitate digestion of BME.
CRITICAL STEP Improper digestion of BME will result in substantial background in the SEM imaging.
49. Top up to 10 mL with cold DMEM.
50. Spin for 5 min at 300g, and discard the supernatant.
! CAUTION From this step onward, protocol steps should be performed in a chemical safety cabinet owing to volatile toxic reagents.
51. Fix in 1% glutaraldehyde in PBS at 4 °C overnight.
52. Spin for 5 min at 300g, and resuspend in PBS.
53. Using a cut-off P1000 tip, transfer the organoids to the top of a coverslip coated with poly-L-lysine, and allow them to sediment and adhere to the surface for 10 min.
54. Using a pipette tip, carefully remove the supernatant.
55. Place each coverslip in a well of a 12-well plate, the organoid-coated side facing upward.
56. To initiate serial dehydration of the samples, add 1 mL of 10% ethanol in PBS to each well. After 10 min, remove the supernatant.
57. Using a pipette tip, carefully remove the supernatant and wash consecutively with 25%, 50% ethanol in PBS, 75%, 90% and 100% (twice) ethanol in water, followed by 50% and 100% hexamethyldisilazane in ethanol.
58. Dry coverslips in a chemical safety cabinet overnight.
59. Mount coverslips on specimen stubs, and place them under an overhead microscope for further manipulation.
60. To expose the interior of organoids injected with bacteria, use 0.5 mm tungsten needles to break the upper organoid wall under an overhead microscope (an example of a broken organoid is shown in Fig. 3d).

61. Coat the specimen surface with a 1 mm layer of gold using a Q150R sputter coater at 20 mA.
62. Proceed to SEM imaging of the samples (example shown in Fig. 3e).

(Optional) Assessment of transcriptional changes • Timing 2 h hands-on time, 5h in total

Organoids offer the ability to profile host and microbial gene expression changes with high experimental control and clear attribution to cell types. Here we describe the considerations on how to harvest and process human and bacterial RNA.

63. Isolate RNA using a commercial kit such as Qiagen RNeasy Mini Kit or RNeasy Protect Bacteria Mini Kit. Organoid–bacteria cocultures can be harvested by directly lysing the domes with Trizol or RLT lysis buffers.
64. Treat samples with RNase-free DNase to remove any residual DNA contamination.
CRITICAL STEP If bacterial RNA is isolated, proper lysis of bacterial cell walls is critical for good isolation yield. Importantly, Gram⁺ bacteria require a more extensive lysis than Gram⁻ microbes. Extensive DNase treatment to remove any genomic DNA content is particularly important for bacterial samples owing to their lack of intronic material, which hampers distinguishing between genomic and transcriptomic amplification.

(Optional) Assessment of mutational effects • Timing ~3 d hands-on time, ~40 d in total

CRITICAL Detecting mutational effects of bacteria in organoids requires starting with a clonal organoid line, followed by a second clonal expansion step after exposure. Comparing the genomes of both clonal lines before and after the exposure allows the analysis of mutations occurring in individual cells during the coculture.

65. Inject organoids with bacteria as described in Steps 22–26.
66. Assess organoid cell viability (Steps 38–42) after 1–7 d of coculture at different starting MOIs, which helps to establish a coculture MOI and timeframe suitable for detecting a mutagenic effect. A slight viability decrease (>10% and <50%) is a good indicator for acceptable genotoxicity for a long-term coculture.
67. Using the parameters established in Step 67, inject organoids as described in Steps 22–26.
68. After a suitable coculture duration (typically 3 d), kill bacteria by adding 100 mg/mL primocin.
69. Let organoids recover from the exposure for 4 d.
CRITICAL STEP Premature passage of organoids after coculture can result in drastically reduced organoid viability.
70. Passage organoids, and allow them to grow to injectable size again.
71. Repeat Steps 68–71 at least two further times to allow mutations to accumulate.

72. Trypsinize organoids to single cells as described before¹⁶ (basic protocol 5).
73. Seed at a density of 100 cells/ μ L, and grow in expansion medium containing 10 μ m RhoKi.
74. Once organoids reach a diameter of >50 μ m, pick individual organoids and grow them into new organoid lines.
75. As soon as the lines are expanded successfully, harvest one well of a 12-well plate full of organoids and proceed to DNA isolation using commercially available kits.
76. Analyze the DNA of clonal organoids before and after exposure to bacteria using whole-genome sequencing as described previously³⁸ (section 'Whole-genome sequencing and read alignment' and following).

Viral coculture of sheared organoids • Timing 1 h hands-on time, 3.5 h in total

77. Start with organoids as prepared in Steps 1–3. Harvest organoids in cold DMEM, and spin for 5 min at 300g and discard supernatant.
CRITICAL STEP Alternative routes of exposure, such as injection and virus addition to the media, can be used for specifically apical or basal access. The mechanical shearing protocol described here ensures both apical and basal access of the virus and yields the best infection efficiency in our experience.
78. Break cystic organoids with a narrowed glass pipette in 1 mL of DMEM. When differentiated organoids are infected, a brief 1–2 min incubation with TrypLE at 37 °C can be performed to aid in breaking the epithelial layer.
79. Spin for 5 min at 300g, and discard supernatant.
80. Wash organoids once with cold DMEM.
81. Thaw virus stock and dilute to appropriate MOI (see Steps 10–21) for MOI calculation). For virus infections of sheared organoids, the total cell number per dome is used (see Steps 11 and 12) for calculating the MOI instead of the number of injected organoids.
82. Resuspend organoid fragments in virus diluted in expansion or differentiation medium, depending on the cell types required (use 100 μ L of diluted virus per well of a 12-well plate of harvested organoids).
83. Incubate for 2 h at 37 °C 5% CO₂.
84. Wash twice with cold DMEM to remove unbound virus.
85. Resuspend thoroughly in BME by pipetting, and plate in domes of ~15 μ L.
86. *Optional step* For extended exposure to the virus, it can also be added to the BME during Step 86 before plating.
87. Leave to solidify bottom-up in a 37 °C CO₂ incubator for 10–20 min.
88. Add organoid expansion or differentiation medium on top (1 mL per well of a 12-well plate), and place in an incubator for the desired coculture duration.

TROUBLESHOOTING

Troubleshooting advice can be found in Table 1.

Table 1. Troubleshooting table

Step	Problem	Possible causes	Solution
25	Insufficient injection mix is coming out of needle Insufficient percentage of organoids is injectable	Needle opening is too small Injection pressure is too low Bacteria clump together Premature differentiation of organoids Injection needle not sharp enough Too dense plating	Increase needle opening by cutting it off more Increase injection pressure Pipette injection mix up and down every time before loading the needle Optimize media composition (especially the source of Wnt) Cut the needle under a sharper angle and increase injection pressure to facilitate perforation of organoid wall Include another step of passing organoids sparsely a few days before injection
26	Bacterial overgrowth	Contamination with different bacterium MOI too high or antibiotics concentration too low Ineffective antibiotics	Decontaminate all equipment and check culture media and dye are clean. Perform 16S sequencing to determine bacteria identity (Steps 34–37) Decrease MOI and/or perform Minimal Inhibitory Concentration (MIC) test to determine the required dose of antibiotics. Perform 16S sequencing to determine bacteria identity (Steps 34–37) Test antibiotics on pure bacterial cultures and acquire alternative non-diffusible antibiotics if needed. Perform 16S sequencing to determine bacteria identity (Steps 34–37)
33	Poor bacterial viability	Remaining antibiotics in organoids Unsuitable oxygen levels Suboptimal media condition	Ensure to remove antibiotics from the culture at least 3 days before adding the bacteria and change the medium in between Perform all steps up until filling the needle in a suitable environment for the bacterial strain at hand Withdraw individual media components which may interfere with bacterial viability. If necessary, add essential media components to the medium and use appropriate controls for any downstream assay

Table 1. (continued)

Step	Problem	Possible causes	Solution
Box 1, step 10	No confluent monolayer forms	Poor cell state upon seeding Inadequate cell number seeded Suboptimal media condition	Start with organoids in optimal expansion state (typically 2-5 d after passaging). Minimize the time of enzymatic digestion by pipetting repeatedly during the dissociation process. Include RhoKi inhibitor from the time of dissociation onwards. Vary the number of seeded cells. Ensure an appropriate Wnt source and RhoKi inhibitor are present in the medium for outgrowth. Don't initiate differentiation until the monolayer is close to reaching confluence.

TIMING

From thawing an established organoid line, it takes ~2 weeks before organoids are in the right growth state, size and density for injections. When a new organoid line is established¹⁷ for injections, it takes ~4 weeks before the right organoid number, growth state, size and density is reached.

Preparation of bacteria takes 6–48 h, depending on the species and strain used. The duration of the coculture and assays is dependent on the research question asked and can range from a few hours for imaging and transcriptional response studies to months for studies on mutations induced by bacteria. The expected duration of each procedure is indicated in the protocol and in the list below:

- Organoid preparation for microinjection (Steps 1–3): 3 weeks (5 h hands-on) when starting from cryostocks; 5–10 d (3 h hands-on) when starting from a growing organoid culture
- Bacterial preparation: 1–2 d (1.5 h hands-on) depending on strain used
- Establishing MOI: 1.5 h (1 h hands-on)
- Microinjection: 5 min hands-on time per dome
- Characterizing the coculture:
 - » Bacterial viability: 1–2 d in total (30 min hands-on)
 - » Bacterial identity: 1 d (30 min hands-on)
 - » Organoid viability: 1–2 d (1.5 h hands-on)
 - » Live microscopy: 2 h (15 min hands-on)
 - » SEM: 2 d (2 h hands-on)
 - » Transcriptional effects: 5 h (2 h hands-on)
 - » Mutational effects: 40 d (3 d hands-on)

ANTICIPATED RESULTS

We anticipate that this protocol will be used to perform diverse experiments to study the direct effects of the microbiota in the intestinal epithelium for cancer, infection and homeostasis studies. In particular, it provides a guide to culture intestinal organoids, cocultures with single bacteria species or viruses and their downstream analysis by confocal or electron microscopy, qPCR or RNA and wholegenome sequencing.

By loading the bacteria/dye suspension mix into a microinjection needle (Fig. 2a–e), microbes can be delivered into the lumen of the organoids (Fig. 2f). If the microinjection has been successful, the dye should remain visible inside the lumen of the organoid and not spread outside its boundaries (Fig. 2f,g). When the bacteria are injected in high numbers or actively divide during the coculture period, they can be visible by light microscopy as a dark area inside the organoid lumen (Fig. 2h). Seeding sparse organoids that become big cysts with culture time will increase the injection success rate (Fig. 2f) In contrast, too dense, small or differentiated organoids will make it practically impossible to inject the entirety of the organoids from one culture (Fig. 2i–k). If bacteria overgrow

outside the lumen, organoids generally show increased levels of cell death, which hampers the interpretability of coculture experiments (Fig. 2l).

In the case of suitable coculture conditions, viable bacteria can be retrieved from organoids to perform colony formation assays to quantify their viability and proliferation rate. Visible bacterial colonies should form within 2 d after plating on agar plates. 16S sequencing of colonies after coculture can also be used to rule out contaminations during the exposure period.

Organoid cell viability can be validated by DAPI exclusion flow cytometry analysis. Excessive exposure of organoids to bacteria or rapid degradation of medium components (e.g., during uncontrolled overgrowth of bacteria) decreases the proportion of viable epithelial cells. However, even under monoculture conditions, a fraction of 5–40% of organoid cells is expected to be stained by DAPI owing to cell turnover and stress during the digestion to single cells.

Cocultures of organoids and microbes stained with the chemical dyes described in this manuscript typically retain the signal for several days in the case of slowly dividing bacteria. Standard fluorescent microscopes can be used to follow the coculture regularly, while confocal microscopy is needed to reveal details of microbial positioning as shown in Fig. 3b. The formation of bacterial structures inside of organoids can be closely visualized by SEM within hours after injection (Fig. 3e), and variations in the bacterial number can be used to reveal different aspects of bacterium–host interactions.

The timing of genomic and transcriptional changes depends heavily on the interaction mechanism between microorganism and epithelial cells. In our experience, at least 9–15 d of exposure over time frame of several weeks and followed by a clonal expansion step allows the detection of mutagenic processes. Transcriptional changes in both microbe and host cells can be detected faithfully by qPCR and RNA sequencing. Monitoring the fraction of injected organoids and location of bacteria is key to proper interpretation of the obtained expression changes.

In the case of viral infection of intestinal organoids, it is important to take into consideration the cell type tropism of the viral infection and the expression of the entry receptor by the epithelial cells. In the case of successful infection, the viral titer should increase after 1 d of infection.

REPORTING SUMMARY

Further information on research design is available in the Nature Research Reporting Summary linked to this article.

DATA AVAILABILITY

All previously unpublished data are included in the figures. Raw image files are available from the corresponding author upon request.

ACKNOWLEDGEMENTS

We thank E. Allen-Vercoe and A. Robinson for provision of bacterial strains and discussions on bacterial culturing conditions. The development of the methods was supported by CRUK grant OPTIMISTIC (C10674/A27140) (J.P., C.P.-M. and H.C.), the Gravitation projects CancerGenomiCs.nl, and the Netherlands Organ-on-Chip Initiative (024.003.001) from the Netherlands Organisation for Scientific Research (NWO) funded by the Ministry of Education, Culture and Science of the government of the Netherlands (J.P., C.P.-M. and H.C.), the Onco Institute (partly financed by the Dutch Cancer Society), the European Research Council under ERC Advanced Grant Agreement no. 67013 (J.P., D.D., I.H. and H.C.) and NETRF/Petersen Accelerator (J.B.).

AUTHOR CONTRIBUTIONS

All authors contributed to the development of the organoid co-culture methods described in this protocol. J.P., C.P.M. and H.C. wrote the manuscript with input and corrections from all authors. A.M.S., C.P.M. and J.P. prepared figures. Competing interests H.C. is inventor on multiple patents held by the Dutch Royal Netherlands Academy of Arts and Sciences that cover organoid technology: PCT/NL2008/050543, WO2009/022907; PCT/NL2010/000017, WO2010/090513; PCT/IB2011/002167, WO2012/014076; PCT/IB2012/ 052950, WO2012/168930; PCT/EP2015/060815, WO2015/173425; PCT/EP2015/077990, WO2016/083613; PCT/EP2015/077988, WO2016/083612; PCT/EP2017/054797, WO2017/149025; PCT/EP2017/065101, WO2017/220586; PCT/EP2018/086716; and GB1819224.5. H.C.'s full disclosure is given at <https://www.uu.nl/staff/JCClevers/>.

REFERENCES

1. Sato, T. et al. Single Lgr5 stem cells build crypt-villus structures in vitro without a mesenchymal niche. *Nature* 459, 262–265 (2009).
2. Dutta, D., Heo, I. & Clevers, H. Disease modeling in stem cell-derived 3D organoid systems. *Trends Mol. Med.* 23, 393–410 (2017).
3. Min, S., Kim, S. & Cho, S.-W. Gastrointestinal tract modeling using organoids engineered with cellular and microbiota niches. *Exp. Mol. Med.* 52, 227–237 (2020).
4. Leslie, J. L. & Young, V. B. A whole new ball game: stem cell-derived epithelia in the study of host-microbe interactions. *Anaerobe* 37, 25–28 (2016).
5. Heo, I. et al. Modelling *Cryptosporidium* infection in human small intestinal and lung organoids. *Nat. Microbiol.* 3, 814–823 (2018).
6. Bartfeld, S. et al. In vitro expansion of human gastric epithelial stem cells and their responses to bacterial infection. *Gastroenterology* 148, 126–136.e6 (2015).
7. Ettayebi, K. et al. Replication of human noroviruses in stem cell-derived human enteroids. *Science* 353, 1387–1393 (2016).
8. Lamers, M. M. et al. SARS-CoV-2 productively infects human gut enterocytes. *Science* <https://doi.org/10.1126/science.abc1669> (2020).
9. Zhou, J. et al. Infection of bat and human intestinal organoids by SARS-CoV-2. *Nat. Med.* 26, 1077–1083 (2020).
10. Pleguezuelos-Manzano, C. et al. Mutational signature in colorectal cancer caused by genotoxic pks+ *E. coli*. *Nature* 580, 269–273 (2020).
11. Andersson-Rolf, A., Fink, J., Mustata, R. C. & Koo, B.-K. A video protocol of retroviral infection in primary intestinal organoid culture. *J. Vis. Exp.* <https://doi.org/10.3791/51765> (2014).
12. Holthaus, D., Delgado-Betancourt, E., Aebischer, T., Seeber, F. & Klotz, C. Harmonization of protocols for multi-species organoid platforms to study the intestinal biology of *Toxoplasma gondii* and other protozoan infections. *Front. Cell. Infect. Microbiol.* 10, 610368 (2021).
13. Dutta, D., Heo, I. & O'Connor, R. Studying *Cryptosporidium* infection in 3D tissue-derived human organoid culture systems by microinjection. *J. Vis. Exp.* <https://doi.org/10.3791/59610> (2019).
14. Sato, T. et al. Long-term expansion of epithelial organoids from human colon, adenoma, adenocarcinoma, and Barrett's epithelium. *Gastroenterology* 141, 1762–1772 (2011).
15. Fakhiri, J. et al. Novel chimeric gene therapy vectors based on adeno-associated virus and four different mammalian bocaviruses. *Mol. Ther. Methods Clin. Dev.* 12, 202–222 (2019).
16. Pleguezuelos-Manzano, C. et al. Establishment and culture of human intestinal organoids derived from adult stem cells. *Curr. Protoc. Immunol.* 130, (2020).
17. Beumer, J. et al. High-resolution mRNA and secretome atlas of human enteroendocrine cells. *Cell* 181, 1291–1306.e19 (2020).
18. Boonekamp, K. E., Dayton, T. L. & Clevers, H. Intestinal organoids as tools for enriching and studying specific and rare cell types: advances and future directions. *J. Mol. Cell Biol.* <https://doi.org/10.1093/jmcb/mjaa034> (2020).
19. Bar-Ephraim, Y. E., Kretzschmar, K. & Clevers, H. Organoids in immunological research. *Nat. Rev. Immunol.* 20, 279–293 (2020).
20. Dijkstra, K. K. et al. Generation of tumor-reactive T cells by co-culture of peripheral blood lymphocytes and tumor organoids. *Cell* 174, 1586–1598.e12 (2018).
21. Greicius, G. et al. PDGFR α + pericyptal stromal cells are the critical source of Wnts and RSPO3 for murine intestinal stem cells in vivo. *Proc. Natl Acad. Sci. USA* 115, E3173–E3181 (2018).
22. Noel, G. et al. A primary human macrophage-enteroid co-culture model to investigate mucosal gut physiology and host-pathogen interactions. *Sci. Rep.* 7, 45270 (2017).
23. Round, J. L. & Mazmanian, S. K. The gut microbiome shapes intestinal immune responses during health and disease. *Nat. Rev. Immunol.* 9, 313–323 (2009).
24. Spence, J. R. et al. Directed differentiation of human pluripotent stem cells into intestinal tissue in vitro. *Nature* 470, 105–109 (2011).
25. McCauley, H. A. & Wells, J. M. Pluripotent stem cell-derived organoids: using principles of developmental biology to grow human tissues in a dish. *Development* 144, 958–962 (2017).
26. Forbester, J. L. et al. Interaction of *Salmonella enterica* serovar Typhimurium with intestinal organoids derived from human induced pluripotent stem cells. *Infect. Immun.* 83, 2926–2934 (2015).
27. Holokai, L. et al. Increased programmed death ligand-1 is an early epithelial cell response to *Helicobacter pylori* infection. *PLoS Pathog.* 15, e1007468 (2019).
28. Finkbeiner, S. R. et al. Stem cell-derived human intestinal organoids as an infection model for rotaviruses. *mBio* 3, e00159-12 (2012).
29. Nikolaev, M. et al. Homeostatic mini-intestines through scaffold-guided organoid morphogenesis. *Nature* 585, 574–578 (2020).
30. Jalili-Firoozinezhad, S. et al. A complex human gut microbiome cultured in an anaerobic intestine-on-a-chip. *Nat. Biomed. Eng.* 3, 520–531 (2019).
31. Steinway, S. N., Saleh, J., Koo, B.-K., Delacour, D. & Kim, D.-H. Human microphysiological models of intestinal tissue and gut microbiome. *Front. Bioeng. Biotechnol.* 8, 725 (2020).
32. Hinman, S. S., Wang, Y. & Allbritton, N. L. Photopatterned membranes and chemical gradients enable scalable phenotypic organization of primary human colon epithelial models. *Anal. Chem.* 91, 15240–15247 (2019).
33. Avraham, R. et al. A highly multiplexed and sensitive RNA-seq protocol for simultaneous analysis of host and pathogen transcriptomes. *Nat. Protoc.* 11, 1477–1491 (2016).
34. Marsh, J. W., Humphrys, M. S. & Myers, G. S. A. A laboratory methodology for dual RNA-sequencing of bacteria and their host cells in vitro. *Front. Microbiol.* 8, 1830 (2017).
35. Westermann, A. J. et al. Dual RNA-seq unveils noncoding RNA functions in host-pathogen interactions. *Nature* 529, 496–501 (2016).
36. Sezonov, G., Joseleau-Petit, D. & D'Ari, R. *Escherichia coli* physiology in Luria-Bertani broth. *J. Bacteriol.* 189, 8746–8749 (2007).
37. Sim, K. et al. Improved detection of bifidobacteria with optimised 16S rRNA-gene based pyrosequencing. *PLoS ONE* 7, e32543 (2012).
38. Blokzijl, F. et al. Tissue-specific mutation accumulation in human adult stem cells during life. *Nature* 538, 260–264 (2016).

5

MUTATIONAL SIGNATURE IN COLORECTAL CANCER CAUSED BY *PKS⁺ E. COLI*

Cayetano Pleguezuelos-Manzano^{1,2,15}, Jens Puschhof^{1,2,15}, Axel Rosendahl Huber^{2,3,15},
Arne van Hoeck^{2,4}, Henry M. Wood⁵, Jason Nomburg^{6,7,8}, Carino Gurjao^{7,8},
Freek Manders^{2,3}, Guillaume Dalmasso⁹, Paul B. Stege¹⁰, Fernanda L. Paganelli¹⁰,
Maarten H. Geurts^{1,2}, Joep Beumer¹, Tomohiro Mizutani^{1,2}, Yi Miao¹¹,
Reinier van der Linden¹, Stefan van Elst¹, Genomics England Research Consortium*,
K. Christopher Garcia¹¹, Janetta Top¹⁰, Rob J. L. Willems¹⁰, Marios Giannakis^{7,8},
Richard Bonnet^{9,12}, Phil Quirke⁵, Matthew Meyerson^{7,8}, Edwin Cuppen^{2,4,13,14},
Ruben van Boxtel^{2,3} & Hans Clevers^{1,2,3}

¹Hubrecht Institute, Royal Netherlands Academy of Arts and Sciences (KNAW) and UMC Utrecht, Utrecht, The Netherlands. ²Oncode Institute, Hubrecht Institute, Utrecht, The Netherlands. ³The Princess Máxima Center for Pediatric Oncology, Utrecht, The Netherlands. ⁴Center for Molecular Medicine and Oncode Institute, University Medical Centre Utrecht, Utrecht, The Netherlands. ⁵Pathology and Data Analytics, Leeds Institute of Medical Research at St James's, University of Leeds, Leeds, UK. ⁶Graduate Program in Virology, Division of Medical Sciences, Harvard Medical School, Boston, MA, USA. ⁷Department of Medical Oncology, Dana-Farber Cancer Institute and Harvard Medical School, Boston, MA, USA. ⁸Broad Institute of MIT and Harvard, Cambridge, MA, USA. ⁹University Clermont Auvergne, Inserm U1071, INRA USC2018, M2iSH, Clermont-Ferrand, France. ¹⁰Department of Medical Microbiology, University Medical Center Utrecht, Utrecht, The Netherlands. ¹¹Howard Hughes Medical Institute, Depts. of Molecular and Cellular Physiology, and Structural Biology, Stanford University School of Medicine, Stanford, CA 94305, USA ¹²Department of Bacteriology, University Hospital of Clermont-Ferrand, Clermont-Ferrand, France. ¹³Hartwig Medical Foundation, Amsterdam, The Netherlands. ¹⁴CPCT Consortium, Rotterdam, The Netherlands. ¹⁵These authors contributed equally: Cayetano Pleguezuelos-Manzano, Jens Puschhof, Axel Rosendahl Huber.

*A list of authors and their affiliations appears at the end of the paper.

ABSTRACT

Various species of the intestinal microbiota have been associated with the development of colorectal cancer (CRC)^{1,2}, yet a direct role of bacteria in the occurrence of oncogenic mutations has not been established. *Escherichia coli* can carry the pathogenicity island *pks*, which encodes a set of enzymes that synthesize colibactin³. This compound is believed to alkylate DNA on adenine residues^{4,5} and induces double strand breaks in cultured cells³. Here, we expose human intestinal organoids to genotoxic *pks*⁺ *Escherichia coli* by repeated luminal injection over a period of 5 months. Whole genome sequencing of clonal organoids before and after this exposure reveals a distinct mutational signature, absent from organoids injected with isogenic *pks*-mutant bacteria. The same mutational signature is detected in a subset of 5876 human cancer genomes from two independent cohorts, predominantly in CRC. Our study describes a distinct mutational signature in CRC and implies that the underlying mutational process directly results from past exposure to bacteria carrying the colibactin-producing *pks* pathogenicity island.

The intestinal microbiome has long been suggested to be involved in colorectal cancer (CRC) tumorigenesis^{1,2}. Various bacterial species are reportedly enriched in stool and biopsies of CRC patients⁶⁻⁹, including genotoxic strains of *Escherichia coli* (*E. coli*)^{3,6,10,11}. The genome of these genotoxic *E. coli* harbors a 50 kb hybrid polyketide-nonribosomal peptide synthase operon (*pks*, also referred to as *clb*) responsible for the production of the genotoxin colibactin. *pks*⁺ *E. coli* are present in a substantial fraction of individuals (~20% healthy individuals, ~40% inflammatory bowel disease, ~60% familial adenomatous polyposis and CRC)^{6,10,11}. *pks*⁺ *E. coli* induce - amongst others - interstrand crosslinks (ICLs) and double strand breaks (DSBs) in epithelial cell lines^{3,10-12} and in gnotobiotic mouse models of CRC, in which they can also contribute to tumorigenesis^{6,10,11}. Recently, two studies have reported colibactin-adenine adducts, which are formed in mammalian cells exposed to *pks*⁺ *E. coli*^{4,5}. While the chemistry of colibactin's interaction with DNA is thus well-established, the outcome of this process in terms of recognizable mutations remains to be determined. Recent advances in sequencing technologies and the application of novel mathematical approaches allow classification of somatic mutational patterns. Stratton and colleagues have pioneered a mutational signature analysis which includes the bases immediately 5' and 3' to the single base substitution (SBS), and a number of different contexts characterizing insertions and deletions (indels)^{13,14}. More than 50 mutational signatures have thus been defined in cancers. For some, the underlying causes (e.g., tobacco smoke, UV light, specific genetic DNA repair defects) are known^{13,15,16}. However, for many the underlying etiology remains unclear. Human intestinal organoids, established from primary crypt stem cells¹⁷, have been useful to identify underlying causes of mutational signatures¹⁸: After being exposed to a specific mutational agent in culture, the organoids can be subcloned and analyzed by Whole Genome Sequencing (WGS) to reveal the consequent mutational signature^{16,19,20}.

In order to define the mutagenic characteristics of *pks*⁺ *E. coli*, we developed a co-culture protocol in which a *pks*⁺ *E. coli* strain (originally derived from a CRC biopsy²¹) was microinjected into the lumen of clonal human intestinal organoids²² (Fig. 1a, b). An isogenic *clbQ* knock-out strain, incapable of producing active colibactin^{21,23}, served as negative control. Both bacterial strains were viable for at least 3 days in co-culture and followed similar growth dynamics (Fig. 1c). DSBs and ICLs, visualized by γ H2AX and FANCD2 immunofluorescence, were induced specifically in epithelial cells exposed to *pks*⁺ *E. coli* (Fig. 1d, e, Extended Data Fig. 1a), confirming that *pks*⁺ *E. coli* induced DNA damage in our model. This co-culture induced no substantial viability difference between organoids exposed to *pks*⁺ and *pks* Δ *clbQ* *E. coli*, although there was a modest decrease when compared to the dye-only injected organoids (Extended Data Fig. 1b, c). We then performed repeated injections (with *pks*⁺ *E. coli*, *pks* Δ *clbQ* *E. coli* or dye-only) into single cell-derived organoids, in order to achieve long-term exposure over a period of 5 months. Subsequently, sub-clonal organoids were established from individual cells extracted from the exposed organoids. For each condition, three subclones were subjected to WGS (Fig. 2a). We also subjected the original clonal cultures to WGS to subtract the somatic

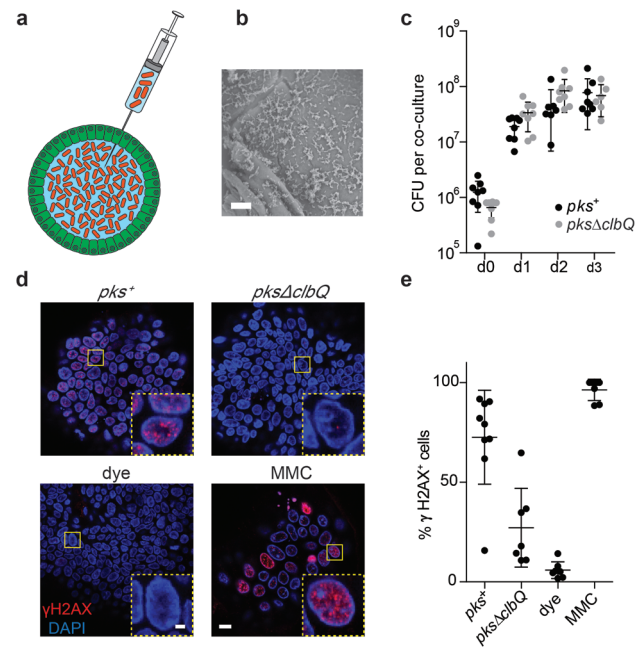


Figure 1. Co-culture of healthy human intestinal organoids with genotoxic *E. coli* induces DNA damage. **a**, Schematic representation of microinjection of genotoxic *E. coli* into the lumen of human intestinal organoids. **b**, Scanning electron microscopy image illustrating direct contact between organoid apical side and *pks*⁺ *E. coli* after 24 h co-culture. Scale bar, 10 μ m. **c**, Mean \pm s.d. bacterial load of *pks*⁺ or *pks* Δ *clbQ* at 0, 1, 2 and 3 days after co-culture establishment (n = 8 co-cultures per condition and time point, except *pks*⁺ day 2 (n = 7) and *pks* Δ *clbQ* day 3 (n = 6)). CFU, colony-forming units. **d**, Representative images of DNA damage induction after 1 day of co-culture, measured by γ H2AX immunofluorescence. One organoid is shown per image with one nucleus in the inset (expansion of boxed area). Scale bars, 10 μ m (main image); 2 μ m (inset). MMC (mitomycin C), positive control for double-strand break induction. **e**, Quantification of data from d: mean \pm s.d. percentage of nuclei positive for γ H2AX foci in organoids injected with *pks*⁺ *E. coli* (n = 9 organoids), *pks* Δ *clbQ* *E. coli* (n = 7 organoids), dye (n = 7 organoids) or mitomycin C (MMC) (n = 7 organoids) after 1 day of co-culture.

mutations that were already present before co-culture. Organoids exposed to *pks*⁺ *E. coli* presented increased SBS levels compared to *pks* Δ *clbQ*, with a bias towards T>N substitutions (Fig. 2b). These T>N substitutions occurred preferentially at ATA, ATT and TTT (of which the middle base is mutated). From this, we defined a *pks*-specific single base substitution signature (SBS-*pks*; Fig. 2c). This mutational signature was not observed in organoids exposed to *pks* Δ *clbQ* *E. coli* or dye (Fig. 2b, c, Extended Data Fig. 2a–c), proving this to be a direct consequence of the *pks*⁺ *E. coli* exposure. Furthermore, exposure to *pks*⁺ *E. coli* induced a characteristic small indel signature (ID-*pks*), which was characterized by single T deletions at T homopolymers (Fig. 2d, e, Extended Data Fig. 2d–f). SBS-*pks* and ID-*pks* were replicated in an independent human intestinal organoid line (Extended Data Fig. 3a–d; SBS cosine similarity = 0.77; ID cosine

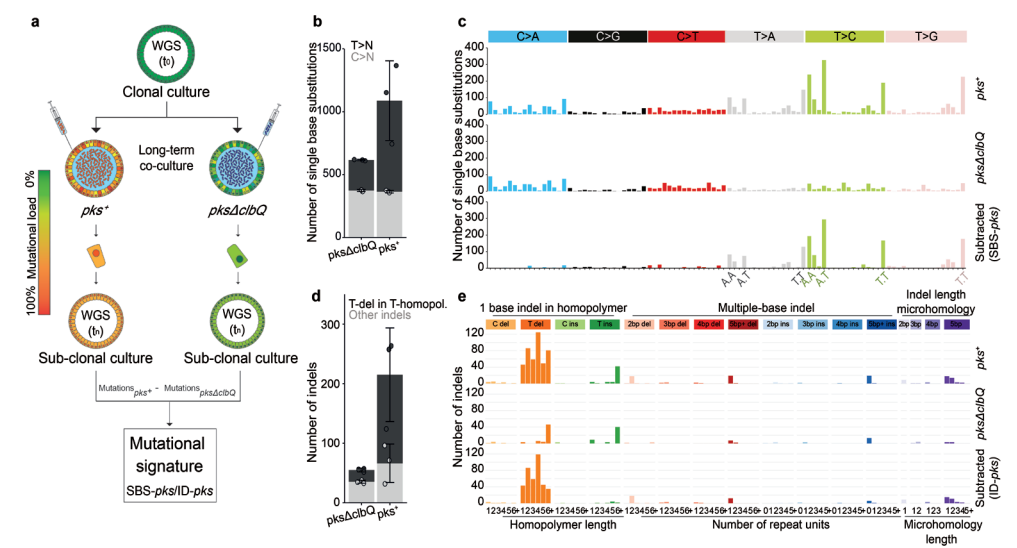


Figure 2. Long-term co-culture with *pks*⁺ *E. coli* induces SBS-*pks* and ID-*pks* mutational signatures. **a**, Schematic representation of the experimental setup. **b**, Bar segment height indicates the mean \pm s.d. number of SBSs that accumulated in organoids co-cultured with either *pks*⁺ or *pks* Δ *clbQ* *E. coli* (n = 3 clones). Dot position above the bottom of the corresponding bar segment (T > N, black; C > N, grey) indicates the number of mutations for each clone. **c**, SBS 96-trinucleotide mutational spectra in organoids exposed to either *pks*⁺ (top) or *pks* Δ *clbQ* (middle) *E. coli*. The bottom panel depicts the SBS-*pks* signature, which was defined by subtracting SBS mutations under the *pks* Δ *clbQ* condition from those under the *pks*⁺ condition. SBSs are indicated above the plot. Most mutated trinucleotide sequences are highlighted below the bottom axis as '5' base.3' base', with the dot indicating the position of the substituted nucleotide. **d**, Bar segment height indicates the mean \pm s.d. number of indels that accumulated in organoids co-cultured with either *pks*⁺ or *pks* Δ *clbQ* *E. coli* (n = 3 clones). Dot position above the bottom of the corresponding bar segment (T deletion in T-homopolymer, black; other indels, grey) indicates the number of mutations for each clone. **e**, Indel mutational spectra observed in organoids exposed to either *pks*⁺ (top) or *pks* Δ *clbQ* (middle) *E. coli*. The bottom panel depicts the ID-*pks* signature, which was defined by subtracting indel mutations under the *pks* Δ *clbQ* condition from those under the *pks*⁺ condition.

similarity = 0.93) and with a *clbQ*-knockout *E. coli* strain complemented with the *clbQ* locus (*pks* Δ *clbQ*:*clbQ*) (Extended Data Fig. 3e–h; SBS cosine similarity = 0.95; ID cosine similarity = 0.95).

Next, we asked if the SBS-*pks* and ID-*pks* mutations were characterized by other recurrent patterns. First, the assessed DNA stretch was extended beyond the nucleotide triplet. This uncovered the preferred presence of an adenine residue 3bp upstream to the mutated SBS-*pks* T>N site (Fig. 3a). Similarly, mutations that contributed to the ID-*pks* signature in poly-T stretches showed an enrichment of adenines immediately upstream of the affected poly-T stretch (Fig. 3b). Intriguingly, the lengths of the adenine stretch and the T-homopolymer were inversely correlated, consistently resulting in a combined length of 5 or more A/T nucleotides (Extended Data Fig. 4a). While SBS-*pks* and ID-*pks*

are the predominant mutational outcomes of colibactin exposure, we also observed longer deletions at sites containing the ID-*pks* motif in organoids treated with *pks*⁺ *E. coli* (Fig. 3c). Additionally, the SBS-*pks* signature exhibited a striking transcriptional strand bias (Fig. 3d, e). We speculate that these observations reflect preferential repair of alkylated adenosines on the transcribed strand by transcription-coupled nucleotide excision repair. These features clearly distinguish the *pks* signature from published signatures of alkylating agents or other factors¹⁹.

We then assessed if the experimentally deduced SBS-*pks* and ID-*pks* signatures occur in human tumors by interrogating WGS data from a Dutch collection of 3668 solid cancer metastases²⁴. The mutations a cancer cell has acquired at its primary site will be preserved even in metastases, so that these provide a view on the entire mutational history of a tumor. We first performed non-negative matrix factorization (NMF) on genome-wide mutation data obtained from 496 CRC metastases in this collection. Encouragingly, this unbiased approach identified an SBS signature that highly resembled SBS-*pks* (cosine similarity = 0.95; Extended Data Fig. 5a, b). We then determined the contribution of SBS-*pks* and ID-*pks* to the mutations of each sample in the cohort. This analysis revealed a strong enrichment of the two *pks* signatures in CRC-derived metastases when compared to all other cancer types (Fisher's exact test p-value < 0.0001, Extended Data Table 1), as is displayed for SBS-*pks* in Figure 4a and for ID-*pks* in Figure 4b. We noted 7.5% SBS-*pks*, 8.8% ID-*pks* and 6.25% SBS/ID-*pks* high samples when applying a cutoff contribution value at 0.05 (Extended Data Table 1, Fig. 4c). As expected, the SBS-*pks* and ID-*pks* signatures were positively correlated in this metastasis dataset ($R^2 = 0.46$ (all samples); $R^2 = 0.70$ (CRC-only); Fig. 4c), in line with their co-occurrence in our *in vitro* data set. The longer deletions at ID-*pks* sites were also found to co-occur with SBS-*pks* and ID-*pks* (Fig. 4e, f). Additionally, we evaluated the levels of the SBS-*pks* or ID-*pks* mutational signatures in an independent cohort, generated in the framework of the Genomics England 100,000 Genomes Project. This dataset is comprised of WGS data from 2208 CRC tumors, predominantly of primary origin. SBS-*pks* and ID-*pks* were enriched in 5.0% and 4.4% of patients respectively, while 44 samples were high in both SBS-*pks* and ID-*pks* (Fig. 4d). The relative contribution of both *pks*-signatures correlated with an R^2 of 0.35 (Fig. 4d).

Finally, we also investigated to what extent the *pks* signatures can cause oncogenic mutations. To this end, we investigated the most common driver mutations found in 7 CRC patient cohorts²⁵ for hits matching the extended SBS-*pks* or ID-*pks* target motifs (Fig. 3a, b). This analysis revealed that 112 out of 4,712 (2.4%) CRC driver mutations matched the colibactin target motif (Supplementary Table 1). *APC*, the most commonly mutated gene in CRC, contained the highest number of mutations matching SBS-*pks* or ID-*pks* target sites, with 52 out of 983 driver mutations (5.3%) matching the motifs (Fig. 4g). We then explored the mutations of the 31 SBS/ID-*pks* high CRC metastases from the HMF cohort for putative driver mutations matching the extended motif. In total, this approach detected 209 changes in protein coding sequences (displayed in Supplementary Table 2).

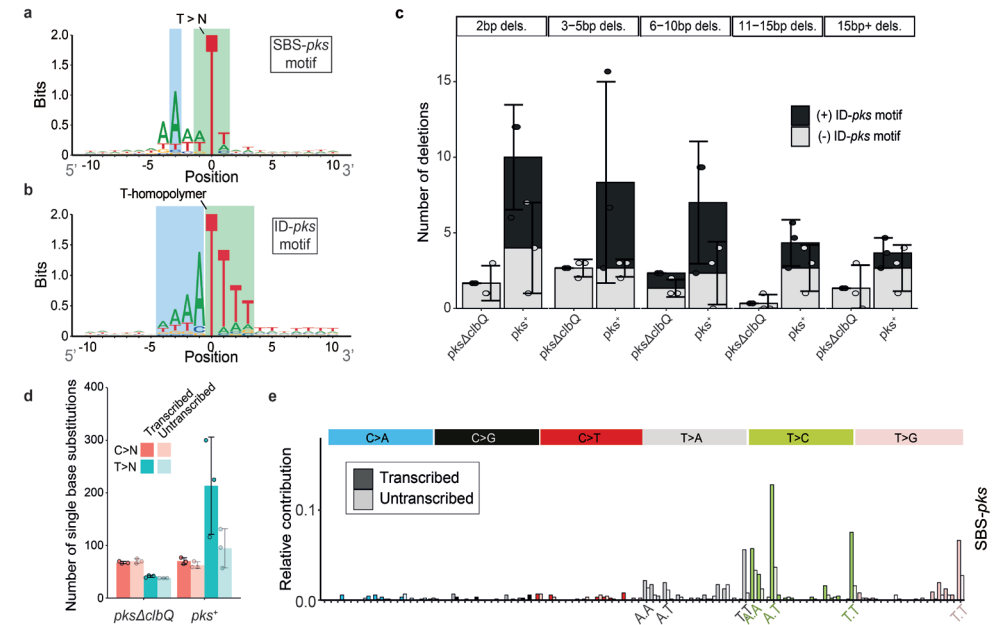


Figure 3. Consensus motifs and extended features of SBS-*pks* and ID-*pks* mutational signatures. **a**, Two-bit representation of the extended sequence context of T > N mutations observed in organoids exposed to *pks*⁺ *E. coli*. Green, highlighted T > N trinucleotide sequence; blue, highlighted A-enriched position characteristic of the SBS-*pks* mutations. **b**, Two-bit representation of the extended sequence context of single T deletions in T homopolymers observed in organoids exposed to *pks*⁺ *E. coli*. Green, highlighted T homopolymer with deleted T; blue, highlighted characteristic poly-A stretch. **c**, Bar segment height indicates the mean \pm s.d. occurrence of deletions comprising more than 1 bp in organoids exposed to *pks*⁺ or *pks* Δ *clbQ* *E. coli* ($n = 3$ clones). Dot position above the bottom of the corresponding bar segment (matching ID-*pks* motif, black; lacking ID-*pks* motif, grey) indicates the number of mutations for each clone. **d**, Transcriptional strand bias of T > N and C > N mutations in organoids exposed to *pks*⁺ *E. coli* or *pks* Δ *clbQ* *E. coli*. Pink, C > N; blue, T > N; dark colour, transcribed strand; bright colour, untranscribed strand; mean \pm s.d. number of events ($n = 3$ clones). **e**, Transcriptional strand bias of the 96-trinucleotide SBS-*pks* mutational signature. Colour, transcribed strand; white, untranscribed strand.

Remarkably, an identical *APC* driver mutation matching the SBS-*pks* motif was found in two independent donors (Fig. 4h).

A recent publication²⁶ identified mutational signatures occurring in healthy human colon crypts. The authors of that study note the cooccurrence of two mutational signatures in subsets of crypts from some of the subjects. These signatures were termed SBS-A and ID-A. The authors derived hierarchical lineages of the sequenced crypts, which allowed them to conclude that the -unknown- mutagenic agent was active only during early childhood. Intriguingly, SBS-A and ID-A closely match SBS-*pks* and ID-*pks*, respectively. Our data imply that *pks*⁺ *E. coli* is the mutagenic agent that is causative to the SBS-A and ID-A signatures observed in healthy crypts. We assessed if the SBS-*pks* mutational signature contributed early to the mutational load of metastatic samples

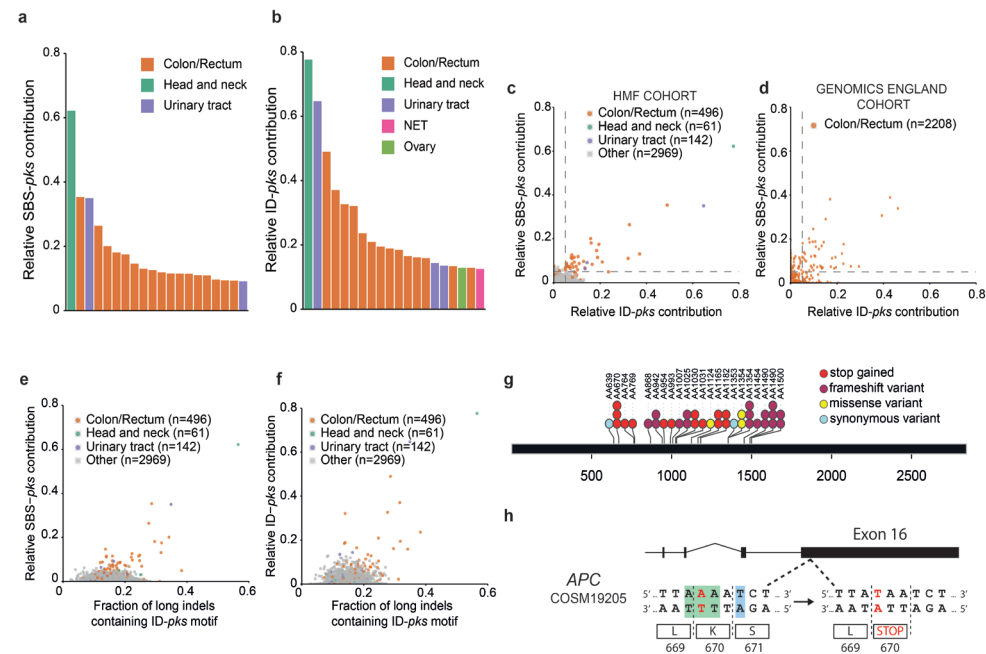


Figure 4. SBS-*pks* and ID-*pks* mutational signatures are present in a subset of CRC samples from two independent cohorts. **a**, Top 20 out of 3,668 metastases from the HMF cohort, ranked by the fraction of SBSs attributed to SBS-*pks*. CRC metastases (orange) are enriched. **b**, Top 20 out of 3,668 metastases from the HMF cohort. Samples are ranked by the fraction of indels attributed to ID-*pks*. CRC metastases (in orange) are also enriched here. NET, neuroendocrine tumour. **c**, Scatterplot of the fraction of SBSs and indels attributed to SBS-*pks* and ID-*pks* in 3,668 metastases from the HMF cohort. Each dot represents one metastasis. Samples high for both SBS-*pks* and ID-*pks* (more than 5% contribution, dashed lines) are enriched in CRC (orange). SBS-*pks* and ID-*pks* are correlated ($R^2 = 0.46$; only CRC, $R^2 = 0.7$). **d**, Scatterplot of SBS-*pks* and ID-*pks* contributions in 2,208 CRC tumour samples, predominantly of primary origin, from the Genomics England cohort. SBS-*pks* and ID-*pks* are correlated ($R^2 = 0.35$). Each dot represents one primary tumour sample. Dashed lines delimit samples with high SBS-*pks* or ID-*pks* contribution (more than 5%). **e**, Scatterplot of SBS-*pks* and deletions longer than 1 bp with ID-*pks* pattern in the HMF cohort. **f**, Scatterplot of ID-*pks* and deletions longer than 1 bp with ID-*pks* pattern in the HMF cohort. **a–f**, Colours indicate tissue of origin. **g**, Exonic APC driver mutations found in the IntOGen collection matching the colibactin target SBS-*pks* or ID-*pks* motifs. **h**, Schematic representation of a driver mutation in APC causing a premature stop codon matching the SBS-*pks* motif, found in the IntOGen collection and in two independent patients from the HMF cohort with high SBS-*pks* and high ID-*pks*.

from the Dutch cohort by evaluating their levels separately in clonal (pre-metastasis) or non-clonal (post-metastasis) mutations. The accumulation of SBS-*pks* and ID-*pks* at the primary tumor site or even earlier was substantiated by the abundant presence of SBS-*pks* in clonal mutations in the cohort (Extended Data Fig. 5c). In addition to CRCs, one head and neck- and three urinary tract-derived tumors from this cohort also displayed a clear SBS-*pks* and ID-*pks* signature (Fig. 4c). Both tissues have been described as sites

of *E. coli* infection^{27–29}. This rare occurrence of the *pks* signatures in non-CRC tumors was substantiated by a preprint report³⁰ of signatures closely resembling SBS-*pks* and ID-*pks* in an oral squamous cell carcinoma patient.

The distinct motifs at sites of colibactin-induced mutations may serve as a starting point for deeper investigations into the underlying processes. Evidence is accumulating that colibactin forms interstrand crosslinks between two adenosines^{4,5,12}, and our data imply a distance of 3–4 bases between these adenosines. These crosslinks formed by a bulky DNA adduct could be resolved in different ways, including induction of DSBs, Nucleotide Excision Repair or translesion synthesis, which in turn could result in various mutational outcomes. While our study unveils single base substitutions and deletions as a mutational consequence, the underlying mechanisms will need to be elucidated in more detailed DNA-repair studies.

In summary, we find that prolonged exposure of wild-type human organoids to genotoxic *E. coli* allows the extraction of a unique SBS and indel signature. As organoids do not model immune/inflammation effects or other microenvironmental factors, this provides evidence for immediate causality between colibactin and mutations in the host epithelial cells. The adenine-enriched target motif is in agreement with the proposed mode of action of colibactin's 'double-warhead' attacking closely spaced adenine residues^{4,5,12}. The pronounced sequence specificity reported here may inspire more detailed investigations on the interaction of colibactin with specific DNA contexts. As stated above, Stratton and colleagues²⁶ likely describe SBS-*pks* and ID-*pks* mutational signatures of the same etiology in primary human colon crypts. This agrees with the notion that *pks*⁺ *E. coli*-induced mutagenesis indeed occurs in the healthy colon of individuals that harbor genotoxic *E. coli* strains³¹ and that such individuals may be at an increased risk of developing CRC. The small number of *pks* signature-positive urogenital and head-and-neck cancer cases suggests that *pks*⁺ bacteria act beyond the colon. Intriguingly, presence of the *pks* island in another strain of *E. coli* Nissle 1917, is closely linked to its probiotic effect³². This strain has been investigated for decades for diverse disease indications³³. Our data suggest that *E. coli* Nissle 1917 may induce the characteristic SBS/ID-*pks* mutational patterns. Future research should elucidate if this is the case *in vitro*, and in patients treated with *pks*⁺ bacterial strains. This study implies that detection and removal of *pks*⁺ *E. coli*, as well as re-evaluation of probiotic strains harboring the *pks* island, could decrease the risk of cancer in a large group of individuals.

ONLINE CONTENT

Any methods, additional references, Nature Research reporting summaries, source data, extended data, supplementary information, acknowledgements, peer review information; details of author contributions and competing interests; and statements of data and code availability are available at <https://doi.org/10.1038/s41586-020-2080-8>.

METHODS

Human material and organoid cultures

Ethical approval was obtained from the ethics committees of the University Medical Center Utrecht, Hartwig Medical Foundation and Genomics England. Written informed consent was obtained from patients. All experiments and analyses were performed in compliance with relevant ethical regulations.

Organoid culture

Clonal organoid lines were derived and cultured as described previously^{16,17}. In brief, wild type human intestinal organoids (clonal lines ASC-5a and ASC-6a, previously used in Blokzijl et al.,³⁴) were cultured in domes of Cultrex Pathclear Reduced Growth Factor Basement Membrane Extract (BME) (3533-001, Amsbio) covered by medium containing Advanced DMEM/F12 (Gibco), 1x B27, 1x Glutamax, 10 mmol/L HEPES, 100 U/mL Penicillin-Streptomycin (all Thermo-Fisher), 1.25 mM *N*-acetylcysteine, 10 μ M Nicotinamide, 10 μ M p38 inhibitor SB202190 (all Sigma-Aldrich) and the following growth factors: 0.5 nM Wnt Surrogate-Fc Fusion Protein, 2% Noggin conditioned medium (both U-Protein Express), 20% Rspo1 conditioned medium (in-house), 50 ng/mL EGF (Peprotech), 0.5 μ M A83-01, 1 μ M PGE2 (both Tocris). For derivation of clonal lines, cells were FACS sorted and grown at a density of 50 cells/ μ l in BME. 10 μ M ROCK inhibitor Y-27632 (Abmole, M1817) was added for the first week of growth. Upon reaching a size of >100 μ m diameter, organoids were picked and transferred to one well per organoid. All organoid lines were regularly tested to rule out mycoplasma infection and authenticated using SNP profiling.

Organoid bacteria co-culture

The genotoxic *pk^s⁺ E. coli* strain was previously isolated from a CRC patient and isogenic *pk^s Δ clbQ* knock out and *pk^s Δ clbQ:clbQ* complemented strains were generated based on this strain²¹. Bacteria were initially cultured in Advanced DMEM (Gibco) supplemented with Glutamax and HEPES to an O.D. of 0.4. They were then microinjected into the lumen of organoids as previously described^{22,35}. Bacteria were injected at a multiplicity of infection of 1 together with 0.05% (w/v) FastGreen dye (Sigma) to allow tracking of injected organoids. At this point, 5 μ g/mL of the non-permeant antibiotic Gentamicin were added to the media to prevent overgrowth of bacteria outside the organoid lumen. Cell viability was assessed as follows: Organoids were harvested after 1, 3 or 5 days (bacteria were removed by primocin treatment at day 3) of co-culture in cold DMEM (Gibco) and incubated in TrypLE Express (Gibco) at 37°C for 5 minutes with repeated mechanical shearing. Single cells were resuspended in DMEM with added DAPI, incubated on ice for at least 15 minutes and assessed for viability on a BD FACS Canto™. Cells positive for DAPI were considered dead, while cells maintaining DAPI exclusion were counted as viable. Bacterial growth kinetics were assessed by harvesting, organoid dissociation with

0.5% saponin for 10 minutes and re-plating of serial dilutions on LB plates. Colony forming units were quantified after overnight culture at 37°C. *E. coli* were killed with 1x Primocin (InvivoGen) after 3 days of co-culture, after which organoids were left to recover for 4 days before being passaged. When the organoids reached a cystic stage again (typically after 2–3 weeks), the injection cycle was repeated. This procedure was repeated 5 times (3 times for ASC Clone 6-a and the *clbQ* complementation experiment in ASC Clone 5-a) to reduce injection heterogeneity and ensure accumulation of enough mutations for reliable signature detection.

Whole-mount organoid immunofluorescence, DNA damage quantification and scanning electron microscopy

Organoids co-cultured with *pk^s⁺/pk^s Δ clbQ E. coli*²¹ were collected in Cell Recovery Solution (Corning) and incubated at 4°C for 30 minutes with regular shaking in order to free them from BME. For FANCD2 staining, organoids were pre-permeabilized with 0.2% Triton-X (Sigma) for 10 minutes at room temperature. Then, organoids were fixed in 4% formalin overnight at 4°C. Subsequently, organoids were permeabilized with 0.5% Triton-X (Sigma), 2% donkey serum (BioRad) in PBS for 30 minutes at 4°C and blocked with 0.1% Tween-20 (Sigma) and 2% donkey serum in PBS for 15 minutes at room temperature. Organoids were incubated with mouse anti- γ H2AX (Millipore; clone JBW301; 1:1000 dilution) or rabbit anti-FANCD2 (affinity purified in Pace et al.³⁶; 1mg/ml) primary antibody overnight at 4°C. Then, organoids were washed 4 times with PBS and incubated with either secondary goat anti-mouse AF-647 (Thermo Fisher, catalog number A-21235, 1:500 dilution) or goat anti-rabbit AF-488 (Life Technologies, catalog number A21206, 1:500 dilution) antibodies, respectively, for 3h at room temperature in the dark and washed again with PBS. Organoids were imaged using an SP8 confocal microscope (Leica). Fluorescent microscopic images of γ H2AX foci were quantified as follows: Nuclei were classified as containing either 0 or one or more foci. The fraction of nuclei containing foci over all nuclei is displayed as one datapoint per organoid. Organoids co-cultured with bacteria for 24h were harvested as described above and processed for scanning electron microscopy as previously described³⁵.

WGS and read alignment

For WGS, clonal and subclonal cultures were generated for each condition. From these clonal cultures DNA was isolated using the DNeasy Blood and Tissue Kit (Qiagen) using manufacturer's instructions. Illumina DNA libraries were prepared using 50 ng of genomic DNA isolated from the (sub-)clonal cultures isolated using TruSeq DNA Nano kit. The parental ASC 5a clone was sequenced on a HiSeq XTEN instrument at 30x base coverage. All other samples were sequenced using an Illumina Novaseq 6000 with 30x base coverage. Reads were mapped against the human reference genome version GRCh37 by using Burrows-Wheeler Aligner³⁷ (BWA) version v0.7.5 with settings `bwa`

mem -c 100 -M. Sequences were marked for duplicates using Sambamba (v0.4.732) and realigned using GATK IndelRealigner (GATK version 3.4–46). The full description and source code of the pipeline is available at <https://github.com/UMCUGenetics/IAP>.

Mutation calling and filtration

Mutations were called using GATK Haplotypecaller (GATK version 3.4–46) and GATK Queue producing a multi-sample Vcf file²⁰. The quality of the variants was evaluated using GATK VariantFiltration v3.4–46 using the following settings: -snpFilterName SNP_LowQualityDepth -snpFilterExpression "QD < 2.0" -snpFilterName SNP_MappingQuality -snpFilterExpression "MQ < 40.0" -snpFilterName SNP_StrandBias -snpFilterExpression "FS > 60.0" -snpFilterName SNP_HaplotypeScoreHigh -snpFilterExpression "HaplotypeScore > 13.0" -snpFilterName SNP_MQRankSumLow -snpFilterExpression "MQRankSum < -12.5" -snpFilterName SNP_ReadPosRankSumLow -snpFilterExpression "ReadPosRankSum < -8.0" -snpFilterName SNP_HardToValidate -snpFilterExpression "MQ0 >= 4 && ((MQ0 / (1.0 * DP)) > 0.1)" -snpFilterName SNP_LowCoverage -snpFilterExpression "DP < 5" -snpFilterName SNP_VeryLowQual -snpFilterExpression "QUAL < 30" -snpFilterName SNP_LowQual -snpFilterExpression "QUAL >= 30.0 && QUAL < 50.0" -snpFilterName SNP_SOR -snpFilterExpression "SOR > 4.0" -cluster 3 -window 10 -indelType INDEL -indelType MIXED -indelFilterName INDEL_LowQualityDepth -indelFilterExpression "QD < 2.0" -indelFilterName INDEL_StrandBias -indelFilterExpression "FS > 200.0" -indelFilterName INDEL_ReadPosRankSumLow -indelFilterExpression "ReadPosRankSum < -20.0" -indelFilterName INDEL_HardToValidate -indelFilterExpression "MQ0 >= 4 && ((MQ0 / (1.0 * DP)) > 0.1)" -indelFilterName INDEL_LowCoverage -indelFilterExpression "DP < 5" -indelFilterName INDEL_VeryLowQual -indelFilterExpression "QUAL < 30.0" -indelFilterName INDEL_LowQual -indelFilterExpression "QUAL >= 30.0 && QUAL < 50.0" -indelFilterName INDEL_SOR -indelFilterExpression "SOR > 10.0".

Somatic single base substitution and indel filtering

To obtain high confidence catalogues of mutations induced during culture, we applied extensive filtering steps previously described by Jager et al.²⁰. First, only variants obtained by GATK VariantFiltration with a GATK phred-scaled quality score ≥ 100 for single base substitutions and ≥ 250 for indels were selected. Subsequently, we only considered variants with at least 20x read coverage in control and sample. We additionally filtered base substitutions with a GATK genotype score (GQ) lower than 99 or 10 in WGS(tn) or WGS(t0), respectively. Indels were filtered when GQ scores were higher than 60 WGS(tn) or 10 in WGS(t0). All variants were filtered against the Single Nucleotide Polymorphism Database v137.b3730, from which SNPs present in the COSMICv76 database were excluded. To exclude recurrent sequencing artefacts, we excluded all variants variable in at least three individuals in a panel of bulk-sequenced mesenchymal stromal cells³⁸. Next, all variants present at the start of co-culture (denominated WGS(t0) in Fig. 2a) were filtered

from those detected in the clonal *pks⁺ E. coli*, *pksΔclbQ E. coli* co-cultures (denominated WGS(tn) in Fig. 2a) or dye culture. Indels were only selected when no called variants in WGS(t0) were present within 100bp of the indel and if not shared in WGS(t0). In addition, both indels and SNVs were filtered for the additional parameters: mapping quality (MQ) of at least 60 and a variant allele (VAF) of 0.3 or higher to exclude variants obtained during the clonal step. Finally, all multi-allelic variants were removed. Scripts used for filtering single base substitutions (SNVFlv1.2) and indels (INDELFlv1.5) are deposited on <https://github.com/ToolsVanBox/>.

Mutational profile analysis

In order to extract mutational signatures from the high-quality mutational catalogues after filtering, we used the R package "MutationalPatterns" to obtain 96-trinucleotide single base substitution and indel subcategory counts for each clonally cultured sample³⁹ (Extended Data Fig. 1a, d). In order to obtain the additional mutational effects induced by *pks⁺ E. coli* (SBS and ID) we pooled mutation numbers for each culture condition (*pksΔclbQ* and *pks⁺*), and subtracted mutational counts of *pksΔclbQ* from *pks⁺* (Fig. 2c, e, Extended Data Fig 2b, d). For the clones exposed to *pksΔclbQ:clbQ*, we subtracted relative levels of the *pksΔclbQ* mutations in the same organoid line. This enabled us to correct for the background of mutations induced by *pksΔclbQ E. coli* and injection dye. To determine transcriptional strand bias of mutations induced during *pks⁺ E. coli* exposure, we selected all single base substitutions within gene bodies and checked whether the mutated C or T was located on the transcribed or non-transcribed strand. We defined the transcribed area of the genome as all protein coding genes based on Ensembl v75 (GCRh37)⁴⁰ and included introns and untranslated regions. The extended sequence context around mutation sites was analyzed and displayed using an in-house script ("extended_sequence_context.R"). 2-bit sequence motifs were generated using the R package "ggseqlogo". Cosine similarities between indel and single-base substitution profiles were calculated using the function 'cos_sim_matrix' from the MutationalPatterns package.

Analysis of clonal mutations in the SBS/ID-*pks* high CRC tumors

From the 31 SBS/ID-*pks* high CRC tumors clonal and subclonal single base substitutions were defined to contain a purity/ploidy adjusted allele-fraction (PURPLE_AF) of < 0.4 or > 0.2 , respectively⁴¹. Signature re-fitting on both fractions was performed with the same signatures as described above for the initial re-fitting of the HMF cohort.

Analysis of >1bp deletions matching *pks*-motif

For each > 1 bp T-deletion observed in organoid clones or the HMF cohort, the sequence of the deleted bases and 5 base-pair flanking regions was retrieved using the R function "getSeq" from the package "BSgenome". Retrieved sequences were examined for

the presence of a 5 base-pair motif matching the *pks*-motifs identified (Extended Data Fig. 4a) "AAAAT", "AAATT", "AATTT" or "ATTTT". Sequences containing one or more matches with the motifs were marked as positive for containing the motif.

NMF extraction of signatures from HMF Colorectal cancer cohort

In order to identify SBS-*pks* in an unbiased manner, signature extraction was performed on all 496 samples from colorectal primary tumors present in the HMF metastatic cancer database²⁴. All variants containing the 'PASS' flag were used for analysis. Signature extraction was performed using non-negative matrix factorization (NMF), using the R package "MutationalPatterns" function "extract_signatures" with the following settings: rank = 17, nrun = 200. The cosine similarity of the extracted signature matching SBS-*pks* was re-fitted to the COSMIC SigProfiler signatures and SBS-*pks* was determined as described above to determine similarity (Extended Data Fig. 5a, b).

Signature re-fitting on HMF cohort

Mutation catalogues containing somatic variants processed according to Priestley et al, 2019 were obtained from the HMF. All variants containing the 'PASS' flag in the HMF dataset were selected. Single base trinucleotide and indel subcategory counts were extracted using the R package "MutationalPatterns" and in house-written R scripts respectively. In order to determine the contribution of SBS-*pks* and ID-*pks* to these mutational catalogues, we re-fitted the COSMIC SigProfiler mutational SBS and ID signatures v3 (<https://cancer.sanger.ac.uk/cosmic/signatures/>), in combination with SBS-*pks* and ID-*pks*, to the mutational catalogues using the MutationalPatterns function "fit_to_signatures". Signatures marked as possible sequencing artefacts were excluded from the re-fitting. Cutoff values for high SBS-*pks* and ID-*pks* levels were manually set at 5%, each. Numbers of SBS/ID-*pks* positive samples were compared between CRC and other cancer types by Fisher's exact test (two-tailed).

Mutation calling and filtration (Genomics England cohort)

As part of the Genomics England 100,000 Genomes Project (main programme version 7)⁴² standard pipeline, 2208 CRC genomes were sequenced on the Illumina HiSeq X platform. Reads were aligned to the human genome (GRCh38) using the Illumina iSAAC aligner 03.16.02.1⁴³. Mutations were called using Strelka and filtered in accordance with the HMF dataset²⁴. Before examining somatic mutations for the *pks* mutational signature, mutation calls were first subjected to additional filtering steps similar to those previously described²⁴. All calls present in the matched normal sample were removed. The calls were split into high and low confidence genomic regions according to lists available at ftp://ftp-trace.ncbi.nlm.nih.gov/giab/ftp/release/NA12878_HG001/NISTv3.3.1/GRCh38/. Somatic mutation calls in high confidence regions were passed with a somatic score (QSI or QSS) of 10, whilst calls in low confidence regions were passed with a score of 20.

A pool of 200 normal samples was constructed, and any calls present in three or more normal samples were removed. Any groups of single nucleotide variants within 2bp were considered to be miss-called multiple nucleotide variants and were removed. Finally, all calls had to pass the Strelka "PASS" filter. Mutational signatures were then analysed as described above for the HMF cohort.

Detection of *pks*-signature mutations in protein coding regions

Mutations were extracted from the 31 SBS/ID-*pks* high CRC-samples. Exonic regions were defined as all autosomal exonic regions reported in Ensembl v75 (GCRh37)40. All extracted CRC mutations were filtered for localization in exonic regions using the Bioconductor packages "GenomicRanges"⁴⁴ and "BSgenome". In a second filtering step, the sequence context of mutations was required to match the following criteria: For SBS-*pks*: T>N mutation, A or T directly upstream and downstream, A 3 bases upstream. For ID-*pks*: Single T deletion, A directly upstream, a stretch of an A homopolymer followed by a T polymer with combined length of at least 5 nucleotides, but no stretch exceeding 10 nucleotides in length. Mutations passing both filter steps were further filtered for presence of a predicted "HIGH" or "MODERATE" score in the transcript with highest impact score according to the reported SnpEff annotation. To assess the mutagenic impact of *pks*, we obtained all mutations from the 50 highest mutated genes in CRC from IntOGen²⁵, release 2019.11.12. Mutations were filtered matching the *pks* motif according to the sequence criteria stated above apart from the predicted impact score. Mutations in APC were plotted using the R package "rtrackViewer", using only exonic mutations.

Data availability

Whole-genome sequence data have been deposited in the European Genome-Phenome Archive (<https://ega-archive.org/>); accession number EGAS00001003934. The data used from the Hartwig Medical Foundation and Genomics England databases consist of patient-level somatic variant data (annotated variant call data) and are considered privacy sensitive and available through access-controlled mechanisms. Patient-level somatic variant and clinical data were obtained from the Hartwig Medical Foundation under data request number DR-084. Somatic variant and clinical data are freely available for academic use from the Hartwig Medical Foundation through standardized procedures. Privacy and publication policies, including co-authorship policies, can be retrieved from: <https://www.hartwigmedicalfoundation.nl/en/data-policy/>. Data request forms can be downloaded from <https://www.hartwigmedicalfoundation.nl/en/applying-for-data/>. To gain access to the data, this data request form should be emailed to info@hartwigmedicalfoundation.nl, upon which it will be evaluated within six weeks by the HMF Scientific Council and an independent Data Access Board. When access is granted, the requested data become available through a download link provided by HMF. Somatic variant data from the Genomics England data set were analysed within

the Genomics England Research Environment secure data portal, under Research Registry project code RR87, and exported from the Research Environment following data transfer request 1000000003652 on 3 December 2019. The Genomics England data set can be accessed by joining the community of academic and clinical scientist via the Genomics England Clinical Interpretation Partnership (GeCIP), <https://www.genomicsengland.co.uk/about-gecip/>. To join a GeCIP domain, the following steps have to be taken: 1. Your institution has to sign the GeCIP Participation Agreement, which outlines the key principles that members of each institution must adhere to, including our Intellectual Property and Publication Policy. 2. Submit your application using the relevant form found at the bottom of the page (<https://www.genomicsengland.co.uk/join-a-gecip-domain/>). 3. The domain lead will review your application, and your institution will verify your identity for Genomics England and communicate confirmation directly to Genomics England. 4. Your user account will be created. 5. You will be sent an email containing a link to complete Information Governance training and sign the GeCIP rules (https://www.genomicsengland.co.uk/wp-content/uploads/2019/07/GeCIP-Rules_29-08-2018.pdf). Completing the training and signing the GeCIP Rules are requirements for you to access the data. After you have completed the training and signed the rules, you will need to wait for your access to the Research Environment to be granted. 6. This will generally take up to one working day. You will then receive an email letting you know your account has been given access to the environment, and instructions for logging in (for more detail, see: <https://www.genomicsengland.co.uk/join-a-gecip-domain/>). Details of the data access agreement can be retrieved from https://figshare.com/articles/GenomicEnglandProtocol_pdf/4530893/5. All requests will be evaluated by the GenomicsEngland Access Review Committee taking into consideration patient data protection, compliance with legal and regulatory requirements, resource availability and facilitation of high-quality research. All analysis of the data must take place within the Genomics England Research Environment secure data portal, <https://www.genomicsengland.co.uk/understanding-genomics/data/> and exported following approval of a data transfer request. Regarding co-authorship, all publications using data generated as part of the Genomics England 100,000 Genomes Project must include the Genomics England Research Consortium as co-authors. The full publication policy is available at <https://www.genomicsengland.co.uk/about-gecip/publications/>. All other data supporting the findings of this study are available from the corresponding author upon request.

Code availability

All analysis scripts are available at <https://github.com/ToolsVanBox/GenotoxicEcoli>.

GENOMICS ENGLAND RESEARCH CONSORTIUM

J. C. Ambrose¹⁹, P. Arumugam¹⁹, E. L. Baple¹⁹, M. Bleda¹⁹, F. Boardman-Pretty^{19,20}, J. M. Boissiere¹⁹, C. R. Boustred¹⁹, H. Brittain¹⁹, M. J. Caulfield^{19,20}, G. C. Chan¹⁹, C. E. H. Craig¹⁹,

L. C. Daugherty¹⁹, A. de Burca¹⁹, A. Devereau¹⁹, G. Elgar^{19,20}, R. E. Foulger¹⁹, T. Fowler¹⁹, P. Furió-Tarí¹⁹, J. M. Hackett¹⁹, D. Halai¹⁹, A. Hamblin¹⁹, S. Henderson^{19,20}, J. E. Holman¹⁹, T. J. P. Hubbard¹⁹, K. Ibáñez^{19,20}, R. Jackson¹⁹, L. J. Jones^{19,20}, D. Kasperaviciute^{19,20}, M. Kayikci¹⁹, L. Lahnstein¹⁹, L. Lawson¹⁹, S. E. A. Leigh¹⁹, I. U. S. Leong¹⁹, F. J. Lopez¹⁹, F. Maleady-Crowe¹⁹, J. Mason¹⁹, E. M. McDonagh^{19,20}, L. Moutsianas^{19,20}, M. Mueller^{19,20}, N. Murugaesu¹⁹, A. C. Need^{19,20}, C. A. Odhams¹⁹, C. Patch^{19,20}, D. Perez-Gil¹⁹, D. Polychronopoulos¹⁹, J. Pullinger¹⁹, T. Rahim¹⁹, A. Rendon¹⁹, P. Riesgo-Ferreiro¹⁹, T. Rogers¹⁹, M. Ryten¹⁹, K. Savage¹⁹, K. Sawant¹⁹, R. H. Scott¹⁹, A. Siddiq¹⁹, A. Sieghart¹⁹, D. Smedley^{19,20}, K. R. Smith^{19,20}, A. Sosinsky^{19,20}, W. Spooner¹⁹, H. E. Stevens¹⁹, A. Stuckey¹⁹, R. Sultana¹⁹, E. R. A. Thomas^{19,20}, S. R. Thompson¹⁹, C. Tregidgo¹⁹, A. Tucci^{19,20}, E. Walsh¹⁹, S. A. Watters¹⁹, M. J. Welland¹⁹, E. Williams¹⁹, K. Witkowska^{19,20}, S. M. Wood^{19,20} & M. Zarowiecki¹⁹, Genomics England, London UK.¹⁹, William Harvey Research Institute, Queen Mary University of London, London, UK.²⁰

ACKNOWLEDGEMENTS

We thank J. H. J. Hoeijmakers, P. Knipscheer and J. I. Garaycochea for discussions on DNA damage, and P. Robinson, K. Vervier, T. Lawley, and M. Stratton for explorative analysis and discussions. This publication and the underlying study have been made possible partly on the basis of the data that Hartwig Medical Foundation and the Center of Personalised Cancer Treatment (CPCT) have made available to the study. This research was made possible through access to the data and findings generated by the 100,000 Genomes Project. The 100,000 Genomes Project is managed by Genomics England Limited (a wholly owned company of the Department of Health and Social Care). The 100,000 Genomes Project is funded by the National Institute for Health Research and NHS England. The Wellcome Trust, Cancer Research UK and the Medical Research Council have also funded research infrastructure. The 100,000 Genomes Project uses data provided by patients and collected by the National Health Service as part of their care and support. This work was supported by CRUK grant OPTIMISTIC (C10674/A27140), the Gravitation projects CancerGenomics.nl and the Netherlands Organ-on-Chip Initiative (024.003.001) from the Netherlands Organisation for Scientific Research (NWO) funded by the Ministry of Education, Culture and Science of the government of the Netherlands (C.P.-M., J.P.), the Onco Institute (partly financed by the Dutch Cancer Society), the European Research Council under ERC Advanced Grant Agreement no. 67013 (J.P., T.M., H.C.), a VIDI grant from the NWO (no. 016.Vidi.171.023) to R.v.B. that supports A.R.H. and NWO building blocks of life project: Cell dynamics within lung and intestinal organoids (737.016.009) (M.H.G.). With financial support from ITMO Cancer AVIESAN (Alliance Nationale pour les Sciences de la Vie et de la Santé, National Alliance for Life Sciences & Health) within the framework of the Cancer Plan (HTE201601) (G.D., R.B.) as well as Howard Hughes Medical Institute, Mathers Foundation, and NIH-1R01DK115728-01A1 (Y.M., K.C.G.).

AUTHOR CONTRIBUTIONS

C.P.-M., J.P., A.R.H. and H.C. conceived the study; C.P.-M., J.P., A.R.H., R.v.B. and H.C. wrote the manuscript; A.R.H., H.M.W., F.M. and R.v.B. performed signature analysis; A.R.H., A.v.H., H.M.W., J.N., C.G., P.Q., M.G., M.M. and E.C. provided access to and analysed patient WGS data; G.D. and R.B. isolated bacterial strains and generated knockouts; C.P.-M., J.P., T.M., R.v.d.L., M.H.G. and S.v.E. established and performed organoid cloning experiments; C.P.-M., J.P. and J.B. performed organoid co-culture experiments; P.B.S., F.L.P., J.T. and R.J.L.W. performed bacteria validation and assays. Y.M. and K.C.G. provided and advised on the use of the Wnt surrogate-Fc fusion reagent.

COMPETING INTERESTS

H.C. is inventor on several patents related to organoid technology; his full disclosure is given at <https://www.uu.nl/staff/JCClevers/>. M.M. is scientific advisory board chair and a consultant for OrigiMed, receives research support from Bayer, Janssen, and Ono, and receives royalty payments from Labcorp. H.C. and K.C.G. are co-founders of Surrozen.

ADDITIONAL INFORMATION

Supplementary information is available for this paper at <https://doi.org/10.1038/s41586-020-2080-8>. Correspondence and requests for materials should be addressed to R.v.B. or H.C.

PEER REVIEW INFORMATION

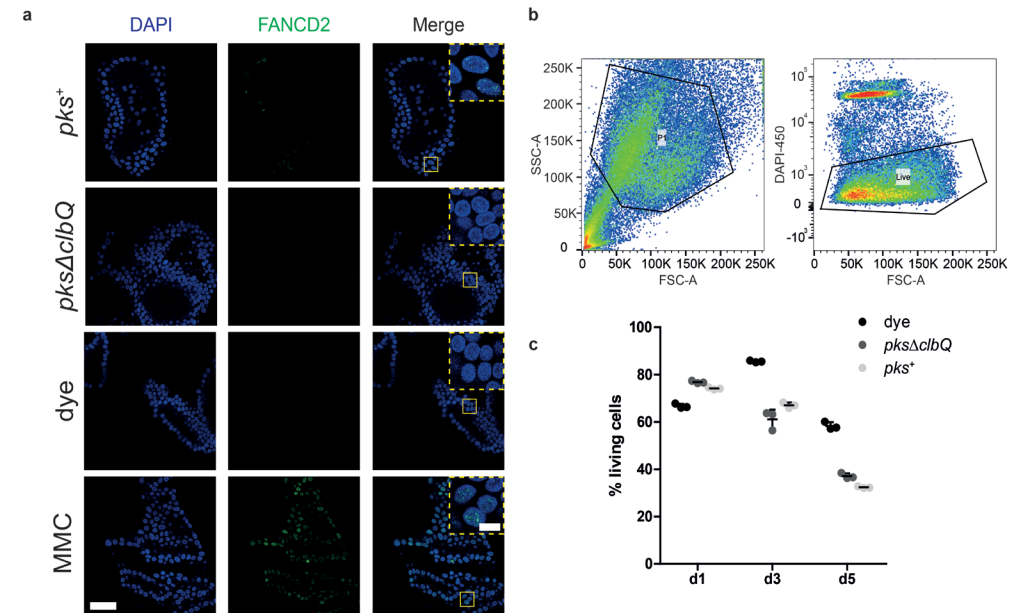
Nature thanks Bogdan Fedeles, Christian Jobin and the other, anonymous, reviewer(s) for their contribution to the peer review of this work.

REFERENCES

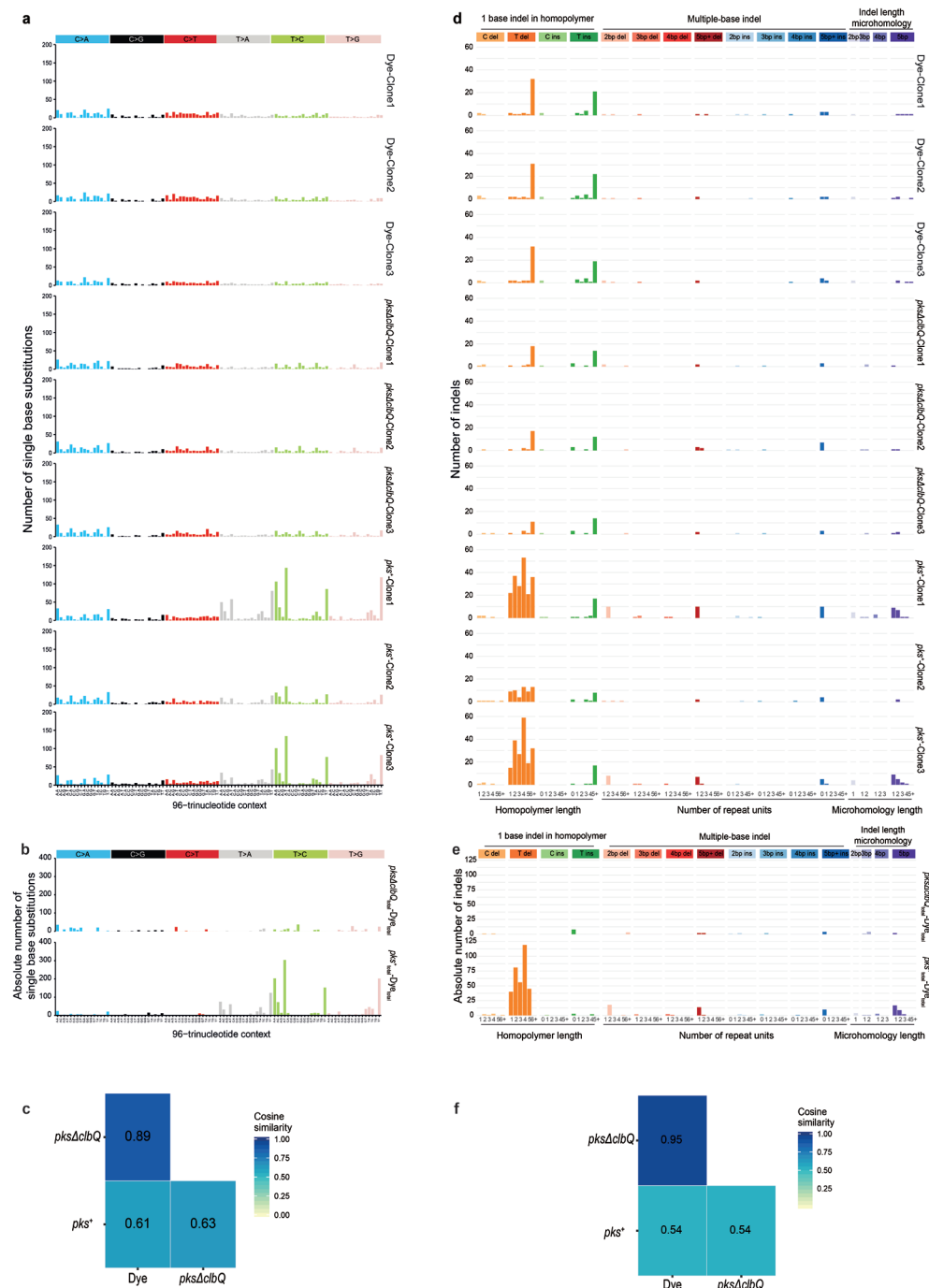
- Allen, J. & Sears, C. L. Impact of the gut microbiome on the genome and epigenome of colon epithelial cells: contributions to colorectal cancer development. *Genome Med.* 11, 11 (2019).
- Gagnaire, A., Nadel, B., Raoult, D., Neefjes, J. & Gorvel, J.-P. Collateral damage: insights into bacterial mechanisms that predispose host cells to cancer. *Nat. Rev. Microbiol.* 15, 109–128 (2017).
- Nougayrède, J.-P. et al. *Escherichia coli* induces DNA double-strand breaks in eukaryotic cells. *Science* 313, 848–851 (2006).
- Wilson, M. R. et al. The human gut bacterial genotoxin colibactin alkylates DNA. *Science* 363, eaar7785 (2019).
- Xue, M. et al. Structure elucidation of colibactin and its DNA cross-links. *Science* 365, eaax2685 (2019).
- Dejea, C. M. et al. Patients with familial adenomatous polyposis harbor colonic biofilms containing tumorigenic bacteria. *Science* 359, 592–597 (2018).
- Bullman, S. et al. Analysis of *Fusobacterium* persistence and antibiotic response in colorectal cancer. *Science* 358, 1443–1448 (2017).
- Kostic, A. D. et al. *Fusobacterium nucleatum* potentiates intestinal tumorigenesis and modulates the tumor-immune microenvironment. *Cell Host Microbe* 14, 207–215 (2013).
- Wirbel, J. et al. Meta-analysis of fecal metagenomes reveals global microbial signatures that are specific for colorectal cancer. *Nat. Med.* 25, 679–689 (2019).
- Buc, E. et al. High prevalence of mucosa-associated *E. coli* producing cyclomodulin and genotoxin in colon cancer. *PLoS One* 8, e56964 (2013).
- Arthur, J. C. et al. Intestinal inflammation targets cancer-inducing activity of the microbiota. *Science* 338, 120–123 (2012).
- Bossuet-Greif, N. et al. The colibactin genotoxin generates DNA interstrand cross-links in infected cells. *mBio* 9, e02393-17 (2018).
- Alexandrov, L. B. et al. The repertoire of mutational signatures in human cancer. *Nature* 578, 94–101 (2020).
- Alexandrov, L. B. et al. Signatures of mutational processes in human cancer. *Nature* 500, 415–421 (2013).
- Nik-Zainal, S. et al. Mutational processes molding the genomes of 21 breast cancers. *Cell* 149, 979–993 (2012).
- Drost, J. et al. Use of CRISPR-modified human stem cell organoids to study the origin of mutational signatures in cancer. *Science* 358, 234–238 (2017).
- Sato, T. et al. Long-term expansion of epithelial organoids from human colon, adenoma, adenocarcinoma, and Barrett's epithelium. *Gastroenterology* 141, 1762–1772 (2011).
- Tuveson, D. & Clevers, H. Cancer modeling meets human organoid technology. *Science* 364, 952–955 (2019).
- Kucab, J. E. et al. A compendium of mutational signatures of environmental agents. *Cell* 177, 821–836.e16 (2019).
- Jager, M. et al. Measuring mutation accumulation in single human adult stem cells by whole-genome sequencing of organoid cultures. *Nat. Protocols* 13, 59–78 (2018).
- Cougnoux, A. et al. Bacterial genotoxin colibactin promotes colon tumour growth by inducing a senescence-associated secretory phenotype. *Gut* 63, 1932–1942 (2014).
- Bartfeld, S. et al. In vitro expansion of human gastric epithelial stem cells and their responses to bacterial infection. *Gastroenterology* 148, 126–136.e6 (2015).
- Li, Z.-R. et al. Divergent biosynthesis yields a cytotoxic aminomalonate-containing precolibactin. *Nat. Chem. Biol.* 12, 773–775 (2016).
- Priestley, P. et al. Pan-cancer whole-genome analyses of metastatic solid tumours. *Nature* 575, 210–216 (2019).
- Gonzalez-Perez, A. et al. IntOGen-mutations identifies cancer drivers across tumor types. *Nat. Methods* 10, 1081–1082 (2013).
- Lee-Six, H. et al. The landscape of somatic mutation in normal colorectal epithelial cells. *Nature* 574, 532–537 (2019).
- McLellan, L. K. & Hunstad, D. A. Urinary tract infection: pathogenesis and outlook. *Trends Mol. Med.* 22, 946–957 (2016).
- Zawadzki, P. J. et al. Identification of infectious microbiota from oral cavity

- environment of various population group patients as a preventive approach to human health risk factors. *Ann. Agric. Environ. Med.* 23, 566–569 (2016).
29. Banerjee, S. et al. Microbial signatures associated with oropharyngeal and oral squamous cell carcinomas. *Sci. Rep.* 7, 4036 (2017).
 30. Boot, A. et al. Identification of novel mutational signatures in Asian oral squamous cell carcinomas associated with bacterial infections Preprint at <https://doi.org/10.1101/368753> (2019).
 31. Payros, D. et al. Maternally acquired genotoxic *Escherichia coli* alters offspring's intestinal homeostasis. *Gut Microbes* 5, 313–325 (2014).
 32. Olier, M. et al. Genotoxicity of *Escherichia coli* Nissle 1917 strain cannot be dissociated from its probiotic activity. *Gut Microbes* 3, 501–509 (2012).
 33. Jacobi, C. A. & Malfertheiner, P. *Escherichia coli* Nissle 1917 (Mutaflor): new insights into an old probiotic bacterium. *Dig. Dis.* 29, 600–607 (2011).
 34. Blokzijl, F. et al. Tissue-specific mutation accumulation in human adult stem cells during life. *Nature* 538, 260–264 (2016).
 35. Heo, I. et al. Modelling *Cryptosporidium* infection in human small intestinal and lung organoids. *Nat. Microbiol.* 3, 814–823 (2018).
 36. Pace, P. et al. FANCE: the link between Fanconi anaemia complex assembly and activity. *EMBO J.* 21, 3414–3423 (2002).
 37. Li, H. & Durbin, R. Fast and accurate long-read alignment with Burrows-Wheeler transform. *Bioinformatics* 26, 589–595 (2010).
 38. Osorio, F. G. et al. Somatic mutations reveal lineage relationships and age-related mutagenesis in human hematopoiesis. *Cell Rep.* 25, 2308–2316.e4 (2018).
 39. Blokzijl, F., Janssen, R., van Boxtel, R. & Cuppen, E. MutationalPatterns: comprehensive genome-wide analysis of mutational processes. *Genome Med.* 10, 33 (2018).
 40. Cunningham, F. et al. Ensembl 2015. *Nucleic Acids Res.* 43, D662–D669 (2015).
 41. Cameron, D. L. et al. GRIDSS, PURPLE, LINX: unscrambling the tumor genome via integrated analysis of structural variation and copy number. Preprint at <https://doi.org/10.1101/781013> (2019).
 42. Genomics England The National Genomics Research and Healthcare Knowledgebase <https://www.genomicsengland.co.uk/the-national-genomics-research-and-healthcareknowledgebase/>(2017).
 43. Raczy, C. et al. Isaac: ultra-fast whole-genome secondary analysis on Illumina sequencing platforms. *Bioinformatics* 29, 2041–2043 (2013).
 44. Lawrence, M. et al. Software for computing and annotating genomic ranges. *PLOS Comput. Biol.* 9, e1003118 (2013).

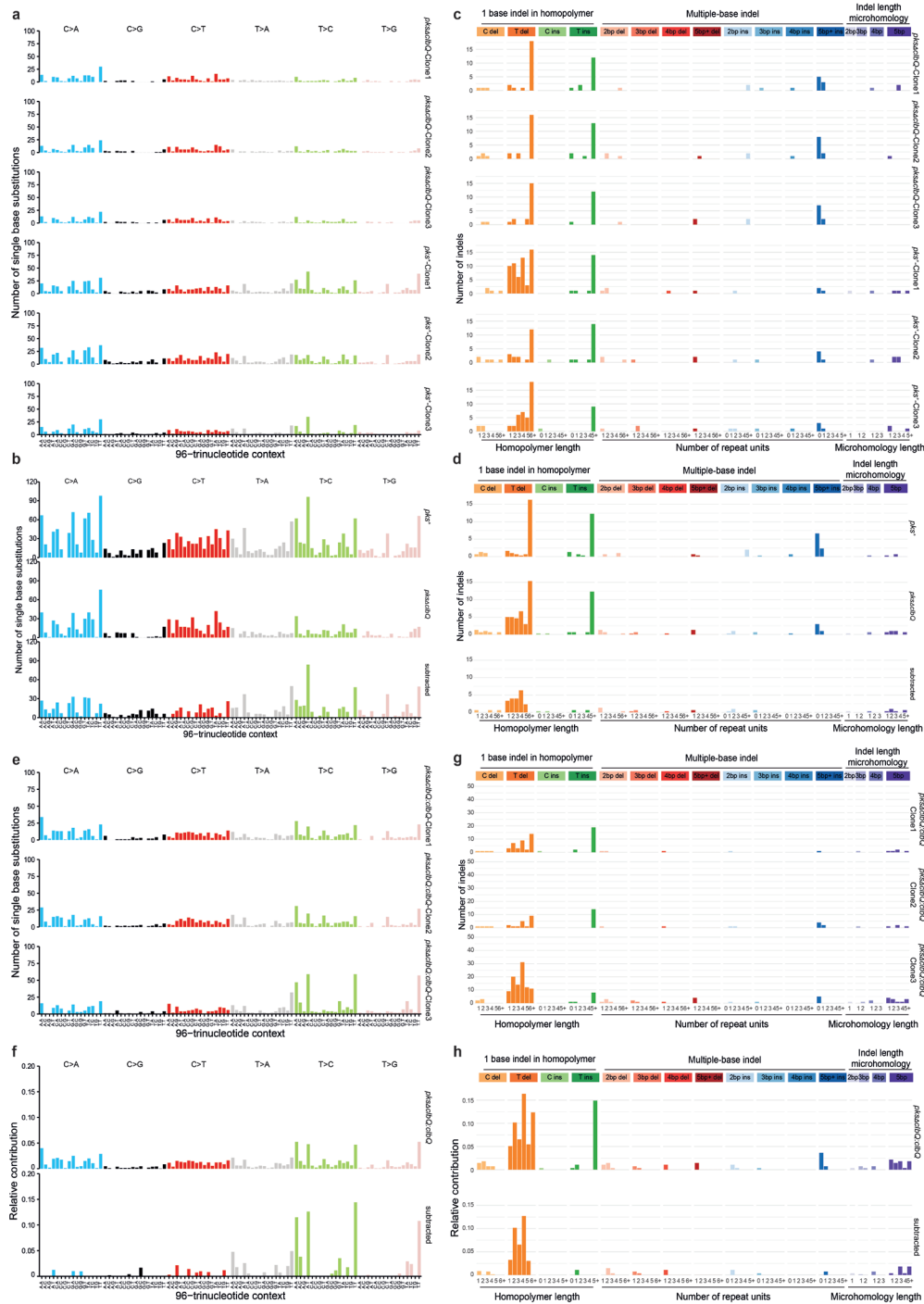
EXTENDED DATA



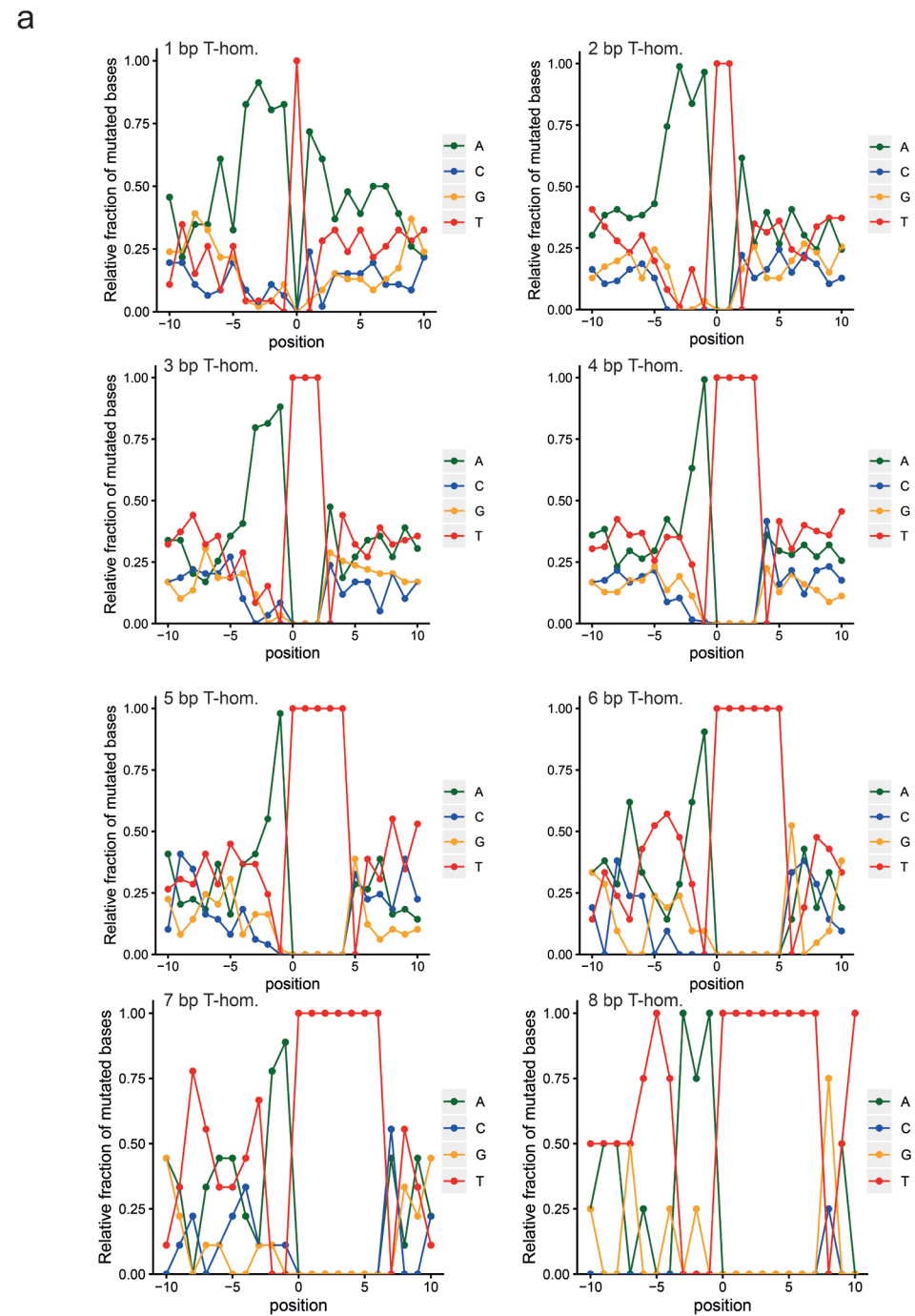
Extended Data Figure 1. Co-culture with genotoxic *pks⁺* *E. coli* induces DNA interstrand crosslinks in healthy human intestinal organoids. **a**, Representative images (out of n = 5 organoids per group) of DNA interstrand crosslink formation after 1 day of co-culture, measured by FANCD2 immunofluorescence (green). Nuclei were stained with DAPI (blue). Yellow boxes represent inset area. Scale bars, 50 μ m (main image); 10 μ m (inset). Experiment was repeated independently twice with similar results. **b**, Gating strategy to select epithelial cells (left) and to quantify viable cells (right). **c**, Mean \pm s.d. viability of intestinal organoid cells after 1, 3 or 5 days of co-culture (n = 3 technical replicates) (bacteria eliminated after 3 days of co-culture). Points are independent replicates.



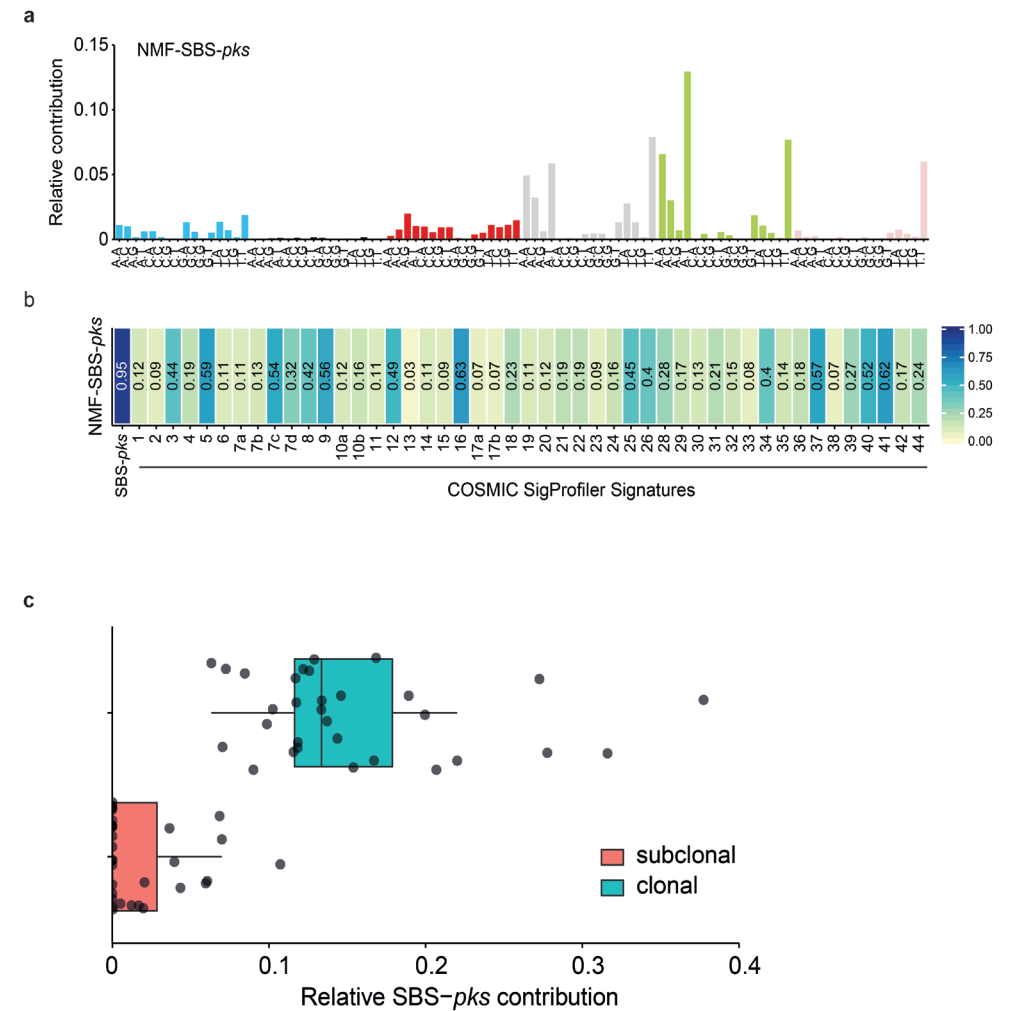
◀ **Extended Data Figure 2. Genotoxic *pks⁺* *E. coli* induce SBS-*pks* and ID-*pks* mutational signatures after long-term co-culture with wild-type intestinal organoids.** **a**, Ninety-six-trinucleotide mutational spectra of SBSs in each of the three individual clones sequenced per condition. Top three, dye; middle three, *pksΔclbQ* *E. coli*; bottom three, *pks⁺* *E. coli*. **b**, Total 96-trinucleotide mutational spectra of organoids injected with *pks⁺* *E. coli* or *pksΔclbQ* *E. coli* from which SBSs in dye-injected organoids have been subtracted. **c**, Heatmap depicting cosine similarity between 96-trinucleotide mutational profiles of organoids injected with dye, *pks⁺* *E. coli* or *pksΔclbQ* *E. coli*. **d**, Indel mutational spectra plots from each of the three individual clones sequenced per condition. Top three, dye; middle three, *pksΔclbQ* *E. coli*; bottom three, *pks⁺* *E. coli*. **e**, Total indel mutational spectra of organoids injected with *pks⁺* *E. coli* and *pksΔclbQ* *E. coli* from which indels in dye-injected organoids have been subtracted. **f**, Heatmap depicting cosine similarity between indel mutational profiles of organoids injected with dye, *pks⁺* *E. coli* or *pksΔclbQ* *E. coli*.



◀ **Extended Data Figure 3. Genotoxic *pks*⁺ *E. coli* and isogenic strain reconstituted with *pks* Δ *clbQ:clbQ* induce SBS-*pks* and ID-*pks* mutational signatures after co-culture.** **a**, Ninety-six-trinucleotide mutational spectra of SBSs in three individual clones from the independent human healthy intestinal organoid line ASC-6a co-cultured for three rounds with *pks*⁺ or *pks* Δ *clbQ* *E. coli*. **b**, Top, total 96-trinucleotide mutational spectra from the three clones cocultured with from *pks*⁺ or *pks* Δ *clbQ* *E. coli* shown in a. Bottom, resulting 96-trinucleotide mutational spectrum from ASC-6a organoids co-cultured with *pks*⁺ *E. coli* after the subtraction of background mutations from three parallel *pks* Δ *clbQ* *E. coli* co-cultures (cosine similarity to SBS-*pks* = 0.77). **c**, Indel mutational spectra from the three independent ASC-6a clones co-cultured for three rounds with *pks*⁺ or *pks* Δ *clbQ* *E. coli*. **d**, Top, total indel mutational spectra from the three clones co-cultured with *pks*⁺ or *pks* Δ *clbQ* *E. coli* shown in c. Bottom, resulting indel mutational spectrum from the independent ASC-6a organoids co-cultured with *pks*⁺ *E. coli* after the subtraction of background mutations from three parallel *pks* Δ *clbQ* *E. coli* co-cultures (cosine similarity to ID-*pks* = 0.93). **e**, Ninety-six-trinucleotide mutational spectra from three individual clones of the ASC-5a line co-cultured for three rounds with the isogenic complemented *E. coli* strain *pks* Δ *clbQ:clbQ*. **f**, Top, total 96-trinucleotide mutational spectrum from the three clones co-cultured with *pks* Δ *clbQ:clbQ* *E. coli* shown in e. Bottom, resulting mutational spectrum after subtracting *pks* Δ *clbQ* background (cosine similarity to SBS-*pks* = 0.95). **g**, Indel mutational spectra from three individual clones of the ASC-5a line co-cultured for three rounds with the isogenic complemented *E. coli* strain *pks* Δ *clbQ:clbQ*. **h**, Top, total indel mutational spectrum from the three clones co-cultured with *pks* Δ *clbQ:clbQ* *E. coli* shown in g. Bottom, resulting mutational spectrum after subtracting *pks* Δ *clbQ* background (cosine similarity to ID-*pks* = 0.95).



Extended Data Figure 4. Detailed sequence context for ID-*pks* and longer deletions by length. **a**, Ten-base up- and downstream profile shows an upstream homopolymer of adenosines that favours induction of T deletions. The length of the adenosine stretch decreases with increasing T homopolymer length (1–8, top left to bottom right).



Extended Data Figure 5. Signature extraction and clonal contribution of SBS-*pks* in CRC metastases. **a**, De novo NMF-SBS-*pks* signature extracted by NMF on all 496 CRC metastases in the HMF data set. **b**, Cosine similarity scores between the de novo extracted SBS signature in **a** and COSMIC SigProfiler signatures, including our experimentally defined SBS-*pks* signature (left). **c**, Relative contribution of SBS-*pks* to clonal (corrected variant allele frequency >0.4, blue) and subclonal fractions (corrected variant allele frequency <0.2, red) of mutations in the 31 SBS/ID-*pks* high CRC metastases from the HMF cohort. Box, upper and lower quartiles; centre line, mean; whiskers, largest value no more than 1.5 times the interquartile range extending from the box; points, individual CRC metastases.

Extended Data Table 1. SBS-*pks* and ID-*pks* levels across tissue types. Sample numbers are displayed by primary tumor type per row. Numbers of samples with more than 5% contribution of ID-*pks*, SBS-*pks* or both are shown; the percentage of positive samples per tissue is indicated in parentheses.

Primary Tumor Location	Total number	SBS- <i>pks</i> > 0.05	ID- <i>pks</i> > 0.05	SBS- <i>pks</i> > 0.05 & ID- <i>pks</i> > 0.05
CRC	496	37 (7.5%)	44 (8.8%)	31 (6.25%)
Head & Neck	61	1 (1.6%)	1 (1.6%)	1 (1.6%)
Urinary Tract	142	3 (2.1%)	6 (4.2%)	3 (2.1%)
Other	2969	12 (0.4%)	134 (4.5%)	1 (0.03%)

6

AN ANALYTICAL FRAMEWORK TO DETECT COLIBACTIN-INDUCED MUTATIONS IN COLORECTAL CANCER AND *E. COLI* NISSLE-EXPOSED ORGANOIDS

Axel Rosendahl Huber^{1,3,4*}, Cayetano Pleguezuelos-Manzano^{2,3*},
Jens Puschhof^{2,3,5*,#}, Charel Boot^{2,3}, Aurelia Saftien^{2,3},
Henry Wood⁶, Phil Quirke⁶,
Hans Clevers^{2,3,#}, Ruben van Boxtel^{1,3,#}

¹Princess Máxima Center for Pediatric Oncology, Heidelberglaan 25, 3584 CS Utrecht, The Netherlands.

²Hubrecht Institute, Royal Netherlands Academy of Arts and Sciences (KNAW) and UMC Utrecht, 3584 CT Utrecht, The Netherlands. ³Oncode Institute, Utrecht, The Netherlands. ⁴Institute for Research in Biomedicine (IRB Barcelona), The Barcelona Institute of Science and Technology, Carrer de Baldori Reixac, 10, 08028 Barcelona, Spain ⁵Microbiome and Cancer Division, German Cancer Research Center (DKFZ), Im Neuenheimer Feld 280, 69120 Heidelberg, Germany. ⁶Pathology and Data Analytics, Leeds Institute of Medical Research at St James's, University of Leeds, Leeds, UK

*These authors contributed equally: Axel Rosendahl Huber, Jens Puschhof, Cayetano Pleguezuelos-Manzano

ABSTRACT

The co-culture of human intestinal organoids with *pks*⁺ *E. coli* producing colibactin induces mutational signatures, which also occur in a subset of colorectal cancer (CRC) tumors¹. *E. coli* Nissle 1917 (EcN) remains a commonly used probiotic, despite harboring the *pks*⁺ operon and inducing double strand DNA breaks^{2,3}. We evaluated the mutagenic activity of EcN by an analytical framework based on the extended motif characteristic of colibactin-induced mutations. EcN showed low, but detectable mutagenic activity compared to previously tested *pks*⁺ *E. coli* strains (estimated at 9-25.9% within a 95% confidence interval)¹. This improved analytic pipeline revealed that 16% of whole genome-sequenced CRC samples show detectable levels of colibactin-induced mutations, more than previously reported using mutational signature refitting. It also reliably detects colibactin-induced mutations in whole exome sequencing data, where conventional mutational signature refitting results in a high false positive rate. Furthermore, this method allows detection of low levels of colibactin-induced mutations in diverse sequencing datasets and represents a crucial step towards pinpointing the genotoxic activity of colibactin in patients.

INTRODUCTION

E. coli strains harboring the polyketide synthase (*pks*) operon produce the genotoxin colibactin and have been associated with an increased risk for colorectal cancer (CRC)⁴⁻⁶. Recent studies have demonstrated that colibactin can alkylate adenines bivalently and thereby cause DNA cross-links^{7,8}. Indeed, in cultured cells *pks*⁺ strains were demonstrated to induce DNA-double strand breaks (DSB)². Furthermore, the co-culture of *pks*⁺ *E. coli* with intestinal organoids and subsequent whole genome sequencing (WGS) revealed its ability to cause single base substitutions (SBS) and short insertions-deletions (ID) in the form of mutational signatures SBS88 and ID18. Because mutational signatures are specific to the effect of individual mutagens⁹, the prevalence of colibactin-induced mutagenesis in CRC genomes could be uncovered. Furthermore, SBS88- and ID18-related mutations are characterized by T>N substitutions and T deletions in adenine-/thymine-rich genomic regions¹. This is in line with other reports indicating similar patterns in colibactin-induced DSBs¹⁰.

E. coli Nissle 1917 (EcN) is a well-studied probiotic strain, commonly used to treat inflammatory bowel disease (IBD) and ulcerative colitis (UC)¹¹. Notably, EcN harbors the *pks* operon in its genome². Despite its probiotic effects, the presence of the *pks* operon suggests that EcN may induce mutations in human cells, which could result in an increased cancer risk. Current evidence on the mutagenicity of EcN shows that it has diminished but detectable ability to cause DSBs compared to other *pks*⁺ strains³. Recently, a study using the *HPRT* gene mutation assay indicated a mutagenic effect of EcN in CHO cells¹². However, no sequencing-based evidence for colibactin-induced mutations in primary human cells by EcN exists to date, and its mutagenic effect has not yet been evaluated systematically at a genome-wide level. To address this, we determined the mutational consequences of EcN exposure in healthy human intestinal organoids using the previously established co-culture system followed by WGS analyses^{1,13}. This revealed that EcN can induce genomic mutations, but to a lesser extent than the CRC-derived *pks* strain tested previously (EcC)^{1,14}. By developing a novel analytical framework based on the extended sequence motif of colibactin-induced SBS mutations, we improved the detection of mutagenesis by EcN exposure. This approach also allowed enhanced detection of colibactin-induced mutations in cancer genome sequencing datasets. Importantly, its improved performance enabled the detection of colibactin-induced mutagenesis in whole-exome sequencing (WES) datasets, which had not been possible with classical mutational signature refitting due to lower mutation burden per sample. Furthermore, this framework allowed discrimination of hypermutated samples enriched in the SBS28 mutational signature bearing *POLE* mutations, initially classified as false positives using the motif-based approach.

RESULTS

We exposed human intestinal organoids to EcN using the microinjection co-culture system (Fig. 1a) previously established to study the mutagenic effect of EcC, a CRC patient-derived *pks*⁺ *E. coli* strain^{1,14}. Both *E. coli* strains showed comparable growth dynamics in co-culture (Fig. 1b). EcN caused DNA damage in organoids exposed for 24h, measured by the presence of nuclear γ H2AX foci, a DSBs marker (Fig. 1c,d). While EcN does not induce the same level of DSBs as the EcC strain, DNA damage level was considerably increased over both negative controls, which were either injected with dye or EcC Δ *clbQ*, an EcC *pks* mutant strain that is unable to produce colibactin (FDR-adjusted p-values, EcN: 0.004; EcC: 0.004, EcC Δ *clbQ*: 0.0313, dye: 0.25) (Fig. 1c,d)^{1,14}.

In order to characterize EcN mutagenic effects, we set up a long-term co-culture of human intestinal organoids injected either with EcN or dye as negative control for 3 days. Then, organoids were treated with non-diffusible antibiotics in order to kill the bacteria. After recovery, organoids were passed and expanded. This co-culture process was repeated for 3 rounds and clonal organoid lines were derived afterwards. These organoids were then subjected to WGS and mutational signature analysis. We compared the mutations in EcN-exposed organoids to those accumulated in dye-exposed organoids. The total number of SBSs and IDs detected did not vary significantly between organoids in both conditions (Fig. 2a, b). Furthermore, the SBS and ID mutational spectra of EcN-treated organoids were similar to those of dye-exposed organoids (Fig. 2c, d), with a cosine similarity of 0.91 and 0.90 respectively (Fig. 2e, f). These results indicate that the overall mutational processes active in the genomes of EcN- and control-exposed organoids are similar when evaluated using mutational signature analysis. To test whether a fraction of the mutations in EcN-exposed organoids could be explained by colibactin-signatures, we performed signature refitting using colibactin (SBS88 and ID18), *in vitro* culture and aging signatures (SBS1, 5 and 18 for SBSs and ID1 and 2 for IDs), since these are basal signatures occurring in organoid cultures^{15,16}. EcN-exposed organoid clones showed a trend towards an increased contribution of SBS88 compared to control clones ($p = 0.064$) (Fig. 2g), but not of ID18 (Fig. 2h). Despite these clear trends (Fig. 2a, c, g), neither comparison of the SBS88 and ID18 signatures in EcN exposed organoids reached a significant enrichment compared to negative control (Fig. 2g, h)). Thus, we asked if other analytical approaches could be used to quantify the contribution of the *pks* signatures to the mutation profiles in EcN-exposed organoids in a more sensitive manner.

Mutational signature analysis only considers the 5' and 3' bases flanking the substitution, however colibactin-induced mutations are characterized by a wider adenine enrichment upstream the occurring T>N SBSs. This enrichment contributes to the colibactin extended sequence motif (Fig. 3a, left). While EcN-exposed organoids also present this motif at a lower level (Fig. 3a, middle), it was not observed in control-treated organoids (Fig. 3a, right) or organoids treated with EcC Δ *clbQ*. Thus, we set to use the motif information to improve the detection of colibactin-induced mutations.

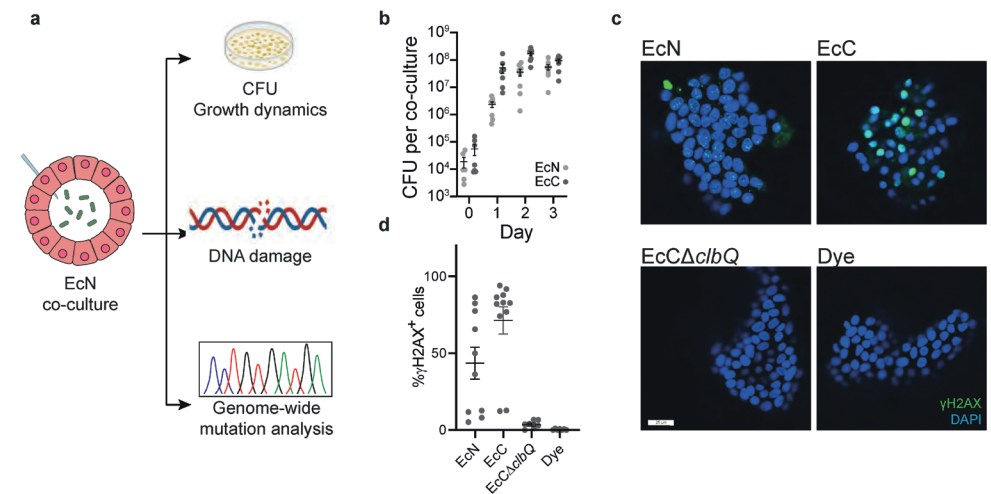


Figure 1. Exposure of intestinal organoids to EcN induces DNA-damage. **a**, Schematic depicting the experimental workflow starting with microinjection of *E. coli* Nissle into the lumen of intestinal organoids. **b**, EcN (grey) and EcC (black) co-culture growth dynamics measured as colony forming units (CFU). Each single dot denotes a single experimental replicate. **c**, DNA double-strand breaks measured by the presence of γ H2AX foci (green) in nuclei (blue) of injected organoids. Exposed conditions: EcN, EcC as positive control. EcC Δ *clbQ* and injection dye as negative control. **d**, Quantification of the percentage of γ H2AX⁺ cells. Cells containing a single γ H2AX focus or more are classified as positive. Each single dot denotes an individual organoid. Scale bar = 25 μ m.

First, we used EcC-induced mutations to evaluate which extended sequence motif best characterizes the colibactin from background mutations present in negative control-exposed organoids. The presence of two adenines 3 and 4 bases upstream of the T>N mutation (-3-4AA) gave the most significant result (p -value = 2.87×10^{-210} , one-sided Fisher's exact test) (Fig. 3b), indicating that this motif can be used to determine activity of colibactin. Using this approach, colibactin-induced mutations with adenines at the -3-4AA positions upstream of the substituted base can be detected more frequently (Fig. 3c) and are significantly enriched in EcN-treated organoids compared to negative control (Fig. 3d, p -value = 5.402×10^{-6} , one-sided Fisher's exact test). These results highlight that considering the -3-4AA base context improves the sensitivity to reliably detect SBS88 mutations in EcN-exposed organoids, which harbor a relatively high background mutation rate (Fig. 3e, Supplementary Fig. 1). In addition, we further increased the specificity of detecting colibactin-induced mutagenesis by only assessing mutations that occur at the most predominantly mutated trinucleotides of SBS88. To determine the optimal subset of mutations to use, we started comparing those from EcC-treated and negative control organoids occurring at the most frequently mutated SBS88 trinucleotide. Then, substitutions occurring at less frequent trinucleotides were included in the comparing cohort in a stepwise manner, from most to least frequent SBS88 trinucleotide. Thus, using the mutations occurring at the 17 most frequent SBS88 trinucleotides resulted in the most

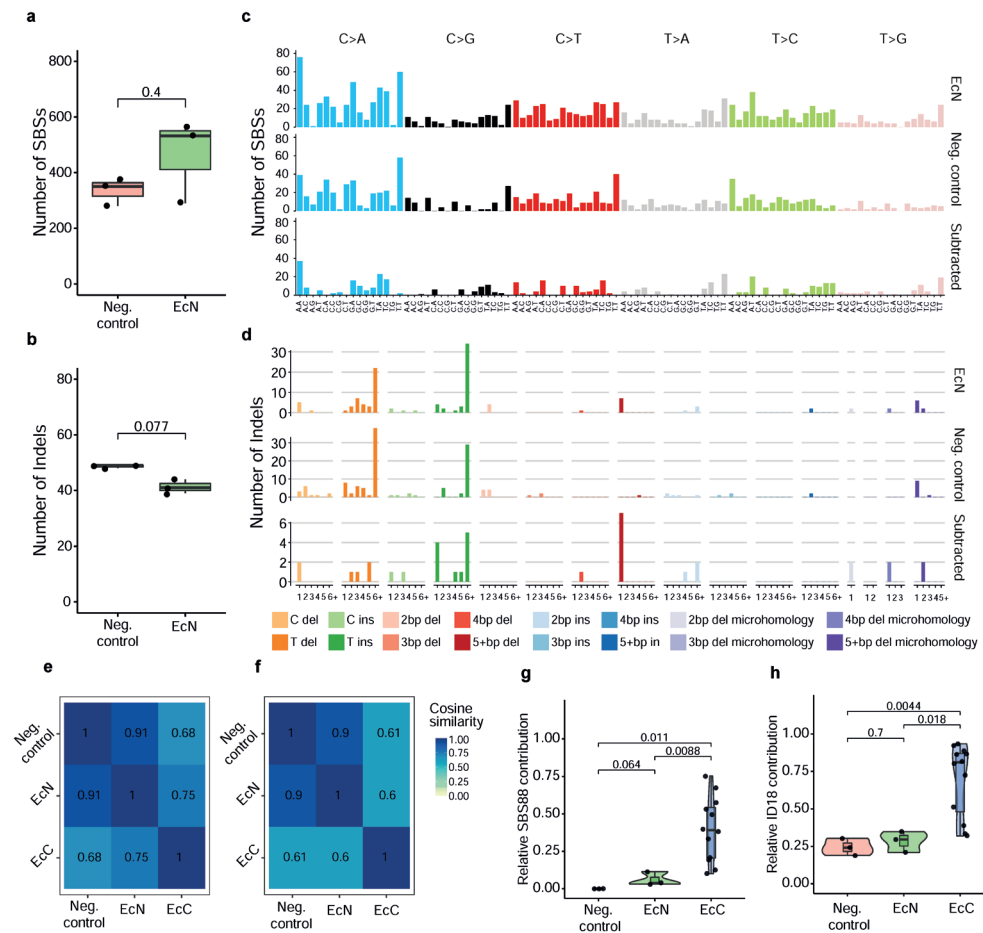


Figure 2. EcN co-culture does not induce a clear mutational signature on intestinal organoid WGS. **a**, Total number of SBSs detected in organoid co-cultured with EcN or negative control (dye). Each dot indicates a single organoid clone. Box indicates upper and lower quartiles with the center line indicating the mean. Whiskers indicate largest or smallest value no more than 1.5 times the interquartile range of the box. **b**, Total number of IDs detected in organoids co-cultured with EcN or negative control (dye). Boxplot specifications according to **a**. **c**, SBS 96-trinucleotide mutational spectra observed in organoids co-cultured with EcN (top) or negative control (dye; middle). Bottom panel depicts the spectra resulting from the subtraction of negative control background mutations from EcN. **d**, ID mutational spectra observed in organoids co-cultured with EcN (top) or negative control (dye; middle). Bottom panel depicts the spectra resulting from the subtraction of negative control background mutations from EcN. **e**, **f**, Cosine similarities between the SBS (**e**) or ID (**f**) mutational spectra between organoids exposed to EcN, control (dye) or EcC (previously derived¹). **g**, Relative SBS88 contribution in organoids co-cultured with EcN, EcC or dye. Mutational signatures considered: SBS1, SBS5, SBS18 (*in vitro* culture) and SBS88 (colibactin). **h**, Relative ID18 contribution in organoids co-cultured with EcN, EcC or dye. Mutational signatures considered: ID1, ID2 (*in vitro* culture) and ID18 (colibactin).

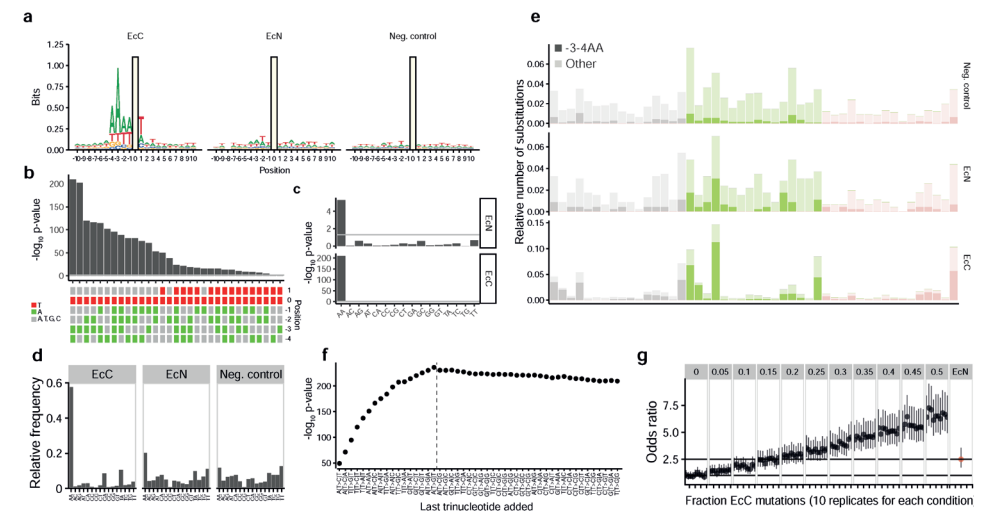


Figure 3. A colibactin-specific -3-4AA motif is enriched in EcN-exposed organoids. **a**, Sequence logo indicating the frequencies of base occurrence in the 10 base pairs upstream and downstream of T>N mutations in organoids exposed to EcC (left), EcN (middle) and control (dye and EcCΔ*clbQ*, right). Size of nucleotide bases indicates information content. Yellow box indicates mutated thymine base. **b**, $-\log_{10}$ transformed p -values from one-tailed fisher's exact test comparing the enrichment of nucleotide motifs between colibactin-exposed organoids (comprising EcC and EcCΔ*clbQ*:*clbQ*) to control-organoids (dye control and EcCΔ*clbQ*). The motifs which were tested are depicted as columns in the lower figure panel. **c**, Relative levels of dinucleotide occurrence at -3 and -4 position from T>N mutations in organoids exposed to EcC, EcN or negative controls. **d**, p -values for enrichment of dinucleotide occurrence at -3 and -4 position from T>N mutations in organoids exposed to EcC and EcN relative to negative control organoids. **e**, T>N trinucleotide SBS mutations by -3 and -4 upstream bases. Dark: SBS mutations having AA at -3 and -4 position. Light: Trinucleotides having any other dinucleotide at the -3 and -4 position. **f**, Stepwise optimization of trinucleotide motifs: $-\log_{10}$ transformed p -values from a one-tailed fisher's exact test, for sequentially accumulating mutations by trinucleotide motif, ordered by occurrence in SBS88/ID18. **g**, Estimation of the relative mutagenicity of EcN by comparison of sampled mixtures of EcC and negative control mutations (10 replicates each) to all negative control mutations. Dots: Indicating odds ratios obtained from a two-tailed fisher's exact test. Lines: 95% confidence interval. On x-axis stepwise increase of EcC-derived mutations in steps of 5%. Last column: Actual enrichment score of EcN-exposed organoids.

significant enrichment of -3-4AA presence against the control cohort (Fig. 3f, p -values = 6.49×10^{-237} and 3.12×10^{-7} for EcC or EcN versus control-exposed organoids, respectively, one-sided Fisher's exact test). Finally, we estimated the relative fraction of colibactin-induced mutations in EcN-treated organoids scoring for AA-enrichment at the -3 and -4 position at the 17 selected trinucleotides. By generating a range of *in silico* sampled mixtures from mutations derived from EcC- and negative control-treated organoids we were able to evaluate the relative mutational effect of EcN compared to EcC. Odds ratios obtained from Fisher's enrichment test estimated that EcN has 16.3% (95% confidence interval between 9.5% and 25.9%) of the mutagenicity compared to the EcC strain in our organoid model (Fig. 3g).

To determine if this analytical framework could be used to improve the detection of colibactin mutagenesis in cancer samples, we determined the presence of the colibactin motif in a WGS cohort consisting of more than 4,800 tumors, of which the majority were metastatic cancers (Hartwig Medical foundation; HMF)¹⁷. 119 out of 4858 samples (2.4%) displayed a significant ($p < 0.001$, Fisher's exact test, one-sided) enrichment of the colibactin motif with an -3-4AA fraction higher than 0.22. This cutoff value was chosen to exclude false positive samples from tissues where colibactin exposure would be implausible, such as brain and bone tumors. The cohort contained 656 CRC samples, 105 of which were colibactin motif positive (16%)(Fig. 4a, b). In addition, colibactin mutagenesis could be detected in 2 out of 22 anal (9.1%), 2 out of 66 small intestine (3%), 5 out of 191 urothelial tract (2.6%), 1 out of 73 head and neck (1.3%) and 1 out of 622 lung (0.16%) samples from the HMF cohort (Fig 4 a, b). Next, we compared the motif classification method to mutational signature refitting of SBS88 and ID18. Applying our previously described mutational signature refitting approach¹ to an extended patient cohort allows detection of 50 samples with high contribution of these mutational signatures, 40 of which were of CRC origin. Of these 50 samples, 47 (94%) were also detected by the motif detection method (Fig. 4b, c). Interestingly, out of the 3 samples detected only by mutational signature refitting, two originate from bone or soft tissue, and thus are likely detected as false positives, since these tissues do not harbor microbiota. Direct comparison of the -3-4AA fraction to the contribution of either SBS88 or ID18 to the mutational load of

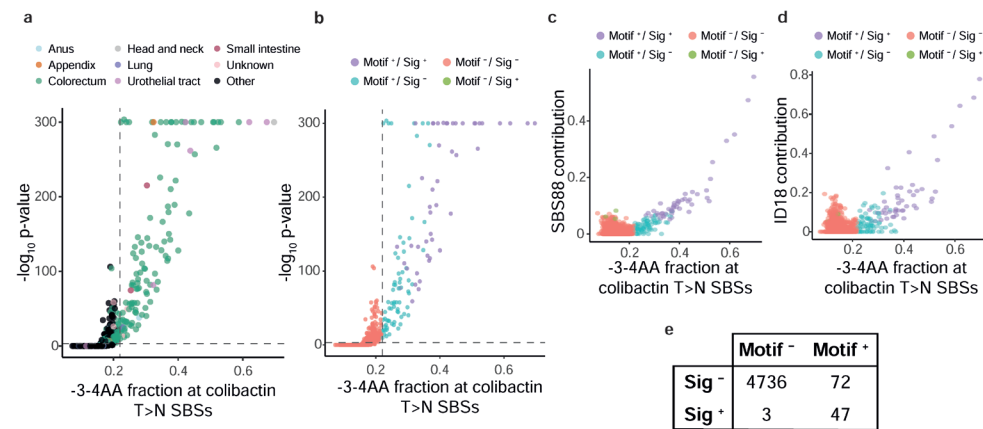


Figure 4. Motif-based classification improves the detection of colibactin mutations in HMF WGS cohort. **a, b**, Scatter plot of $-\log_{10}$ transformed p -values (one-sided fisher's exact test with FDR correction) versus the fraction of -3-4AA at colibactin T>N mutations for each sample ($n = 4848$) of the HMF cohort. Color code indicates the site of primary origin (a) or the sample classification according to motif and mutational signature refitting (b) for each sample. **c**, Summary of HMF WGS sample classification using motif-based and mutational signature refitting-based approaches. **d, e**, Scatter plot of SBS88 (d) or ID18 (e) against the fraction of -3-4AA at colibactin T>N mutations for each sample of the HMF cohort. Color code indicates sample classification according to motif and mutational signature refitting.

each sample shows that the motif-based method allows for the detection of samples with lower levels of both SBS88 and ID18 mutational signatures or with high contribution of other mutational processes (Fig. 4d, e). These findings highlight the advantage of using the colibactin motif to detect the effect of the toxin, allowing to detect the mutagenic effect of colibactin in a larger fraction of samples than using mutational signature refitting.

The motif-based filtering analysis revealed a cluster of 4 positive samples characterized by a high mutational load (Fig. 5a). Interrogation of the dataset for the presence of mutations in genes related to the hypermutator phenotype revealed that 3 out of 4 of these samples harbored oncogenic *POLE* mutations (*POLE*^{mut}), whereas the rest of the cohort did not present such mutations (Fig. 5a). *POLE* encodes the catalytic subunit of DNA

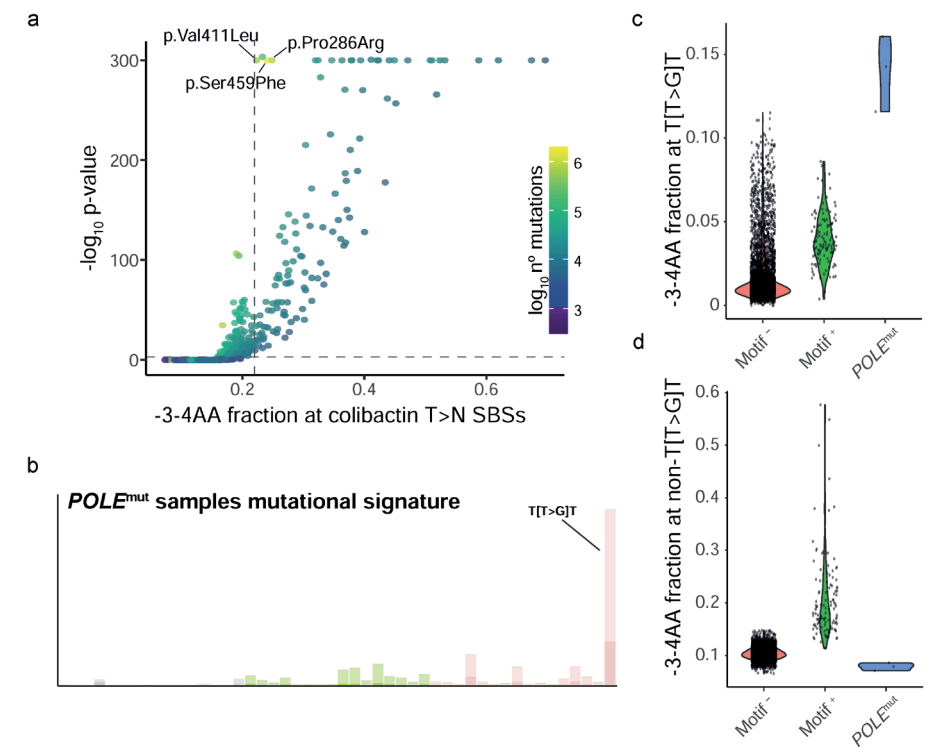


Figure 5. *POLE*^{mut} samples present the -3-4AA motif at T[T>G]T trinucleotide mutations in a colibactin-independent manner. **a**, Scatter plot of $-\log_{10}$ transformed p -values (one-sided fisher's exact test with FDR correction) versus the fraction of -3-4AA at colibactin T>N mutations for each sample ($n = 4848$) of the HMF cohort. Color scale indicates the total number of mutations per sample. Oncogenic mutations in hypermutated *POLE*^{mut} samples, classified as colibactin motif-positive, are indicated. **b**, Trinucleotide mutational spectra for all T>N mutations present in *POLE*^{mut} samples classified as colibactin-motif positive. Dark color shading indicates the fraction of mutations with -3-4AA presence per trinucleotide. Light color indicates any other base combination. **c**, Fraction of T[T>G]T mutations with -3-4AA presence in colibactin-motif negative, colibactin-motif positive (*POLE*^{wt}) or *POLE*^{mut} samples. **d**, Fraction of non-T[T>G]T mutations at colibactin trinucleotides with -3-4AA presence in colibactin-motif negative, colibactin-motif positive (*POLE*^{wt}) or *POLE*^{mut} samples.

polymerase epsilon and oncogenic mutations in this gene result in a hypermutator phenotype^{18,19}. *POLE*^{mut}-associated mutations display an extended DNA context similar to those observed in colibactin induced DSBs¹⁰. One of the mutational signatures associated with *POLE*^{mut}, SBS28, is predominantly characterized by T[T>G]T mutations²⁰ (Fig. 5b). Importantly, SBS28 mutations occurring at the T[T>G]T trinucleotide are also taken into consideration in our motif classification model (Fig 3b, f). To test whether this overlap caused the classification of SBS28-positive samples as colibactin-motif positive, we scrutinized the samples from the HMF cohort for -3-4AA enrichment specifically at SBS28-related T[T>G]T substitutions (Fig. 5c) or in the 47 remaining T>N (non-T[T>G]T) trinucleotides (Fig. 5d). This analysis revealed that SBS28-enriched samples present a -3-4AA enrichment only at T[T>G]T mutations compared to colibactin motif negative samples. However, no difference is detected between these groups when only the other T>N occurring substitutions are taken into consideration (Fig. 5 c,d). Besides, when only non-T[T>G]T substitutions are considered, colibactin-positive samples with *POLE*^{wt} status showed an enrichment of -3-4AA which is absent in *POLE*^{mut} samples (Fig. 5 c,d). This analysis indicates that *POLE*^{mut} SBS28-enriched samples are classified as false positive because of the presence of -3-4AA enrichment specifically at T[T>G]T substitutions contributing to SBS28. Whether this pattern is biologically independent from colibactin-induced mutations or colibactin lesions rather interact with either *POLE*^{wt} or *POLE*^{mut} is not clear. Additionally, this highlights the importance to assess hypermutated CRC genomes for the presence of *POLE* driver mutations, SBS28 mutations or a T[T>G]T bias before concluding on colibactin activity.

Large whole exome sequencing (WES) datasets from cancer genomes hold great promise to shed further light on the prevalence and timing of colibactin-induced mutagenicity. However, the overall mutation load to be analyzed is drastically reduced compared to WGS data, leading to spurious refitting of mutational signatures and less reliable interpretations. Thus, we assessed whether colibactin-induced mutations could be more confidently detected using the motif-based analytical framework on exonic mutations present in the HMF metastatic WGS cohort. First, we determined the status of each sample using the colibactin motif classification on WGS data. Second, the same HMF set was downsampled to consider only exonic regions and each sample was evaluated using both mutational signature refitting or the colibactin motif classification. Third, the motif evaluation of the WGS set was used to cross-validate the results obtained considering the exonic regions only (Fig. 6a). This analysis revealed that mutational signature refitting on WES performs worse than motif classification on WES at discerning between samples that were classified as motive positive or negative based on WGS (WES Sig.Ref. FPR=0.006, WES motif FPR=0) (Fig. 6b, c, g). Increasing the -3-4AA threshold to 0.26 to filter out all samples containing *POLE* proofreading exonuclease domain mutations allowed distinction of a subset of colibactin positive samples (45/119) (Fig. 6c, g), mostly of CRC origin in the WES data (Fig. 6d). Receiver-operator characteristic analysis revealed that the motif classification approach is both more sensitive and specific than mutational

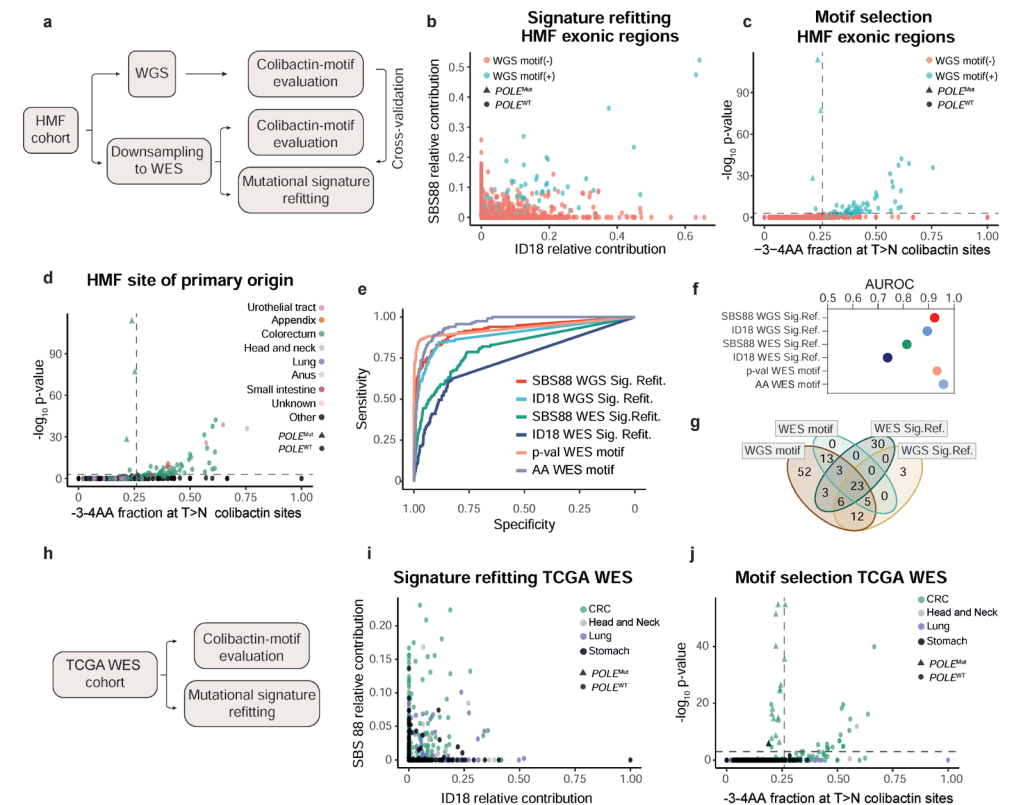


Figure 6. Colibactin-motif enables reliable detection of pks mutagenesis in WES cohorts. **a**, Scheme depicting the validation strategy based on down sampling of WGS data to their exonic components. **b**, Scatterplot of the SBS88 and ID18 contribution to exonic mutations in HMF cohort samples. Colors represent motif-based classification on whole genome level, shapes *POLE* mutation status. **c**, Scatterplot of the -3-4AA motif levels and statistical significance of enrichment in the exonic mutations of HMF cohort samples. Colors represent motif-based classification on whole genome level, shapes *POLE* mutation status. **d**, Scatterplot of the -3-4AA motif levels and statistical significance of enrichment in the exonic mutations of HMF cohort samples. Colors represent primary tumor origin; shapes represent *POLE* mutation status. **e**, ROC analysis of motif-based (-3-4AA contribution and significance on WES level) and signature refitting-based (ID18 and SBS88 on both WGS and WES level) classification using the motif-based classification on WGS level as ground truth. **f**, AUC values resulting from the ROC analyses depicted in e. **g**, Venn diagram depicting overlaps between sample classification using signature refitting and the -3-4AA motif on both whole genome and whole exome levels. **h**, Scheme depicting the analysis performed on the TCGA WES cohort. **i**, Scatterplot of the SBS88 and ID18 contribution to a set of WES samples from the TCGA cohort. Colors represent motif-based classification on whole exome level, shapes *POLE* mutation status. **j**, Scatterplot of the -3-4AA motif levels and statistical significance of enrichment in a set of WES samples from the TCGA cohort. Colors represent motif-based classification on whole exome level, shapes *POLE* mutation status.

signature refitting when used on WES datasets (AUROC values for the *p*-value and -3-4AA presence = 0.93 and 0.96, respectively; Fig. 6e,f,g). Finally, we validated this approach

on a large WES cohort consisting of 2825 cancer WES from The Cancer Genome Atlas (TCGA) (Fig. 6h). As for the HMF cohort, mutational signature refitting did not allow to reliably detect colibactin mutated (Fig. 6i). However, the motif-based method allows detection of a sizable fraction of CRC cases (17/619; 2.7%) with enrichment of the motif (Fig. 6j), a lower percentage compared to WGS analysis due to the lower number of mutations present at exonic regions only.

DISCUSSION

Here, we present an analytical framework that improves the detection of colibactin-induced mutations. This approach relies on the significant enrichment of adenines present 3 and 4 bases upstream the most characteristic T>N substitutions of the SBS88 mutational signature. Filtering for these motif requirements increases the performance of the mutation classification since T>N mutations not matching the colibactin-target motif are excluded (Fig. 3e). Its application allowed to detect the mutagenic activity of the probiotic *pks*⁺ strain EcN in the genome of healthy organoids exposed bacteria in co-culture. Furthermore, it improves the detection of colibactin-linked samples in WGS cohorts and enables the reliable detection of colibactin exposure in WES samples, previously not possible using mutational signatures.

The motif-based approach allows to distinguish a larger group of WGS samples with enrichment of colibactin-linked mutations compared to mutational signature refitting (Table 1). The 119 colibactin-motif positive samples detected were composed mainly by CRC cases (105 out of 551 CRC samples, 18.5%). The rest of the positive samples originated from organs harboring a microbiota, like the urinary tract, head and neck, lung, anus or small intestine. The fact that we can distinguish more colibactin-motif positive samples in the same cohort is indicative of an increased sensitivity, while the absence of samples of primary origins which do not harbor a microbiota is indicative of preserved specificity. In addition, the fraction of colibactin motif positive samples is more in line with the 21% SBS88 and ID18-positive samples detected in healthy colorectal crypts^{21,22}. The slightly lower fraction we observe may be the result of additional processes greatly increasing mutation loads, such as a hypermutator phenotype, which reduces the relative levels of colibactin signatures and/or extended motifs below detection thresholds.

Because of its increased performance, the motif-based approach enables interrogation of WES cohorts reliably (Table 1), not feasible with signature refitting due to the lower mutational load present in WES samples. Considering the HMF WGS dataset as a gold-standard, we evaluated the motif-based and signature refitting performance in the same dataset downsampled to contain only exonic mutations. This showed that signature refitting has a high false positive rate leading to an unreliable detection of the colibactin mutations and 30 samples being falsely classified as colibactin-linked by WES signature refitting. However, the motif-based approach enables reliable distinction of a subset of true positive samples. This advance opens the door to systematically interrogating

Table 1. Summary of colibactin-motif classification per tumor organ of origin in the 3 datasets analyzed in this study. POLE^{mut} samples are excluded. Samples without exonic mutations in HMF WES and TCGA WES datasets are excluded.

HMF WGS	Motif-	Motif+	%	HMF WES	Motif-	Motif+	%	TCGA WES	Motif-	Motif+	%
Anus	20	2	9.1	Anus	21	1	4.5	Colorectum	619	17	2.7
Appendix	5	1	16.7	Appendix	5	1	16.7	Head and neck	510	1	0.2
Colorectum	551	102	15.6	Colorectum	613	37	5.7	Lung	1225	0	0
Head and neck	72	1	1.4	Head and neck	72	1	1.4	Stomach	433	0	0
Lung	621	1	0.2	Lung	620	0	0				
Other	3094	0	0	Other	3070	0	0				
Small intestine	64	2	3	Small intestine	60	1	1.6				
Unknown	126	2	1.6	Unknown	126	0	0				
Urothelial tract	186	5	2.6	Urothelial tract	188	3	1.6				

the large amount of WES datasets that are currently available. To date, WES remains frequently used in clinical setups. Thus, the motif-based classification can be a useful tool for the future evaluation of the action of colibactin for medical purposes.

The colibactin motif-based approach revealed that initially, hypermutated samples harboring oncogenic mutations in *POLE* and an enrichment in SBS28 were classified as colibactin-motif positive. Closer evaluation of their mutational signature profiles revealed that the *POLE*^{mut}-associated mutational signature SBS28 is characterized only by T[T>G]T mutations which also exhibit an enrichment of adenines 3 and 4 bases upstream the substitution. Because of these similarities *POLE*^{mut} samples were initially classified as colibactin-positive. Strikingly, mutational similarities between *POLE*^{mut} and colibactin-linked samples have been pointed out before¹⁰. However, whether these two observations are biologically independent, or the adenine enrichment observed in both colibactin-induced mutations and the genomes from tumors with mutated polymerase epsilon are part of one DNA repair mechanism is not completely clear.

Whereas this study contributes to a growing body of evidence highlighting the DNA-damaging and mutagenic properties of EcN¹², the explanation for decreased levels of DNA damage and mutations compared to other colibactin-producing bacteria^{1,10} remains unsolved. Additionally, whether this heterogeneity is indicative of divergent strain mutagenicity in humans is not known. Different production levels of rate limiting components of the PKS enzymatic machinery, or differences in how the toxin is exported and reaches the eukaryotic nuclei could possibly explain these observations. Several regulatory mechanisms related to the metabolism of iron, spermidine, glucose or inulin have been proposed to affect colibactin production ability²³⁻²⁷. Intrinsic EcN differences affecting these pathways could potentially explain the mutagenic heterogeneity observed in our co-culture system. Furthermore, the human gut with a complete microbiota, mature mucus layer and immune system, inter-individual differences in DNA repair efficiency and the duration of the exposure could influence the mutagenic potential of *pks*⁺ bacteria, including EcN. However, given that healthy colon cells accumulate only ~40 SBS each year^{21,28}, prolonged exposure of the human gut to even lowly mutagenic *pks*⁺ strains could result in a markedly increased mutation load. Whether cell-intrinsic or -extrinsic, the factors regulating colibactin production could be of clinical interest to target and reduce the mutagenic ability of *pks*⁺ bacteria. We speculate that the reduced mutagenicity of EcN in combination with a lower induction of ID compared to SBS by colibactin results in the lack of an identifiable ID signature after EcN exposure.

The functional consequences of colibactin-induced mutations *in vivo* are only beginning to be elucidated. While early studies report hotspots of target sequences in truncating *APC* mutations^{1,3,29}, *in vivo* evidence of colibactin-induced mutagenesis leading to transformation is lacking. Future studies in mouse models of CRC will be essential to filling these gaps in knowledge. Comparison of EcN with other *pks*⁺ bacterial strains in such *in vivo* studies will help to further contribute to elucidating the specific risk caused by this probiotic strain. We envision that the sensitive detection of colibactin-

linked mutations in animal models and patients treated with EcN will be of paramount importance to determine the safety of this commonly prescribed probiotic. The analytical framework presented in this manuscript is expected to translate well to *in vivo* datasets and could thereby make a valuable contribution in the future clinical assessment of EcN mutagenicity.

METHODS

Organoid culture

Ethical approval was obtained from the ethics committee of the University Medical Center Utrecht. Written informed consent was obtained from the tissue donor. All experiments and analyses were performed in compliance with the applicable ethical regulations.

Organoid experiments were performed as previously described³⁰ based on the protocols described in Pleguezuelos-Manzano et al., 2020^{1,13}. The clonal wild-type human intestinal organoid line ASC-5a (described in Blokzijl et al., 2016²⁸) was cultured in 10 µl domes of Cultrex Pathclear Reduced Growth Factor Basement Membrane Extract (BME) (3533-001, Amsbio) submerged in a growth medium consisting of Advanced DMEM/F12 (Gibco), 1× B27, 1× glutamax, 10 mmol/l HEPES, 100 U/ml penicillin-streptomycin (all Thermo Fisher), 1.25 mM N-acetylcysteine, 10 µM nicotinamide, 10 µM p38 inhibitor SB202190 (all Sigma-Aldrich) and the following growth factors: 0.5 nM Wnt surrogate-Fc fusion protein, 2% noggin conditioned medium (both U-Protein Express), 20% Rspo1 conditioned medium (in-house), 50 ng/ml EGF (PeproTech), 0.5 µM A83-01, and 1 µM PGE2 (both Tocris). To derive clonal lines, organoids were dissociated to single cells using TrypLE express (Gibco) and subjected to fluorescence-activated cell sorting (FACS). After sorting, cells were seeded at a density of 50 cells per µl in BME. The Rho kinase inhibitor Y-27632 (10 µM; Abmole, M1817) was added for the first week of growth. Upon reaching a size of >100 µm diameter, organoids were picked and transferred to separate wells of a 48 well plate per organoid. The organoid line identity was regularly confirmed using SNP testing and WGS. Mycoplasma tests were consistently negative throughout the experiments.

EcN co-culture with organoids

The EcN bacterial cultures were performed according to previously described protocols^{1,13}. Bacteria were cultured in Advanced DMEM (Gibco) supplemented with glutamax and HEPES to an optical density (OD) of 0.4. Luminal microinjection into human intestinal organoids was performed as previously described^{13,31}. Bacteria were injected at a multiplicity of infection of 1 together with 0.05% (w/v) FastGreen dye (Sigma) visualize injected organoids. 5 µg/ml of the non-permeant antibiotic gentamicin was added to the medium right after injection to prevent overgrowth of bacteria outside the organoid lumen. Bacterial growth was determined by harvesting, organoid dissociation with 0.5% saponin for 10 min and re-plating of serial dilutions on LB plates. Colony forming units

(CFUs) were counted after a 16 h culture at 37 °C. For long-term co-cultures, the bacteria were killed with 1× Primocin (InvivoGen) after 3 days of co-culture, after which organoids were kept in culture to recover for 4 days before being passaged. Upon reaching a cystic organoid phenotype again (typically after 2–3 weeks), the injection cycle was repeated. This procedure was repeated three times to enable accumulation of mutations and ensure an even exposure of most cells.

DNA damage quantification

Organoids co-cultured with EcN, EcC or EcCΔ*clbQ* (as described in Cougnoux et al., 2014¹⁴) were collected in cell recovery solution (Corning) and incubated at 4 °C for 30 min under gentle rocking in order to remove attached BME from the organoids. The samples were fixed in 4% formalin for 16 h at 4 °C. Organoids were permeabilized with 0.5% Triton-X (Sigma), 2% donkey serum (BioRad) in PBS for 30 min at 4 °C and blocked with 0.1% Tween-20 (Sigma) and 2% donkey serum in PBS for 15 min at room temperature. Subsequently, the samples were incubated with primary mouse anti-γH2AX antibody (Millipore; clone JBW301; 1:1,000 dilution) for 16 h at 4 °C. Then, organoids were washed four times with PBS and incubated with secondary goat anti-mouse AF-647 antibody (Thermo Fisher, catalogue number A-21235, 1:500 dilution) for 3 h at room temperature under the exclusion of light and washed again with PBS. The samples were imaged on an SP8 confocal microscope (Leica). Fluorescent microscopic images of γH2AX foci were quantified by classifying each nucleus as having either no foci or one or more foci. The fraction of nuclei containing foci divided by the sum of all nuclei is displayed as one datapoint per organoid. Statistical significance was evaluated using Prism GraphPad software version 8.4.3 (686). Wilcoxon test was performed to obtain p-values. FDR correction was applied using the R function `p.adjust()` with the parameter method set to "BH".

DNA isolation and sequencing

Genomic DNA was isolated from organoid pellets using the Qiagen DNeasy Blood & Tissue kit. DNA was eluted in 50 μL Low EDTA (10 mM Tris base, 0.1 mM EDTA). DNA sequencing libraries were made with a TruSeq Nano kit (Illumina) from 50 ng of genomic DNA using manufacturers' instructions. These libraries were sequenced at a depth of 15x or 30x using a Novaseq 6000 at the Hartwig Medical foundation (www.hartwigsequencing.nl).

Mapping and variant calling

Aligned sequencing data from previously sequenced organoids co-cultured with CCR, CCR Δ*clbQ*, Δ*clbQ* CCR:Δ*clbQ*:*clbQ* and injection dye were included in the analysis (Supplementary table 1), and all analyses were performed starting from the FASTQ raw sequencing data (PMID: 32106218). Clones were sequenced at 30x base coverage

using an Illumina Novaseq 6000, except for the clones exposed for a single injection round. These clonal lines, and the parental clonal line were sequenced at 30x using an Illumina Hiseq X10 sequencing machine. Sequencing reads from all samples were mapped to the human reference GRCh38 genome using the Burrows-Wheeler Aligner v0.7.17 "BWA-MEM -c 100 -M". Duplicate sequencing reads were marked using Sambamba MarkDup v0.6.8. A full description and source code for the NF-IAP version 1.2 pipeline can be retrieved from: <https://github.com/UMCUGenetics/NF-IAP>. Variants in the mapped data were called using GATK Haplotypecaller version 4.1.3.0 using default settings. Variants were filtered using GATK 4.1.3.0 using the following filter settings for SBS: `--filter-expression 'QD < 2.0' --filter-expression 'MQ < 40.0' --filter-expression 'FS > 60.0' --filter-expression 'HaplotypeScore > 13.0' --filter-expression 'MQRankSum < -12.5' --filter-expression 'ReadPosRankSum < -8.0' --filter-expression 'MQ0 >= 4 && ((MQ0 / (1.0 * DP)) > 0.1)' --filter-expression 'DP < 5' --filter-expression 'QUAL < 30' --filter-expression 'QUAL >= 30.0 && QUAL < 50.0' --filter-expression 'SOR > 4.0' --filter-name 'SNP_LowQualityDepth' --filter-name 'SNP_MappingQuality' --filter-name 'SNP_StrandBias' --filter-name 'SNP_HaplotypeScoreHigh' --filter-name 'SNP_MQRankSumLow' --filter-name 'SNP_ReadPosRankSumLow' --filter-name 'SNP_HardToValidate' --filter-name 'SNP_LowCoverage' --filter-name 'SNP_VeryLowQual' --filter-name 'SNP_LowQual' --filter-name 'SNP_SOR' -cluster 3 -window 10". The following settings were used to filter all other variants: filter_criteria = "--filter-expression 'QD < 2.0' --filter-expression 'ReadPosRankSum < -20.0' --filter-expression 'FS > 200.0' --filter-name 'INDEL_LowQualityDepth' --filter-name 'INDEL_ReadPosRankSumLow' --filter-name 'INDEL_StrandBias'".`

Variant filtering

To filter out mutations induced during sequencing, clonal expansion or library preparation, we filtered genomic variants using an in-house filtering pipeline, SMuRF v2.1.1 (<https://github.com/ToolsVanBox/SMuRF>). Briefly, the variant allele frequency (VAF) was calculated for each variant by pileup of all bases mapped at the mutation position. Variant data derived from organoid clones sequenced at 30x depth were filtered for the following criteria: VAF ≥ 0.3, base coverage ≥ 10 and an MQ quality ≥ 60. For organoid clones sequenced at 15x depth two deviations from the filter settings were introduced: VAF ≥ 0.15, base coverage ≥ 5. To select only mutations occurring during *in-vitro* culture, variants present in the clonal parental organoid line were removed. Recurrent mapping or sequencing artifacts were removed by filtering against a blacklist containing variants present in healthy bone marrow mesenchymal stromal cells³².

Mutational signature analysis

The resulting filtered variants were analyzed using the R package MutationalPatterns v3.0.1³³ to generate 96-trinucleotide and indel plots. (<https://github.com/UMCUGenetics/MutationalPatterns>). In brief, mutations were categorized in 96-trinucleotide categories

for SBS mutations and 83 categories for indel mutations. To compare profiles against COSMIC mutational signatures, version 3.1, the cosine similarity measure was used³⁴. Mutational signatures for the HMF cohort were extracted in the same manner as in Pleguezuelos-Manzano *et al.*, 2020¹. For refitting of EcN clones to SBS and ID mutational profiles, we used the colibactin-induced (SBS88 and ID18) mutational signatures, COSMIC version v3.2, (<https://cancer.sanger.ac.uk/signatures/>). In the re-fitting, we included aging clock-like (SBS1 and 5 for SBSs and ID1 and 2 for IDs)¹⁵ and cell-culture induced signatures (SBS18) active in organoids during cell culture²⁸.

Extended context selection and enrichment testing

For all analyses, only unique T>N SBS mutations occurring in each exposed culture condition were taken into account. For this, a negative population consisting of WGS from 6 samples exposed to dye and 6 samples exposed to EcCΔ*clbQ* strain no longer capable of producing colibactin were used. This was compared to 9 samples exposed to EcC and 3 samples exposed to EcN. To determine the presence of extended context patterns of *pks* profiles, we selected all base occurrences present in *pks* mutations with a frequency of 45% or higher¹. We tested the enrichment of these motifs in all pairwise combinations using a one-tailed Fisher's exact test, using 'greater' as an alternative hypothesis, comparing against all unique mutations present in organoids exposed to dye control and CCR Δ*clbQ* exposure. The most significant position, AA at -3 and -4 was selected for further analysis. To compare enrichments, enrichment for all dinucleotide occurrences was tested using a one-tailed Fisher's exact test, using 'greater' as an alternative hypothesis.

To select the optimal trinucleotide, we tested AA enrichment within selected *pks* trinucleotides, selecting only mutations with the most frequent trinucleotide in the SBS88 signature. We tested against the control mutations using a one-tailed Fisher's exact test, and stepwise added the next most occurring trinucleotide for all T>N mutations. In this manner all T>N trinucleotides were tested. The most specific *pks* trinucleotide combination was determined as the combination of trinucleotides which exhibited the lowest p-value using a one-tailed Fisher's test, testing for enrichment. The lowest p-value ($p = 3.51 \times 10^{-206}$) was obtained when selecting the 17 trinucleotides with the highest contribution to SBS88: A[T>C]T, A[T>C]A, T[T>G]T, T[T>C]T, T[T>A]T, A[T>A]A, A[T>C]C, A[T>A]T, T[T>G]A, A[T>A]C, T[T>G]C, T[T>A]A, G[T>A]T, G[T>G]T, G[T>C]T, A[T>G]A, A[T>G]T.

Estimation of relative mutagenicity of EcN with respect to EcC

We generated synthetic mixtures of control and CCR *pks+* *E. coli* mutations by sampling mutations from all unique mutations present in control (control dye and EcCΔ*clbQ*-exposed) and EcC-exposed organoids. For each concentration, increasing in steps of 5% EcC-content, we generated 10 mixtures containing 0 to 50% EcC mutations. The same total number of mutations (983) as present in EcN exposed organoids (983 mutations) was sampled for each replicate. The '-3-4AA' fraction of mutations was determined by taking

the extended context of mutations at positions -3 and -4 at the previously defined 17 *pks* motif trinucleotides. Enrichment for these motifs was tested against all control mutations using a one-sided Fisher's exact test.

Assessment of extended context motifs enrichment in a cohort of metastatic cancer samples

Ethical approval was obtained from the ethics committee of the HMF. Written informed consent was obtained from all patients. All experiments and analyses were performed in compliance with the applicable ethical regulations. Three cancer genomes containing < 100 somatic SBS mutations were removed from all subsequent analyses from the HMF data. Trinucleotide counts for all mutations in the HMF dataset were determined as in Pleguezuelos-Manzano *et al.*¹ The occurrence of -3-4AA was determined for all 17 *pks* trinucleotides across the cohort. Enrichment of mutations with 'AA' at the -3 and -4 position was determined compared against AA and other dinucleotide presence in all other samples of the HMF cohort using a one-sided Fisher's exact test with *fdr* correction. Colibactin-motif enrichment per sample was defined as having a $p < 0.001$ (Fisher's exact test, one-sided) and a -3-4AA fraction higher than 0.22. Nervous system and bone/soft tissue samples were considered to be unlikely to be exposed to *pks+* bacteria prior to carcinogenesis and used as negative population to set thresholds. For analyses of *POLE*-hypermuted samples in the HMF cohort, somatic mutations were checked to contain any of the 21 mutations in the *POLE* and *POLD1* hotspot mutations¹⁹.

Simulation of whole-exome (WES) data from the HMF cohort

To simulate WES data, only mutations in coding sequences in the GRCh37. Exonic sites were considered when reported as exonic region in Ensembl v75 (GCRh37) and coordinates were converted to GCRh38 genome using UCSC liftOver. 36 cancer genomes containing no exonic SBS or no exonic indel mutations were removed from the dataset. Mutational signature re-fitting and calculation of -3-4AA fraction were performed similarly as for the whole-genome mutations in the HMF-cohort. Receiver-operator curves (ROCs) and Area under the curve (AUCs) were determined using the R-package 'ROCR', using the WGS motif classification as true positive and negative values.

TCGA analysis

Whole exome mutation calls from TCGA cohorts STAD (stomach adenocarcinoma)³⁵, COAD (colon adenocarcinoma)³⁶, READ (rectal adenocarcinoma)³⁶, LUAD (lung adenocarcinoma)³⁷, LUSC (lung squamous cell carcinoma)³⁸ and HNSC (head and neck squamous cell carcinoma)³⁹ were downloaded from the National Cancer Institute GDC data portal <https://portal.gdc.cancer.gov/>.

MuTect2⁴⁰ output was chosen from the various called mutation files available as the filters used in the TCGA MuTect2 pipeline most closely matched those from the HMF

cohort, namely “alt_allele_in_normal” (Evidence seen in the normal sample), “bPcr” (variant allele shows a bias towards one PCR template), “bSeq”, (Variant allele shows a bias towards one sequencing strand), “clustered_events” (Clustered events observed in the tumor), “germline_risk”, (Evidence indicates this site is germline, not somatic), “homologous_mapping_event”, (More than three events were observed in the tumor), “multi_event_alt_allele_in_normal”, (Multiple events observed in tumor and normal), “oxog” (Failed dToxoG), “panel_of_normals” (Seen in at least 2 samples in the panel of normal), “str_contraction” (Site filtered due to contraction of short tandem repeat region), “t_lod_fstar” (Tumor does not meet likelihood threshold), “triallelic_site” (Site filtered because more than two alt alleles pass tumor LOD). Additionally, any SNV calls less than 2bp from another call were removed. The same mutational analyses were then performed as described for the HMF WES data.

Data and code availability

Raw sequencing reads are deposited at the European Genome-Phenome Archive (EGA), under the dataset accession numbers (EGAD00001005416 and EGAD00001008687). Filtered vcf files and R scripts used to perform all analyses can be retrieved from: <https://github.com/AxelRosendahlHuber/Nissle>

ACKNOWLEDGEMENTS

CRUK grant OPTIMISTIC (C10674/A27140), the Gravitation projects CancerGenomiCs.nl and the Netherlands Organ-on-Chip Initiative (024.003.001) from the Netherlands Organisation for Scientific Research (NWO) funded by the Ministry of Education, Culture and Science of the government of the Netherlands (JP, CP-M, CB, AS and HC). In addition, this work has been supported by a VIDI grant from the Netherlands Organisation for Scientific research (NWO) (no. 016.Vidi.171.023) (ARH, RvB) and the OncoCode Institute (partly financed by the Dutch Cancer Society) (ARH, JP, CP-M, CB, AS, HC). The results published here are in whole or part based upon data generated by The Cancer Genome Atlas managed by the NCI and NHGRI. Information about TCGA can be found at <http://cancergenome.nih.gov>.

CONFLICT OF INTEREST

H.C. is inventor on several patents related to organoid technology; his full disclosure is given at <https://www.uu.nl/staff/JCClevers/>. H.C. became head of Pharma, Research and Early Development of F. Hoffmann-La Roche Ltd, Basel, Switzerland.

REFERENCES

- Pleguezuelos-Manzano, C. et al. Mutational signature in colorectal cancer caused by genotoxic pks+ E. coli. *Nature* 580, 269–273 (2020).
- Nougayrède, J.-P. et al. Escherichia coli Induces DNA Double-Strand Breaks in Eukaryotic Cells. *Science* 313, 848–851 (2006).
- Iftexhar, A. et al. Genomic aberrations after short-term exposure to colibactin-producing E. coli transform primary colon epithelial cells. *Nat. Commun.* 12, 1003 (2021).
- Yachida, S. et al. Metagenomic and metabolomic analyses reveal distinct stage-specific phenotypes of the gut microbiota in colorectal cancer. *Nat. Med.* 25, 968–976 (2019).
- Wirbel, J. et al. Meta-analysis of fecal metagenomes reveals global microbial signatures that are specific for colorectal cancer. *Nat. Med.* 25, 679–689 (2019).
- Pleguezuelos-Manzano, C., Puschhof, J. & Clevers, H. Gut Microbiota in Colorectal Cancer: Associations, Mechanisms, and Clinical Approaches. *Annu. Rev. Cancer Biol.* 6, 65–84 (2022).
- Xue, M. et al. Structure elucidation of colibactin and its DNA cross-links. *Science* 365, eaax2685 (2019).
- Wilson, M. R. et al. The human gut bacterial genotoxin colibactin alkylates DNA. *Science* 363, eaar7785 (2019).
- Alexandrov, L. B. et al. The repertoire of mutational signatures in human cancer. *Nature* 578, 94–101 (2020).
- Dziubańska-Kusibab, P. J. et al. Colibactin DNA-damage signature indicates mutational impact in colorectal cancer. *Nat. Med.* 26, 1063–1069 (2020).
- Schultz, M. Clinical use of E. coli Nissle 1917 in inflammatory bowel disease. *Inflamm. Bowel Dis.* 14, 1012–1018 (2008).
- Nougayrède, J.-P. et al. A Toxic Friend: Genotoxic and Mutagenic Activity of the Probiotic Strain Escherichia coli Nissle 1917. *mSphere* 6, e00624-21 (2021).
- Puschhof, J. et al. Intestinal organoid cocultures with microbes. *Nat. Protoc.* 16, 4633–4649 (2021).
- Cougnoux, A. et al. Bacterial genotoxin colibactin promotes colon tumour growth by inducing a senescence-associated secretory phenotype. *Gut* 63, 1932–1942 (2014).
- Alexandrov, L. B. et al. Clock-like mutational processes in human somatic cells. *Nat. Genet.* 47, 1402–1407 (2015).
- Kuijk, E. et al. The mutational impact of culturing human pluripotent and adult stem cells. *Nat. Commun.* 11, 2493 (2020).
- Priestley, P. et al. Pan-cancer whole-genome analyses of metastatic solid tumours. *Nature* 575, 210–216 (2019).
- Campbell, B. B. et al. Comprehensive Analysis of Hypermutation in Human Cancer. *Cell* 171, 1042–1056.e10 (2017).
- Rayner, E. et al. A panoply of errors: polymerase proofreading domain mutations in cancer. *Nat. Rev. Cancer* 16, 71–81 (2016).
- Hodel, K. P. et al. POLE Mutation Spectra Are Shaped by the Mutant Allele Identity, Its Abundance, and Mismatch Repair Status. *Mol. Cell* 78, 1166–1177.e6 (2020).
- Lee-Six, H. et al. The landscape of somatic mutation in normal colorectal epithelial cells. *Nature* 574, 532–537 (2019).
- Cagan, A. et al. Somatic mutation rates scale with lifespan across mammals. *Nature* 604, 517–524 (2022).
- Oliero, M. et al. Oligosaccharides increase the genotoxic effect of colibactin produced by pks+ Escherichia coli strains. *BMC Cancer* 21, 1–10 (2021).
- Wallenstein, A. et al. ClbR Is the Key Transcriptional Activator of Colibactin Gene Expression in Escherichia coli. *mSphere* 5, e00591-20 (2020).
- Tronnet, S. et al. Iron Homeostasis Regulates the Genotoxicity of Escherichia coli That Produces Colibactin. *Infect. Immun.* 84, 3358–3368 (2016).
- Chagneau, C. V. et al. The Polyamine Spermidine Modulates the Production of the Bacterial Genotoxin Colibactin. *mSphere* 4, e00414-19 (2019).
- Dougherty, M. W. & Jobin, C. Shining a Light on Colibactin Biology. *Toxins* 13, 346 (2021).
- Blokzijl, F. et al. Tissue-specific mutation accumulation in human adult stem cells during life. *Nature* 538, 260–264 (2016).
- Terlouw, D. et al. Recurrent APC Splice Variant c.835-8A>G in Patients With

- Unexplained Colorectal Polyposis Fulfilling the Colibactin Mutational Signature. *Gastroenterology* 159, 1612-1614.e5 (2020).
30. Sato, T., et al. Single Lgr5 stem cells build crypt-villus structures in vitro without a mesenchymal niche. *Nature* 459, 262–265 (2009).
 31. Bartfeld, S. et al. In Vitro Expansion of Human Gastric Epithelial Stem Cells and Their Responses to Bacterial Infection. *Gastroenterology* 148, 126-136.e6 (2015).
 32. Osorio, F. G. et al. Somatic Mutations Reveal Lineage Relationships and Age-Related Mutagenesis in Human Hematopoiesis. *Cell Rep.* 25, 2308-2316.e4 (2018).
 33. Manders, F. et al. MutationalPatterns: the one stop shop for the analysis of mutational processes. *BMC Genomics* 23, 1–18 (2022).
 34. Blokzijl, F., Janssen, R., van Boxtel, R. & Cuppen, E. MutationalPatterns: comprehensive genome-wide analysis of mutational processes. *Genome Med.* 10, 1–11 (2018).
 35. Cancer Genome Atlas Research N. Comprehensive molecular characterization of gastric adenocarcinoma. *Nature.* 2014;513(7517):202-9.
 36. Cancer Genome Atlas N. Comprehensive molecular characterization of human colon and rectal cancer. *Nature.* 2012;487(7407):330-7.
 37. Cancer Genome Atlas Research N. Comprehensive molecular profiling of lung adenocarcinoma. *Nature.* 2014;511(7511):543-50.
 38. Cancer Genome Atlas Research N. Comprehensive genomic characterization of squamous cell lung cancers. *Nature.* 2012;489(7417):519-25.
 39. Cancer Genome Atlas N. Comprehensive genomic characterization of head and neck squamous cell carcinomas. *Nature.* 2015;517(7536):576-82.
 40. Benjamin D, Sato T, Cibulskis K, Getz G, Stewart C, Lichtenstein L. Calling Somatic SNVs and Indels with Mutect2. *bioRxiv.* 2019.

7.1

THE HUMAN RESPIRATORY TRACT, CYSTIC FIBROSIS, AND THE ROLE OF *PSEUDOMONAS AERUGINOSA* IN THE PROGRESSION OF THE DISEASE

Cayetano Pleguezuelos-Manzano^{1,2}, Hans Clevers^{1,2}

¹ Hubrecht Institute-KNAW and University Medical Center Utrecht, Utrecht, The Netherlands. ² Oncode Institute, Hubrecht Institute-KNAW and University Medical Center, Utrecht, The Netherlands.

THE HUMAN RESPIRATORY TRACT, CYSTIC FIBROSIS, AND THE ROLE OF *PSEUDOMONAS AERUGINOSA* IN THE PROGRESSION OF THE DISEASE

The airway epithelium expands from the upper tract -nasal cavity, pharynx, and larynx-, to the lower tract -trachea, bronchi, and bronchioles-, and the respiratory zone -respiratory bronchioles and alveoli⁻¹. Gas exchange takes place in the alveoli, which are composed of alveolar type (AT)1 and AT2 cells forming a very thin single layer epithelium. In contrast, the epithelium from the upper and lower respiratory tracts is pseudo-stratified. There, basal cells marked by the expression of *TP63* or *KRT5* act as tissue-resident adult stem cells¹. As basal cells differentiate, they give rise to secretory and ciliated cells, which populate most of the apical surface of the epithelium¹. Secretory cells (Goblet and club cells) produce and secrete mucins (mainly MUC5AC) and secretoglobins (SCGB1A1). These form the mucus layer, a physical and chemical barrier that prevents bacteria from reaching the epithelium. By the coordinated movement of their cilia, ciliated cells are responsible for the clearance of this mucus. Other rare cell types of the airway include pulmonary neuroendocrine cells or PNECs, ionocytes and tuft cells. PNECs serve as bridge between external stimuli and the nervous system¹. Ionocytes are suggested to be the main regulators of mucosal osmolarity and pH^{2,3}. Lastly, tuft cells act as sensors mediating downstream responses by the innate immune system⁴.

Cystic fibrosis (CF) is one of the most prevalent monogenic diseases to date, affecting approximately 100.000 people globally⁵, 50.000 of them in Europe⁶. This disease impacts most severely the respiratory tract. CF is caused by mutations in the *cystic fibrosis transmembrane conductance regulator (CFTR)* gene. This gene encodes a chloride channel essential to the osmoregulation and pH control of the epithelial surface⁷. In the airway, absent or malfunctioning CFTR leads to excessive accumulation of viscous mucus, followed by the obstruction of the airways and development of bronchiectasis. This, in turn, induces chronic inflammation and contributes to the appearance of bacterial infections⁷.

P. aeruginosa is one of the main pathogens causing chronic infections in people with CF⁸. This Gram-negative bacterium is ubiquitously present in water and soil milieux, and normally colonizes the airways of people with CF during the first decade of life. Once established, this pathogen undergoes genomic and phenotypic adaptations to the CF airway, leading to health-threatening chronic infections⁹. These adaptations range from mutations of genes related to biofilm formation and antibiotic resistance to altered bacterial metabolism⁹. Thus, understanding how the interaction between the bacteria and the CF airway contributes to *P. aeruginosa* adaptation might help to improve the life conditions of people with CF. To this end, improved *in vitro* infection models will be of importance for discovering novel targets, as well as testing novel antimicrobial compounds against *P. aeruginosa*.

Adult stem cell (ASC)-derived organoids have been established from the human respiratory tract^{10,11}, and they consist mostly of basal, goblet and ciliated cells. Airway ASC organoids recapitulate CF pathogenesis and can be used as a platform to test treatment efficacy^{10,11}, as the correct functioning of CFTR directly correlates with the swelling ability of these organoids. Additionally, they have been useful to model respiratory syncytial virus¹⁰ and SARS-CoV-2 infections¹² *in vitro*. Thus, ASC-derived organoids from healthy and CF individuals offer a valuable opportunity to develop novel *in vitro* models of *P. aeruginosa* infection. Chapter 7.2 describes our approach to establish 2D airway organoid co-cultures with *P. aeruginosa* and the characterization of their interaction by dual RNA sequencing¹³.

REFERENCES

- Hewitt RJ, Lloyd CM. Regulation of immune responses by the airway epithelial cell landscape. *Nat Rev Immunol*. 2021;21(6):347-362. doi:10.1038/s41577-020-00477-9
- Montoro DT, Haber AL, Biton M, et al. A revised airway epithelial hierarchy includes CFTR-expressing ionocytes. *Nature*. 2018;560(7718):319-324. doi:10.1038/s41586-018-0393-7
- Plasschaert LW, Žilionis R, Choo-Wing R, et al. A single-cell atlas of the airway epithelium reveals the CFTR-rich pulmonary ionocyte. *Nature*. 2018;560(7718):377-381. doi:10.1038/s41586-018-0394-6
- Ting HA, von Moltke J. The Immune Function of Tuft Cells at Gut Mucosal Surfaces and Beyond. *The Journal of Immunology*. 2019;202(5):1321-1329. doi:10.4049/jimmunol.1801069
- Allen L, Allen L, Carr SB, et al. Future therapies for cystic fibrosis. *Nat Commun*. 2023;14(1):693. doi:10.1038/s41467-023-36244-2
- Bierlaagh MC, Muilwijk D, Beekman JM, van der Ent CK. A new era for people with cystic fibrosis. *Eur J Pediatr*. 2021;180(9):2731-2739. doi:10.1007/s00431-021-04168-y
- Ratjen F, Bell SC, Rowe SM, Goss CH, Quittner AL, Bush A. Cystic fibrosis. *Nat Rev Dis Primers*. 2015;1(1):1-19. doi:10.1038/nrdp.2015.10
- Malhotra S, Hayes D, Wozniak DJ. Cystic Fibrosis and *Pseudomonas aeruginosa*: the Host-Microbe Interface. *Clinical Microbiology Reviews*. 2019;32(3):e00138-18. doi:10.1128/CMR.00138-18
- Rossi E, La Rosa R, Bartell JA, et al. *Pseudomonas aeruginosa* adaptation and evolution in patients with cystic fibrosis. *Nat Rev Microbiol*. 2021;19(5):331-342. doi:10.1038/s41579-020-00477-5
- Sachs N, Papaspyropoulos A, Zomer-van Ommen DD, et al. Long-term expanding human airway organoids for disease modeling. *The EMBO Journal*. 2019;38(4):e100300. doi:10.15252/embj.2018100300
- Amatngalim GD, Rodenburg LW, Aalbers BL, et al. Measuring cystic fibrosis drug responses in organoids derived from 2D differentiated nasal epithelia. *Life Science Alliance*. 2022;5(12). doi:10.26508/lsa.202101320
- Lamers MM, van der Vaart J, Knoops K, et al. An organoid-derived bronchioalveolar model for SARS-CoV-2 infection of human alveolar type II-like cells. *The EMBO Journal*. 2021;40(5):e105912. doi:10.15252/embj.2020105912
- Aprianto R, Slager J, Holsappel S, Veening JW. Time-resolved dual RNA-seq reveals extensive rewiring of lung epithelial and pneumococcal transcriptomes during early infection. *Genome Biol*. 2016;17(1):1-16. doi:10.1186/s13059-016-1054-5

7.2

ESTABLISHMENT AND CHARACTERIZATION OF A NEW *PSEUDOMONAS AERUGINOSA* INFECTION MODEL USING 2D AIRWAY ORGANOIDS AND DUAL RNA SEQUENCING

Cayetano Pleguezuelos-Manzano^{1,2#}, Wouter A. G. Beenker^{1#}, Gijs J.F. van Son^{2,3},
Charelle Boot^{1,2}, Harry Begthel¹, Gimano D. Amatngalim^{4,5}, Jeffrey M. Beekman^{4,5,6},
Hans Clevers^{1,2†}, Jeroen den Hertog^{1,7}

¹ Hubrecht Institute-KNAW and University Medical Center Utrecht, Utrecht, The Netherlands.

² Oncode Institute, Hubrecht Institute-KNAW and University Medical Center, Utrecht, The Netherlands.

³ Princess Máxima Center for Pediatric Oncology, Utrecht, Netherlands. ⁴ Department of Pediatric Pulmonology, Wilhelmina Children's Hospital, University Medical Center Utrecht, Utrecht University, Member of ERN-LUNG, Utrecht, The Netherlands. ⁵ Regenerative Medicine Center Utrecht, University Medical Center Utrecht, Utrecht University, Utrecht, The Netherlands. ⁶ Centre for Living Technologies, Eindhoven-Wageningen-Utrecht Alliance, Utrecht, The Netherlands. ⁷ Institute Biology Leiden, Leiden University, Leiden, The Netherlands.

[#] Contributed equally

[†] Current affiliation: Roche Institute for Translational Bioengineering (ITB), Roche Pharma Research and Early Development, Roche Innovation Center Basel, CH-4070 Basel, Switzerland

ABSTRACT

Pseudomonas aeruginosa is a Gram-negative bacterium that is notorious for infections in the airway of cystic fibrosis (CF) subjects. Often, these infections become chronic, leading to higher morbidity and mortality rates. Bacterial quorum sensing (QS) coordinates the expression of virulence factors and the formation of biofilms at a population level. QS has become the focus of attention for development of alternatives to antimicrobials targeting *P. aeruginosa* infections. However, a better understanding of the bacteria-host interaction, and the role of QS in infection, is required. In this study, we set up a new *P. aeruginosa* infection model, using 2D airway organoids derived from healthy and CF individuals. Using dual RNA-sequencing, we dissected their interaction, focusing on the role of QS. As expected, *P. aeruginosa* induced epithelial inflammation. However, QS signaling did not affect the epithelial airway cells. The epithelium influenced several infection-related processes of *P. aeruginosa*, including metabolic changes, induction of type 3 and type 6 secretion systems (T3SS and T6SS), and increased expression of antibiotic resistance genes, including *mexXY* efflux pump and several porins. Interestingly, the epithelium influenced the regulation by QS of the type 2 (T2SS) and T6SS. Finally, we compared our model with *in vivo* *P. aeruginosa* transcriptomic datasets, from samples directly isolated from the airways of CF subjects. This shows that our model recapitulates important aspects of *in vivo* infection, like enhanced denitrification, betaine/choline metabolism, increased antibiotic resistance, as well as an overall decrease of motility-related genes. This relevant infection model is interesting for future investigations, helping to reduce the burden of *P. aeruginosa* infections in CF.

Keywords: Airway organoids, *Pseudomonas aeruginosa*, 2D co-culture, Infection model, Dual RNA-sequencing, Quorum sensing

INTRODUCTION

Pseudomonas aeruginosa is a Gram-negative opportunistic bacterium, which is known to chronically infect the airways of people with cystic fibrosis (CF). CF is a genetic disorder caused by mutations in the gene coding for the cystic fibrosis transmembrane conductance regulator (CFTR) protein. Mutated CFTR leads to an osmotic imbalance of the epithelial surface in multiple organs¹⁻³. However, the airways are most affected due to their obstruction by desiccated mucus, which can lead to pulmonary failure^{4,5}. This CF mucus presents a perfect condition for *P. aeruginosa* growth⁶. Because *P. aeruginosa* has a high intrinsic resistance to antibiotics, infections often become chronic⁷⁻¹¹, contributing to the high morbidity and mortality observed in people with CF¹⁰.

A growing field of research focuses on quorum sensing (QS) as an alternative target to treat *P. aeruginosa* infections. Via QS, bacteria regulate a broad range of cellular processes based on their local cell density. QS in Gram-negative bacteria is highly conserved: a LuxI-type synthase produces a signal molecule (an acyl-homoserine lactone (AHL)) that can diffuse across membranes and bind to its cognate LuxR-type receptor, altering the expression of target genes^{12,13}. Thus, when bacterial density is high, the concentration of AHLs increases, inducing downstream processes like biofilm formation and the production of virulence factors¹².

P. aeruginosa presents a relatively complex QS network, involving three different systems: two typical LuxI/R systems (*las*-encoded and *rhl*-encoded system) and a unique *Pseudomonas* Quinolone Signal (PQS)-based system. These systems are hierarchical and highly interconnected. The Las system is the QS master regulator that induces the expression of the Rhl and PQS systems¹⁴. Importantly, inhibition of QS reduces the toxicity of *P. aeruginosa* in animal models and leads to faster clearing and prolonged survival of the infected animal¹⁵⁻¹⁷. However, the exact role of QS in human infection and CF is still underexplored¹⁸.

To date, *P. aeruginosa* CF infection models vary from the study of *P. aeruginosa* isolates from CF subjects¹⁹⁻²¹ to growing *P. aeruginosa* *in vitro* in artificial CF sputum and other bacterial media²²⁻²⁶, using various CF animal models²⁷⁻²⁹, working with *ex vivo* CF lungs^{30,31}, or co-culture systems using cancer cell lines and primary cells³²⁻³⁷. Each of these models present distinct advantages and disadvantages³⁸.

Human airway organoids derived from adult stem cells faithfully resemble the cellular composition and physiology of the airway³⁹. Additionally, airway organoids derived from CF subjects capture the molecular characteristics of the disorder and therefore are a useful tool to study CF phenotypes *in vitro*⁴⁰. Furthermore, organoid co-cultures have recently been used to investigate the role of bacteria in colorectal cancer^{41,42}. In the current study, we describe a new co-culture method using upper airway organoids grown in 2D -derived from healthy individuals and CF subjects- to study *P. aeruginosa* infections. By performing dual RNA-seq⁴³, this analysis captures the interaction between the host cells and the bacteria.

MATERIALS AND METHODS

Bacterial strains and growth conditions

For this study, we used *P. aeruginosa* PAO1 strains, which constitutively express GFP. Stocks were stored in -80 °C in 20 % glycerol solutions. PAO1 strains were plated on Luria agar (LA) at 37 °C and grown in medium specific for the assay. *E. coli* RHO3 strains were used for conjugation and medium was supplemented with 400 µg/mL 2,6-Diaminopimelic acid (Sigma-Aldrich, Merck Life Science, Amsterdam, The Netherlands) to support growth. The PAO1 $\Delta pq s A$ strain has been described before⁴⁴. The PAO1 $\Delta las I / \Delta rh I I$ strain was generated using allelic exchange following the method described before⁴⁵. For the generation of the mutants we inserted upstream (using UP.Fw and UP.Rv primers) and downstream (using DN.Fw and DN.Rv primers) regions of the gene of interest in pEX18Gm plasmids using Gibson assembly restriction cloning, using the restriction enzymes ScaI and SphI (Primers and plasmids are listed in Supplementary table 1 and 2). After Gibson assembly, the plasmid was transformed into RHO3 *E. coli* donor strains before conjugation via puddle mating with PAO1 GFP strain. Mutant colonies were identified with colony PCR (using seq.FW and seq.Rv primers) and confirmed by sequencing (performed by Macrogen Europe BV).

Organoid cultures

Nasal brushing-derived epithelial stem cells were collected and stored with informed consent of all donor and was approved by a specific ethical board for the use of biobanked materials TcBIO (Toetsingscommissie Biobanks), an institutional Medical Research Ethics Committee of the University Medical Center Utrecht (protocol ID: 16/586). Nasal epithelial stem cells were isolated and expanded in 2D cell cultures as previously described⁴⁶. After initial expansion, nasal cells were grown as organoids and cultured as previously described³⁹. In brief, organoids were cultured in expansion medium containing Advanced DMEM F12, 1X GlutaMax (Life Technologies; 12634-034), 10mM HEPES (Life Technologies; 15630-056) (AdvDMEMF12++), supplemented with penicillin and streptomycin (10,000IU/ml each; Life Technologies; 15140-122) 1× B27 supplement (Life Technologies; 17504-044), 1.25mM N-acetyl-L-cysteine (Sigma-Aldrich; A9165), 10mM nicotinamide (Sigma-Aldrich; N0636), 500nM A83-01 (Tocris; 2939), 5µM Y-27632 (Abmole; Y-27632), 1µM SB202190 (Sigma-Aldrich; S7067), 100ng/ml human FGF10 (PeproTech; 100-26), 25ng/ml FGF7 (PeproTech; 100-19), 1% (vol/vol) RSPO3, and Noggin (produced via the r-PEX protein expression platform at U-Protein Express BV). For its passage, organoids were collected, washed and resuspended in TrypLE (Gibco) and incubated at 37°C for 15 minutes. Then, organoids were mechanically disrupted into single cells and plated in droplets of Cultrex growth factor reduced BME type 2 (Biotechne | R&D systems 3533-010-02). For the 2D culture of airway organoids, 10⁵ cells were seeded into 24-well polystyrene membranes (Greiner Bio-One) and cultured for one week in expansion medium in both top and bottom compartments until confluency.

After confluency, cells were differentiated in air liquid interface (ALI) during 1 month using PneumaCult™-ALI Medium (Stem cell technologies) supplemented with Hydrocortisone stock solution (5 µl/ml; Stem cell technologies #07925) and Heparin solution (2 µl/ml; Stem cell technologies #07980). ALI culture performed without addition of antibiotics.

2D airway organoid - *Pseudomonas aeruginosa* co-culture

Bacterial colonies were picked and grown in DMEM medium (ThermoFisher Scientific, 31966-021), supplemented with 10mM HEPES (ThermoFisher Scientific, 15630080) and 1X GlutaMAX (ThermoFisher Scientific, 35050061), without antibiotics, until an OD₆₀₀ = 0.35 – 0.45. 1 mL of early log-phase bacterial culture was taken and centrifuged for 3 min at 15,000 g, before washing once with PBS. Bacterial cells were pelleted again and resuspended in AdvDMEMF12++ to normalize to OD₆₀₀ = 0.4. Bacteria were diluted 100 x in the same medium before adding 50 µL to the organoids to reach a multiplicity of infection (MOI) of 0.1. Organoids in transwells were washed three times in DMEM/F12 before addition of the bacteria. Co-cultures were incubated at 37°C with 5 % CO₂ for 14 h. In parallel, 50 µL of bacteria were grown in a 96-well plate and organoid transwells without bacteria were incubated as controls. The epithelial cells were checked for damage using the fluorescent EVOS FL Auto 2 microscope (ThermoFisher Scientific) at 14 h. Damaged co-cultures were excluded for analysis.

Imaging of organoid 2D cultures and PAO1-GFP co-culture

Organoid 2D culture and PAO1 co-cultures were fixed with 4% formaldehyde for 2 hours at room temperature. Then, 2D cultures were processed for immunohistochemistry following standard techniques and embedded in paraffin. After sectioning, hematoxylin/eosin staining was performed according to manufacturer instructions. After blocking, the used primary antibodies included anti-MUC5AC (Thermo, MA5-12175), anti-acetylated Tubulin (SantaCruz, sc-23950) and anti-P63 (Abcam, ab735). Co-cultures were processed for wholemount immunofluorescence imaging using standard techniques⁴¹. Then, co-culture was stained with Phalloidin Atto-647 (65906-10NMOL) and DAPI and imaged with SP8 confocal microscope (Leica).

Colony forming unit (CFU) test

For the CFU test, organoid infection protocol was followed as described before. For time point 0 h, plates were incubated for only 5 min. For time point 14 h, plates were incubated 14 h. After incubation, 50 µL of 0.5% saponin was added to the wells and incubated for 10 min at room temperature. Then, the volume was resuspended and transferred to Eppendorf tubes before centrifugation for 10 min at 15,000 g. Supernatant was aspirated and pellets were resuspended in PBS before making 10-fold dilutions. 5 µL of the dilutions were plated on tryptic soy agar and plates were incubated overnight at 34 °C before the colonies were counted.

RNA isolation

RNA was isolated from the cultures using the MasterPure Complete DNA and RNA Purification Kit (Immunosource, Belgium) following manufacturer instructions. To remove all the gDNA, two additional rounds of DNase treatment were performed using TURBO DNase (ThermoFisher Scientific) following manufacturer's protocol. RNA was subsequently isolated again using the MasterPure RNA isolation kit and the RNA was dissolved in MQ and stored at -80 °C until further use. For RNA-sequencing, RNA libraries were validated with Agilent 2100 bioanalyzer. Samples were sent for sequencing to the Utrecht Sequencing Facility (Useq), for library preparation using Truseq RNA stranded ribo-zero. RNAseq was performed using the Illumina NextSeq2000 platform.

Mapping of raw-reads to the genome

To analyze the dataset, a variety of bioinformatics tools were used and we followed a similar protocol as described before, with minor modifications (Supplementary figure 1)⁴⁷. First, the reads were mapped to the human genome (hg19) using STAR mapping software⁴⁸. Unmapped reads were written into a new FastQ-file. Gene counts were assigned to the mapped reads using FeatureCounts⁴⁹. Unmapped reads were then mapped against the PAO1 genome (NCBI: txid208964)^{48,50,51}. Gene counts were again assigned using FeatureCounts. The code for this pipeline is available on Github (https://github.com/GJFvanSon/Hubrecht_clevers.git).

Bioinformatic analysis

Human and PAO1 count tables were independently analyzed using DESeq2⁵². DEGs were calculated using the lfcShrink function with argument type set to "apglm". Volcano plots were generated using EnhancedVolcano package⁵³. For the human dataset, GO enrichment analysis was performed using the function enrichGO() from the package clusterProfiler⁵⁴ with arguments OrgDb=org.Hs.eg.db, ont="BP", pAdjMethod="fdr", minGSSize="1", maxGSSize="2000", qvalueCutoff="0.05" and readable="TRUE". For PAO1 dataset, GO enrichment analysis was performed using the online tool PANTHER 17.0, with the following settings: analysis type: PANTHER overrepresentation test (Released 20221013), annotation version and release date: GO ontology database DOI: 10.5281/zenodo.6799722 released 2022-07-01, reference list: *Pseudomonas aeruginosa* (all genes in database), annotation data set: GO biological process complete, test type: Fisher's exact, correction: calculate false discovery rate. KEGG pathway was generated using the Pathview R package. *Pseudomonas* category and GO gene lists were downloaded from *Pseudomonas* Genome DB version 21.1 (2022-11-20)⁵⁵. Protein-protein association network analysis was performed using the STRING v11 online tool⁵⁶. Common genes with a $\log_2\text{Foldchange} / \log\text{SE} > |4|$ were used as input. The input parameters were set as follow: Organism = "*Pseudomonas aeruginosa* PAO1", Network Type = "full string network", Required score = "high confidence (0.700)", and FDR stringency = "medium

(5 percent)". MCL clustering was performed on the resulting network using the following parameters: inflation parameter = "3", and edges between clusters = "Don't show".

RESULTS

Establishment of 2D airway organoid co-cultures with *P. aeruginosa*

We aimed to study the interaction between *P. aeruginosa* and the airway epithelium during early infection. For this, we established an epithelial co-culture system composed of upper airway (nasal) organoids cultured in 2D and the well-characterized *P. aeruginosa* PAO1 strain constitutively expressing GFP. Organoid cultures were differentiated for 1 month in 2D air liquid interface (ALI) (Figure 1A). This approach gave rise to a pseudostratified epithelium containing the main cell types of the mature airway epithelium: goblet cells marked by MUC5AC, ciliated cells marked by acetylated tubulin, and basal cells marked by TP63 (Figure 1B). 2D ALI cultures allow for easy apical exposure to bacteria. PAO1

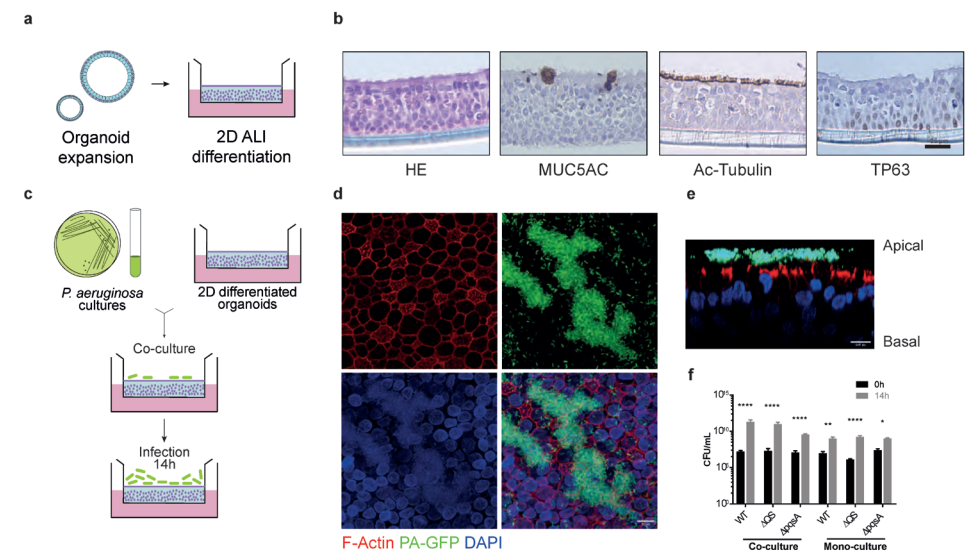


Figure 1. Co-culture establishment of 2D-airway organoids with *P. aeruginosa* PAO1. **a**, Schematic representation of organoid 2D culture establishment and ALI differentiation. **b**, HE and staining of the major cell types present in ALI differentiated airway organoids, goblet cells stained by MUC5AC, ciliated cells by acetylated (Ac) tubulin and basal cells by TP63. Scale bar indicates 25 μm . **c**, Schematic representation of co-culture establishment of PAO1-GFP and differentiated airway organoids. **d**, Z projections and **e**, cross-section of confocal imaging of the co-culture after 14h. Red: F-Actin; green: PAO1-GFP; blue: DAPI. Scale bar indicates 10 μm . **f**, CFU assay of WT PAO1 bacteria and PAO1 ΔQS and ΔpqxA strains following co-culture with organoids and in liquid medium at time points 0h and 14h. The mean of the triplicates was plotted and error bars represent standard error of the mean (SEM). To determine statistical significance between the time points, log-transformed data was analyzed using two-way ANOVA, corrected for multiple comparisons using Sidak's test (*, $P < 0.05$; **, $P < 0.005$; ****, $P < 0.0001$).

bacteria were pipetted apically at a multiplicity of infection (MOI) of 0.1 (Figure 1C). After 14 hours, bacterial aggregates had formed on the epithelial cells implying that downstream pathways including biofilm formation are active in co-culture (Figure 1D, E). Longer co-culture time was not feasible due to elevated epithelial cell death caused by the bacteria. Wild type PAO1 cells and PAO1 strains ΔQS (*rhlI/lasI* KO) and $\Delta pqsA$ (*pqsA* knockout) that display impaired QS were alive and proliferated during this time span (Figure 1F).

Dual RNA-sequencing of the co-culture model

To study the interplay between upper airway epithelial organoids and *P. aeruginosa*, we subjected the 14 hours co-cultures to dual RNA-seq, in order to capture the transcriptomic response of both components. For this, we used organoid lines derived from a healthy donor or from a CF subject and either WT, $\Delta pqsA$ or ΔQS PAO1 cells (Figure 2A). Organoid cultures without bacteria and pure bacterial cultures were used as controls. As an initial step to validate the feasibility of our approach, we performed bacterial RNA sequencing of PAO1-WT strain, both in co-culture and by itself (Supplementary figure 1). We added these samples to the analysis of the dual RNA-seq cohort unless otherwise stated. After a two-step mapping approach (Supplementary Figure 1A), approximately half of the reads from co-culture samples were aligned to the bacterial or human genome, indicating that the dual RNA-seq approach efficiently captured the transcriptome of both components. As expected, the analysis of separately cultured 2D organoids and bacteria yielded almost 100% reads of the corresponding species (Figure 2B).

We first validated the differential expression of the bacterial KO genes in the bacterial strains. As expected, the PAO1 $\Delta pqsA$ strain showed inhibition of *pqsA*, while not affecting *lasI* and *rhlI*. PAO1 ΔQS showed inhibition of all three QS pathways, including inhibition of *pqsA* due to the hierarchical QS system in *P. aeruginosa* PAO1 (Figure 2C). These three strains allowed us to study and compare the effect of QS and of the PQS system in co-culture. Comparison of the PAO1 transcriptomes showed a major difference between PAO1 cells grown in mono-culture and in co-culture with organoids (Figure 2D). The effect of ΔQS was also evident in co-culture and in bacterial mono-culture (Figure 2D). However, $\Delta pqsA$ did not show a marked transcriptional change, other than *pqsA* expression itself, compared to WT bacteria, irrespective of the culture method (Figure 2D). Since our analysis included only one healthy and CF organoid line, conclusions about CF-specific effects of PAO1 cannot be drawn. Nevertheless, both organoid lines showed a clear transcriptional response to the presence of PAO1 irrespective of the bacterial genotype (Figure 2E).

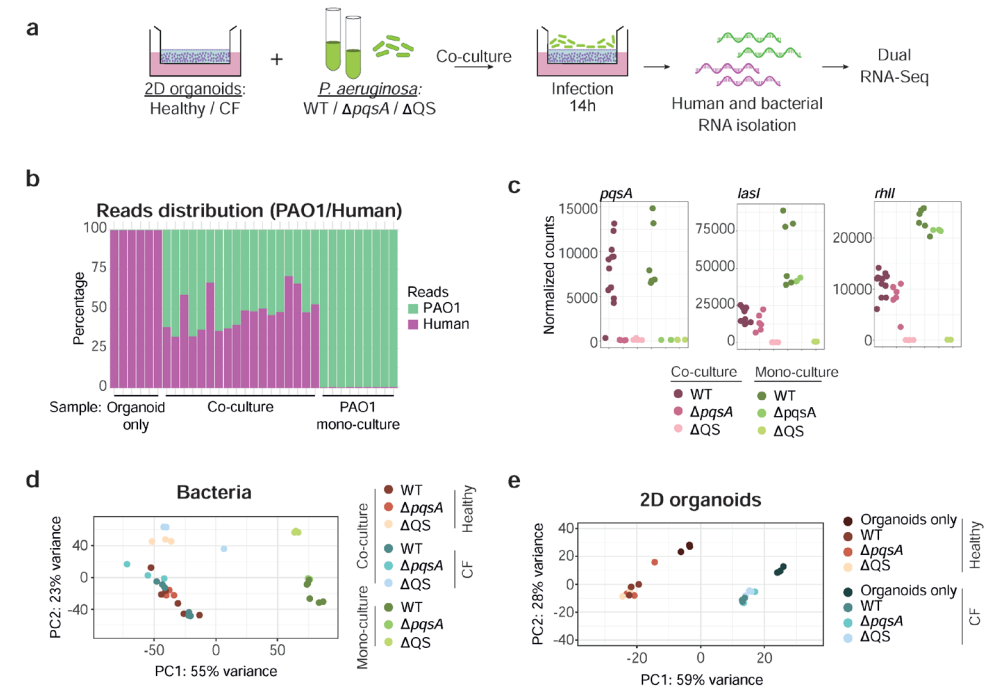


Figure 2. Co-culture characterization by Dual RNA-seq. **a**, Schematic representation of the Dual RNA-seq experiment. **b**, Distribution of human and bacterial reads across the different samples included in the run after performing the mapping and count assignment (as in Supplementary figure 1). **c**, Knock-out validation by gene expression. Normalized counts of *pqsA*, *lasI* and *rhlI* across the different samples of the cohort. Color code indicates culture condition (Green: mono-culture; magenta: co-culture) and PAO1 genotype (Dark: WT; middle: $\Delta pqsA$; light: ΔQS). **d**, PCA plot of PAO1 samples. **e**, PCA plot of 2D organoid samples. Color code indicates PAO1 genotype, culture condition (co-culture or mono-culture) and organoid genotype (Healthy or CF).

P. aeruginosa induces epithelial inflammation

Next, we focused on the effect induced by the different PAO1 strains on the 2D organoid cultures (Figure 3A). Coculture with PAO1 cells led to upregulation of 1610 genes in 2D organoids and downregulation of 638 genes. This occurred irrespectively of the PAO1 genotype (Fig. 3B) For both healthy and CF 2D organoids, these changes reflected pathways involved in NF- κ B-mediated inflammation and response to lipopolysaccharides (LPS), including *IL1A/B*, *TNFA*, and various *CXCL* chemokines (Figure 3D and E). Whereas previous studies have shown that QS molecules affect epithelial cells^{57–59}, no clear QS-derived effect was observed when organoids were exposed to PAO1 WT compared to $\Delta pqsA$ and ΔQS strains (Figure 3B). Since the $\Delta pqsA$ and ΔQS strains lack expression of some or most QS signaling molecules, this observation contrasted with a previous report suggesting that the epithelium can sense and respond to QS molecules⁵⁷.

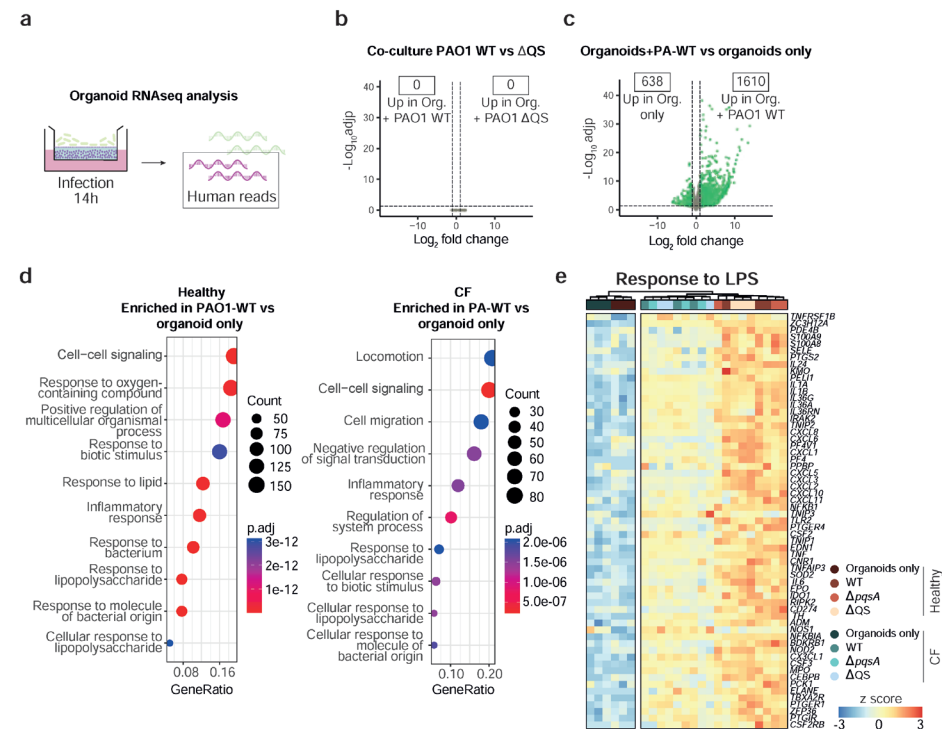


Figure 3. Transcriptional response of the epithelium to infection with the different PAO1 strains. **a**, Schematic representation of the analysis. **b**, Volcano plot showing the \log_2 fold change and $-\log_{10}$ adjusted p-value of all genes, when comparing the transcriptome of 2D organoids exposed to PAO1 WT or PAO1 Δ QS. **c**, Volcano plot showing the \log_2 fold change and $-\log_{10}$ adjusted p-value per gene comparing the transcriptome of 2D organoids exposed to PAO1 WT or unexposed controls. Green indicates differentially expressed genes (DEGs) (\log_2 fold change > 1 and adjusted p value < 0.05). **d**, Gene ontology enrichment analysis showing top 10 categories enriched in 2D organoids exposed to PAO1 WT. Left panel: Healthy organoid line. Right: CF organoid line. **e**, Gene expression heatmap of genes from "Response to lipopolysaccharide" GO term category (GO:0032496). Color code indicates culture condition (co-culture or mono-culture) and PAO1 genotype (WT, Δ pqsA or Δ QS).

The epithelium induces *P. aeruginosa* transcriptional changes associated with infection

We next focused on the effect of the organoids on *P. aeruginosa* PAO1 (Figure 4A). Comparing the gene expression profile of PAO1 grown in co-culture versus mono-culture revealed a total of 2215 differentially expressed genes (DEGs) (979 upregulated in co-culture; 1136 upregulated in mono-culture) (Figure 4B). Gene ontology enrichment analysis of these genes revealed broad metabolic differences between the two culture modes. Genes involved in iron acquisition (e.g., siderophore and pyoverdine processes) showed higher expression in pure bacterial cultures (Supplementary Figure 2A). This contrasted with what has been observed in human infections^{19,60}, but was in agreement with previous co-culture attempts³⁵.

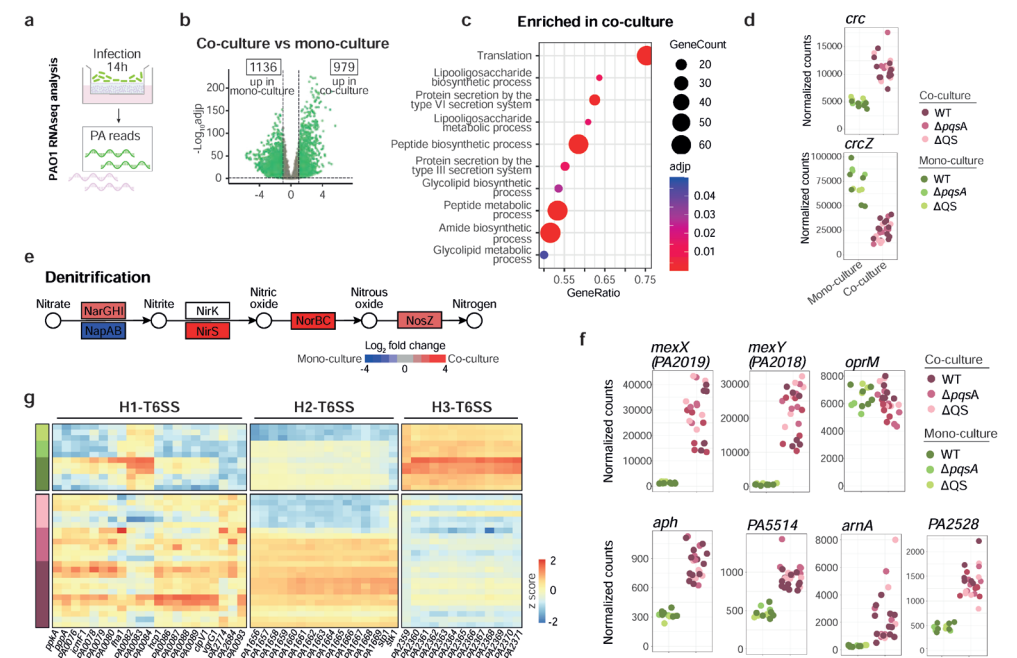


Figure 4. Transcriptional response of PAO1 to the presence of airway epithelium. **a**, Schematic representation of the analysis. **b**, Volcano plot displaying the \log_2 fold change and $-\log_{10}$ adjusted p-value of all genes, when comparing the PAO1 transcriptomes of co-culture and bacterial mono-culture samples. Green indicates differentially expressed genes (DEGs) (\log_2 fold change > 1 and adjusted p value < 0.05). The number of genes upregulated in co-culture and bacterial mono-culture is indicated. **c**, Gene ontology enrichment analysis showing top 10 categories enriched in PAO1 exposed to airway epithelium in co-culture. **d**, Normalized count plots of genes involved in CCR pathway, *crc* and *crcZ*. **e**, KEGG pathway pae00910 plot displaying the \log_2 fold change of genes involved in denitrification. DEGs from co-culture vs bacterial culture mono-culture comparison of PAO1 transcriptomes. **f**, Normalized count plots of genes involved in *P. aeruginosa* antibiotic resistance. **g**, Heat map displaying expression of genes involved in *P. aeruginosa* T6SS. Genes grouped by H1, H2 or H3 T6SS subtype^{68,69}. Samples grouped by culture condition. Color code indicates culture condition (Green: bacterial mono-culture; magenta: co-culture) and PAO1 genotype (Dark: WT; middle: Δ pqsA; light: Δ QS).

PAO1 cells co-cultured with airway cells increased their expression of genes related to peptide, glycolipid and amide biosynthetic pathways (Figure 4C), suggesting major metabolic rearrangements. Interestingly, co-cultured PAO1 cells presented increased *crc* and decreased *crcZ* levels (Figure 4D), two main regulators of the carbon catabolite repression (CCR) pathway^{61,62}. This pathway is central to the hierarchical utilization of preferred carbon sources by *P. aeruginosa*. This finding suggested that the epithelium provides a source of preferred nutrients compared to the medium alone. Interestingly, expression change was observed in only a subset of genes known to be regulated by the CCR pathway (Supplementary Figure 2B). This highlights the complexity of metabolic regulation.

Another important aspect of *P. aeruginosa* infection of individuals with CF is its ability to perform denitrification⁶³. This mechanism enables the utilization of nitrogenous oxides (nitrate, nitrite, and nitrous oxide) as electron acceptor for respiratory growth in anoxic conditions, such as during the course of infection⁶⁴. We found that co-cultured PAO1 expressed increased levels of many genes involved in nitrogen metabolism (Supplementary Figure 2C), and particularly those used in denitrification (Figure 4E). This suggests that there is local anoxia due to the oxygen consumption by the epithelium and high-density bacterial population, which is similar as observed in airway infections^{6,65}. Beyond metabolism, the bacteria also showed elevated levels of genes involved in resistance to antibiotics (Supplementary Figure 2D). Particularly striking was the effect of the epithelium on genes encoding the MexXY efflux pump, porins, and genes like *aph*, *PA5514*, *arnA* and *PA2528* encoding antibiotic degrading enzymes (Figure 4F and Supplementary Figure 2E). Of note, our co-culture system is performed in antibiotic-free conditions. Finally, the presence of epithelial cells induced the expression of type 3 (Supplementary Figure 2F) and type 6 (Figure 4G) secretion systems (T3SS and T6SS). These bacterial secretion systems are syringe-like structures used to inject toxins into the cytoplasm of target cells⁶⁶⁻⁶⁹. The epithelium mainly induced the expression of the H2-T6SS, and to a lesser extent H1-T6SS, but it repressed those belonging to the H3-T6SS subtype. H1 and H2 subtypes are known to act against other prokaryotes and eukaryotes, respectively^{68,70}. Little is known about the role and regulation of H3-T6SS in infection.

The epithelium influences aspects of *P. aeruginosa* QS regulation

Next, we investigated how the presence of the epithelium affected QS-regulated processes in *P. aeruginosa* PAO1. Since only the dual RNA-seq run contained samples from all three bacterial conditions (WT, $\Delta pq s A$, and $\Delta Q S$), only samples from this run were included in the analysis to avoid batch-induced bias. In general, LasR- and RhlR-regulated genes and only some PQS-regulated genes were downregulated in PAO1 WT co-culture conditions compared to bacterial mono-cultures (Figure 5A). This correlates with previous descriptions of stronger QS-induced responses in pure bacterial cultures than in clinical infections^{19,65,71}. Interestingly, the QS receptor levels (*mvfR*, *lasR* and *rhIR*) seemed to be more affected by $\Delta Q S$ when the bacteria were co-cultured with the epithelium than in mono-culture. This could impact the QS regulatory network and therefore it is worth taking into consideration when interpreting results of QS regulation using *in vitro* models. Only 46 and 23 DEGs were found when comparing WT PAO1 with $\Delta pq s A$ in co-culture and in mono-culture respectively (Supplementary Figure 3A-B). From these, the *antABC* operon was affected only in mono-culture (Supplementary Figure 3C). This operon encodes the enzymes responsible for derivatizing the PqsA substrate anthranilic acid to catechol, before degradation to intermediates of the tricarboxylic acid (TCA) cycle⁷². The loss of PqsA in the $\Delta pq s A$ strain could lead to an accumulation of anthranilic acid.

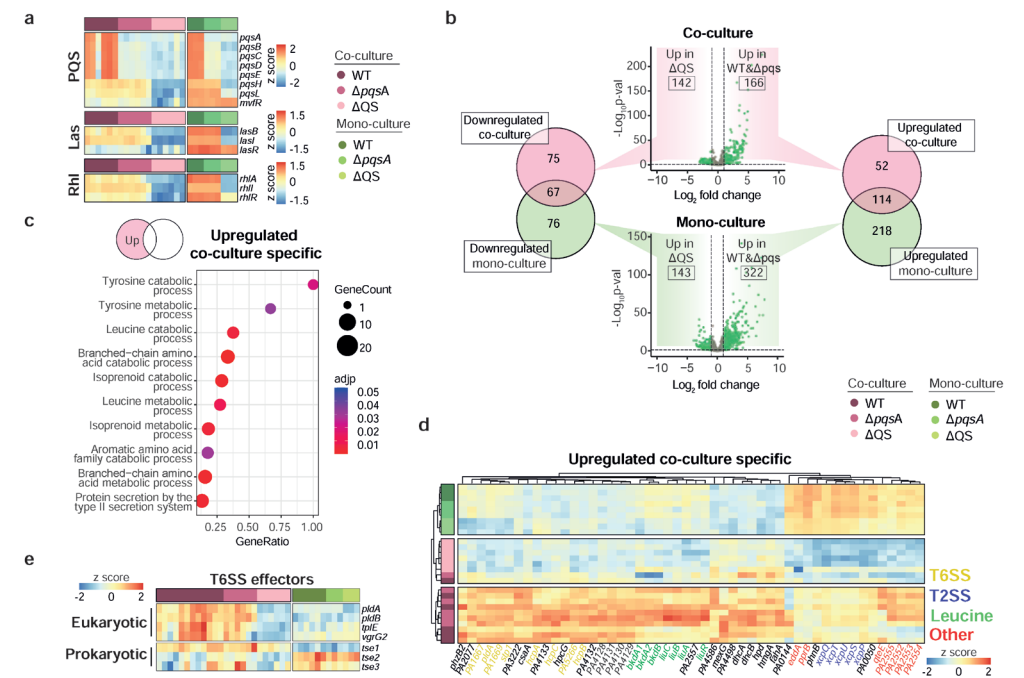


Figure 5. Epithelial effect on PAO1 QS regulation. **a**, Gene expression heat map of genes involved in PQS, Las or Rhl QS pathways. **b**, Volcano plots displaying gene \log_2 fold change and $-\log_{10}$ adjusted p-value when comparing the transcriptomes of WT and $\Delta pq s A$ PAO1 to those of $\Delta Q S$ in co-culture (top) and in pure bacterial cultures (bottom). Venn diagrams display the overlap between genes up (right) and downregulated (left) in the comparisons. **c**, Gene ontology enrichment analysis showing top 10 categories enriched in genes that are specifically upregulated in co-culture in WT and $\Delta pq s A$ PAO1 transcriptomes compared to $\Delta Q S$. **d**, Gene expression heat map showing top 50 co-culture-specific DEGs. Genes are color-coded according to the following categories (Yellow: T6SS; purple: T2SS; green: Leucine metabolism; red: other pathways). **e**, Gene expression heat map of T6SS eukaryotic and prokaryotic effectors. Sample color code indicates culture condition (Green: bacterial culture mono-culture; magenta: co-culture) and PAO1 genotype (Dark: WT; middle: $\Delta pq s A$; light: $\Delta Q S$).

Via upregulation of *antABC* in bacterial mono-cultures, anthranilic acid might be used as a nutrient.

In contrast, deletion of *rhII* and *lasI* in $\Delta Q S$ led to 308 and 465 DEGs in co-culture and in mono-culture, respectively (Figure 5B). In order to dissect which QS-regulated processes were affected by the epithelium, we identified DEGs that occurred specifically in co-culture (52 up and 75 downregulated). Iron uptake pathways were downregulated only in $\Delta Q S$ co-culture condition (Supplementary Figure 3D). This highlighted the differences of the two culture systems regarding iron utilization by the bacteria. On the other hand, genes involved in leucine and tyrosine catabolism were upregulated (Figure 5C-D). The amino acid utilization by *P. aeruginosa* is thought to be a key element of *P. aeruginosa* adaptation to the human airways, since amino acid auxotrophy is common in CF clinical

isolates. This could explain why the QS effect is not observed in isolated bacterial cultures⁷³. Furthermore, we found genes regulated by QS specifically in co-culture involved in bacterial adhesion and biofilm formation (*pprB*), and phosphatase and phosphodiesterase activities (*eddA*)^{74,75}. Additionally, a number of T2SS and T6SS related genes (Figure 5C-D) were specifically regulated by QS in co-culture. T2SS-related genes from WT PAO1 in co-culture showed slightly reduced levels compared to mono-culture. In contrast, QS mutants in co-culture showed a greatly reduced expression of T2SS-related genes. This suggested that the epithelium potentially inhibits T2SS, which can be counteracted by QS-regulated molecules in WT bacteria. The expression of T6SS-related genes was low in all PAO1 strains in mono-culture. Co-culture conditions specifically showed a QS-regulatory effect on the expression of these genes. This suggested that a combination of epithelial and QS factors induce the expression of some T6SS genes. In addition, T6SS effectors that are involved in pathogenicity of eukaryotic cells were both induced by a combination of epithelial and QS signals (Figure 5E).

Benchmarking 2D co-culture model with chronic clinical samples

Next, we addressed which aspects from *in vivo* *P. aeruginosa* infections were recapitulated in our 2D co-culture model. We compared the transcriptional profiles of clinical *P. aeruginosa* strains directly isolated from airway biopsies from CF subjects to the PAO1 co-culture samples. Pure bacterial culture samples from this and other studies were included in the comparison^{19,65,76} (Supplementary Figure 4). After dataset integration, PCA analysis revealed that the origin of the bacterial samples (*in vivo*, co-culture, or mono-culture) explained the clustering of the samples best (Figure 6A). The comparison of the *in vivo* and co-culture transcriptomes to all mono-culture samples revealed a total of 1382 and 2045 DEGs, respectively (Figure 6B). Despite the fact that our co-culture represented an early stage of infection compared to the chronic state of the clinical samples, 269 genes were common between both comparisons (4.7% of all PAO1 genes) (Figure 6C-D). This core gene signature captured the aspects of an *in vivo* infection present in our co-culture model. In order to understand pathways enriched in this core gene signature, we performed protein-protein interaction network analysis (Figure 6E). This confirmed that denitrification is an important process for *P. aeruginosa* infection and that this was captured by our model (Figure 6E-F, Figure 4E and Supplementary Figure 5). Increased expression of *mexYX* antibiotic efflux pump (Figure 6E-F, Figure 4F, Supplementary Figure 5) was also confirmed *in vivo*. Additionally, the expression of some T2SS proteins (Figure 6E-F, Supplementary Figure 5) was reduced in the core signature compared to *in vitro* cultures, which is in line with our previous analysis (Figure 5D).

Beyond confirming the relevance of some of the pathways previously discovered by our cohort, the comparative analysis (Figure 6) uncovered other processes relevant for *in vivo* infection. This included elevated levels of choline/betaine metabolic genes (*betAB*), responsible for the production of glycine-betaine (GB) (Figure 6E-F, Supplementary

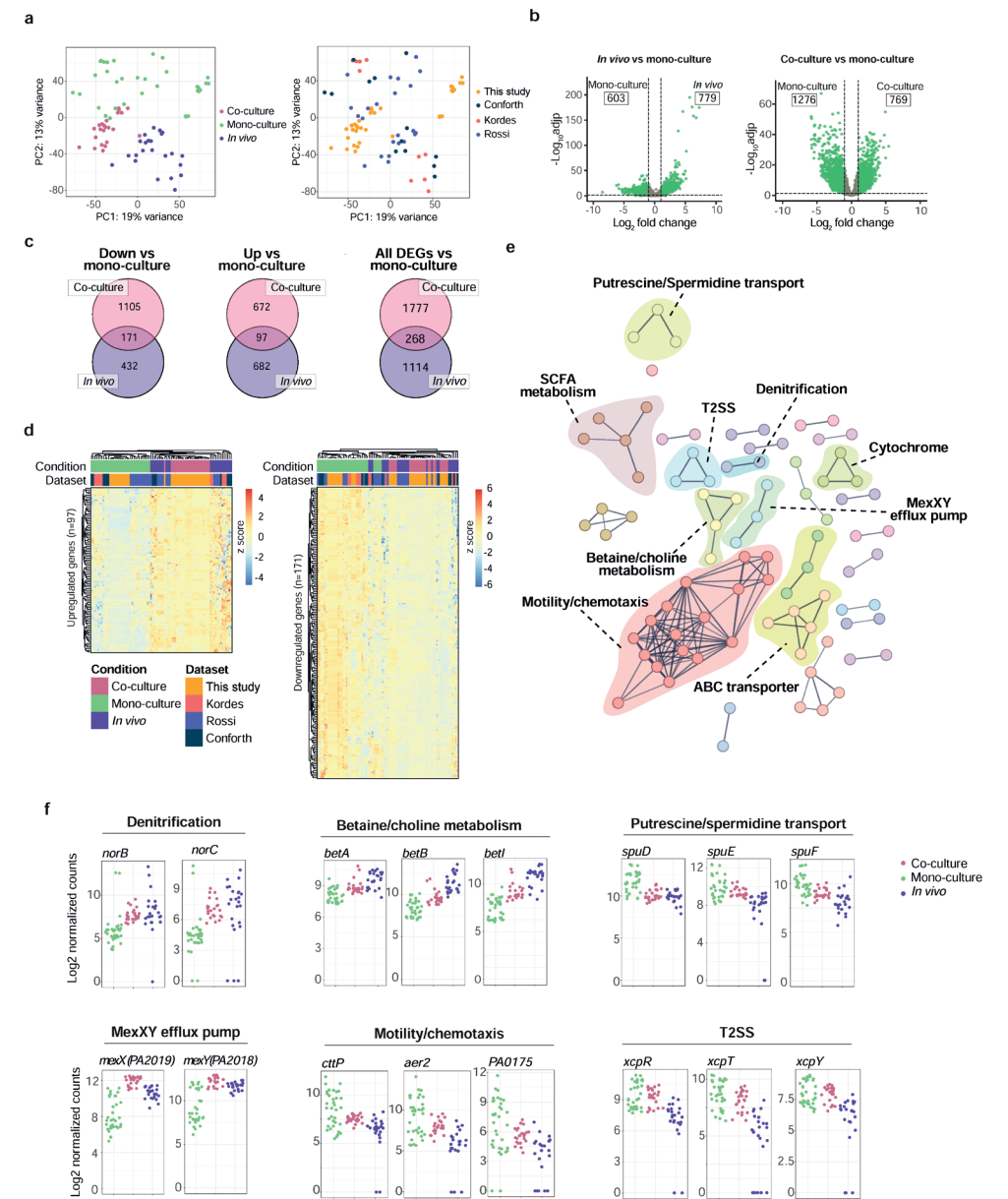


Figure 6. Benchmarking co-culture model with *in vivo* *P. aeruginosa* transcriptomic datasets directly isolated from the airways of CF subjects. **a**, PCA plots showing sample distribution by condition (Magenta: co-culture; green: bacterial culture in isolates; purple: *in vivo*) or by study of origin (Orange: this study; purple: Cornforth et al., 2018¹⁹; pink: Kordes et al., 2019⁷⁶; blue: Rossi et al., 2018⁶⁵). **b**, Volcano plots displaying gene log₂ fold change and -log₁₀ adjusted p-value comparing transcriptomes of *in vivo* *P. aeruginosa* (left) or co-cultured PAO1 (right) to those of all pure bacterial culture samples. Green indicates differentially expressed genes (DEGs) (log₂ fold change > 1 and adjusted p value < 0.05). Indicated in the boxes the number of up- or downregulated DEGs. **c**, Venn diagrams displaying the overlap between genes that are upregulated (left), downregulated

- (middle), or both (right) in the previous *in vivo* and co-culture comparison to *in vitro* and mono-culture samples (b). **d**, Expression heat map displaying the common up-(left) and downregulated (right) genes. Samples clustered based on the expression of all genes plotted per heat map. Color-code indicates condition (Magenta: co-culture; green: pure bacteria; purple: *in vivo*) and study of origin (Orange: this study; purple: Cornforth et al., 2018; pink: Kordes et al., 2019; blue: Rossi et al., 2018). **e**, Protein-protein interaction network of common DEGs (*in vivo* and co-culture). Each node represents a protein encoded by a DEG. Edges represent known protein-protein association (either physical or functional) with a confidence level higher than 0.7. Node color represent clusters generated MCL method. Highlighted the pathway to which the cluster proteins belong. **f**, Log2 normalized count plots of representative genes from pathways highlighted by the network analysis. Color-code indicates Magenta: co-culture, green: pure bacteria and purple: *in vivo*.

Figure 5). The accumulation of GB has been proposed as a bacterial osmo-protective mechanism⁶⁵, and to be important in *P. aeruginosa* infection in mice⁷⁷. Additionally, our 2D co-culture model captured the reduced levels of motility- and chemotaxis-related genes that are observed *in vivo* compared to pure bacterial cultures (Figure 6E-F, Supplementary Figure 5), which is another important aspect for biofilm formation.

DISCUSSION

In this study, we describe a novel *P. aeruginosa* co-culture system using 2D human airway organoids derived from healthy and CF individuals. Subjecting the co-culture to dual RNA-seq allowed us to gain insight into how both components interact with, and respond to each other, focusing on the role of QS molecules and downstream signaling. Finally, we benchmarked our findings with a cohort of publicly available RNA-seq datasets from clinical samples of *P. aeruginosa* infected airways. Our co-culture model recapitulates metabolic aspects, CCR and nitrogen usage, as well as the expression of several secretion systems, important for *P. aeruginosa* persistence and virulence. Furthermore, the upregulation of genes involved in *P. aeruginosa* antibiotic resistance could be of particular relevance for research of bacterial mechanisms of antibiotic resistance and discovery of novel antibacterial compounds. This is highly relevant in the case of *P. aeruginosa* due to its high intrinsic resistance¹¹. Since it is not possible to study early stages of infection using clinical isolates, our model offers a tool to understand the initial steps of the infectious process in near-physiological conditions.

Previous attempts to co-culture *P. aeruginosa* in 2D have been performed using cancer cell lines^{32–36,78,79} or primary human airway cultures^{34,37}. The latter offers clear advantages over the former, because of the non-cancerous nature of the primary cultures. Human airway organoids allow for the indefinite biomass expansion and thus for longitudinal experiments using a defined and constant organoid source. Additionally, the indefinite expansion of airway organoids will enable *P. aeruginosa* co-culture with genetically engineered organoid lines and isogenic WT controls, once genome editing of airway organoids becomes efficient enough to perform experiments at this scale⁸⁰. This will open

the door to understanding which epithelial factors shape the course of *P. aeruginosa* infection and how to harness them to fight the infection.

In this dataset, we do not observe a major organoid response specific to QS pathways. Using live co-cultures could lead to lower effective concentrations of QS-induced molecules, compared to what has been used in studies testing the effect of single QS compounds on epithelial cells^{81,82}. In addition, the strong LPS-induced inflammation, present in all conditions, might abrogate the effect of QS-derived molecules. Particularly, LPS is not accounted for in studies that solely focus on QS-derived molecules. Additionally, it is likely that only specific cell types respond to QS molecules, i.e. chemosensory tuft cells^{83,84}, and therefore bulk RNAseq would not allow the study of these cell-specific effects.

Future expansion of the co-culture infection models, with the addition of immune cells, will yield insight into how this important aspect affects the behavior of the *P. aeruginosa* infections. Importantly, co-culture models that recapitulate a more complex tissue architecture⁸⁵ will also help to understand biofilm formation under more physiological conditions. Furthermore, QS pathways coordinate the population-scale behavior of individual bacteria, which leads to the functional and spatial heterogeneity found in bacterial biofilms. The recent application of spatial transcriptomics to *P. aeruginosa* biofilms grown on solid surfaces have allowed detailed study of these two aspects^{86,87}. It will be very interesting to address this spatial and functional heterogeneity in the presence of the epithelial and immune cells using co-cultures. Furthermore, our 14-hour co-culture system represents an early stage of the infectious process. While this time span allows studying QS regulation, it is too short to focus on biofilm development and other aspects of chronic infections. Longer incubation using our method was technically challenging due epithelial damage caused by the bacterial cells. Developing co-culture strategies that enable sustained chronic infection of the mucosa will help to investigate these aspects of later infection stages.

In conclusion, 2D organoid co-cultures with *P. aeruginosa* represent a new development of the current methods to study host-bacterium interplay. The system recapitulates major infection traits from both bacteria and epithelium, including bacterial metabolism, expression of virulence factors and the induction of an inflammatory response in the epithelium.

ACKNOWLEDGEMENTS

We acknowledge the Utrecht Sequencing Facility (USEQ) for providing sequencing service and data. USEQ is subsidized by the University Medical Center Utrecht and The Netherlands X-omics Initiative (NWO project 184.034.019). We would also like to thank Dr. Tim Holm Jakobsen for kindly providing PAO1-GFP strain, Dr. Bart Bardoel for kindly providing *E. coli* RHO3 strain, and Joe J. Harrison for kindly providing the pEX18Gm plasmid.

CONFLICT OF INTEREST

H.C. is inventor on several patents related to organoid technology; his full disclosure is given at <https://www.uu.nl/staff/JCClevers/>. H.C. became head of Pharma, Research and Early Development of F. Hoffmann-La Roche Ltd, Basel, Switzerland.

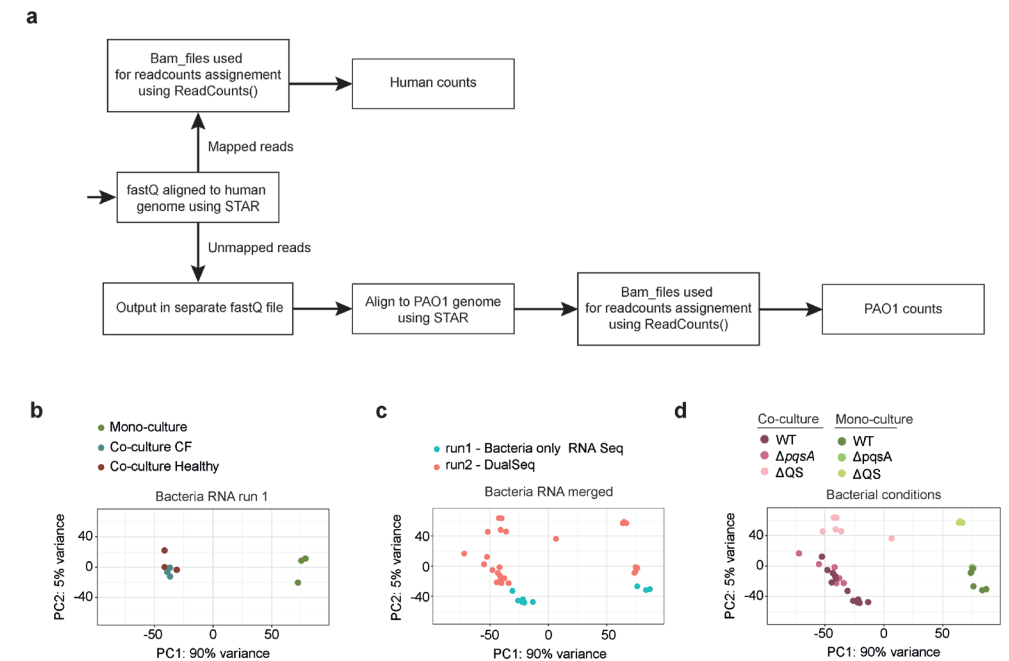
REFERENCES

- Malhotra, S., Hayes, D. & Wozniak, D. J. Cystic fibrosis and pseudomonas aeruginosa: The host-microbe interface. *Clin. Microbiol. Rev.* 32, 1–46 (2019).
- Quinton, P. M. Cystic fibrosis: impaired bicarbonate secretion and mucoviscidosis. *Lancet* 372, 415–417 (2008).
- Kunzelmann, K., Schreiber, R. & Hadorn, H. B. Bicarbonate in cystic fibrosis. *J. Cyst. Fibros.* 16, 653–662 (2017).
- Forbes, E. & Abu-Sbaih, R. Cystic fibrosis. *Nat. Rev. Dis. Prim.* (2015) doi:10.1038/nrdp.2015.49.
- De Boeck, K. Cystic fibrosis in the year 2020: A disease with a new face. *Acta Paediatr. Int. J. Paediatr.* 109, 893–899 (2020).
- Rossi, E. et al. *Pseudomonas aeruginosa* adaptation and evolution in patients with cystic fibrosis. *Nat. Rev. Microbiol.* 19, (2021).
- LiPuma, J. J. The changing microbial epidemiology in cystic fibrosis. *Clin. Microbiol. Rev.* 23, 299–323 (2010).
- Fischer, A. J. et al. Sustained Coinfections with *Staphylococcus aureus* and *Pseudomonas aeruginosa* in Cystic Fibrosis. *Am. J. Respir. Crit. Care Med.* 203, 328–338 (2021).
- Foundation, C. F. Cystic Fibrosis Foundation Patient Registry, 2021 Annual Data Report. *Cyst. Fibros. Found. Publ.* (2022).
- Parkins, M. D., Somayaji, R. & Waters, V. J. Epidemiology, biology, and impact of clonal *pseudomonas aeruginosa* infections in cystic fibrosis. *Clin. Microbiol. Rev.* 31, (2018).
- Botelho, J., Grosso, F. & Peixe, L. Antibiotic resistance in *Pseudomonas aeruginosa* – Mechanisms, epidemiology and evolution. *Drug Resist. Updat.* 44, 100640 (2019).
- Bassler, B. L. & Losick, R. Bacterially Speaking. *Cell* 125, 237–246 (2006).
- Whitehead, N. A., Barnard, A. M. L., Slater, H., Simpson, N. J. L. & Salmond, G. P. C. Quorum-sensing in Gram-negative bacteria. *FEMS Microbiol. Lett.* 25, 365–404 (2001).
- Lee, J. & Zhang, L. The hierarchy quorum sensing network in *Pseudomonas aeruginosa*. *Protein Cell* 6, 26–41 (2014).
- Hentzer, M. et al. Attenuation of *Pseudomonas aeruginosa* virulence by quorum sensing inhibitors. *EMBO J.* 22, 3803–3815 (2003).
- SINGH, V. K. et al. Tackling Recalcitrant *Pseudomonas aeruginosa* Infections In Critical Illness via Anti-virulence Monotherapy. *Nat. Commun.* 13, (2022).
- Tang, H. et al. Epigallocatechin-3-Gallate Ameliorates Acute Lung Damage by Inhibiting Quorum-Sensing-Related Virulence Factors of *Pseudomonas aeruginosa*. *Front. Microbiol.* 13, (2022).
- Azimi, S., Klementiev, A. D., Whiteley, M. & Diggle, S. P. Bacterial Quorum Sensing During Infection. 201–219 (2020).
- Cornforth, D. M. et al. *Pseudomonas aeruginosa* transcriptome during human infection. *Proc. Natl. Acad. Sci. U. S. A.* 115, (2018).
- Marvig, R. L., Sommer, L. M., Molin, S. & Johansen, H. K. Convergent evolution and adaptation of *Pseudomonas aeruginosa* within patients with cystic fibrosis. *Nat. Genet.* 47, 57–64 (2015).
- Smith, E. E. et al. Genetic adaptation by *Pseudomonas aeruginosa* to the airways of cystic fibrosis patients. *Proc. Natl. Acad. Sci. U. S. A.* 103, 8487–8492 (2006).
- Turner, K. H., Wessel, A. K., Palmer, G. C., Murray, J. L. & Whiteley, M. Essential genome of *Pseudomonas aeruginosa* in cystic fibrosis sputum. *Proc. Natl. Acad. Sci.* 112, 4110–4115 (2015).
- Gannon, A. D. & Darch, S. E. Tools for the Real-Time Assessment of a *Pseudomonas aeruginosa* Infection Model. *J. Vis. Exp.* 1–17 (2021) doi:10.3791/62420.
- Tata, M. et al. RNAseq based transcriptional profiling of *Pseudomonas aeruginosa* PA14 after short and long-term anoxic cultivation in synthetic cystic fibrosis sputum medium. *PLoS One* 11, 1–18 (2016).
- Palmer, K. L., Aye, L. M. & Whiteley, M. Nutritional cues control *Pseudomonas aeruginosa* multicellular behavior in cystic fibrosis sputum. *J. Bacteriol.* 189, 8079–8087 (2007).
- Fung, C. et al. Gene expression of *Pseudomonas aeruginosa* in a mucin-containing synthetic growth medium mimicking cystic fibrosis lung sputum. *J. Med. Microbiol.* 59, 1089–1100 (2010).

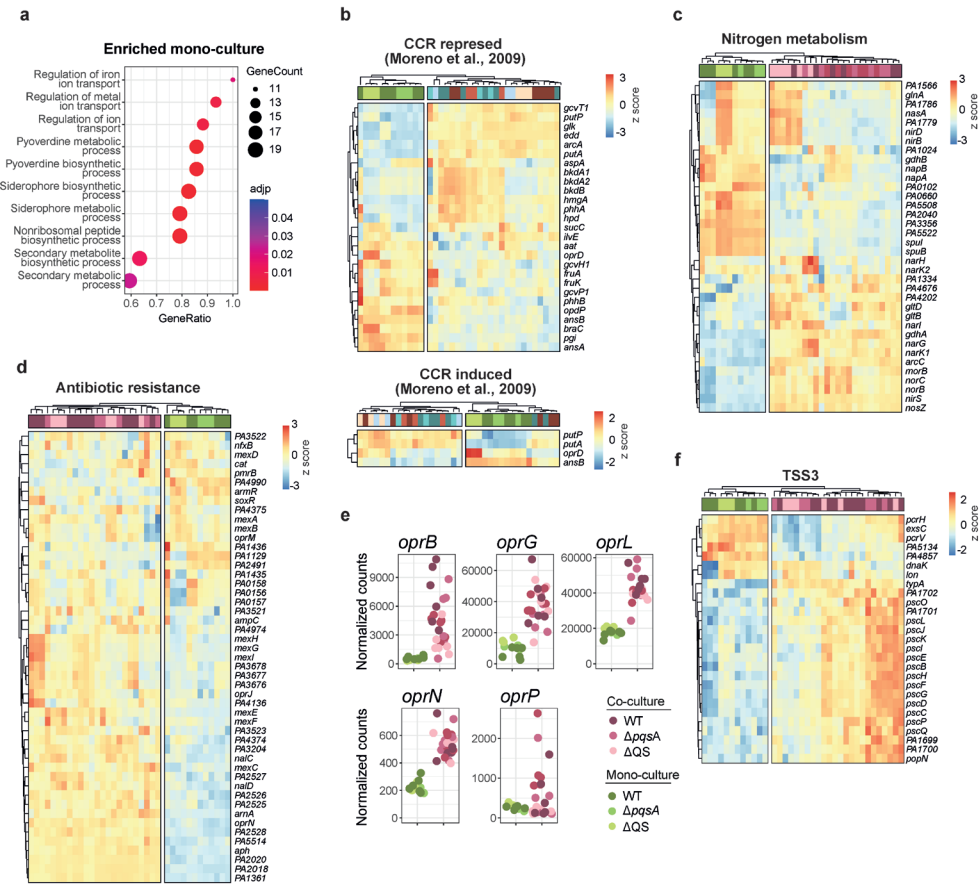
27. Rosen, B. H. et al. Animal and Model Systems for Studying Cystic Fibrosis. *J. Cyst. Fibros.* 17, S28–S34 (2018).
28. O'Toole, G. A. et al. Model Systems to Study the Chronic, Polymicrobial Infections in Cystic Fibrosis: Current Approaches and Exploring Future Directions. *MBio* 12, 1–8 (2021).
29. McCarron, A., Donnelley, M. & Parsons, D. Airway disease phenotypes in animal models of cystic fibrosis. *Respir. Res.* 19, 1–12 (2018).
30. Harrington, N. E. et al. Antibiotic efficacy testing in an Ex vivo model of pseudomonas aeruginosa and staphylococcus aureus biofilms in the cystic fibrosis lung. *J. Vis. Exp.* 2021, 1–16 (2021).
31. Harrington, N. E., Littler, J. L. & Harrison, F. Transcriptome Analysis of Pseudomonas aeruginosa Biofilm Infection in an Ex Vivo Pig Model of the Cystic Fibrosis Lung. *Appl. Environ. Microbiol.* 88, (2022).
32. Joseph, T., Look, D. & Ferkol, T. NF- κ B activation and sustained IL-8 gene expression in primary cultures of cystic fibrosis airway epithelial cells stimulated with Pseudomonas aeruginosa. *Am. J. Physiol. - Lung Cell. Mol. Physiol.* 288, 471–479 (2005).
33. Balloy, V. et al. Bronchial epithelial cells from cystic fibrosis patients express a specific long non-coding RNA signature upon Pseudomonas aeruginosa infection. *Front. Cell. Infect. Microbiol.* 7, 1–9 (2017).
34. Tang, M. et al. Evaluating Bacterial Pathogenesis Using a Model of Human Airway Organoids Infected with Pseudomonas aeruginosa Biofilms. *Microbiol. Spectr.* (2022).
35. Frisk, A. et al. Transcriptome analysis of Pseudomonas aeruginosa after interaction with human airway epithelial cells. *Infect. Immun.* 72, 5433–5438 (2004).
36. Zulianello, L. et al. Rhamnolipids are virulence factors that promote early infiltration of primary human airway epithelia by Pseudomonas aeruginosa. *Infect. Immun.* 74, 3134–3147 (2006).
37. Tseng, J., Do, J., Widdicombe, J. H. & Machen, T. E. Innate immune responses of human tracheal epithelium to Pseudomonas aeruginosa flagellin, TNF- α , and IL-1 β . *Am. J. Physiol. - Cell Physiol.* 290, 678–690 (2006).
38. Laucirica, D. R., Garratt, L. W. & Kicic, A. Progress in Model Systems of Cystic Fibrosis Mucosal Inflammation to Understand Aberrant Neutrophil Activity. *Front. Immunol.* 11, 1–12 (2020).
39. Sachs, N. et al. Long-term expanding human airway organoids for disease modeling. *EMBO J.* 38, 1–20 (2019).
40. Dekkers, J. F. et al. A functional CFTR assay using primary cystic fibrosis intestinal organoids. *Nat. Med.* 19, 939–945 (2013).
41. Pleguezuelos-Manzano, C. et al. Establishment and Culture of Human Intestinal Organoids Derived from Adult Stem Cells. *Curr. Protoc. Immunol.* 130, (2020).
42. Puschhof, J. et al. Intestinal organoid cocultures with microbes. *Nat. Protoc.* 16, 4633–4649 (2021).
43. Westermann, A. J. & Vogel, J. Host-pathogen transcriptomics by dual RNA-seq. *Methods Mol. Biol.* 1737, 59–75 (2018).
44. Beenker, W. A. G., Hoeksma, J., Bannier-Hélaouët, M., Clevers, H. & den Hertog, J. Paecilomyces inhibits quorum sensing in Gram-negative bacteria. *BioRxiv* (2022).
45. Hmelo, L. R. et al. Precision-engineering the Pseudomonas aeruginosa genome with two-step allelic exchange. *Nat. Protoc.* 10, 1820–1841 (2015).
46. Amatngalim, G. D. et al. Measuring cystic fibrosis drug responses in organoids derived from 2D differentiated nasal epithelia. *Life Sci. Alliance* 5, 1–14 (2022).
47. Aprianto, R., Slager, J., Holsappel, S. & Veening, J. W. Time-resolved dual RNA-seq reveals extensive rewiring of lung epithelial and pneumococcal transcriptomes during early infection. *Genome Biol.* 17, 1–16 (2016).
48. Dobin, A. et al. STAR: Ultrafast universal RNA-seq aligner. *Bioinformatics* 29, 15–21 (2013).
49. Liao, Y., Smyth, G. K. & Shi, W. FeatureCounts: An efficient general purpose program for assigning sequence reads to genomic features. *Bioinformatics* 30, 923–930 (2014).
50. Stover, C. K. et al. Complete genome sequence of Pseudomonas aeruginosa PAO1, an opportunistic pathogen. *Nature* 406, 959–964 (2000).
51. Schoch, C. L. et al. NCBI Taxonomy: A comprehensive update on curation, resources and tools. *Database* 2020, 1–21 (2020).
52. Love, M. I., Huber, W. & Anders, S. Moderated estimation of fold change and dispersion for RNA-seq data with DESeq2. *Genome Biol.* 15, 1–21 (2014).
53. Blighe, K., Rana, S. & Lewis, M. EnhancedVolcano: Publication-ready volcano plots with enhanced colouring and labeling. <https://github.com/kevinblighe/EnhancedVolcano> (2018).
54. Yu, G., Wang, L. G., Han, Y. & He, Q. Y. ClusterProfiler: An R package for comparing biological themes among gene clusters. *Omi. A J. Integr. Biol.* 16, 284–287 (2012).
55. Winsor, G. L. et al. Enhanced annotations and features for comparing thousands of Pseudomonas genomes in the Pseudomonas genome database. *Nucleic Acids Res.* 44, 646–653 (2016).
56. Szklarczyk, D. et al. STRING v11: Protein-protein association networks with increased coverage, supporting functional discovery in genome-wide experimental datasets. *Nucleic Acids Res.* 47, D607–D613 (2019).
57. Moura-Alves, P. et al. Host monitoring of quorum sensing during Pseudomonas aeruginosa infection. *Science (80-.)*. 366, (2019).
58. Hughes, D. T. & Sperandio, V. Interkingdom signalling: communication between bacteria and their hosts. *Nat. Rev. Microbiol.* 6, 111–120 (2008).
59. Kendall, M. M. & Sperandio, V. What a dinner party! Mechanisms and functions of interkingdom signaling in host-pathogen associations. *MBio* 7, 1–14 (2016).
60. Vasil, M. L. & Ochsner, U. A. The response of Pseudomonas aeruginosa to iron: genetics, biochemistry and virulence. *Mol. Microbiol.* 34, 399–413 (1999).
61. Bharwad, K. & Rajkumar, S. Rewiring the functional complexity between Crc, Hfq and sRNAs to regulate carbon catabolite repression in Pseudomonas. *World J. Microbiol. Biotechnol.* 35, 1–12 (2019).
62. Rojo, F. Carbon catabolite repression in Pseudomonas: Optimizing metabolic versatility and interactions with the environment. *FEMS Microbiol. Rev.* 34, 658–684 (2010).
63. Line, L. et al. Physiological levels of nitrate support anoxic growth by denitrification of Pseudomonas aeruginosa at growth rates reported in cystic fibrosis lungs and sputum. *Front. Microbiol.* 5, 1–11 (2014).
64. Palmer, K. L., Brown, S. A. & Whiteley, M. Membrane-bound nitrate reductase is required for anaerobic growth in cystic fibrosis sputum. *J. Bacteriol.* 189, 4449–4455 (2007).
65. Rossi, E., Falcone, M., Molin, S. & Johansen, H. K. High-resolution in situ transcriptomics of Pseudomonas aeruginosa unveils genotype independent patho-phenotypes in cystic fibrosis lungs. *Nat. Commun.* 9, 1–13 (2018).
66. Hauser, A. R. The Type III Secretion System of Pseudomonas aeruginosa: Infection by Injection. *Nat. Rev. Microbiol.* 7, 654–665 (2009).
67. Hernandez, R. E., Gallegos-Monterrosa, R. & Coulthurst, S. J. Type VI secretion system effector proteins: Effective weapons for bacterial competitiveness. *Cell. Microbiol.* 22, 1–9 (2020).
68. Chen, L., Zou, Y., She, P. & Wu, Y. Composition, function, and regulation of T6SS in Pseudomonas aeruginosa. *Microbiol. Res.* 172, 19–25 (2015).
69. Sana, T. G., Berni, B. & Bleves, S. The T6SSs of Pseudomonas aeruginosa strain pao1 and their effectors: Beyond bacterial-cell targeting. *Front. Cell. Infect. Microbiol.* 6, (2016).
70. Sana, T. G. et al. The second type VI secretion system of Pseudomonas aeruginosa strain PAO1 is regulated by quorum sensing and fur and modulates internalization in epithelial cells. *J. Biol. Chem.* 287, 27095–27105 (2012).
71. Gifford, A. H. et al. Use of a multiplex transcript method for analysis of Pseudomonas aeruginosa gene expression profiles in the cystic fibrosis lung. *Infect. Immun.* 84, 2995–3006 (2016).
72. Bundy, B. M., Campbell, A. L. & Neidle, E. L. Similarities between the antABC-encoded anthranilate dioxygenase and the benABC-encoded benzoate dioxygenase of Acinetobacter sp. strain ADP1. *J. Bacteriol.* 180, 4466–4474 (1998).
73. Thomas, S. R., Anjana, R., Hodson, M. E. & Pitt, T. L. Increased sputum amino acid concentrations and auxotrophy of Pseudomonas aeruginosa in severe cystic fibrosis lung disease. *Thorax* 55, 795–797 (2000).

74. Huang, H. *et al.* An integrated genomic regulatory network of virulence-related transcriptional factors in *Pseudomonas aeruginosa*. *Nat. Commun.* 10, (2019).
75. Wilton, M., Halverson, T. W. R., Charron-Mazenod, L., Parkins, M. D. & Lewenza, S. Secreted phosphatase and deoxyribonuclease are required by *Pseudomonas aeruginosa* to defend against neutrophil extracellular traps. *Infect. Immun.* 86, 1–12 (2018).
76. Kordes, A. *et al.* Genetically diverse *Pseudomonas aeruginosa* populations display similar transcriptomic profiles in a cystic fibrosis explanted lung. *Nat. Commun.* 10, (2019).
77. Wargo, M. J. Choline Catabolism to Glycine Betaine Contributes to *Pseudomonas aeruginosa* Survival during Murine Lung Infection. *PLoS One* 8, 1–7 (2013).
78. Randell, S. H., Fulcher, M. L., O’Neal, W. & Olsen, J. C. Primary epithelial cell models for cystic fibrosis research. *Methods Mol. Biol.* 742, 285–310 (2011).
79. Liu, Y. C. *et al.* Contribution of the Alkylquinolone Quorum-Sensing System to the Interaction of *Pseudomonas aeruginosa* With Bronchial Epithelial Cells. *Front. Microbiol.* 9, (2018).
80. Geurts, M. H. & Clevers, H. CRISPR engineering in organoids for gene repair and disease modelling. *Nat. Rev. Bioeng.* 1, 32–45 (2023).
81. Moura-Alves, P. *et al.* Host monitoring of quorum sensing during *Pseudomonas aeruginosa* infection. *Science (80-.).* 366, (2019).
82. Moura-Alves, P. *et al.* AhR sensing of bacterial pigments regulates antibacterial defence. *Nature* 512, 387–392 (2014).
83. Nadjisombati, M. S. *et al.* Detection of Succinate by Intestinal Tuft Cells Triggers a Type 2 Innate Immune Circuit. *Immunity* 49, 33–41.e7 (2018).
84. Tizzano, M. *et al.* Nasal chemosensory cells use bitter taste signaling to detect irritants and bacterial signals. *Proc. Natl. Acad. Sci. U. S. A.* 107, 3210–3215 (2010).
85. Rossy, T. *et al.* *Pseudomonas aeruginosa* contracts mucus to rapidly form biofilms in tissue-engineered human airways. *bioRxiv* 2, 2022.05.26.493615 (2022).
86. Dar, D., Dar, N., Cai, L. & Newman, D. K. Spatial transcriptomics of planktonic and sessile bacterial populations at single-cell resolution. *Science (80-.).* 373, (2021).
87. Shi, H. *et al.* Highly multiplexed spatial mapping of microbial communities. *Nature* 588, 676–681 (2020).
88. Moreno, R., Martínez-Gomariz, M., Yuste, L., Gil, C. & Rojo, F. The *Pseudomonas putida* Crc global regulator controls the hierarchical assimilation of amino acids in a complete medium: Evidence from proteomic and genomic analyses. *Proteomics* 9, 2910–2928 (2009).

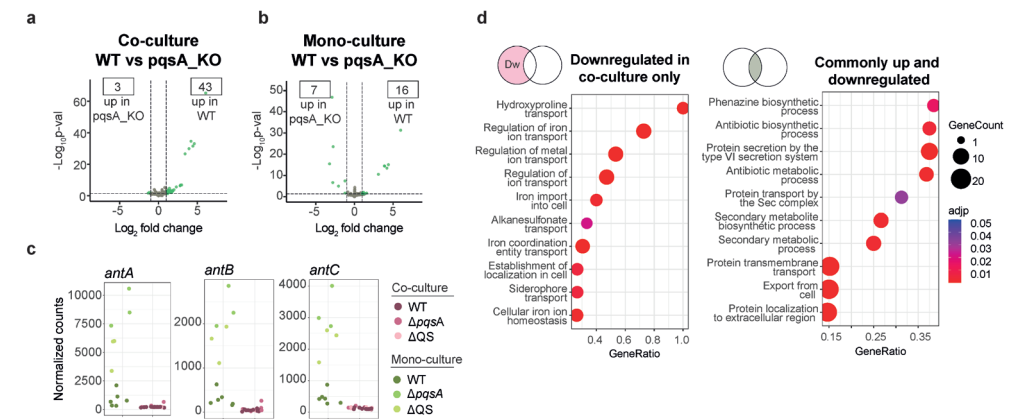
SUPPLEMENTARY DATA



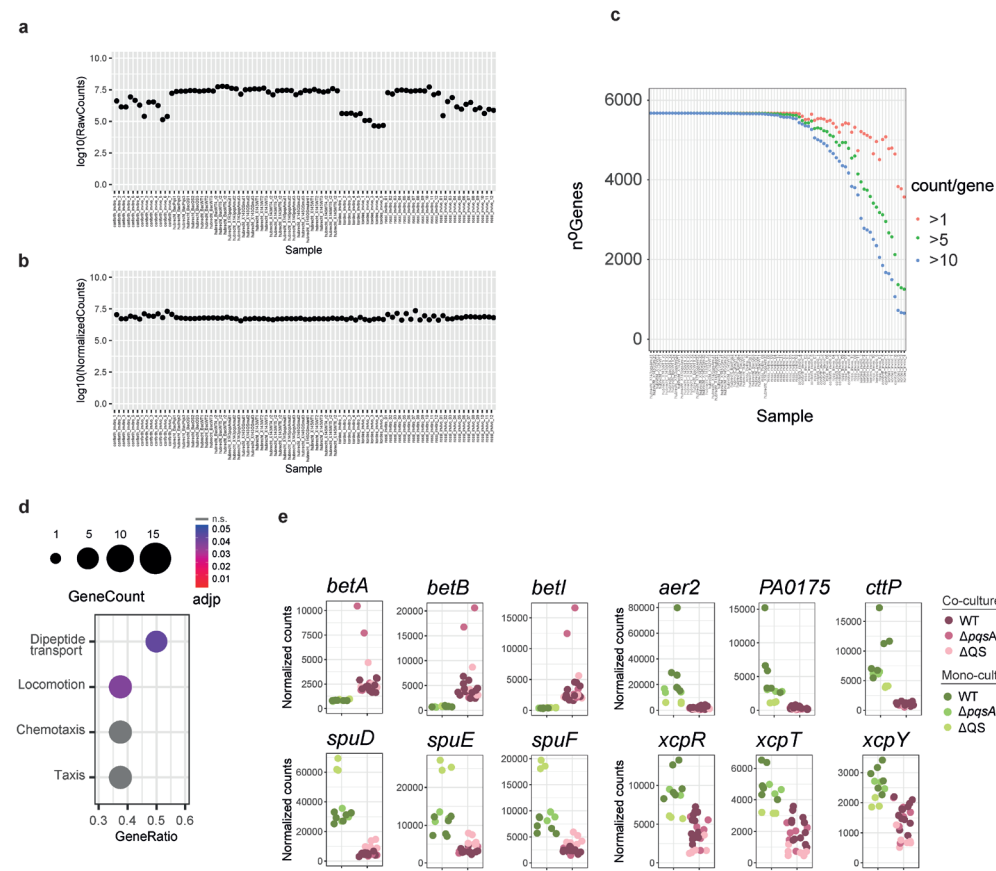
Supplementary figure 1. Mapping strategy and PAO1 bulk dataset integration. **a**, Mapping and count assignment strategy. **b**, PCA plot of PAO1-only bulk RNA samples from run 1. **c**, PCA plot showing samples by run (PAO1-only bulk RNA-seq or Dual RNA-seq). **d**, PCA plot of the integrated dataset color-coded by culture type and PAO1 genotype.



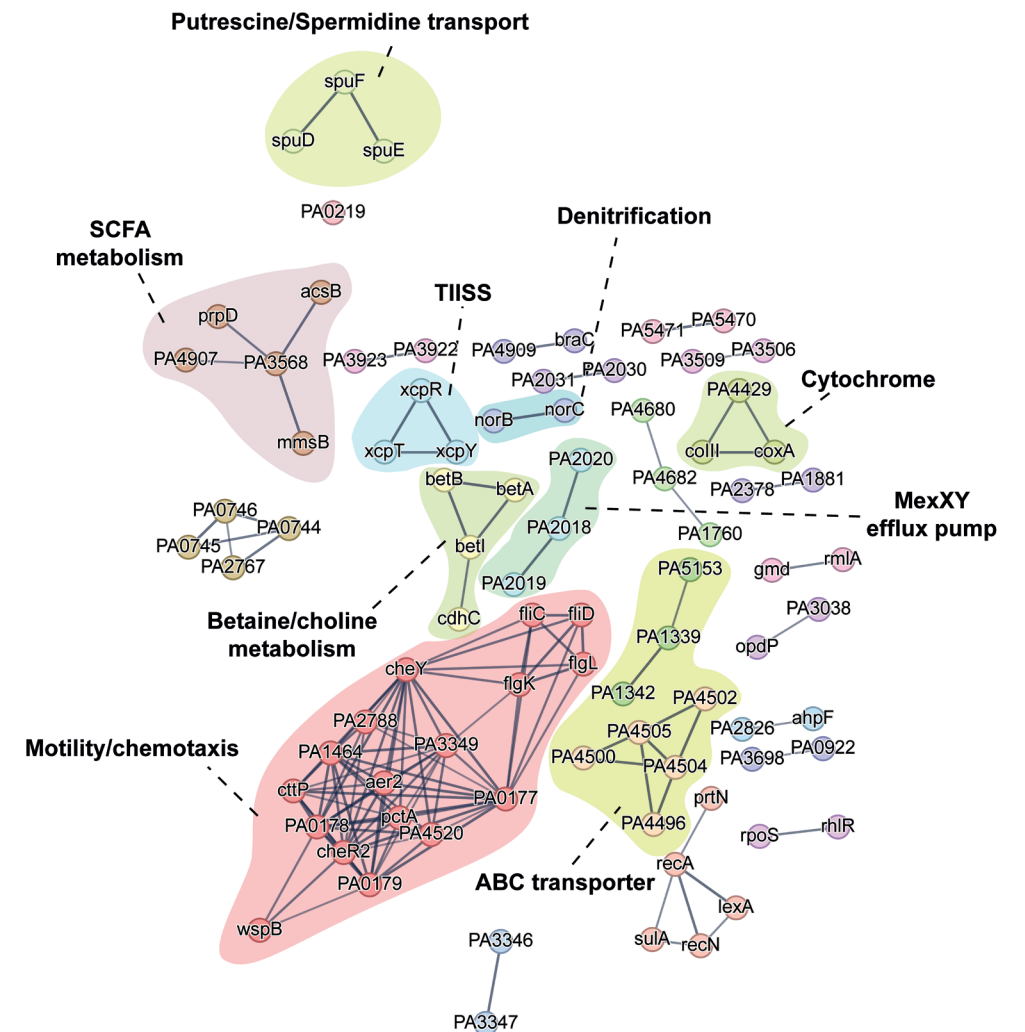
Supplementary figure 2. Extended transcriptional response of PAO1 to the presence of airway epithelium. **a**, Gene ontology enrichment analysis showing top 10 categories enriched in PAO1 mono-culture **b**, Expression heat map of genes regulated by the Carbon catabolite repression (CCR) pathway in the related bacterium *Pseudomonas putida* (Moreno et al., 2009⁸⁸). **c**, Expression heat map of genes from the KEGG pathway nitrogen metabolism (pae00910). **d**, Expression heat map of genes known to confer antibiotic resistance to *P. aeruginosa*. **e**, Normalized count plots of DEGs encoding *P. aeruginosa* porins. **f**, Expression heat map of T3SS genes (GO:0030254).



Supplementary figure 3. Extended effects of the epithelium on PAO1 QS regulation. **a**, Volcano plot displaying gene \log_2 fold change and $-\log_{10}$ adjusted p-value when comparing the transcriptomes of WT to $\Delta pq s A$ PAO1 in co-culture. **b**, Volcano plot displaying gene \log_2 fold change and $-\log_{10}$ adjusted p-value when comparing the transcriptomes of WT to $\Delta pq s A$ PAO1 in mono-culture. **c**, Normalized count plots of genes from the anthranilic acid metabolic pathway. **d**, Gene ontology enrichment analysis showing top 10 categories enriched in genes that are specifically downregulated in co-culture in WT and $\Delta pq s A$ PAO1 transcriptomes compared to ΔQS (left) or those that are common to both (right, up and downregulated).



Supplementary figure 4. Cohort integration quality control. **a**, \log_{10} of total raw counts per sample before DESeq2 normalization. **b**, \log_{10} of normalized counts per sample after DESeq2 normalization. **c**, Number of genes with more than 1 (red), 5 (green) or 10 (blue) counts per sample. **d**, Gene ontology enrichment analysis showing categories enriched in top common DEGs from co-culture and *in vivo* samples. **e**, Normalized count plots of genes from Figure 6 f, performing the analysis only in the samples from our cohort, to exclude bias in the results due to the integration process with the extra datasets.



Supplementary figure 5. Extended protein-protein network results. Protein-protein interaction network of common DEGs (*in vivo* and co-culture). Each node represents a protein encoded by DEG. Individual gene names are highlighted over the nodes. Edges represent known protein-protein association (either physical or functional) with a confidence level higher than 0.7. Node color represent clusters generated MCL method. Highlighted the pathway to which the cluster proteins belong.

Supplementary table 1. Primers used.

Primer name	Primer sequence
<i>lasI</i> .UP.Fw	GCCAGTGCCAAGCTTGCATGCGAGGCCAACCGTTTCATG
<i>lasI</i> .UP.Rv	GCTGTTCCACCAGTACGATCATCTTCACTTCCTCCAA
<i>lasI</i> .DN.Fw	GAAGATGATCGTACTGGTGGAACAGCGACTGG
<i>lasI</i> .DN.Rv	CATGATTACGAATTCGAGCTTTCCTGCCCTGGATAGAAC
<i>lasI</i> .seq.Fw	GCTCGGAAGCCAATGTGAACTT
<i>lasI</i> .seq.Rv	AACTGGAACGCCTCAGCCAG
<i>rhII</i> .UP.Fw	CATGATTACGAATTCGAGCTCGACCAGCAGAACATCTC
<i>rhII</i> .UP.Rv	TGAAGCTAATTCGATCATGCATGAGCTCCAGCGATTGAGAGCAA
<i>rhII</i> .DN.Fw	ATCCCAATTCGATCGTCCGGCTACCACCCGGAATGGCT
<i>rhII</i> .DN.Rv	GCCAGTGCCAAGCTTGCATGCCAGGTTGATCGAGATGC
<i>rhII</i> .seq.Fw	ATGTCCTCCGACTGAGAGGG
<i>rhII</i> .seq.Rv	CAGAGAGACTACGCAAGTCGG

Supplementary table 2. Plasmids used.

	Use	Reference
pEX18Gm	Backbone plasmid used for the generation of deletion constructs	Hmelo (2015) ⁴⁵
pEX18Gm:: Δ <i>lasI</i>	Plasmid containing <i>lasI</i> deletion construct for use in PAO1	This study
pEX18Gm:: Δ <i>rhII</i>	Plasmid containing <i>rhII</i> deletion construct for use in PAO1	This study

8

SUMMARIZING DISCUSSION

INTRODUCTION

The advent of adult stem cell (ASC)-derived organoids during the last decade has revolutionized the way biologists study the epithelium. Today, organoids are one of the main tools used to study stem cell biology, tissue homeostasis, regenerative medicine, and cancer biology. Additionally, ASC-derived organoids have the potential to replace animal models as an essential part in the drug-testing platform in the future. A powerful characteristic of ASC-derived organoids is that they enable reductionistic experimentation as they solely contain epithelial cells. This reductionist approach enabled by organoids has been at the base of the work presented in this thesis.

The simplicity of organoids is in stark contrast with the complexity of the human gut microbiota. More than 10^{13} bacteria inhabit our gut, outnumbering our own somatic cells¹. Collectively, the microbiota encodes numerous genes, constituting a versatile metabolic machinery. Understanding which (group of) bacteria or bacterial metabolites are responsible for the development of gastrointestinal diseases, like inflammatory bowel disease (IBD) or colorectal cancer (CRC), is one of the main challenges today. The emergence of metagenomics has shed light on which species and metabolites are enriched in CRC patients. However, these associations do not prove whether these microbes cause the disease(s). Therefore, the main focus of this thesis has been to investigate mechanisms by which bacteria drive CRC, making use of organoid-bacteria co-cultures, following a reductionist approach.

Chapter 1 aims to describe bacteria recurrently associated with CRC development in previous metagenomic studies. Additionally, it highlights the existing knowledge of how these bacteria may contribute to CRC. However, the interspecies differences and the limited physiological relevance of cancer cell lines are major limitations of these approaches. Therefore, establishing human intestinal organoid co-cultures with a single bacteria strain, in combination with isogenic knock outs for the gene of interest, offers a unique opportunity to study the contribution of specific microbial factors. Thus, **Chapter 2** describes previous attempts to establish intestinal organoid and organ-on-a-chip co-cultures with bacteria, giving a perspective on the biological aspects best captured by the different co-culture platforms. This chapter is not restricted to the study of bacterial contribution to CRC tumorigenesis, but includes research covering the microbial contribution to gut health and other infectious diseases. A brief outline on the methodology used for organoid culture is given in **Chapter 3**. Additionally, the methodology that we developed to perform 3D organoid co-cultures with single bacterial strains is described in **Chapter 4**, including details on common downstream co-culture characterization techniques.

PKS⁺ E. COLI INDUCE MUTATIONS IN COLORECTAL CANCER

One bacteria strain associated with CRC is *pkS⁺ E. coli*, which produce the genotoxin colibactin². Using intestinal organoid-bacteria co-cultures, in **Chapter 5** we were able to

identify colibactin-specific mutational signatures (SBS88 for single based substitutions and ID18 for short insertions and deletions) caused by the bacteria in organoids. Besides, this mutational signature was enriched in a subset of CRC samples, indicating that in those patients *pks*⁺ *E. coli* induced mutations in colonocytes that eventually gave rise to a colorectal tumor. Independent observations were made reaching the same conclusions^{3,4}. Importantly, *APC* mutations -a main driver of CRC- could be caused by colibactin, although to date direct experimental evidence is still missing.

This discovery led to new questions, many remaining unanswered to date. Are all *pks*⁺ bacteria equally genotoxic? Is it safe to use *pks*⁺ probiotics? When in life are we most vulnerable to the mutagenic effect of *pks*⁺ bacteria? What intrinsic (genetic predisposition, chronic inflammation) and/or extrinsic (antibiotics intake, diet, life style) factors could affect this susceptibility? Could the presence of *pks*⁺ bacteria in fecal samples be used in a clinical setup to identify individuals at risk of developing CRC? Could *pks*⁺ bacteria be the cause of the increasing early-onset CRC trend? Are there other genotoxic gut microbes?

Chapter 6 focuses on the first two of these questions. *E. coli* Nissle 1917 is a *pks*⁺ strain widely used as a probiotic to treat intestinal inflammatory diseases⁵. Hence, we assessed its mutagenic activity by long-term co-cultures with intestinal organoids and subsequent whole genome sequencing. By developing a novel analytical framework based on the characteristic adenine enrichment of colibactin-induced mutations, we observed that despite its reduced mutagenic activity, Nissle 1917 can induce mutations in human healthy intestinal organoids. This finding suggests that other factors might contribute to the differential regulation of *pks*-induced mutagenicity observed across strains. These might relate to heterogeneous production levels of colibactin itself, or in contrast, by the ability of *pks*⁺ *E. coli* to perform other processes relevant for colibactin ability to reach the epithelium and induce mutations. Nevertheless, our observation invites for a critical re-evaluation of the use of Nissle 1917 as probiotic. In the future, dedicated epidemiological studies should address if its use is appropriate and under which circumstances, considering the potential benefits for the patient and the possible side effects^{6,7}, including risk of CRC development.

To this end, it will be important to determine how age contributes to *pks*⁺ susceptibility. Evidence from mutational signature analyses of healthy colon⁸ and small intestine⁹ samples suggests that *pks*-induced mutations tend to occur during the first decade of life in most cases. The mucus layer is a physical and chemical barrier that protects the intestinal epithelium from the negative effect of the gut microbiota, while enabling our symbiotic relation with the microbes¹⁰⁻¹². At birth, our gut becomes colonized and it takes several years until the microbial community becomes stable¹³. Additionally, this microbial colonization contributes to the full maturation of the mucus layer¹². Thus, we can hypothesize that if *pks*⁺ bacteria penetrate the mucus layer and reach the gut epithelium at this stage, they might have increased possibilities to become one of the dominant members of the microbiota. Once established, their ability to reach the otherwise sterile

intestinal crypt and induce mutations might be increased. It is important to note that the mutations eventually leading to CRC can be induced many years before the onset of the disease, as mutations in cancer driver genes may occur decades before tumor development^{14,15}. If this hypothesis turns out to be correct, the use of Nissle 1917 in infants should be discouraged. Furthermore, prospective cohorts monitoring the composition of the microbiota, years before the onset of disease (CRC or IBD), might help to elucidate some aspects about the timing of *pks*⁺ bacterial infection in relation with the disease onset timing. Some of these prospective cohorts already exists¹⁶, although to date they have not been focused on CRC.

Additionally, colibactin-induced mutational signatures have been identified in IBD patients¹⁷, again posing the association-vs-causation problem. Could IBD progression be caused by the presence of *pks*⁺ bacteria? Or does the disease create an environment favoring this bacteria's growth? Despite being a multifactorial disease, IBD has a clear genetic component, as many single nucleotide polymorphisms (SNPs) are associated with the disease. Considering the latter, it is likely that other SNPs, even though not involved in IBD, might also enable *pks*⁺ bacteria to reach and deliver colibactin to the epithelial genome. Following this line of thought, it will be interesting to perform genome-wide association studies (GWAS), evaluating the link between the presence of colibactin-derived mutational signatures and the presence of SNPs at a populational level. This approach might identify SNPs in genes involved in immune defense against *pks*⁺ bacteria, like HLAs or immunoglobulins. Additionally, other important factors might be antibacterial peptides secreted by the epithelium or mucins and enzymes involved in the determination of their glycosylation patterns.

Besides, other extrinsic factors should be included when considering the susceptibility to *pks*⁺ *E. coli*. The use of antibiotics has been shown to have a dramatic effect on the composition of the human gut microbiota¹⁸, and in hospitals they are associated with antibiotic multi-resistant infections (AMR)¹⁹. Thus, this negative impact by antimicrobials might represent a colonization opportunity for *pks*⁺ bacteria. However, to date no evidence supporting this hypothesis. Additionally, a recent study has associated red meat consumption with an elevated CRC incidence in samples with high load of *pks*⁺ *E. coli*²⁰. However, the association with other life style factors, like tobacco smoking, is still unexplored.

Once we have an epidemiological overview on how these parameters (i.e., current/past exposure to *pks*⁺ bacteria, presence of intrinsic/extrinsic risk factors) affect the risk of developing CRC, we might be able to establish whether an individual is at higher risk of developing CRC. In turn, this could help developing early measures to decrease this risk by eliminating the bacteria, and/or to introduce closer monitoring of individuals at risk. Along the same lines, the rate of early-onset CRC has been increasing over the past decades in western countries²¹, although the reason for this is still unclear. Changes in the gut microbiota and the presence of pathogenic bacteria are among the common

suspects to be behind this trend. Thus, evaluating if CRC-associated bacteria are a contributing factor to early-onset disease is of high importance.

CRC AND BACTERIA: BEYOND *PKS*⁺ *E. COLI*

As mentioned earlier, the gut microbiota can be understood as an entity with an incommensurable potential to produce a vast array of metabolites, most of which remain unknown²². Thus, it is plausible that colibactin is not the only bacterial metabolite inducing mutations in the colonic epithelium. In fact, there are other microbial *pks* operons, producing metabolites with different properties and functions²³. Additionally, a recent publication has identified novel genotoxic bacteria isolated from the gut of IBD patients²⁴.

Beyond mutagenic bacteria, other microbes have been implicated in CRC tumorigenesis. As indicated in **Chapter 1**, Enterotoxigenic *Bacteroides fragilis* (ETBF), *Fusobacterium nucleatum*, bile-acid-producing *Clostridiales*, *Parvimonas micra*, (*Pepto*) *Streptococcus* sp., among others have been linked with CRC. As future associative studies refine the core CRC-associated bacterial signature and provide (additional) mechanistic insights, we will gain a better understanding on how to use this knowledge in future therapies. These treatment strategies could range from the development of small molecules inhibitors, targeting the ability of these pathogens to colonize the gut microbiota, to those directed towards the inhibition of their pathogenic feature e.g., the enzymatic production of colibactin or other toxins. Interestingly, another alternative could be the development of prophylactic and therapeutic oncomicrobial vaccines that would elicit cellular and humoral immune responses²⁵. Again, these could be directed against specific bacterial effectors, but also towards bacterial antigens presented by HLA molecules on tumor cells. Currently, only vaccines against oncoviruses (HPV) exist, none have been developed against oncomicrobes. Despite its appeal, oncomicrobe vaccination remains a futuristic approach and many technical and theoretical hurdles need to be overcome before making it a reality.

ORGANOID BACTERIA CO-CULTURES TO MODEL INFECTION: *P. AERUGINOSA* AND THE AIRWAY

Bacterial infections have historically been a major cause of death for humankind. Only during the 20th century, with the development of health care systems, vaccination, antibiotics becoming readily available, the mortality rate caused by bacteria has decreased. However, the number of AMR bacterial infection cases is increasing, while the development of new class antibiotics has been halted during the last decades²⁶. Quorum sensing (QS) is a signaling network that governs the collective behavior of bacteria during infection²⁷, leading to the formation of 3D structures or biofilms and the acquisition of extrinsic antibiotic resistance mechanisms. The presence of biofilms from several Gram-negative bacteria, and particularly of *P. aeruginosa*, is associated with chronic AMR infections in the airway of cystic fibrosis (CF) patients²⁸. Therefore,

targeting the QS network of *P. aeruginosa* to sensitize the bacteria to the effect of other antibiotics has become an appealing approach. However, to date, QS inhibitors are only used in pre-clinical stages²⁹. Thus, the characteristics of airway epithelium, CF disease and *P. aeruginosa* infections of the airway are summarized in **Chapter 7.1**. Additionally, the organoid-*P. aeruginosa* co-culture model described in **Chapter 7.2** offers a more physiologically relevant platform (compared to previous studies) to gain knowledge about the mechanistic role of *P. aeruginosa* QS regulation during infection. Our co-culture model recapitulates several *P. aeruginosa* QS-related processes that have been described previously in human infection: lower QS pathway level, reduced motility, utilization of denitrification pathway, as well as the upregulation of antibiotic efflux pumps and virulence factors like type 3 and 6 secretion systems. Thus, this platform might be useful in future research aiming to tackle the severity of *P. aeruginosa* infections in CF patients. Additionally, we believe that this co-culture system might offer an alternative pre-clinical test model for antibiotic discovery and prediction of clinical response³⁰.

OUTLOOK

Despite the advances brought by organoid-bacteria co-cultures, this model system is still at an early stage. Although organoid-bacteria co-culture systems have already shown exciting potential for biological discovery, we recognize that the current approach is low-throughput and technically challenging for its widespread use among the scientific community. In our view, devising strategies to upscale easy and reliable co-culture systems will be important. Advances in tissue engineering³¹ and microfluidic³² technologies in combination with automated microinjection devices³³ might enable this upscaling. Once the technology reaches this point, its combination with (unbiased) CRISPR and small molecule screens, as well as the development of drug screening platform will bring co-cultures to the next level. Hopefully, these advances will help understanding the role of bacteria in diseases like cancer, immune-related diseases like IBD, chronic obstructive pulmonary disease, autoimmunity, and allergies among others. Additionally, organoid-bacteria co-culture systems may serve as a platform for the discovery of new antibacterial and antiviral compounds and the understanding of infectious diseases.

Efficient incorporation of the immune cells to the co-culture system will be a crucial step, since immune system plays a key role shaping the microbiota status, as well as being a rely component in the development of the aforementioned diseases. Furthermore, organ-on-a-chip technologies already incorporate relevant factors like a more complex 3D structure, nutrient and oxygen gradients, and flow, as well as serving as a structural platform to assemble the different bacterial and host compartments. However, their implementation should be according with the idea of the reductionistic approach. Therefore, the experimental setting must be carefully designed in each case to address the research question efficiently.

CONCLUDING REMARKS

The work presented in this thesis explores the mechanisms by which bacteria cause disease by developing different organoid-bacteria co-cultures systems. The identification of *pks*-derived colibactin as a mutagen contributing to CRC is one of the main findings described in this work. Additionally, we describe the reduced, but detectable, ability of *pks*⁺ probiotics to induce mutations in healthy organoids. In this thesis, we also established an airway infection model with *P. aeruginosa*, which commonly causes chronic infections in CF patients. Since antibiotic resistance is a growing problem, co-cultures may offer a future platform to develop new antibacterial molecules. Despite these findings, to date, most of the gut microbiota continues being a big black box. As our understanding of the microbiota grows, so will the opportunities to harness its potential for human benefit, not only in cancer research but also in many other scientific areas. Organoids represent a powerful tool to this end, and I believe they will be at the core of these future advances.

REFERENCES

1. Sender R, Fuchs S, Milo R. Revised Estimates for the Number of Human and Bacteria Cells in the Body. *PLOS Biology*. 2016;14(8):e1002533. doi:10.1371/journal.pbio.1002533
2. Nougayrède JP, Homburg S, Taieb F, et al. Escherichia coli Induces DNA Double-Strand Breaks in Eukaryotic Cells. *Science*. 2006;313(5788):848-851. doi:10.1126/science.1127059
3. Dziubańska-Kusibab PJ, Berger H, Battistini F, et al. Colibactin DNA-damage signature indicates mutational impact in colorectal cancer. *Nature Medicine*. 2020;26(7):1063-1069. doi:10.1038/s41591-020-0908-2
4. Boot A, Ng AWT, Chong FT, et al. Characterization of colibactin-associated mutational signature in an Asian oral squamous cell carcinoma and in other mucosal tumor types. *Genome Res*. 2020;30(6):803-813. doi:10.1101/gr.255620.119
5. Zhao Z, Xu S, Zhang W, Wu D, Yang G. Probiotic Escherichia coli NISSLE 1917 for inflammatory bowel disease applications. *Food Funct*. 2022;13(11):5914-5924. doi:10.1039/D2FO00226D
6. Guenther K, Straube E, Pfister W, Guenther A, Huebler A. Severe Sepsis After Probiotic Treatment With Escherichia coli NISSLE 1917. *The Pediatric Infectious Disease Journal*. 2010;29(2):188. doi:10.1097/INF.0b013e3181c36eb9
7. Olier M, Marcq I, Salvador-Cartier C, et al. Genotoxicity of Escherichia coli Nissle 1917 strain cannot be dissociated from its probiotic activity. *Gut Microbes*. 2012;3(6):501-509. doi:10.4161/gmic.21737
8. Lee-Six H, Olafsson S, Ellis P, et al. The landscape of somatic mutation in normal colorectal epithelial cells. *Nature*. 2019;574(7779):532-537. doi:10.1038/s41586-019-1672-7
9. Wang Y, Robinson PS, Coorens THH, et al. APOBEC mutagenesis is a common process in normal human small intestine. *Nat Genet*. 2023;55(2):246-254. doi:10.1038/s41588-022-01296-5
10. Hansson GC. Role of mucus layers in gut infection and inflammation. *Current Opinion in Microbiology*. 2012;15(1):57-62. doi:10.1016/j.mib.2011.11.002
11. Johansson MEV, Hansson GC. Immunological aspects of intestinal mucus and mucins. *Nat Rev Immunol*. 2016;16(10):639-649. doi:10.1038/nri.2016.88
12. Gustafsson JK, Johansson MEV. The role of goblet cells and mucus in intestinal homeostasis. *Nat Rev Gastroenterol Hepatol*. 2022;19(12):785-803. doi:10.1038/s41575-022-00675-x
13. Enav H, Bäckhed F, Ley RE. The developing infant gut microbiome: A strain-level view. *Cell Host & Microbe*. 2022;30(5):627-638. doi:10.1016/j.chom.2022.04.009
14. Martincorena I. Somatic mutation and clonal expansions in human tissues. *Genome Med*. 2019;11(1):1-3. doi:10.1186/s13073-019-0648-4
15. Balmain A. The critical roles of somatic mutations and environmental tumor-promoting agents in cancer risk. *Nat Genet*. 2020;52(11):1139-1143. doi:10.1038/s41588-020-00727-5
16. Gacesa R, Kurilshikov A, Vich Vila A, et al. Environmental factors shaping the gut microbiome in a Dutch population. *Nature*. 2022;604(7907):732-739. doi:10.1038/s41586-022-04567-7
17. Olafsson S, McIntyre RE, Coorens T, et al. Somatic Evolution in Non-neoplastic IBD-Affected Colon. *Cell*. 2020;182(3):672-684. e11. doi:10.1016/j.cell.2020.06.036
18. Willing BP, Russell SL, Finlay BB. Shifting the balance: antibiotic effects on host-microbiota mutualism. *Nat Rev Microbiol*. 2011;9(4):233-243. doi:10.1038/nrmicro2536
19. Blake KS, Choi J, Dantas G. Approaches for characterizing and tracking hospital-associated multidrug-resistant bacteria. *Cell Mol Life Sci*. 2021;78(6):2585-2606. doi:10.1007/s00018-020-03717-2
20. Arima K, Zhong R, Ugai T, et al. Western-Style Diet, *pks* Island-Carrying Escherichia coli, and Colorectal Cancer: Analyses From Two Large Prospective Cohort Studies. *Gastroenterology*. 2022;163(4):862-874. doi:10.1053/j.gastro.2022.06.054
21. Sinicrope FA. Increasing Incidence of Early-Onset Colorectal Cancer. *New England*

- Journal of Medicine*. 2022;386(16):1547-1558. doi:10.1056/NEJMra2200869
22. Pasolli E, Asnicar F, Manara S, et al. Extensive Unexplored Human Microbiome Diversity Revealed by Over 150,000 Genomes from Metagenomes Spanning Age, Geography, and Lifestyle. *Cell*. 2019;176(3):649-662.e20. doi:10.1016/j.cell.2019.01.001
 23. Nivina A, Yuet KP, Hsu J, Khosla C. Evolution and Diversity of Assembly-Line Polyketide Synthases. *Chem Rev*. 2019;119(24):12524-12547. doi:10.1021/acs.chemrev.9b00525
 24. Cao Y, Oh J, Xue M, et al. Commensal microbiota from patients with inflammatory bowel disease produce genotoxic metabolites. *Science*. 2022;378(6618):eabm3233. doi:10.1126/science.abm3233
 25. Holt RA. Oncomicrobial vaccines: The potential for a *Fusobacterium nucleatum* vaccine to improve colorectal cancer outcomes. *Cell Host & Microbe*. 2023;31(1):141-145. doi:10.1016/j.chom.2022.11.014
 26. Lewis K. The Science of Antibiotic Discovery. *Cell*. 2020;181(1):29-45. doi:10.1016/j.cell.2020.02.056
 27. Mukherjee S, Bassler BL. Bacterial quorum sensing in complex and dynamically changing environments. *Nat Rev Microbiol*. 2019;17(6):371-382. doi:10.1038/s41579-019-0186-5
 28. Rossi E, La Rosa R, Bartell JA, et al. *Pseudomonas aeruginosa* adaptation and evolution in patients with cystic fibrosis. *Nat Rev Microbiol*. 2021;19(5):331-342. doi:10.1038/s41579-020-00477-5
 29. Rémy B, Mion S, Plener L, Elias M, Chabrière E, Daudé D. Interference in Bacterial Quorum Sensing: A Biopharmaceutical Perspective. *Frontiers in Pharmacology*. 2018;9. Accessed February 21, 2023. <https://www.frontiersin.org/articles/10.3389/fphar.2018.00203>
 30. Miethke M, Pieroni M, Weber T, et al. Towards the sustainable discovery and development of new antibiotics. *Nat Rev Chem*. 2021;5(10):726-749. doi:10.1038/s41570-021-00313-1
 31. Nikolaev M, Mitrofanova O, Broguiere N, et al. Homeostatic mini-intestines through scaffold-guided organoid morphogenesis. *Nature*. 2020;585(7826):574-578. doi:10.1038/s41586-020-2724-8
 32. Wang Z, Boretto M, Millen R, et al. Rapid tissue prototyping with micro-organospheres. *Stem Cell Reports*. 2022;17(9):1959-1975. doi:10.1016/j.stemcr.2022.07.016
 33. Williamson IA, Arnold JW, Samsa LA, et al. A High-Throughput Organoid Microinjection Platform to Study Gastrointestinal Microbiota and Luminal Physiology. *Cellular and Molecular Gastroenterology and Hepatology*. 2018;6(3):301-319. doi:10.1016/j.jcmgh.2018.05.004



NEDERLANDSE SAMENVATTING

RESUMEN EN ESPAÑOL

CURRICULUM VITAE

LIST OF PUBLICATIONS

ACKNOWLEDGMENTS

NEDERLANDSE SAMENVATTING

Van volwassen stamcellen (ASC) afgeleide organoïden zijn miniatuurreplica's van menselijke organen die in een schaal worden gekweekt. Ze vertrouwen op het intrinsieke vermogen van epitheliale stamcellen om te prolifereren en/of te differentiëren op basis van specifieke moleculaire aanwijzingen. Door deze aanwijzingen in vitro na te bootsen, kunnen ASC-organoïden worden gekweekt uit gezond weefsel en voor onbepaalde tijd worden uitgebreid, terwijl ze aanleiding geven tot de gedifferentieerde cellen die kenmerkend zijn voor hun orgel van oorsprong. Tegenwoordig worden ASC-organoïden gebruikt om diverse biologische aspecten van de menselijke epitheliale biologie te bestuderen.

De focus van dit proefschrift ligt op het begrijpen van de mechanismen waarmee bacteriën ziekten veroorzaken. Verschillende bacteriesoorten, waaronder *pk^s⁺ E. coli*, zijn herhaaldelijk in verband gebracht met de ontwikkeling van colorectale kanker (CRC). Het blijft echter onduidelijk of hun verrijking oorzakelijk is of een gevolg van de ziekte. Bovendien wordt het toenemende aantal antimicrobieel resistente (AMR) bacteriën wereldwijd een groot probleem. Met name AMR-stammen van *P. aeruginosa* veroorzaken chronische infecties bij personen met cystische fibrose, die een belangrijke bijdrage leveren aan het hoge sterftecijfer.

In dit proefschrift ontwikkelen we co-cultuurmodellen voor organoïde-bacteriën om de directe mechanismen te onderzoeken waarmee deze bacteriën (*pk^s⁺ E. coli* en *P. aeruginosa*) ziekten veroorzaken. Vanwege hun reductionistische aard (zijnde puur epitheel), maken ASC-organoïden isolatie en in vitro reconstructie mogelijk van de interacties die optreden tussen het epitheel en bacteriën tijdens infectie.

Hoofdstuk 1 heeft tot doel de bacteriesoorten te definiëren die gewoonlijk geassocieerd worden met CRC. Het blijft focussen op de huidige mechanistische kennis waarmee de microbiota CRC kan veroorzaken. Daarnaast bespreekt het de huidige benaderingen om de darmmicrobiota te gebruiken of aan te pakken bij de behandeling van kanker.

Hoofdstuk 2 bespreekt recente ontwikkelingen van co-culturen van bacteriën met darmorganoïden en organ-on-a-chip-modellen. Bovendien belicht dit hoofdstuk de biologische processen die door elk model beter worden samengevat. Verder bespreekt het de huidige trends en toekomstige richtingen van het gebruik van organoïde-bacterie-co-culturen om interacties tussen gastheer en microbiota te bestuderen.

Hoofdstuk 3 beschrijft de standaardmethode die wordt gebruikt om ASC-afgeleide menselijke 3D-organoïden van de dunne darm en de dikke darm vast te stellen en te kweken, zowel uit gezond als uit tumorweefsel. Het omvat technieken voor cryopreservatie, immunofluorescentiekleuring en differentiatie van organoïden naar specifieke cellijnen.

Hoofdstuk 4 beschrijft de methodologie die we hebben ontwikkeld om co-culturen uit te voeren, met een focus op 3D darmorganoïden en darmbacteriën. Bovendien

behandelt het de meest gebruikelijke technieken die worden gebruikt in downstream-analyses, van de chemische labeling van bacteriën tot de combinatie ervan met organoïde immunolabeling en beeldvorming, evaluatie van bacteriën en organoïde levensvatbaarheid, en het genereren van eencellige klonen uit organoïden voor beoordeling van bacteriële mutagenese op het epitheel.

Hoofdstuk 5 identificeert mutatiesignaturen geïnduceerd door *pk^{s+}* *E. coli* in CRC. Door langdurige co-culturen van intestinale organoïden met *pk^{s+}* *E. coli* tot stand te brengen, identificeren we twee mutatiehandtekeningen die worden veroorzaakt door het *pk^s*-product, colibactine. Deze handtekeningen, SBS88 en ID18 genoemd, kunnen worden opgevat als specifieke voetafdrukken die door colibactine in het genoom zijn achtergelaten. Dit stelt ons dus in staat om het mutagene effect te identificeren van *pk^{s+}*-bacteriën verrijkt in een subgroep van CRC-patiënten. Bovendien suggereren onze resultaten dat door colibactine geïnduceerde mutaties specifiek APC kunnen beïnvloeden, de belangrijkste aanjager van CRC-tumorvorming.

Hoofdstuk 6 is een vervolgstudie waarin we het mutagene vermogen evalueren van een *pk^{s+}*-stam van *E. coli* die wordt gebruikt als algemeen probioticum. Deze stam vertoont dus verminderde, maar detecteerbare mutagene eigenschappen wanneer deze samen met organoïden wordt gekweekt. Als onderdeel van deze analyse ontwikkelen we een analytische benadering die gebruik maakt van de karakteristieke adenineverrijking van door colibactine geïnduceerde mutaties. Deze methode verfijnt hun detectie in datasets voor volledige genoomsequencing. Bovendien maakt het een efficiënte detectie van colibactine-mutaties mogelijk in monsters van complete exome sequencing-cohorten.

Hoofdstuk 7.1 geeft een overzicht van de menselijke luchtwegen en de huidige ASC-organoïdemodellen afgeleid van de luchtwegen. Daarnaast beschrijft het de oorzaak en gevolgen van cystic fibrosis (CF), een monogene ziekte die de luchtwegen ernstig aantast. Vaak gaat CF gepaard met chronische infecties van de Gram-negatieve *P. aeruginosa*, wat ernstige complicaties voor de patiënten veroorzaakt.

Hoofdstuk 7.2 modelleert luchtweginfecties met *P. aeruginosa* met behulp van een 2D organoïde kweekstelsel. Na het vaststellen van de co-cultuurcondities, karakteriseren we tegelijkertijd de transcriptionele respons van het epitheel en de bacteriën, met een focus op quorum sensing regulatie. Met behulp van dubbele RNA-sequencing laten we zien dat het epitheel bacteriële veranderingen in de bacteriën induceert die gerelateerd zijn aan metabolisme, expressie van virulentiefactoren en antibioticaresistentiegenen. Belangrijk is dat verschillende van deze processen

RESUMEN EN ESPAÑOL

Los organoides derivados de células madre adultas son réplicas en miniatura de órganos humanos que pueden ser cultivados en el laboratorio. Estos organoides se basan en la habilidad de las células madre epiteliales para mantener su estado proliferativo y/o diferenciarse, dependiendo de las señales moleculares a las que están expuestas en el organismo. La recapitulación de estas señales de proliferación o diferenciación *in vitro* hace posible mantener su capacidad expansiva, dando lugar a más células madre o de producir otros tipos celulares funcionales. Hoy, los organoides son una herramienta esencial para el estudio de un amplio abanico de aspectos relacionados con la biología molecular de los tejidos epiteliales.

Esta tesis se enfoca en el estudio de los mecanismos por los cuales las bacterias causan enfermedades. La presencia en el colon de varias especies bacterianas, *E. coli pk^{s+}* entre ellas, está asociada con un mayor riesgo de desarrollar cáncer de colon. Sin embargo, todavía no está claro si esta asociación es causa o consecuencia de la enfermedad. Además, el incremento en la tasa de bacterias resistentes a agente antimicrobianos (AMR por sus siglas en inglés) se está convirtiendo en un grave problema a nivel mundial. En particular, cepas resistentes de la bacteria *P. aeruginosa* causan infecciones crónicas en las vías respiratorias de individuos con fibrosis quística, contribuyendo al agravamiento de la enfermedad y su alta tasa de mortalidad.

En esta tesis se desarrollamos co-cultivos de organoides y bacterias para investigar los mecanismos por los cuales *E. coli pk^{s+}* contribuye al desarrollo del cáncer colorrectal, y *P. aeruginosa* al empeoramiento de la fibrosis quística. Debido a la naturaleza reduccionista de los organoides, compuestos puramente de células epiteliales, estos permiten aislar y reconstruir *in vitro* una versión minimalista de las interacciones que ocurren durante la infección entre ambos componentes.

En el **capítulo 1** se definen las especies bacterianas recurrentemente asociadas con el cáncer colorrectal. Después, se cubren los conocimientos actuales sobre los mecanismos por los cuales estas bacterias podrían causar la enfermedad. Finalmente, en este capítulo se discuten las estrategias actuales usadas para modular o utilizar la microbiota intestinal en el tratamiento del cáncer colorrectal.

En el **capítulo 2** se hace una revisión de los avances recientes en el campo de los co-cultivos bacterianos usando organoides intestinales y órganos en chips. Este capítulo señala qué procesos biológicos están mejor representados por cada modelo. Además, se incluye una discusión sobre uso presente y futuro de co-cultivos para el estudio de las interacciones entre las bacterias y el epitelio intestinal.

En el **capítulo 3** se describe la metodología estándar para el establecimiento y cultivo de organoides intestinales de tejido sano y de cáncer colorrectal. Incluye técnicas de criopreservación, inmunomarcaje de fluorescencia y diferenciación de los organoides hacia linajes celulares intestinales como células goblet, enteroendocrinas o enterocitos/colonocitos.

En el **capítulo 4** se describe la metodología desarrollada en esta tesis para el establecimiento de co-cultivos de organoides intestinales en 3D y bacterias intestinales. Además, este capítulo recoge técnicas comúnmente utilizadas para la caracterización de estos co-cultivos; Desde el marcaje fluorescente de bacterias y su combinación con inmunomarcaje de organoides, hasta la evaluación de la viabilidad de bacterias y organoides. Además, se detalla el método para la generación de clones derivados de una sola célula para la evaluación de la mutagénesis bacteriana en organoides.

En el **capítulo 5** se identifica una signatura mutacional inducida por *E. coli pks*⁺ en organoides, presente en muestras de cáncer colorrectal. Estableciendo co-cultivos de organoides intestinales con *E. coli pks*⁺ a largo plazo, se identifican dos signaturas mutacionales inducidas por colibactina, una toxina producto del operón *pks*. Estas signaturas mutacionales, llamadas SBS88 and ID18, pueden ser entendidas como huellas específicas dejadas en el genoma por la acción mutagénica de la colibactina. Esto permite identificar la acción mutagénica de bacterias productoras de colibactina, predominantemente en pacientes de cáncer colorrectal. Además, nuestros resultados sugieren que esta mutagénesis podría afectar especialmente al gen *APC*, cuyas mutaciones son un factor muy importante en el desarrollo del cáncer colorrectal.

En el **capítulo 6** se ahonda en el descubrimiento realizado en el capítulo 5, evaluando la mutagénesis de una cepa de *E. coli pks*⁺ que se usa comúnmente como probiótico. En nuestro análisis, esta cepa presenta una capacidad mutagénesis reducida comparada con la cepa usada previamente. A pesar de ello, este probiótico también causa mutaciones detectables en los organoides. Como parte de este análisis, desarrollamos un método de análisis basado en la presencia predominante de adeninas en las mutaciones causadas por la colibactina. Este método mejora la detección de mutaciones causadas por colibactina en muestras de secuenciación genómica, a la vez que permite su detección en muestras de secuenciación exónica.

En el **capítulo 7.1** se hace una introducción de la biología tracto respiratorio y organoides derivados de este órgano. Además, este capítulo detalla la causa y consecuencias de la fibrosis quística, una enfermedad monogénica que afecta severamente a las vías respiratorias. Comúnmente, la fibrosis quística viene acompañada de infecciones crónicas de la bacteria Gram-negativa *P. aeruginosa*, la cual causa complicaciones importantes en estos pacientes.

En el **capítulo 7.2** se establece un modelo de co-cultivo entre *P. aeruginosa* y organoides nasales en 2D. A continuación, se caracteriza la respuesta transcripcional de ambos componentes, bacteriano y epitelial, prestando particular atención a la regulación la percepción quorum bacteriana. Utilizando secuenciación dual del RNA, mostramos que el epitelio induce cambios importantes en la bacteria, que incluyen cambios metabólicos, la expresión de factores de virulencia y de genes relacionados con la resistencia a antibióticos. Además, pudimos confirmar que varios de estos procesos también están presentes en muestras bacterianas directamente recogidas de individuos con fibrosis quística.

En el **capítulo 8** se discute las implicaciones de los resultados obtenidos en las secciones previas, y del rol que los co-cultivos de bacterias y organoides pueden jugar en futuras investigaciones en el campo de las interacciones entre el huésped y la microbiota humana.

CURRICULUM VITAE

Cayetano Pleguezuelos Manzano was born on June 25th, in Córdoba, Andalucía, España. He graduated from the Instituto de Educación Secundaria Luis de Góngora in Córdoba, with a scientific bachillerato in 2010. After this, he initiated his bachelor's studies in Biotechnology at University of León, in León, Spain. During his bachelor's degree, Cayetano studied for one year at Nottingham Trent University (UK), as part of an Erasmus student exchange program. After finalizing his Bachelor in 2014, he moved to Amsterdam, the Netherlands, to perform an internship at Sanquin in the group of Mar Fernandez-Borja, where he studied the role of prion protein in monocyte-blood vessel interactions. In 2015, Cayetano enrolled in the master's program of Biomolecular Sciences at Vrije Universiteit Amsterdam, graduating in 2017 with *cum laude* mention. During his master's, he performed his first internship at the lab of Prof. Louis Vermeulen at AMC Amsterdam, where he studied the influence of the site-of-origin on colorectal cancer heterogeneity using mouse intestinal organoids. Then, he moved to Utrecht to perform his second internship at the lab of Prof. Hans Clevers to investigate the role of telomerase on the expansion potential of human cholangiocyte organoids. In November 2017, after finalizing his master's degree, Cayetano joined the lab of Prof. Clevers as PhD student to study host-microbiota interactions in disease establishing human organoid co-cultures with pathogenic bacteria. The results of this are presented in this thesis.

LIST OF PUBLICATIONS

Pou Casellas, C., **Pleguezuelos-Manzano, C.**, Rookmaaker, M. B., Verhaar, M. C., & Clevers, H. (2023). Transcriptomic profile comparison reveals conservation of ionocytes across multiple organs. *Scientific Reports*, 13(1).

Pleguezuelos-Manzano, C.*; Beenker, W. A. G.*; Son, G. J. F. van; Begthel, H.; Amatngalim, G. D.; Beekman, J. M.; Clevers, H.; Hertog, J. den. Establishment and Characterization of a New Pseudomonas Aeruginosa Infection Model Using 2D Airway Organoids and Dual RNA Sequencing. *bioRxiv* March 11, 2023, p 2023.03.11.532178. (Preprint)

Juan, L. S., Freije, A., Sanz-Gómez, N., Jiménez-Matías, B., **Pleguezuelos-Manzano, C.**, Sanz, J. R., de Diego, E., Naranjo, S., Clevers, H., & Gandarillas, A. (2023). DNA damage triggers squamous metaplasia in human lung and mammary cells via mitotic checkpoints. *Cell Death Discovery*, 9(1).

Pleguezuelos-Manzano, C.*, Puschhof, J.*, & Clevers, H. (2022). Gut Microbiota in Colorectal Cancer: Associations, Mechanisms, and Clinical Approaches. *Annual Review of Cancer Biology*, 6(1), 65–84.

Allen, J., Rosendahl Huber, A., **Pleguezuelos-Manzano, C.**, Puschhof, J., Wu, S., Wu, X., Boot, C., Saftien, A., O'Hagan, H. M., Wang, H., van Boxtel, R., Clevers, H., & Sears, C. L. (2022). Colon Tumors in Enterotoxigenic Bacteroides fragilis (ETBF)-Colonized Mice Do Not Display a Unique Mutational Signature but Instead Possess Host-Dependent Alterations in the APC Gene. *Microbiology Spectrum*, 10(3), e01055-22.

Rosendahl Huber, A.*, **Pleguezuelos-Manzano, C.***, & Puschhof, J.* (2021). A bacterial mutational footprint in colorectal cancer genomes. *British Journal of Cancer*, 124(11).

Puschhof, J.*, **Pleguezuelos-Manzano, C.***, Martinez-Silgado, A., Akkerman, N., Saftien, A., Boot, C., de Waal, A., Beumer, J., Dutta, D., Heo, I., & Clevers, H. (2021). Intestinal organoid cocultures with microbes. *Nature Protocols*, 16(10).

Geurts, M. H., Poel, E. de*, **Pleguezuelos-Manzano, C.***, Oka, R., Carrillo, L., Andersson-Rolf, A., Boretto, M., Brunsveld, J. E., Boxtel, R. van, Beekman, J. M., & Clevers, H. (2021). Evaluating CRISPR-based prime editing for cancer modeling and CFTR repair in organoids. *Life Science Alliance*, 4(10).

Beumer, J., Geurts, M. H., Lamers, M. M., Puschhof, J., Zhang, J., van der Vaart, J., Mykytyn, A. Z., Breugem, T. I., Riesebosch, S., Schipper, D., van den Doel, P. B., de Lau,

W., **Pleguezuelos-Manzano, C.**, Busslinger, G., Haagmans, B. L., & Clevers, H. (2021). A CRISPR/Cas9 genetically engineered organoid biobank reveals essential host factors for coronaviruses. *Nature Communications*, 12(1).

Puschhof, J.*, **Pleguezuelos-Manzano, C.***, & Clevers, H. (2021). Organoids and organs-on-chips: Insights into human gut-microbe interactions. *Cell Host & Microbe*, 29(6), 867–878.

Pleguezuelos-Manzano, C.*, Puschhof, J.*, Rosendahl Huber, A.*, van Hoeck, A., Wood, H. M., Nomburg, J., Gurjao, C., Manders, F., Dalmaso, G., Stege, P. B., Paganelli, F. L., Geurts, M. H., Beumer, J., Mizutani, T., Miao, Y., van der Linden, R., van der Elst, S., Garcia, K. C., Top, J., Willems, R. J. L., Giannakis, M., Bonnet, R., Quirke, P., Meyerson, M., Cuppen, E., van Boxtel, R., Clevers, H. (2020). Mutational signature in colorectal cancer caused by genotoxic pks+ *E. coli*. *Nature*, 580(7802).

Pleguezuelos-Manzano, C.*, Puschhof, J.*, van den Brink, S., Geurts, V., Beumer, J., & Clevers, H. (2020). Establishment and Culture of Human Intestinal Organoids Derived from Adult Stem Cells. *Current Protocols in Immunology*, 130(1), e106.

Beumer, J., Puschhof, J., Bauzá-Martinez, J., Martínez-Silgado, A., Elmentaite, R., James, K. R., Ross, A., Hendriks, D., Artegiani, B., Busslinger, G. A., Ponsioen, B., Andersson-Rolf, A., Saftien, A., Boot, C., Kretzschmar, K., Geurts, M. H., Bar-Ephraim, Y. E., **Pleguezuelos-Manzano, C.**, Post, Y., Begthel, H., van der Linden, F., Lopez-Iglesias, C.; van de Wetering, W. J., van der Linden, R., Peters, P. J., Heck, A. J. R., Goedhart, J., Snippert, H., Zilbauer, M., Teichmann, S. A., Wu, W., Clevers, H. (2020). High-Resolution mRNA and Secretome Atlas of Human Enteroendocrine Cells. *Cell*, 181(6), 1291-1306.e19.

Miao, Y., Ha, A., de Lau, W., Yuki, K., Santos, A. J. M., You, C., Geurts, M. H., Puschhof, J., **Pleguezuelos-Manzano, C.**, Peng, W. C., Senlice, R., Piani, C., Buikema, J. W., Gbenedio, O. M., Vallon, M., Yuan, J., de Haan, S., Hemrika, W., Rösch, K., Dang, L. T., Baker, D., Ott, M., Depeille, P., Wu, S. M., Drost, J., Nusse, R., Roose, J. P., Piehler, J., Boj, S. F., Janda, C. Y., Clevers, H., Kuo, C. J., Garcia, K. C. (2020). Next-Generation Surrogate Wnts Support Organoid Growth and Deconvolute Frizzled Pleiotropy In Vivo. *Cell Stem Cell*, 27(5), 840-851.e6.

Adam, R. S., van Neerven, S. M., **Pleguezuelos-Manzano, C.**, Simmini, S., Léveillé, N., de Groot, N. E., Holding, A. N., Markowetz, F., & Vermeulen, L. (2020). Intestinal region-specific Wnt signalling profiles reveal interrelation between cell identity and oncogenic pathway activity in cancer development. *Cancer Cell International*, 20(1), 578.

Richardson, D. D., Tol, S., Valle-Encinas, E., **Pleguezuelos, C.**, Bierings, R., Geerts, D., & Fernandez-Borja, M. (2015). The prion protein inhibits monocytic cell migration by stimulating β 1 integrin adhesion and uropod formation. *Journal of Cell Science*, 128(16), 3018–3029.

Manuscripts in preparation

Rosendahl Huber, A.*, **Pleguezuelos-Manzano, C.***, Puschhof, J.*, Boot, C., Saftien, A., Wood, H., Quirke, P., Clevers, H., van Boxtel, R., An analytical framework to detect colibactin-induced mutations in colorectal cancer and *E. coli* Nissle-exposed organoids (Under revision).

* indicates equal contribution

ACKNOWLEDGMENTS

These years at the lab have been an amazing experience. This was possible, no doubt, because of all the people that I encountered on the way. And now, it is the time for me to thank you:

Of course, my acknowledgments need to start with **Hans**. Being at your lab during these years has been very enriching and stimulating. I feel privileged to have had the chance to learn from you. I would like to thank you for creating such a research and human environment, allowing your people to learn, work, and collaborate with such freedom. Your vision and knowledge are immense, although I still wonder how you do it, how is it possible... I have always been amazed at how little information you need to stir entire projects in the right direction. Additionally, you are generous with your people, and if we occasionally got into trouble, you were always there to help us out of it. Unbiased experimentation and reductionistic research, I will try to keep up with the scientific spirit that you inculcate in us. I cannot really wish you more success in your career, but I still do. And of course, all the best in your personal life.

Next are my friends, colleagues and paranymphs, **Amanda** and **Adriana**. Both of you have helped me enormously during this adventure, and no doubt you have contributed to making my PhD such a fantastic experience. Thanks for being great paranymphs already. I am looking forward to seeing how everything goes during the next weeks! I am sure it will be amazing.

Amanda, we started our journey in this lab at the same time, November 2017, and in the same place, the later so-called "other side office". At the beginning it felt a bit like Siberian steppe; however, very quickly this changed, and we all knew that the other side was the proper side. During these years, I was able to discover an incredible scientist, who was and is an example of how to do proper science. With attention to details and exhaustive search for the right approach to prove a point. Additionally, I learnt a lesson that I will take with me for the rest of my life: step1 – paranoia. Apart from this, I think that the time that we spent together in the lab and outside allows me now to call you a friend and I am incredibly happy about that. You have always been there to celebrate in the highs and to cheer up in the lows, with wise words ready for when they are needed. Always you were ready to eat a lot of tasty food together, bike, and for me to join your running sessions again, maybe soon... For all this, thank you. I am sure that you will be able to do everything you want in life successfully. We need to meet in Spain for all the food, sun, hiking, biking, not running, and more food.

Adriana, we met a bit later in my PhD and our relationship started in slightly different circumstances. We have spent a lot of time culturing organoids together, what also casually brought up the opportunity of having a lot of interesting conversations: from philosophical and scientific, to art and culture, always of course, a lot of Spain-related topics, and food. You are very direct, and I appreciate you for that, really. You have an incredible artistic power, never stop with it. You are also a great scientist, with a deep

knowledge of your research topic, and are very thoughtful and creative about your experiments. This marinates really well altogether with your hard work and perseverance. I am sure that your PhD will look amazing, and I am looking forward to it. I also call you a friend now I am happy about that.

Jens and Axel. I could only start writing here how happy I am that I got to work with you during this adventure. You both have been a very, very important part of my PhD and I cannot thank you enough for all of it. Over the years we managed to get to know each other quite well and this made me discover two amazing friends.

Jens, we started working together early after my start as PhD, looking for the right bacteria co-culture project to pursue. We managed to navigate this jungle as proper mowglis, as we liked to say, and it kind of worked out! We spent many days and evenings microinjecting organoids, doing experiments, and working on manuscripts together. And it was always a bit easier because you are a cheerful person, of course always with a joke or meme ready to unarm me with, and very caring for the people you work with. All this accounts for the time we spent in the lab doing science, but of course to cope with such hard work, we needed some recreation time. Transforming the evening lab corridors into tennis, frisbee, football, racing, and shooting fields was something that happened more often that we should admit. But I can only say that it was a lot of fun, and something I really enjoyed. I am very happy that your career brought you back home to do great science in a fantastic institute. Looking forward to see what you are cooking there!

Axel, we first met at Olympos football court while we were both on the bench substituting. After a brief introduction, who would have said that we would go this far together. Together we spent one of the most intense weeks of my life inhabiting the meeting rooms of the Hubrecht and PMC, for days and nights. But obviously, it was for the good. You are a dream Bioinformatician! with so much biological insight and with such an ability to perform your bioinformatic magic in record time. Your passion for science, your easy-going personality, and your ability to make everybody feel comfortable, made all this adventure unique. Now that you have come to spend some time in Spain, I would also like to switch to Spanish for a bit here. Axel, ¡tú eres la leyenda! Me alegra de ver que te lo estás pasando bien y que disfrutas conociendo la cultura española. Siempre es un placer reencontrarme con mi amigo holandés en cualquier parte, pero más ahora en Barcelona. ¡Espero que nos tomemos más de una cervecita en el futuro!

Wouter, we had a blast building the *Pseudomonas*-airway co-cultures. During the way, we had a lot of discussions and continuously imagined the many interesting directions our project could take and that was a lot of fun. At the end, we managed and put everything together, and I am very proud of what we did. You are an example of how to always be positive, despite how hard the circumstances might be, and how to keep going on graciously. I hope that you are enjoying your new job and I wish you all the best in everything you want to do in life.

Thanks to all my fellow PhD students, and all my colleagues during these years:

Carla, you always bring a nice vibe to the office. You have demonstrated an incredible ability to progress through your PhD, even if it did not seem easy for you at the beginning. I am sure that what is left of it is going to be great and very successful. Keep singing please!

Else, I am very happy to have met you in the lab. During the time we overlapped, you were always very impressive, working on a lot of projects, and supervising many students at the same time. Of course, your work is as impressive today. Sometimes, when I stand next to you, I hope some of your superpowers infuse into my brain. This will not happen, but you are an example of how to get ahead by being smart, with hard work, and kindness.

Emma, I am happy to have met you in the lab. I hope that your Clevers/Rios endeavor continues as great as until now. All the best.

Fjodor, it was nice sharing our PhD paths in the lab. Your MD background always brought fresh perspectives to our scientific discussions. Also, your cooking skills brought fresh dishes to the table from time to time! And it was always great. Good luck finishing and all the best in life!

Frans, you left the lab soon after I started my PhD. Your work always looked very developed and serious and at the same time you seemed chill about it, how did you do it? I am still trying to figure it out. I am happy that we stayed connected during this time and wish you all the best in the future.

Jelte, it was great to sit next to you all those years. You were a real driving force for the sociability of the office. You managed to arrange many of our activities, and I thank you for that. I hope your postdoc in the UMC will be successful as everything else you want to do in your life.

Joep, it has been a pleasure to meet you in the lab. Your knowledge and vision were always inspiring. It was always fun to chat over lunch/tc/borrel with you about any topic and to hear about all the fun facts that you shared. Always fun. Thanks very much for everything and I wish you all the best in Basel, and in all your endeavors. See you soon.

Joost, amazing football player and better PhD student. Thanks very much for sharing all your insights about integrins and organoids. You were always ready to help me with any kind of western-related question and beyond. I am sure your PhD will go amazingly.

Kadi, you always had sharp comments ready to highlight my ignorance on diverse topics, either scientific, general life, or Estonia-related. But it was always with a fun touch, and I appreciate them (now xd). Your work seemed extremely focused, thoughtful, and complete. It was great to play tennis together sometimes! Curious if you are keeping up with it, I am trying. I hope all is going good in Denmark and wish you all the best.

Katarina, you are the last person joining the office, and you brought a cheerful spirit. You are going to navigate the lab well, and your PhD will be fantastic. All the best.

Kim, you were a great PhD colleague. Always ready to help and very fun. You are still today famous for your food supplies. It is great to hear that you are happy in Germany, and that everything is going great. All the best and see you soon.

Lulu, it was fun to have you as wet lab neighbor. Your ability to pipet and not to get distracted by my random questions is remarkable. During these years, you have taught me a lot about China, Chinese culture, and food! Good luck finishing your PhD and all the best in the future.

Maarten, we also started together, and sharing this PhD trip with you has been a lot of fun. From the hours of scientific (and less scientific) conversations in the office, mixed with great dart shooting and basketbaling, hours in TC, to all the outside activities together. Your knowledge of genetic engineering, and your drive and focus to bring it to the next level is enviable. All the best in your present and future endeavors, and let's keep in touch.

Martina, you were key contributing to the cheerful atmosphere of the group and still are today. Scientifically, you come up with good research questions and are a pipetting machine. These are valuable qualities that will bring you success for sure. I will remember our invasions of Brava and all the dinners at your place. It was always great. All the best Martina regazza!

Ninouk, we are all sad that you left, but happy that your career has brought you to Basel, such a great place for research. I hope that you have not forgotten about us yet! Working with you during your internship was a great experience for me, from which I learnt a lot. Thanks very much for all your effort! Apart from that, I was glad to discover that we do share many other interests. We have, at least, one future concert to attend together :)

Sam, we have been neighbors for a bit now. During this time, I have discovered two things. That you are already an amazing scientist and that you are also an amazing person. I am incredibly happy that I have been sitting next to you, so that I could learn from you in both regards. I am sure that your PhD is going to be full of success and I wish you all the best in life.

Yorick, it was always fun to be with you in the lab. You always had some ready-made jokes to deliver or some dry-ice-water eppjes ready for surprise. Apart from that, your work in the lab was always inspiring and inventive. I envy now how clear you always had your next step after the PhD. I hope that everything is going well and to see you around soon.

Carola, you are one of the first people I met in the Clevers lab, during your student spot time and I am very happy that we made it until now. You are super smart and hard worker and I am very happy to have been close to you during these years. You always made the lab, especially the TC room, a brighter place to work in. It was nice to be involved somehow in the beginning of your musical career, and I will always remember that great Dutch band Kings of Lions. I wish you all the best and I hope that we stay in touch in the future. Hartelijke bedankt.

Charel, thanks very much for all your work in all the bacteria-related projects that were running in the lab and for being a great colleague in the meantime. You joined during COVID time, but managed to, very quickly, push so many projects forward in a very

impressive way, being passionate about organoids and bacteria. I am not surprised to hear that you are also rocking it in your new job. All the best for the future.

Lisanne, you were always terribly busy pipetting and moving forward millions of organoid lines. It was nice to see your organizational and planning skills from the neighbor desk, still today I try to keep it up myself with your example. I wish you and Tom all the best in life.

Veerle, you are another veteran in the lab. Thanks very much for always being ready to help. It was nice to share this experience with you. All the best.

Anjali, Priyanca, and Sigrid, you are old time lab legends! I am glad that I was there to meet you, because you were always nice, fun, and welcoming. Thanks to all the other technicians that were there a bit afterwards: **Milou, Mandy, Lisanne, and Gijs**. Thanks to the present students, **Julia, Wisse** and **Dirk Jan. Roksan** who was student with me many years ago, and to all the other master students that were at the lab during these years. It has been nice meeting you all here.

Johan, thanks for all the efforts to keep the lab up and running during all these years, and especially now. **Stieneke**, the Clevers lab functions because of you and we do not say it enough. Thanks very much for all you do! **Laura**, during these years, you were always ready to help with anything with a smile, thanks very much for everything. **Wim**, I wish to be able to keep your energy level in the future. Impressive. Thanks to **Harry** and **Jeroen** for your help and work, not only with organoid and tissue fixing, sectioning, and staining, but also for your inventiveness to solve any kind of unforeseen problem. Thanks to **Karien**, you taught me a lot of things during my first months at the lab. I hope you are enjoying your retirement!

Thanks to **Annemieke** for all your help during these years, and especially now organizing my defense. You always bring fresh and cheerful air every time you visit the lab!

Also, I would like to thank my other mentors: **Helmuth**, thanks for your guidance, teaching and mentoring during my internship in the lab. I regard you as one of the most intelligent people that I have met, and I am grateful that I had the chance to be your student in the lab. **Salvatore**, you introduced me to organoids in my first master internship. You also taught me about science, how to do experiments, and to always include positive and negative controls! I remember you did so with patience and care, and I really thank you for that. I wish you and your family all the best. And **Dion**, thank you very much.

Ruben, thanks very much for your guidance, support, and enthusiasm during all these years.

Thanks to the past and present postdocs during my time in the lab: **Helmuth, Kai, Marrit, Yotam, Lena, Inha, Benedetta, Oded, Huili, Tomo, Yoshi, Jasper, DJ, Georg, Jochem, Talya, Matteo, Sangho, Delilah, Rosie, Elena, Daniel, Daisong, Chris, Lin, Théo, Guiwei, Amir, Nella, Sarina, and Xuan**. I learnt a lot from all your different expertise and characters. You all made my experience at the lab enjoyable in one way or another and I am grateful that we crossed our paths!

Kai, you were a postdoc legend when I joined, and I am sure you are a PI one now. **Yotam**, I started as a master student at the time you were defending your PhD in Amsterdam. And here I am now, thanking you for all the help and fun at the lab. **Marrit**, you taught us all about circadian biology, such an interesting topic. Thank you! **Huili**, thanks for sharing those organoid lines with me, I still have them in culture today! **Tomo**, it was awesome sharing the lab with you, thanks for all the insight growing single cell clonal organoids! Also, it was great to meet you and your family in Córdoba. **Yoshi**, you always had the most legendary lab meetings! I hope that everything is going fantastic in Japan. **Jasper**, thanks for all the seniority and guidance during the beginning of my time at the lab, it was really helpful. **Matteo**, you interviewed to join the lab at the same group meeting where I was also presenting! Obviously, I am happy you stayed and to have spent these years together in the lab. As I write these lines, Inter is qualified for the Champions League's final. I hope that reading this in the future will bring you joy rather than pain. Good luck! **Sangho**, your immune work in the lab is impressive, and I am sure that you will be successful with everything you want to do in life. I am only sad that I did not manage to convince you to play more music together during these years. Maybe before I leave? :D **Daniel**, it was a lot of fun to share all the scientific discussions at the lab as well as all the beers and cocktails outside. You are a microscope legend, and everybody knows it. Let's keep in touch! **Rosie**, happy to have met you here. I hope you are enjoying your UK experience. **Chris**, you are the sweetest postdoc obviously! I am happy to collaborate with you these days. **Lin**, good luck pushing all your projects. **Nella**, even if we did not always agree in our discussions, it was nice having you in the office! **Théo**, I am glad that there is somebody else that can appreciate the right side of the host-microbe interaction at the lab. **Sarina**, you are a great scientist and very hardworking. It was always nice talking to you. Good luck in the lab! **Xuan**, good luck with your PhD defence and with your postdoc here. Thanks very much and best wishes for the future to everybody!

Thanks to my PMC colleagues during these years: **Margit, Evelyn, Seok, Laurens, Femke, Karin** and **Marc. Gijs**, thanks very much for all the help with the sequencing and I hope that your PhD goes amazingly.

Thanks to **Rob Willems** and its infectious disease team at UMC, **Fernanda** and **Paul**. You always had great input for my projects and were helpful during all our discussions. Thanks to the **OPTIMISTIC** team: leaders, senior and junior researchers, patient advocates, and administration. Thanks to the **NOCI** team. Especial thanks to my NOCI peers, you were always a great group of people to work and have fun with. Thanks, **Joske** for all your contribution to the *pks* work from the bioinformatics angle. You have pushed it to the next level, for sure. Thanks for their collaboration to **Phil Quirke** and **Henry Wood**. Thanks to **Reinier** and **Stefan** for your help sorting cells and with the Melody machine. Thanks to the personnel of the Hubrecht for making it such a lovely place to work in.

Thanks to all the people outside the lab:

Okke, my friend! It was always a fun to see you in any kind of scenarios, playing board games (one day, maybe, I will beat you and/or Adriana, maybe...), eating food of any

level, drinking more and less alcoholic beers, good wine and always having fun. During this time, I had the chance to appreciate your persona and discover a very nice guy. With your engineering mindset, you always bring a fresh point of view to our discussions that I always enjoyed. PS. I summon you (and Adriana) to share some grilled ibérico pork in Spain at some future point! **Anna**, it was always refreshing and fun meeting you. I hope that you keep enjoying Utrecht and wish you and Daniel all the best. **Juri**, I am glad that we developed a kind of weird music style together. Thanks for all those moments. I hope that everything is going well. **Nick**, thanks for your drum lessons, and your ability to keep it motivating and interesting. Saturday morning is always a time that I look forward to, and that makes my weeks better. **Nick** de Boston, gracias por aguantar esos ritmos impares mientras yo me iba por ahí. Gracias por tu pasión por el flamenco y la cultura andaluza. **Jason** and **Emma** sois fantásticos. Gracias por acogerme en vuestra casa durante estos años. Siempre que estuve allí, me hicisteis sentir genial. Espero que nos podamos ver mucho más en el futuro. **Etienne**, thanks for being great. It was amazing to visit Bordeaux. We will go to a VI Nations match soon! Also, thanks to all the **football** and **tennis people**, it was great fun playing with you.

Sylvie, merci pour tout! Tu es très gentille et sympathique toujours que Marie et moi sommes à Brest. C'est toujours fantastique de visiter toi, et je suis content d'apprendre la culture Bretonne et Française avec toi. Aussi, merci beaucoup pour me dessee courage pour la finalisation de ma thèse, et tout l'attention et aide pour choisi la couverture de ma livre. Evidemment, j'aime tout le Kouign-amann que tu envoyé sur le Pays-Bas. Merci pour ça aussi. Comme Marie avec l'Espagnol, je suis en train de apprend Française pour poudre communique avec toi et ta culture trop facilement. Merci pour tout!

Eider, Dila, Dimi, Manu, and Peri. My Dutch family, thanks very much for taking me into your fantastic group when I first came to the Netherlands. I am super grateful to have met you and I will always bring you with me. Each one of you has inspired me in different ways during these years and I have learnt something from all of you. Even if we are scattered across Europe, I know that we will stay connected.

Gracias a mis **abuelas y abuelos**, porque han sido y son los mejores. A mí abuela **Maruja**, por cuidar tan atentamente siempre de mí con todo el cariño. A mi abuela **Concha** y a mis abuelos **Paco** y **Cayetano**, siempre en el recuerdo. Gracias a mis primos y primas, **Rafa**, **María**, **Mónica**, **Carlos**, **Pedro** e **Inma**. **Inma** muchas gracias por todo el apoyo y el ánimo durante todos estos años de doctorado. ¡Mucha suerte con tus exámenes, vas a ser la mejor profe de tó el sistema de educación andalú! También a mi tita **Conchi** porque durante este tiempo siempre se ha preocupado por cómo me iba por aquí. Gracias a mis tíos **Jose** y **Fafi** y a mi tía **Paqui**. A mi tita **Conchi** y a mi tío **Rafalín**, los mejores.

Marie, you are an inspiration for life and science. I admire the determination, thoughtful consideration, and kindness with which you approach things and people. You are smart in many different ways, and I learn from you every day. You are always listening and always have wise words when needed. You are also fun. You are always ready to

act according to your values, even if that means in a not-so-straightforward way. For all this, thank you. In the lab, you have demonstrated that you are an excellent scientist, have created an incredible research field, and have done so with intelligence, inventiveness and hard work. I am incredibly happy for you and to have witnessed it of course. I am very sure that whatever it is our future, it will be beautiful.

Mi hermana **María**. Mariquilla, eres la mejor. Durante estos años, te has convertido en una joven independiente y responsable. Con las ideas siempre claras y llevándote para adelante todo lo que haga falta. Además de todo esto eres inteligente y rápida. También graciosa (de vez en cuando...-). Aprendo de ti cada vez que hablamos o nos juntamos. Muchas gracias por todos los ánimos que siempre me das. Con permiso de padre y madre, las mejores croquetas del planeta. Estoy seguro de que tendrás éxito en todo lo que te propongas y espero poder estar más por allí para verlo con mis propios ojos :)

Mamá y papá. Gracias por todo desde siempre. Gracias por la educación y los valores que nos habéis dado a María y a mí desde pequeños. Gracias por permitirme estudiar fuera de Córdoba y de España, sin ningún tipo de problema, nunca. Gracias por todos los ánimos y por ayudarme a poner las cosas en perspectiva. **Papá**, recuerdo cuando era pequeño, en casa, siempre andabas arreglando y construyendo cosas, y yo por medio curioseando. Los mejores paseos por el campo, andando y en bici, con mi padre. **Mamá**, gracias por enseñarme a valorar siempre la cultura, la lectura, el arte y la música. Todo esto, de una manera u otra, me inculcó la curiosidad y el espíritu que hace falta, creo, para dedicarse a la ciencia. Por todo, a los dos, ¡gracias!

